UNM | Electrical & Computer Engineering

SUMMA FOUNDATION

AMEREM 2014

BOOK OF ABSTRACTS

www.ece.unm.edu/amerem2014

University of New Mexico

Albuquerque, New Mexico, USA

July 27-31, 2014

Professor Edl Schamiloglu, *General Chair*
Dr. D.V. Giri, *Technical Program Chair*
Dr. William A. Radasky, *Technical ProgramVice Chair*
Mr. William Prather, *Treasurer*

Design Aspects of Korean Half Impulse Radiating Antenna (KOHIRA)

Tae Heon Jang
EMC Technology Center
Korea Testing Laboratory, 516 Haean-ro, Sa-dong,
Sangnok-gu, Ansan-si, Gyeonggi-do
South Korea 326-901
jhjang@ktl.re.kr

D. V. Giri
Dept. of ECE, Univ of New Mexico
Albuquerque, NM, USA and Pro-Tech,
11-C Orchard Ct, Alamo, CA 94507-1541, USA
Giri@DVGiri.com

Abstract— This paper describes the design, fabrication and testing of KOHIRA which is under development. KOHIRA consists of half of a Paraboloidal reflector of diameter 1.164 m, fed by two coplanar arms, each at 45 degrees from the vertical. KOHIRA is energized by a transient pulse generator PBG 3 offered by Kentech in UK. The input pulse has amplitude of 12 kV, a 10-90% risetime of 100 ps and an exponential decay time of 4.2 ns.

Keywords- Impulse Radiating Antenna, Half IRA, Transient pulse

I. INTRODUCTION

KOHIRA is schematically shown in Figure 1.

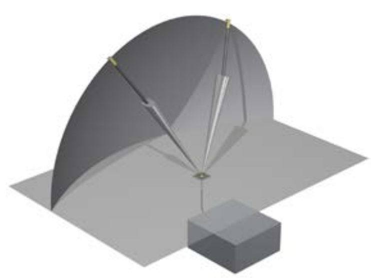

Figure 1. Notional sketch of KOHIRA

Focal length F = 42.3 cm, Diameter D = 116.4 cm
F/D = 0.363 and Depth d = 19.737 cm.
KOHIRA is expected to work over a band of frequencies raging from a low (f_ℓ) to high (f_h) frequencies. The low frequency limit is governed by the reflector size and the high frequency is governed by the rise time of the input pulse and how well the feed is constructed. Considering some risetime degradation between the pulser output and the wavelaunch on to the reflector, KOHIRA is expected to work from about 150 MHz to about 1.75 GHz.

II EXCITATION VOLTAGE WAVEFORM

The voltage waveform is analytically modeled by

$$V(t) = V_0(1+\Gamma)e^{-\beta\left(\frac{t-t_s}{t_d}\right)}\left[0.5\,\mathrm{erfc}\left(-\sqrt{\pi}\frac{t-t_s}{t_d}\right)u(-(t-t_s))+\left[1-0.5\,\mathrm{erfc}\left(-\sqrt{\pi}\frac{t-t_s}{t_d}\right)\right]u(t-t_s)\right]$$

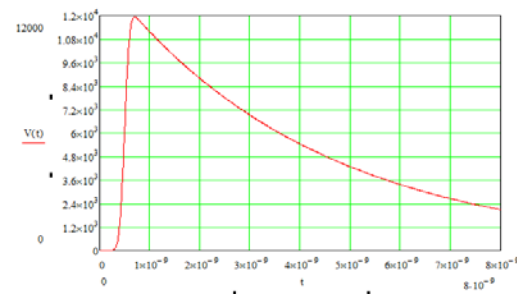

Figure 2. Excitation voltage waveform

With V_0 = 12,000 V, T =0.05, β = 0.048, t_d = 200 ps, t_s = 0.5 ns and is shown plotted in Figure 2. This waveform has a fairly simple Fourier transform. The pulse generator is a 50 Ohm device and the input impedance of the antenna is 100 Ohms and we have inserted an impedance transformer at the feed point.

II RADIATED ELECTRIC FIELDS

The radiated electric fields are estimated and shown plotted in Figure 3.

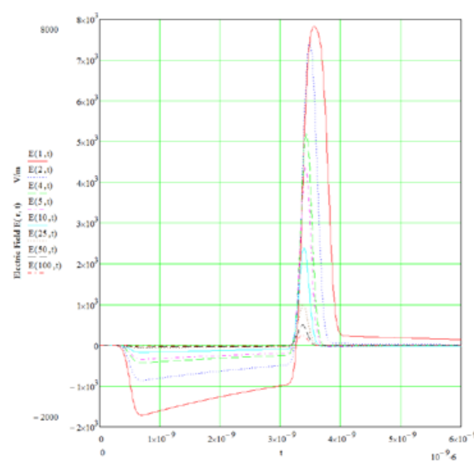

Figure 3. Calculated electric fields at various ranges

We will present detailed design and measurements as it becomes available.

Numerical Simulation of Power-grid Overloads and Short-circuit Protections

Chaouki Kasmi* and Damien Coiffard
Wireless Security Lab
French Network and Information Security Agency
Paris, France
*chaouki.kasmi@ssi.gouv.fr

Muriel Darces and Marc Hélier
Sorbonne Universités
UPMC Univ. Paris 06, UR2, L2E,
F-75005, Paris, France

***Abstract*—Spurious electromagnetic emanations can propagate along the power-grid cable network of critical infrastructures, which poses unacceptable risks for their *security* and *safety*. According to international standards, protective devices have to be inserted in low-voltage distribution networks in order to prevent physical damages due to either overload or short-circuit. We propose here to characterize these devices by measuring their scattering parameters in order to estimate their effects on the conducted propagation of electromagnetic interference along the power network.**

Keywords-component: Protective devices; Power-grid; Electromagnetic interferences;

I. Context

Many studies [1-3] have been devoted to the analysis of the conducted propagation of intentional and unintentional electromagnetic interferences (EMI) along the power-grid. It has been shown that the low-voltage distribution network acts as a guiding structure for these interferences. The use of models [3] has shown that we are able to analyse the conducted propagation of EMI along low-voltage cable networks. Models of such a network have been improved by the integration of appliances impedance [3] in electromagnetic simulation software.

In order to go further in the improvement of power-grid models, we propose to measure the scattering parameters of protective devices, obtained from different manufacturers and of several current-rates, at radio frequencies. Moreover the measurements have been performed with the power-supply turned on and shut off (respectively *off-line* and *on-line* states of devices) in order to know if appliances connected to the power network can be damaged by high-power electromagnetic attacks in both configurations. The measurement results have been inserted in the CRIPTE Code [4] simulation software developed by ONERA.

II. Overload's and Short-circuit's protections

International standards [5] define the protective devices (fuse-based breakers and magnetic-based breakers) that have to be added to the power network structure in order to protect a facility from physical damages that may be due to short-circuits or overloads. Both types of devices have been connected to a Vector Network Analyzer, thanks to simple adapters based on 50 Ω connectors. The scattering parameters of the device under test have been obtained by removing the effects of the test fixture. This has been achieved by using a *software-based de-embedding* procedure [6] and the deterministic modelling of the adapters.

III. Integration in the CRIPTE Code

The CRIPTE code [4] allows analyzing the conducted propagation of electromagnetic interferences in *topological networks* by solving the *BLT* equation. The modelling of complex cable networks is based on the combination of uniform sub-networks by means of *tubes* (representing the cable bundles), connected by *junctions,* as well as end points characterized by *loads*.

The *tubes* can be characterized either by the per-unit-length parameters obtained thanks to a 2D-field solver or by the measured per-unit-length parameters of cable bundles. Concerning the *junctions,* they can be characterized by impedance or scattering parameters. The last approach has been derived to insert the scattering parameters of devices in their *on-line* and *off-line* states as 4-port junctions.

Low-voltage power network models [3] have been improved by using the measured scattering parameters of the tested protective devices. It will be shown how the electromagnetic interferences are affected by those protective devices. Several outcomes will be also presented.

References

[1] Y. V. Parfenov, L. N. Zdoukhov, W. A. Radasky and M. Ianoz, "Conducted IEMI threats for commercial buildings", Electromagnetic Compatibility, IEEE Transactions on, Vol. 46, No. 3, pp. 404-411, August, 2004.

[2] D. Mansson, R. Thottappillil and M. Backstrom, "Propagation of UWB Transients in Low-Voltage Power Installation Networks", Electromagnetic Compatibility, IEEE Transactions on, Vol. 50, pp. 619-629, August, 2008.

[3] C. Kasmi, M. Darces, and M. Hélier, "Statistical analysis of a spurious signal level in a low voltage PLC network," in Electromagnetic Compatibility (EMC EUROPE), 2012 International Symposium on, pp. 1-5, September, 2012.

[4] J.-P. Parmantier and P. Degauque, "Topology Based Modeling of Very Large Systems". Modern Radio Science 1996, pp. 151-177, edited by J. Hamelin. Oxford University Press.

[5] IEEE – "Recommended Practice for Applying Low-Voltage Circuit Breakers Used in Industrial and Commercial Power Systems", IEEE Standard 1015-2006 (Revision of IEEE Std. 1015-1997), pp. 1-182, September, 2006.

[6] C. Kasmi, M. Hélier, M. Darces and P.-M. Ricordel, "A new de-embedding method to measure the RF input impedance of grid-powered devices", Electronics Letters, Vol. 49, Issue 19, p. 1218 – 1219, September, 2013.

Effect of Corona on Lightning-Induced Voltages

Tran Huu Thang
Tsuruoka National College of Technology
Department of Electrical and Electronic Engineering
Yamagata 997-8511, Japan
thangth@tsuruoka-nct.ac.jp

Yoshihiro Baba Naoto Nagaoka Akihiro Ametani
Doshisha University
Department of Electrical Engineering
Kyoto 610-0321, Japan
ybaba/nnagaoka/aametani@mail.doshisha.ac.jp

Naoki Itamoto
Hokuriku Electric Power Company
Institute of Research and Development
Toyama 930-8686, Japan
n.itamoto@rikuden.co.jp

Vladimir A. Rakov
University of Florida
Department of Electrical and Computer Engineering
Gainesville, FL 32611, USA
rakov@ece.ufl.edu

Abstract— **A simplified model of corona discharge for the finite-difference time-domain (FDTD) computations has been applied to analysis of lightning-induced voltages at different points along a single overhead wire in the presence of corona space charge around the wire. The magnitudes of FDTD-computed lightning-induced voltages in the presence of corona discharge are slightly larger than those computed without considering corona.**

Lightning; corona discharge; finite-difference time-domain method; lightning induced voltage

I. Introduction

In this paper, we apply a simplified (engineering) model [1, 2] of corona discharge developed for FDTD computations to analyzing lightning-induced voltages on a single wire above ground, which simulates the configurations employed in *Nucci et al.* [3] and *Dragan et al.* [4]. In the corona model, the progression of corona streamers from the wire is represented as the radial expansion of cylindrical weakly-conducting (40 μS/m) region (sheath) around the wire.

II. Modeling

Figs. 1 (a) and (b) show the plan (*xy*-plane) and side (*yz*-plane) views of a 5-mm radius, 1-km long overhead horizontal perfectly conducting wire located 7.5 m above ground. Lightning channel is represented by a 600-m long, vertical phased ideal current source array. Two cases are considered in which lightning is assumed to terminate on ground at points A (midpoint of the wire) and B (close to one of the line terminations). For FDTD computations, this conductor system is accommodated in a working volume of 400 m × 1200 m × 750 m. Cell sides along *x*, *y* and *z* axes are 2.2 cm in the vicinity of the conductors, and increase gradually to 10 and 200 cm beyond that region. Corona discharge is assumed to occur only on the horizontal wire.

III. Analysis and Results

Figs. 2 (a) and (b) illustrate induced voltages at different points along the overhead wire with and without considering corona on the wire, computed using the FDTD method for a negative lightning return stroke. Fig. 2 (a) is for stroke location A (35-kA current), and Fig. 2 (b) is for stroke location B (55-kA current). It follows from Fig. 2 that the induced voltage magnitudes are larger and the risetimes are longer in the presence of corona discharge on the horizontal wire. This trend agrees with that reported in [3] and [4], although the increase predicted by our full-wave model (up to 5%) is less significant than in their studies based on the circuit-theory approach (up to a factor of 2).

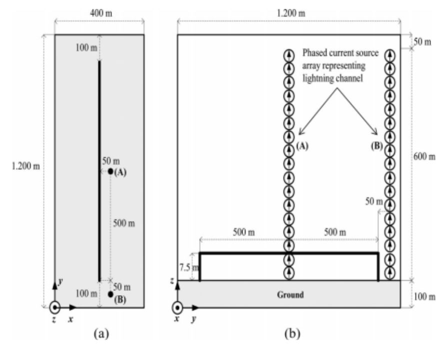

Figure 1. Plan and side views of a 5-mm radius, 1-km long overhead horizontal wire located 7.5-m above the ground.

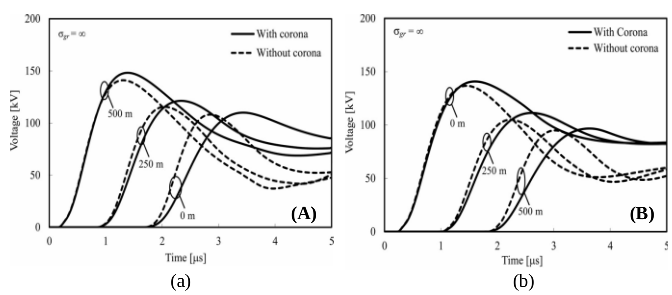

Figure 2. FDTD-computed waveforms of induced voltages at different points along the wire. The computations were performed for perfectly conducting ground with (a) stroke location A (y = 500 m) and (b) stroke location B (near y = 0 m).

References

[1] T. H. Thang, Y. Baba, N. Nagaoka, A. Ametani, J. Takami, S. Okabe, and V. A. Rakov, "A simplified model of corona discharge on overhead wire for FDTD computations," IEEE Trans. Electromagnetic Compatibility, vol. 54, no. 3, pp. 585-593, 2012.

[2] T. H. Thang, Y. Baba, N. Nagaoka, A. Ametani, J. Takami, S. Okabe, and V. A. Rakov, "FDTD simulation of lightning surges on overhead wires in the presence of corona discharge," IEEE Trans. Electromagnetic Compatibility, vol. 54, no. 6, pp. 1234-1243, 2012.

[3] C.A. Nucci, S. Guerrieri, M. T. Correia de Barros, and F. Rachidi, "Influence of corona on the voltages induced by nearby lightning on overhead distribution lines", IEEE Trans. Power Delivery, vol. 15, no. 4, pp.1265-1273, 2000.

[4] G. Dragan, G. Florea, C. A. Nucci, and M. Paolone, "On the influence of corona on lightning-induced overvoltages", Paper presented at 30th International Conference on Lightning Protection, Cagliali, Italy, 2010.

ID 006

IEMI AC Harmonic Vulnerability of Small External Power Supplies

Edward Savage#1, William Radasky#2, and Michael Madrid
Metatech Corporation
358 S. Fairview Ave., Suite E, Goleta, CA 93117-3601, USA
[1] savagee@cox.net
[2] wradasky@aol.com

***Abstract*—A typical IEMI attack on a facility would involve high frequency (or fast transients) high-level radiative or conductive assaults resulting in transients entering equipment on their attached cabling. However, another possible attack uses low frequency and low levels – introducing harmonics onto the AC power system. Such an attack, if possible, has some differences from high-frequency attacks, including that it is less erratic – just as for the AC power itself, any low frequency signal introduced on the AC wiring will appear essentially undiminished at all attached equipment. In this paper we report on tests performed to determine the response of common low voltage power supplies when their AC power feed is distorted by various types and levels of harmonic distortion. It is found that switched mode power supplies are immune to such attacks, but rectifier type supplies are very susceptible, if the harmonic distortion is not symmetrical.**

Keywords— harmonics, wall warts, small power supplies, switched mode power supplies

I. Introduction

Many low power electrical devices are powered by (or their internal battery charged by) "wall warts". These are small converters that typically plug directly into an AC outlet (hence their colloquial name), and put out a low voltage level (typical DC) via a cable, which plugs into the equipment and supplies its power. Older such supplies typically consist of a transformer-rectifier circuit, while newer ones are more likely to use switched mode power supply (SMPS) circuitry (Fig. 1). In our tests we looked at many samples of both types of supplies, introducing various forms of harmonic distortion, and stepping up the distortion level, trying to find damage levels. The basic results were that the rectifier types of units were easily and consistently fully damaged, while the SMPS types could not be damaged.

Figure 1. Samples of wall wart power supplies.

Rectifier Type	SMPS Type
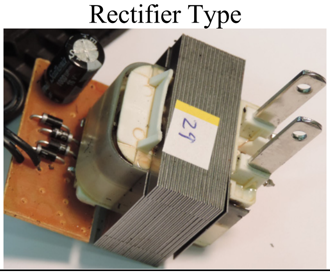	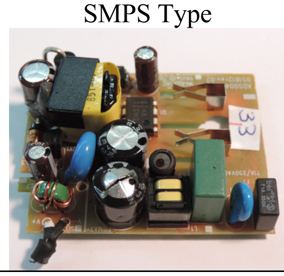

II. Test Setup and Procedures

The basis for our tests was a Schaffner NSG 1007-5-208-413 AC Power Source (harmonic generator). The generator provided the AC power to the test sample, which was loaded on its output side by a 50 Ω resistor. Measurements were made of the input and output waveforms, along with the DC output voltage. We also recorded the case temperature of the test sample. For harmonic distortion we only used single harmonics – either 2nd or 3rd harmonic. For either, the waveform shape varied with harmonic phase. We also did tests with added DC (zeroth harmonic). Each test point (selection of harmonic number, phase, and percent distortion level) was applied for five minutes, while we watched to see if the test sample "died". We gradually increased the distortion level in successive test points, in order to determine damage levels. Four test waveforms were selected, two using 2nd harmonic and two with 3rd harmonic. Three of these waveforms had polarity symmetry – for a given waveform the negative peaks were the same as the positive peaks, while one was asymmetrical, with the negative peaks twice the amplitude of the positive peaks. Additional tests used DC offsets, which also had the effect of producing an asymmetrical waveform.

III. Test Results

Four of the test samples were of the SMPS type (more are to be tested), and these were very hard to damage. (One did die, at the very extremes of our test conditions, in which the AC waveform had peaks of 644 volts, with almost 100% distortion of a 230 V_{RMS} AC fundamental power feed.) Besides this one unit that died at our highest test levels, the devices all easily survived the worse distortion available from the test generator – almost 100% distortion, or up to 70 volts added DC. These devices also did not show the temperature effects noted with the rectifier supplies.

However, our 16 samples of rectifier type supplies were very different – we completely damaged every unit. For symmetrical waveforms, however, the units did not show any adverse effects, up to almost 100% distortion. But with asymmetrical distortion, they died (the transformer primary windings opened) at low distortion levels – typically at a few tens of percent distortion. They also similarly died at added DC levels of a few tens of volts. For both damage modes the units also had extreme temperature increases.

Design Aspects of a RS-105 Facility Using a Conical Transmission Line

D. V. Giri
Dept. of ECE, Univ of New Mexico
Albuquerque, NM, USA and Pro-Tech,
11-C Orchard Ct, Alamo, CA 94507-1541,
USA Giri@DVGiri.com

Tae Heon Jang
EMC Technology Center , Korea Testing Laboratory,
516 Haean-ro, Sa-dong, Sangnok-gu, Ansan-si,
Gyeonggi-do, South Korea 326-901
jhjang@ktl.re.kr

***Abstract*— This paper describes the design, fabrication and preliminary measurements of a facility in Seoul, South Korea to meet the Radiated Susceptibility Standard RS 105. This facility is under development. This facility will be used for susceptibility testing of electronic equipment.**

Key Words - Transient pulse, RS-101, EMP, susceptibility testing

I. Introduction

This facility has been called KEMPS and the goal is to produce the RS-105 compliant e-field environment and the facility is schematically shown in Figure 1.

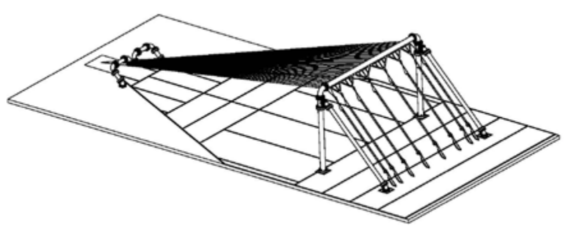

Figure 1. Schematic diagram

The pulser exciting the facility is manufactured by EMC Montena of Switzerland and the model number is EMP 230K-2-23 which is designed to work into a load of 100 Ohms.
The facility is designed for a TEM impedance of 100 Ohms with the overall dimensions of: length l = 18.5 m, maximum height b = 3.71 m and the full width of the top plate 2a = 5.98 m . This makes (l/b) = 4.98 and (b/a) = 1.240 resulting in ~ 100 Ohms to match the pulse generator. The top plate is formed by stretching stainless steel wires. Two catenaries' supports are required, to support and maintain the tension in the wires. Stainless steel wires have been routinely used to prevent corrosion problems and they have adequate electrical conductivity. The sag will be held to less than 5% of the span. The ground plane design accounts for the test object loading factor and are made of galvanized steel mesh of varying sizes except in the pulser region, where it is designed to be a solid plate. A portion of the ground plane is formed by solid plates for test object movement.

II. Spherical TEM Mode Calculations

A spherical TEM mode propagates in the conical transmission line and the excitation pulse has frequency components ranging from DC to about 200 MHz. The low frequencies in the pulse are well terminated by the distributed termination at the end of the line and the high frequencies do not see the termination and get radiated out. Some of the intermediate frequencies can leak to the sides of the facility. The spherical TEM mode is depicted in Figure 2. The radial components of the electric and magnetic fields are zero. The principal components are E_θ and H_ϕ. The spherical TEM mode propagation is shown in Figure 2.

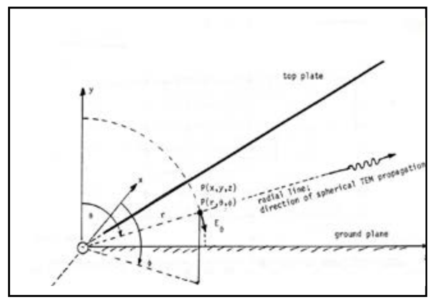

Figure 2. Propagation of spherical TEM mode

III Predicted E-field Levels

The predicted fields in a normalized format are shown in Figure 3 as constant-field contours.

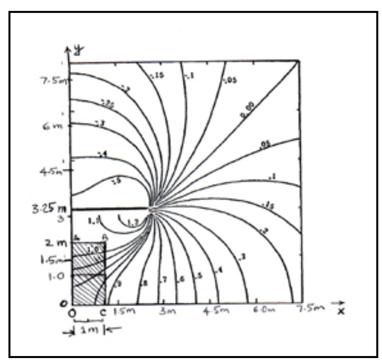

Figure 3. Constant normalized e-field contours in the central plane of the working volume (2m x2mx2m)

The normalized e-field at the center of the working volume is 0.96. The corresponding absolute value for a 230 kV input pulse will be [230kV/3.71m] x 0.96 = 59.5 kV/m. It is noted that since the pulser output is nearly a double exponential, the analysis and results presented here are applicable at any instant of time t during the pulser waveform, in a relative sense. In other words, at every t during the pulser waveform, TEM waveform is propagating. In the frequency domain, the results presented are valid from dc up to a frequency where a non-TEM mode comes in with appreciable amplitude. Details of analyses and preliminary measurements will be presented.

Waveform Averaging and EMP Extrapolation

William D. Prather
Air Force Research Laboratory
Directed Energy Directorate
Kirtland AFB NM, USA
willliam.d.prather@ieee.org

Jory Cafferky
TEAM Technologies, Inc.
EME Programs
Albuquerque NM
jcafferky@team-technologies.com

***Abstract*—The final step in processing measured EMP data on a test object is to extrapolate it to an EMP standard as described in [1]. The extrapolation corrects for simulator inadequacies in amplitude, spectral density, and planarity. Many test programs have used only Type 2 (single point) extrapolation. However, it will be shown in this paper that the use of Type 3A extrapolation, where the data is spatially averaged over the working volume, offers significant improvements in the results.**
Keywords-EMP, CW, waveform averaging, extrapolation

I. Introduction

To estimate the coupling of EMP to an aircraft or other test object, the measured data must be extrapolated to a standard EMP waveform as described in [1]. This is done to correct for simulator inadequacies in field amplitude, spectrum, and uniformity. Many test programs have used only Type 2 (single point) extrapolation. However, it will be shown in this paper that Type 3A extrapolation (where the data is spatially averaged over the working volume) offers significant improvements in the results for both horizontally and vertically polarized simulations.

There are several steps in the extrapolation process.

1. Measure the principal components of E and H across the working volume, with phase.
2. Remove the ground reflection from each measurement using (E + H)/2.
3. Average the results across the working volume.
4. Normalize the cable current measurements to the averaged field value and multiply by the EMP standard.

If the field pattern in the CW and pulse illuminations are uniform, and the CW radiated spectrum is flat, the final CW and pulse results will compare very well. Examples are shown in the paper.

II. Waveform Averaging

A. Horizontal Polarization. For an overhead incident, horizontally polarized wave, there will be a large ground reflection that must be removed.

B. Vertical Polarization. Vertically polarized fields also reflect off of support poles and trailers, causing notches in the field map spectra at every test point. However, these notches are spatially dispersed – they occur at a different frequency at each point in space due to differences in travel time between the arrival of the incident and reflected fields. Therefore, when the measurements are averaged, they will disappear. These notches do not appear in the internal cable current measurements, because the test object responds only to the average field.

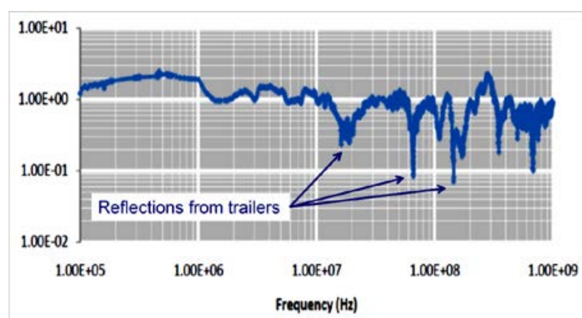

Fig. 1. Measured electric field at one point in space showing the appearance of the spatially dispersed notches.

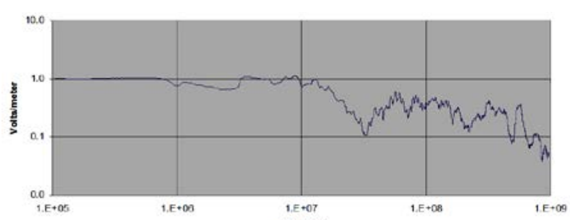

Fig. 2. Averaging 5 TP reduces or eliminates these notches.

References

[1] C.E. Baum, "Extrapolation Techniques for Interpreting the Results of Tests in EMP Simulators in Terms of EMP Criteria," Sensor & Simulation Note 222, AFWL, Kirtland AFB NM, March 1977.

This work was sponsored by the Defense Threat Reduction Agency, Oklahoma City Air Logistics Center, and the Navy Surface Warfare Center at Dahlgren.

A Self-monitored Information System for High Power Electromagnetic Attacks Detection

Chaouki Kasmi[1]*, José Lopes-Esteves[1] and Mathieu Renard[2]
Wireless Security Lab[1], Hardware and Software Security Lab[2]
French Network and Information Security Agency
Paris, France
*chaouki.kasmi@ssi.gouv.fr

***Abstract*—The trend in society is to integrate more and more electronic devices in critical infrastructures which make them more vulnerable to high power electromagnetic attacks. Many studies were devoted to the analysis and the detection of electromagnetic attacks against critical electronic systems. In almost all cases, detection devices are additional hardware devices which need to be placed inside the facility. A new approach, considering the target itself as a sensor, is proposed to detect HPEM attacks.**

Keywords-component; HPEM attacks; HPEM detection; Forensic;

I. Introduction

During the last decades, high power electromagnetic (HPEM) attack [1] against critical systems has become a topic of high interest. The protection from and the detection of such threats becomes of fundamental interest in order to prevent either service disruptions or physical damages. Many studies were devoted to the analysis [2-3] and the detection [4-5] of electromagnetic attacks against electronic systems. Generally, detection devices are additional hardware systems [4-5] which need to be placed inside the facility. In this abstract, it will be shown that the target itself can be naturally used as a sensor and that the statistical analysis of recorded information can be used for HPEM-attacks detection.

II. Fault Detectors

The information system, a computer in what follows, possesses several interfaces (peripherals, communication links) and internal sensors (temperature sensor), as summarized in Table 1, that can be used to monitor any trouble that may occur during its use. The wireless interfaces, known as *front-door* coupling interfaces, can be used to monitor the noise floor, the signal to noise ratio and the received power of the surrounding electromagnetic environment.

Additional parameters can be monitored on the computer using the general commands provided by manufacturers such as CPU load, motherboard sensors status, memory faults or software crashes can provide, when properly correlated, a reliable HPEM-attacks detector system. Mouse deflection errors on a computer running a Microsoft Windows operating system have been reported [5] during immunity testing. In order to obtain further details, we decided to work on a Linux distribution which allows getting deeper in the kernel system logs.

TABLE I. Information available on a computer

	Detectors	**Information available**
Communication interfaces	2G/3G, NFC, PLC WI-FI, Bluetooth	noise floor signal to noise ratio bit error rate received power data rate
	Ethernet	
Hardware	CPU Memories	fault analysis load temperature
Software	Operating system	software crashes
	Drivers	

III. Online Detection and Forensic

The collected data can be analysed in real time or stored, either locally or remotely. Alert messages can be provided to the user of the computer. Moreover, if a computer is physically damaged, a forensic analysis can be applied by extracting and analyzing the collected data in order to estimate if the computer has been hit by HPEM-attacks.

Furthermore, the wide deployment of such software in a large IT-network can lead to the design of a distributed agent mesh which allows increasing the efficiency of HPEM-attacks detection.

During the presentation the test results from HPEM-attacks against a monitored computer will be presented. It will be shown how the proposed method provides a low-cost built-in reliable way to detect HPEM-attacks and their effects on a target.

References

[1] W. A. Radasky, C. E. Baum and M. W. Wik, "Introduction to the special issue on high-power electromagnetics and intentional electromagnetic interference," Electromagnetic Compatibility, IEEE Transactions on, vol.46, no. 3, pp. 314-321, Aug. 2004.

[2] J. Mirschberger, F. Sonnemann, J. Urban and R. H. Stark, "High-Power Electromagnetic effects on Distributed and Automotive CAN-bus systems", In Proc. of EUROEM 2012, pp. 85, July, 2012

[3] M. G. Bäckström and K. G. Lövstrand, "Susceptibility of electronic systems to high-power microwaves: Summary of test experience," IEEE Trans. Electromagn. Compat., vol. 46, no. 3, 2004.

[4] A. Kreth, O. Doering. E. Genender and H. Garbe, "Predetection for the identification of electromagnetic attacks against airports", In Proc. of EUROEM 2012, pp. 81, July, 2012.

[5] R. Hoad, L. Sutherland, "The Forensic Utility of Detecting Disruptive Electromagnetic Interference", In Proc. of the 6th European Conference on I-Warfare and Security, pp. 77-87, July, 2007.

Russian National Primary Standard Facility for realization of lightning impulse current unit

K.Yu. Sakharov, V.A. Turkin, O.V. Mikheev, A.V. Sukhov
All-Russian Research Institute for Optical and Physical Measurements (VNIIOFI)
Moscow, Russia
m12@vniiofi.ru

***Abstract* – The description of the National Primary Standard Facility of lightning impulse current unit, its operation principles and the results of its experimental characterization are presented. The current pulses in the amplitude range from 1 to 100 kA with minimal rise time 140 ns are generated in the standard facility. The expanded uncertainty of the realization of the lightning impulse current unit (*P* = 0.99) is no more than 2.6%.**

Keywords – lightning, impulse current, standard facility, calibration

I. Introduction

It is important to monitor a waveform (amplitude and time characteristics) of the current pulses generated in the simulators during lightning immunity testing of the aerospace vehicles, power systems and communication devices. There are different types of the measuring instruments (MI) used for this purpose (EM 8.4.5 and EM 8.4.6 in accordance with BIMP classification). The development of the standard facility of lightning impulse current solved the problem of calibration of such MI [1].

II. The Standard Facility Construction

The lightning impulse current waveform is normalized in the standards. The amplitude of component A is 200 kA with the rise time $t_R \approx$ 2-5 μs (according to various sources, for example [1, 2]). Consequently the reference current pulses for the MI calibration must have the rise time no more than t_R = 2/3 ≈ ≈ 0.7 μs at the amplitude I_A of order 100 kA (since usually the MI dynamic range is more than 2). These statements formed the basis of the standard facility development.

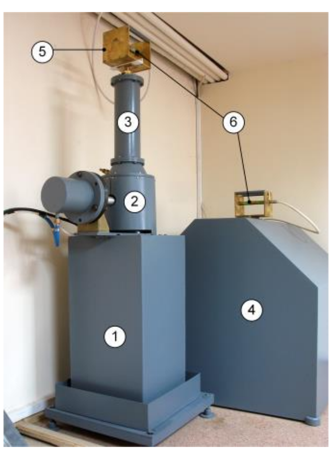

Figure 1. Standard facility for realization of lightning impulse current unit

The standard facility includes the following devices (Fig.1): high-voltage pulse generator (HVPG) consisting of the capacitive storage *1*, high-voltage gas-filled gap *2* and the unit of the discharge resistance *3*; single-turn high impulse current transformer *4*; output terminals *5* and current shunts *6*. Noninductive coaxial shunts are made of the manganin foil and they are used for the determination of the generated pulse waveform parameters.

There are two operating modes in the standard facility. In the first mode the capacitive storage is directly discharged on the output terminals. At the same time the small amplitude current pulse with the short rise time is generated to determine the transient response rise time of calibrated MI. In the second mode the storage discharges through the high impulse current transformer and the current pulse with the amplitude up to 100 kA is generated to determine the conversion ratio of the MI.

III. Facility Characterization Results

The results of standard facility experimental characterization are presented in table 1. The typical oscillograms of the current pulses generated in the standard facility are presented on the Fig. 2 (the voltage-current re-calculation has been made taking into account the shunt conversion ratios).

TABLE I. Metrological Characteristics of the Standard Facility

Op. mode	Amplitude I_A, kA	Rise time t_R, μs	Duration t_P, μs
I	1.0÷8.0	0.14÷0.4	10÷12
II	6.0÷100	9.2÷10.0	35÷36

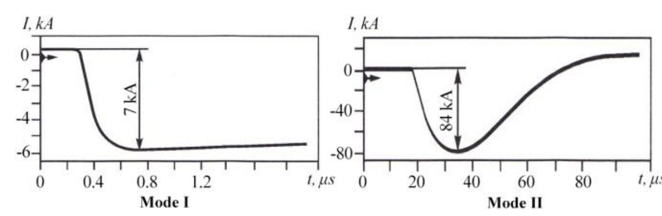

Figure 2. The typical oscillograms of the generated current pulses

The expanded uncertainty of the realization of the lightning impulse current unit (P = 0.99) is no more than 2.6%

References

[1] Gamerota, W.R. et al. "Current Waveforms for Lightning Simulation", Electromagnetic Compatibility, IEEE Transactions on, pp. 235-238, Vol. 54, Issue 4, Aug. 2012
[2] Aviation Rules AP-25. Interstate Aviation Committee. OAO "Aviaizdat", 2004.
[3] K.Yu. Sakharov, V.A. Turkin, O.V. Mikheev, A.V. Sukhov. National Primary Standard of lightning pulse current unit at the range from 1 up to 100 kA // Measurement Techniques, 56, No 11, 1203-1208 (2014)

Lightning Characteristics Analysis of Grounding Devices by Modified Partial Element Equivalent Circuit Method

Jinliang He, Jinpeng Wu, and Bo Zhang
State Key Lab of Power Systems, Department of Electrical Engineering
Tsinghua University
Beijing, 100084, China
hejl@tsinghua.edu.cn

***Abstract*—This paper proposes a time-domain method for the lightning transient performance of the grounding device. Based on the partial element equivalent circuit method, it considers the frequency-dependence in the time-domain, and refers to the alternating direction implicit difference scheme for the unconditionally stable solution.**

Keywords- grounding; partial element equivalent circuit (PEEC); time-domain; frequency-dependent; lightning.

I. INTRODUCTION

The lightning transient characteristic of the grounding device plays an important role in the lightning protection [1]. For evaluating and analyzing, simulation is a very effective approach. There are several kinds of methods such as the transmission line method, the finite-different time-domain method, the method of moment and the PEEC method. Compared with the former three, PEEC gives consideration to both efficiency and accuracy [2].

In this paper, a modified PEEC method is proposed with following characteristic: a) bases on the electromagnetic quasi-static (EMQS) hypothesis and time-domain analysis; b) considers the frequency-dependence, as well as the multi-layer soil and the mutual coupling; c) refers the ADI difference scheme for the unconditionally stable solution.

II. GENERAL PRINCIPLE OF METHOD

Firstly, for conductors buried in the lossy ground, the node voltages $\boldsymbol{V}$ and the branch currents $\boldsymbol{I}$ are arranged alternatively, $\boldsymbol{V}$ are located at the nodes, and $\boldsymbol{I}$ are located at the middle of the branches. Then, the EMQS equivalent circuit is established in the frequency domain, which considers the frequency-dependence, as well as the multi-layer soil and the mutual coupling.

$$\begin{cases} \boldsymbol{Y}_r * \boldsymbol{V} - \boldsymbol{A}\boldsymbol{I} = \boldsymbol{I}_s \\ \boldsymbol{Z}_a * \boldsymbol{I} + \boldsymbol{A}^T \boldsymbol{V} = 0 \end{cases} \tag{1}$$

where $\boldsymbol{I}_s$ is the current source vector, $\boldsymbol{A}$ is the incidence matrix, $\boldsymbol{Y}_r$ and $\boldsymbol{Z}_a$ are respectively the admittance and the impedance, which are full matrixes. By the vector fitting method [4], each of the frequency-dependent elements can be approximated as a rational function in the complex frequency (s) domain:

$$\begin{cases} \boldsymbol{Y}_r = \boldsymbol{s}\boldsymbol{C}_r + \boldsymbol{G}_r + \sum_{q=1}^{Q_r}\left[\boldsymbol{k}_r^q \big/ \left(\boldsymbol{s} + \boldsymbol{p}_r^q\right)\right] \\ \boldsymbol{Z}_a = \boldsymbol{s}\boldsymbol{L}_a + \boldsymbol{R}_a + \sum_{q=1}^{Q_a}\left[\boldsymbol{k}_a^q \big/ \left(\boldsymbol{s} + \boldsymbol{p}_a^q\right)\right] \end{cases} \tag{2}$$

Then, by the inverse Laplace transformation, (1) can be transferred from the frequency domain into the time domain as:

$$\begin{cases} \boldsymbol{C}_r\, d\boldsymbol{v}/dt + \boldsymbol{G}_r \boldsymbol{v} + \boldsymbol{B}_r - \boldsymbol{A}\boldsymbol{i} = \boldsymbol{i}_s \\ \boldsymbol{L}_a\, d\boldsymbol{i}/dt + \boldsymbol{R}_a \boldsymbol{i} + \boldsymbol{B}_a + \boldsymbol{A}^T \boldsymbol{v} = 0 \end{cases} \tag{3}$$

where $\boldsymbol{B}_r$ and $\boldsymbol{B}_a$ are the infinite integral items resulted, and can be calculated by the recursive convolution method [3].

Lastly, by the ADI difference scheme [4], one traditional time step is split into two sub-time steps as (4) and (5). Then, the implicit and explicit difference schemes are respectively applied.

$$\begin{cases} \boldsymbol{C}_r \dfrac{\boldsymbol{v}^{n+1/2} - \boldsymbol{v}^n}{\Delta t/2} + \boldsymbol{G}_r \dfrac{\boldsymbol{v}^{n+1/2} + \boldsymbol{v}^n}{2} + \boldsymbol{B}_r - \boldsymbol{A}\boldsymbol{i}^{n+1/2} = \dfrac{\boldsymbol{i}_s^{n+1} + 3\boldsymbol{i}_s^n}{4} \\ \boldsymbol{A}^T \boldsymbol{v}^{n+1/2} + \boldsymbol{L}_a \dfrac{\boldsymbol{i}^{n+1/2} - \boldsymbol{i}^n}{\Delta t/2} + \boldsymbol{R}_a \dfrac{\boldsymbol{i}^{n+1/2} + \boldsymbol{i}^n}{2} + \boldsymbol{B}_a = 0 \end{cases} \tag{4}$$

$$\begin{cases} \boldsymbol{C}_r \dfrac{\boldsymbol{v}^{n+1} - \boldsymbol{v}^{n+1/2}}{\Delta t/2} + \boldsymbol{G}_r \dfrac{\boldsymbol{v}^{n+1} + \boldsymbol{v}^{n+1/2}}{2} + \boldsymbol{B}_r - \boldsymbol{A}\boldsymbol{i}^{n+1/2} = \dfrac{3\boldsymbol{i}_s^{n+1} + \boldsymbol{i}_s^n}{4} \\ \boldsymbol{A}^T \boldsymbol{v}^{n+1/2} + \boldsymbol{L}_a \dfrac{\boldsymbol{i}^{n+1} - \boldsymbol{i}^{n+1/2}}{\Delta t/2} + \boldsymbol{R}_a \dfrac{\boldsymbol{i}^{n+1} + \boldsymbol{i}^{n+1/2}}{2} + \boldsymbol{B}_a = 0 \end{cases} \tag{5}$$

III. VALIDATION AND CONCLUSION

A typical tower footing device, shown in Fig.1, is tested and simulated by the proposed method. It can be seen that they have quite a good agreement.

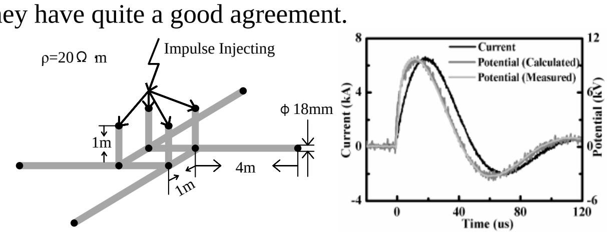

Fig. 1. The validation model and the results

REFERENCES

[1] J. L. He, R. Zeng, and B. Zhang, "Methodology and Technology for Power System Grounding," *Wiley*, 2012.

[2] S. C. Wang, "Time-domain simulation of small thin-wire structures above and buried in lossy ground using generalized modified mesh current method," *IEEE Trans. Power Del.*, vol.26, no.1, pp. 369-377, 2011.

[3] T. B. Lu, et al., "Effect of multilayer soil on the switching transient in substations," *IEEE Trans. Magn.*, vol.42, no.4, pp. 843-846, 2006.

[4] Kantartzis, N.V., et al., "An unconditionally stable higher order ADI-FDTD technique for the dispersionless analysis of generalized 3-D EMC structures," *IEEE Trans. Magn*, 2004. 40(2): p. 1436-1439.

Supported by the National Natural Science Foundation of China under Grant No. 51277107.

ID 013

Radiated Power Calculations for Open TEM-Waveguides

Application of Transmission-Line Super Theory to a Wire Based System

Ronald Rambousky
Electromagnetic Effects and HPEM Branch
Bundeswehr Research Institute (WIS)
29633 Munster, Germany
ronald.rambousky@ieee.org

Heyno Garbe
Institute of Electrical Engineering and
Measurement Technology
Leibniz University Hannover
30167 Hannover, Germany

***Abstract*— Open wire based TEM-waveguides can mathematically be described by an advanced transmission-line theory which involves intrinsically radiation effects. The radiated power is calculated directly from the complex, position and frequency dependent parameter matrix and the potential and current distribution on the wires. The calculated radiated power is compared to emission measurements in a reverberation chamber and good agreement is achieved.**

TEM-Waveguide; Advanced Transmission-Line Theory; Electromagnetic Radiation

I. Introduction

TEM-waveguides are widely accepted for qualification testing in EMC. They provide a dominant TEM electromagnetic wave in the designated test volume. Closed TEM-waveguides, as for example GTEM cells, intrinsically produce higher order field modes above cut-off frequencies. This modal behavior can be analytically described by generalized, but classical multi-conductor transmission-line theory. For open TEM-waveguides radiated electromagnetic energy must be taken into account. Therefore, it is necessary to use an advanced transmission-line theory to describe the electromagnetic field in the waveguide and the radiated power. For a conical wire based TEM-waveguide (like a NEMP simulator) Transmission-Line Super Theory (TLST) was used to calculate the radiated power [1]. For this case the TEM-waveguide can be handled as a nonuniform multi-conductor transmission-line. The theoretical results were compared to power emission measurements in a reverberation chamber.

II. Transmission-Line Super Theory

TLST [2] is a full wave description of Maxwell's equations cast into the form of telegrapher's equations of classical transmission-line theory.

$$\frac{\partial}{\partial \zeta}\begin{bmatrix}\varphi(\zeta,f)\\ \mathbf{i}(\zeta,f)\end{bmatrix} + j\omega\overline{\mathbf{P}}^{*(1)}(\zeta,f)\begin{bmatrix}\varphi(\zeta,f)\\ \mathbf{i}(\zeta,f)\end{bmatrix} = \begin{bmatrix}\mathbf{0}\\ \mathbf{0}\end{bmatrix} \qquad (1)$$

Eq. (1) shows the TLST equation for a nonuniform N-wire system parameterized according a common parameter ζ, describing normalized arc lengths, with excitation only at the ends of the lines. The parameter matrix $\overline{\mathbf{P}}^{*(1)}$ must be evaluated using an iterative process [3]. The matrix elements are now position and frequency dependent complex values. The radiated power can be calculated from the TLST parameter matrix and the potential and current values on the wires of the multi-wire transmission-line system which are available after solving the coupled first order ODE with the appropriate boundary conditions for exciting sources and loads (see Fig. 1).

III. Experimental Validation

Reverberation chambers are very well suited for emission measurements of electronic systems because of their nearly isotropic field distribution. Radiated power measurements on the wire models of an open TEM-waveguide fit very well to the TLST calculations. In our experiments the radiated power calculations using TLST were validated to measurements for the first time [4].

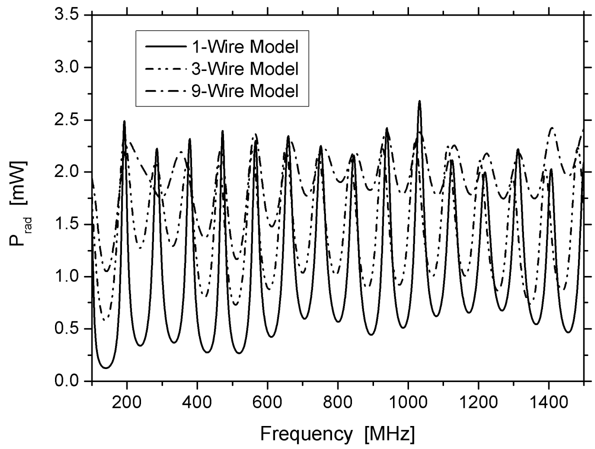

Figure 1. TLST calculated radiated power for open wire based TEM-waveguides made of 1, 3 or 9 wires.

References

[1] R. Rambousky, "Analyse der Feldeigenschaften in offenen TEM-Wellenleitern mit Methoden einer erweiterten Leitungstheorie", PhD thesis, Leibniz University Hannover, accepted, Jan 2014

[2] J. Nitsch, F. Gronwald, and G. Wollenberg, „Radiating Nonuniform Transmission-Line Systems and the Partial Element Equivalent Circuit Method", J. Wiley & Sons Ltd., 2009

[3] R. Rambousky, J. Nitsch, and H. Garbe, „Application of Transmission-Line Super Theory to Multiwire TEM-Waveguide Structures, IEEE Trans. Electromagn. Compat., 55(6):1311-1319, 2009

[4] R. Rambousky, H. Garbe, and H.G. Krauthäuser, „Cross-Validation of Transmission-Line Super Theory Radiated Power Calculations With Measurements for Open Waveguide Structures", 2013 IEEE International Symposium on EMC, 751-756, Denver, Colorado, 2013

ID 014

Fiber-Optic Sensor: A New Tool for Lightning Current Measurement

Truong X. Nguyen, Jay J. Ely and George N. Szatkowski
NASA Langley Research Center
Hampton, VA 23681-0001, U.S.A.
truong.x.nguyen@nasa.gov

***Abstract*— A fiber-optic current sensor is developed for measuring aircraft in-flight lightning current. It is based on Faraday Effect, which causes light polarization in a fiber to rotate when the fiber is exposed to a magnetic field. Advantages include the abilities to measure total enclosed lightning current and to conform to structure geometry. The sensor is capable of measuring 300 A – 300 KA, a 60 dB range. This paper reports test results of lighting direct and in-direct effect current amplitudes. Potential applications extend beyond aircraft and lightning uses.**

Keywords - lightning; Faraday Effect; fiber-optic; current;

I. INTRODUCTION

Sensors used in previous efforts to measure in-flight lightning current suffered from installation issues or inability to directly measure total currents. A fiber-optic current sensor was developed that addressed these concerns for in-flight measurements. When installed around structures of interest the sensor can measure the total current enclosed by the optical fiber sensing loop, much like a Rogowski coil. However, it is self-integrating, and can measure DC current. The fiber is light weight, flexible, and conformable to arbitrary structure shapes. It does not suffer from hysteresis and saturation like current transformers. Being non-conductive, the sensing fiber can be safely routed directly into the aircraft fuselage, eliminating the need for optical converters. Applications are not limited to aircraft and lightning.

II. SENSOR CONCEPT AND TEST RESULTS

Faraday Effect causes light polarization in the sensing fiber to rotate when exposed to an external magnetic field in the direction of light propagation [1,2]

$$\phi = V\int \boldsymbol{B}\cdot dl = \mu_0 V\int \boldsymbol{H}\cdot dl \qquad (1)$$

where ϕ is the polarization rotation angle in radians, V is the Verdet constant, **B** is the magnetic flux density, **H** is magnetic field, and l is length. Forming N fiber loops and applying Ampere's law result in ϕ being directly proportional to the total current enclosed I (Eq. 2). Thus, I can be determined by determining ϕ.

$$\phi = \mu_0 V\oint_N \boldsymbol{H}\cdot dl = \mu_0 VNI \qquad (2)$$

Fig. 1 illustrates a polarimetric detection scheme to determine the rotation angle ϕ. The optical scheme uses a 1310nm wideband laser, a spun highly birefringent sensing fiber [2], a reflective scheme with a Faraday mirror, and a dual-detectors setup for common-mode noise subtraction. Measurement range from 300 A to 300 kA was achieved, a 60 dB range [3].

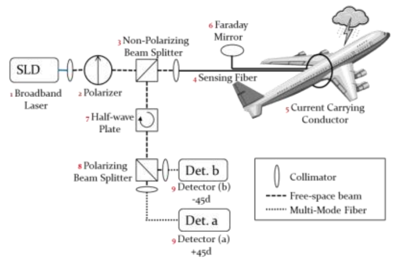

Figure 1. Optical detection scheme.

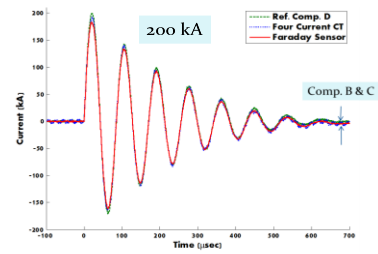

Figure 2. 200 kA current test.

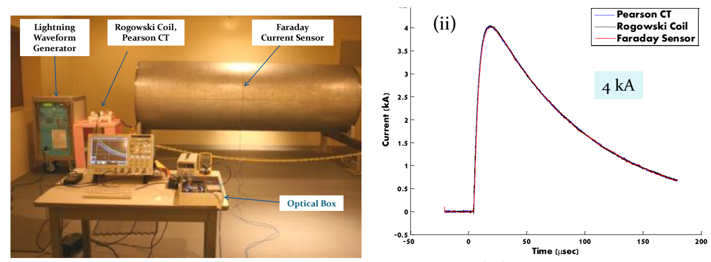

Figure 3. Measurement on a simulated aircraft fuselage.

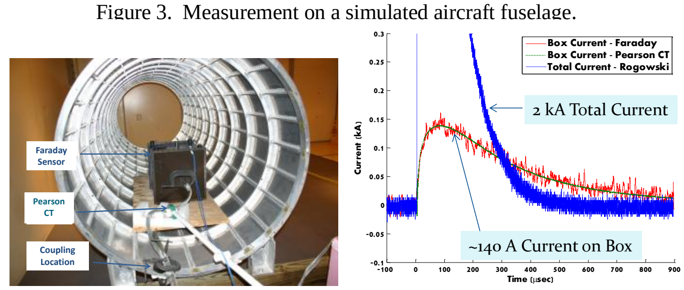

Figure 4. Low level measurement on an internal structure.

A number of tests were performed with good results. Fig. 2 illustrates a 200 kA peak current test at a commercial lightning test facility. Reasonably good results were achieved despite an imperfect setup due to installation limitations. Fig. 3 illustrates measurement on a simulated aircraft fuselage. The peak current was 4 kA, limited by the laboratory test equipment used. Fig. 4 demonstrates excellent isolation for low current measurement on an internal structure (simulating equipment or wire bundles) in the presence of a significantly larger current on the outer aluminum structure. Sensors of the same design also successfully measured triggered lightning [3] with excellent result comparisons though data are not reported here.

III. REFERENCES

[1] J. M. Lopez-Higuera, Editor. Handbook of Optical Fibre Sensing Technology, 2002; Sections 27.2 - 27.4.

[2] R. Laming and D. Payne, "Electric Current Sensors Employing Spun Highly Birefringent Optical Fibers," Journal of Lightwave Technology, Dec. 1989.

[3] T. Nguyen, J. Ely, G. Szatkowski, C. Mata, A. Mata, G. Snyder, "An Intrinsic Fiber-Optic Sensor for Structure Lightning Current Measurement," 2014 Int. Lightning Detection Conference (ILDC).

Electromagnetic Security: Risks Management Improvement using Statistics

Robert L. Gardner, Consultant
6152 Manchester Park Alexandria,
VA 22310, USA
Robert.L.Gardner@verizon.net

Chaouki Kasmi*, Muriel Darces and Marc Hélier
Sorbonne Universités
UPMC Univ Paris 06, UR2, L2E,
F-75005, Paris, France
*chaouki.kasmi@ssi.gouv.fr

Abstract—**The hardening of critical infrastructures against threats of intentional electromagnetic interference is mandatory in order to improve their *safety* and *security*. We propose in this paper to demonstrate how the extreme value statistics can be involved in risks management procedures for the estimation of appropriate protections thanks to the evaluation of a safe margin.**

Keywords-component: Electromagnetic security; Risk management; Extreme Values statistics;

I. Context

Intentional electromagnetic interference (IEMI) poses unacceptable risks for the security and safety of critical infrastructures. The hardening of these structures has been enhanced thanks to risk management procedures. In the same time, the complexity of systems and networks imposes to lay aside experimental tests for a combined use of simulation tools and statistics [1]. The use of models imposes to take into account the uncertainty and the variability of input modeling parameters. This has been achieved by the introduction of stochastic methods, such as the Monte-Carlo approach, which allows estimating the variability of a physical quantity under study.

In *Electromagnetic Compatibility* studies, the *Gaussian* model (computation of the mean and variance of the physical quantity under study) is mainly applied, even if it is known for failing in accurately modeling the probability of *outliers*. We propose to highlight the benefit of extreme value statistics [2] for an accurate design of protective devices.

II. Vulnerabilities and Protections Analysis

The risk has been formulated [3] as a function of the *Exposure* of the target, its *Vulnerability* and its *Criticality* as follows:

$$Risk = \alpha\{Exposure, Vulnerability, Criticality\}$$

Based on the estimated risk, additional protective devices should be inserted in the infrastructure.

In order to define the appropriate protection line (*PL*), it is necessary to estimate accurately the following parameters [4]:

- *Threat Level* (TL), provided by standards;
- *Immunity level* (IL) of the device to be protected;
- *Safe margin* (SM) in order to introduce the parameters uncertainty and variability.

As soon as we focus on the *security* and *safety* of critical system, it is necessary to manage the *worst-case* scenario (as depicted in Fig. 1) where the tails of distributions overlap. It has been shown [2] that the extreme values statistic, and more specifically the *excess model*, is a well-founded methodology for the analysis of highly improbable events.

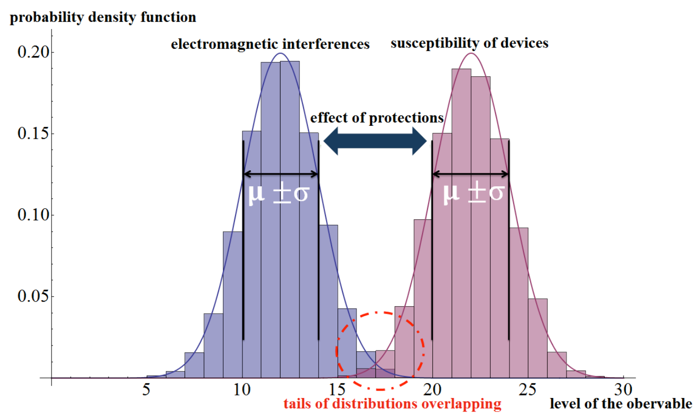

Figure 1. Probability density function of IEMI vs. Device susceptibility

By adjusting the extreme values thanks to the generalized *Pareto* distribution [2], the TL, IL and SM levels can be computed for a given probability.

III. Risks Management

During the presentation, it will be demonstrated how we can capitalize on the prediction of the extreme values statistics of the devices immunity (IL), IEMI level (TL) and protections performance for the design of appropriate protective systems (SM).

References

[1] R. L. Gardner and Christopher W. Jones, "System Lethality: Perspective on High Power Microwaves", System Design and Assessment Note 34, July, 1995.

[2] C. Kasmi, M. Darces, M. Hélier, and E. Prouff, "Generalised Pareto distribution for extreme value modelling in electromagnetic compatibility", Electronics Letters, Vol. 49, pp. 334–335, 2013.

[3] E. F. Vance, "The Relation of Cost to Evaluation and Monitoring of Electromagnetic Protection", System Design and Assessment Note, Note 33, January, 1994.

[4] A. W. Kaelin and M. Nyffler, "Pass/Fail Criteria for HPEM-Protection devices", Proc. Of EUROEM 2012, pp. 89, Toulouse, France, July, 2012.

Shielding Effectiveness research due to antenna polarization characteristic

Ho-Jae Kang, Chang-Su Huh
INHA University
Electrical Engineering
Incheon, Republic of Korea
ghwo1028@nate.com

Woo-Chul Park
KTR
EMP Department
Yongin, Republic of Korea

Sun-Mook Hwang
Hanwha
Gumi, Republic of Korea

***Abstract*— Internationally, Weapons based on EMP are rapidly developed. Meaning of EMP is abbreviation of Electromagnetic pulse. And generally, This meaning is high power electromagnetic wave. But, In the academic world, accurate representation of EMP is HPEM(High power Electromagnetic). And to minimize influence of HEMP, the shielding facility including high shielding effectiveness(SE) is being manufactured. when designing shielding facility, required units like vent, waveguide, shielding door should be included in the shielding facility. The PoEs generating by these units can drop performance of shielding facility. In this paper, To analyze these factors, After artificial the PoEs are installed, we are compared with shielding effectiveness according to vertical and horizontal polarization of antenna. And the operational frequency is 10k~1GHz defined to MIL-STD-188-125-1. But applied antenna according to frequency is different. So, we apply Loop antenna in the 10k ~ 20MHz and biconical antenna in the 20M ~ 100MHz, Log Periodic(LP) antenna in the 100M ~ 1GHz. And As defined to MIL-STD-188-125-1, the position of transmitting antenna is 2.05m away from the shielding wall. Likewise, The position of receiving antenna is 1.00m away from the shielding wall. Used the shielding room has shielding effectiveness more than 90dB. The size of shielding room is 2.4m × 6m × 2.4m. Configuration units of the shielding room are one shielding door, one filter, one waveguide. And we measure electric field strength according to shape of PoE. After we are compared with shielding effectiveness of shielding facility and shielding effectiveness of no shielding facility electric field strength, we calculate shielding effectiveness.**

Keywords- PoE(Point of Entry), Shielding Effectiveness, Antenna, Shielding facility, Electric field strength

I. INTRODUCTION

Currently, the Shielding facilities to block various high-power pulse weapons or electromagnetic wave are manufactured. And, the shielding effectiveness as index to evaluate these facilities is being used. So, After we establish position of antenna and frequency scope applying the standard, the experiment is conducted and we calculate shielding effectiveness(SE).

II. MAIN SUBJECT

In this experiment, we manufacture 1×100 ㎟ slot in the shielding room having shielding effectiveness(SE) more than 90dB. And we measure the shielding effectiveness of the shielding room according to antenna radiation characteristic. Also, In the frequency scope 10k~1GH,we arrange Loop, Biconical, Log Periodic(LP) antenna

Figure 1. Shielding room and PoE(Point of Entry)

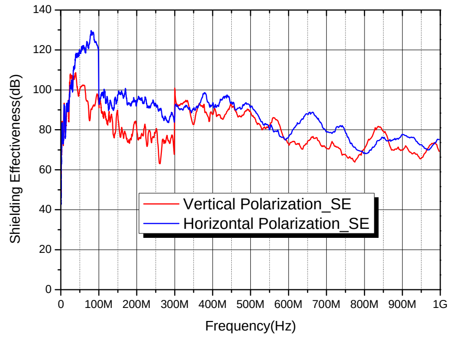

Figure 2. Shielding effectiveness comparison

In lower frequency, shielding effectiveness between horizontal and vertical polarization is almost same. But, In high frequency scope 10MHz~ 300MHz, the shielding effectiveness difference is more than 40dB.

III. CONCLUSION

Through the experiment, the shielding effectiveness of antenna's vertical and horizontal polarization about horizontal shape slot are different[1]. So, we can know the fact that plane wave of antenna according to shape of PoE is differently propagated.

REFERENCE

[1] Lee S, Sung C, Kim E, You S, Lee J, Park D. Shielding Effectiveness of Metallic Enclosure with a Rectangular Slit Aperture. KIEES. 2012;23:652-659

Equipment and Methodology for Destructive High-Power Microwave Testing

Tomas Hurtig, Mose Akyuz, Mattias Elfsberg, Anders Larsson and Sten E Nyholm
Division of Defence & Security, Systems and Technology
FOI – Swedish Defence Research Agency
Norra Sorunda, Sweden
tomas.hurtig@foi.se

***Abstract*— FOI is establishing a facility for destructive HPM testing and is developing an envisaged test methodology for such tests. The methodology consists of two test phases: (1) Determine the lowest power density required to destroy an object within a frequency range, using a reverberation chamber. (2) At this frequency, determine the most sensitive direction of attack using an HPM generator. A reverberation chamber and an HPM-generator adequate for such tests are also presented.**

Keywords- Destructive testing, High-Power Microwave (HPM), Reverberation chamber, Vircator

I. INTRODUCTION

High-power electromagnetic radiation has not only the potential to upset electronics; it may also be used for physically destroying electronic components. The development of HPEM devices has reached a sufficient maturity to form a real threat in this respect, at least in the military context [1]. General mitigation techniques include low-level tests, which can be performed since the system responses are linear. However, when studying destructive effects, the system response becomes non-linear and scaling from low-level tests will not be possible. To be able to perform tests in the destructive, non-linear regime, FOI is developing a relevant test methodology and appropriate facilities.

II. TEST METHODOLOGY

In general, susceptibility testing of electronic equipment is demanding since the electromagnetic coupling into an object is strongly dependent on frequency, polarization and direction of incidence [2]. Thus, during an HPM test, the device under test (DUT) must be irradiated in a broad frequency interval (at least the S-band, 2-4 GHz), in many directions and with at least two polarizations. Destructive HPM testing of electronic equipment requires that the DUT is subjected to very high power densities, usually on the order of several 100 kW/m^2, or over 10 kV/m [3].

The proposed test method consists of the following two test phases:

- First, the DUT is tested in a reverberating chamber (RC) where the minimum power density required to destroy the DUT is established and at which frequency this occur.
- Second, the DUT is tested for its most sensitive direction of attack and polarization using a frequency-tuned HPM generator.

To realize this test method a designated RC and HPM generator must be developed. These are described in the following two sections.

III. DESCRIPTION OF SYSTEM

A. Reverberation Chamber

The RC was designed and delivered by Siepel and has a working volume of 0.72 x 0.56 x 0.4 m^3 and a lowest usable frequency (LUF) of 1 GHz. The time constant of the chamber is below 400 ns and the normalized E-field according to DO-160 varies between 300 V/m and 400 V/m in the frequency range between 1 GHz and 6 GHz [4]. At the time of writing the chamber is powered by a 5 kW pulsed S-band amplifier enabling electric field strengths up to about 25 kV/m in an empty chamber. The 400 ns time constant enables pulsed testing down to about 2 µs according to DO-160, shorter pulses requires loading of the chamber to reduce the time constant.

B. High-Power Microwave Generator

The HPM-source is a modified version of a coaxial virtual cathode oscillator, vircator that will generate a TE_{11} mode in a cylindrical waveguide connected to a medium gain horn antenna [5]. This system can produce a power density on the order of 10 MW/m^2 over an area of a few square decimeters where the far field of the antenna begins. For testing at a lower power density objects are simply moved further away from the antenna. The polarization is changed by rotating the cathode so that the direction of electron emission and hence the polarization of the TE_{11} mode is changed. This simplifies testing of large objects that can be difficult to rotate around the axis of the propagation vector of the radiation in order to facilitate testing at different polarizations.

REFERENCES

[1] M. Gunzinger and Ch. Dougherty, “Changing the game: The promise of directed-energy weapons”, Center for Strategic and Budgetary Assessments, USA, 2012

[2] M. Bäckström and K. Lövstrand, “Susceptibility of Electronic Systems to High-Power Microwaves: Summary of Test Experience”, IEEE Transactions on Electromagnetic Compatibility, vol. 46, pp 396-403, 2004

[3] M. Bäckström, B. Nordström and K. G. Lövstrand, “Is HPM a threat against civil society?”, XXVII General assembly of the International Union of Radio Science, Maastricht Exhibition and Congress Centre, Netherlands, August 17-24, 2002

[4] RTCA, “Environmental Conditions and Test Procedures for Airborne Equipment”, Document number DO-160F, Issue date 12/6/2007

[5] C. Möller, M. Elfsberg, T. Hurtig, A. Larsson and S. E. Nyholm, “Proof of principle experiments on direct generation of the TE11 mode in a Coaxial Vircator”, IEEE Transactions on Plasma Science, Vol 38, pp 26-31, 2010

Trends in Narrowband High Power Microwaves

Edl Schamiloglu

Department of Electrical and Computer Engineering, University of New Mexico
Albuquerque, NM 87131-0001, USA
edls@unm.edu

***Abstract*— Narrowband high power microwave (HPM) sources are coherent hypoband sources of electromagnetic radiation that have been under development for nearly 50 years. Such sources are intense, high perveance, relativistic electron beam-driven vacuum electron devices that follow a power-frequency scaling governed by Pf^2. This presentation reviews historical developments, describes the present state-of-the-art in the field, and suggests recent trends that are shaping the future direction in this field.**

Keywords-high power microwaves, hypoband sources, pulsed power

I. Introduction

Narrowband HPM sources [1,2] are hypoband coherent sources of electromagnetic radiation that have been under development for nearly 50 years. These sources are an outgrowth of the development of modern pulsed power [3]. Such sources are intense, high perveance, relativistic electron beam-driven vacuum electron devices that follow a power-frequency scaling governed by Pf^2 (power times frequency squared). The frequency range over which HPM sources are researched range from <1 GHz – 1 THz.

II. Historical Overview

HPM sources began to appear in the mid-to-late 1960's (see [4] for more details). They have two lines of genesis, one in the United States and one in the Soviet Union. The availability of high-current pulsed power accelerators led researchers, primarily plasma physicists, to revisit conventional electron beam-driven source concepts except this time using high-perveance electron beams. Plasma physicists led this line of research because these high-perveance relativistic electron beams have strong space charge fields, and plasma physicists are those who best understand particle-wave interactions under such extreme conditions, Fig. 1.

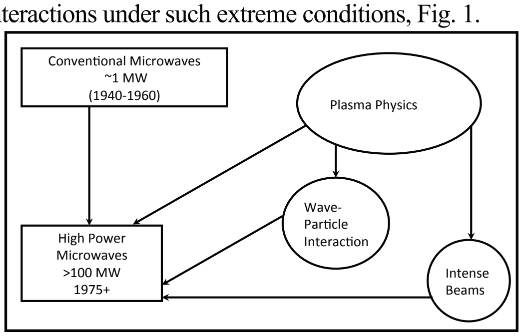

Figure 1. Plasma physicists dominated the development of HPM sources because of their understanding of particle-wave interaction when space charge is dominant [2].

Research supported by AFOSR MURI Grant FA9550-12-1-0489, AFOSR Grant FA9550-11-1-0200.

A. *The Early Years – The HPM Power Derby*

The early years (1960's to 1991) were dominated by a power derby between researchers in the United States and the Soviet Union. This was the era of big machines, exemplified by the Aurora machine at Harry Diamond Laboratories (Army Research Laboratory, Adelphi, MD) and the Gamma machine at the Institute of High Current Electronics, Tomsk, Soviet Union.

B. *Pulse Shortening and Virtual Prototyping*

The HPM power derby came to an end by the mid-1990's. At the time the goal of source researchers was 1 kJ of output energy. This was beyond what was achievable. Inevitably, plasmas generated within the electrodynamic interaction region limited the output pulse duration and pulse repetition rate.

At about the same time, virtual prototyping emerged as a revolutionary tool for designing HPM sources [5]. Prior to the early-mid 1990's experimentalists tinkered; modeling and simulation attempted to match experimental results. Absolute agreement was poor. Today, no metal will be cut until simulation demonstrates optimal performance! Particle-in-cell (PIC) codes have altered the paradigm of HPM source design.

III. Recent Trends

The recent trends in the field are summarized in bullet form below.

- Multi-spectral sources
- Phase-coherent sources
- Metamaterial and metamaterial-like slow wave structures.

Multi-spectral sources pertains to single HPM sources that can concurrently generate two or more frequencies. Phase-coherent sources pertains to recent advances in driving two (N) or more sources using the same pulsed power driver. The phase coherence required to achieve an N^2 scaling in peak output power is <25°. Finally, metamaterials have recently been extensively studied for their use as slow wave structures in HPM sources [6]. This research frontier is at its nascent stage.

References

[1] R.J. Barker and E. Schamiloglu, *High Power Microwave Sources and Technologies* (IEEE Press/John Wiley and Sons, New York, NY, 2001).

[2] J. Benford, J. Swegle, and E. Schamiloglu, *High Power Microwaves, 2nd Ed.* (Taylor and Francis, Boca Raton, FL, 2007).

[3] E. Schamiloglu, R.J. Barker, M. Gundersen, and A.A. Neuber, "Modern Pulsed Power: Charlie Martin and Beyond," (Invited Paper), *Proceedings of the IEEE*, vol. 92, 1014-1020 (2004).

[4] C.E. Baum, "Reminiscences of High-Power Electromagnetics," *IEEE Trans. EMC,* vol. 49, pp. 211-218 (2007).

[5] J.W. Luginsland *et al.,* "Computational Techniques," Chap. 11 in [1].

[6] http://www.ece.unm.edu/FY12MURI/

Design of a Frequency Tunable 75 GHz Resonant TWT Using Serpentine Waveguides

Mikhail Fuks and Edl Schamiloglu

Department of Electrical and Computer Engineering, University of New Mexico
Albuquerque, NM 87131-0001, USA
fuks@ece.unm.edu

***Abstract*— Conventional sources of sub-millimeter wavelength radiation, such as the TWT and BWO, require very small single mode electrodynamic systems in which propagation of intense electron beams is a very complicated problem. An alternative solution is to use oversized slow wave structures; however, this leads to the necessity of providing single mode interaction. The problem of mode selection in such systems is also very challenging. Above all, such a solution strongly limits the range of frequency tuning. Meanwhile, at present there are several designs of sub-millimeter wavelength sources on the basis of serpentine waveguides [1-3], which are essentially traveling wave tube amplifiers. We consider such sources to generate 75 GHz.**

Keywords-millimeter wave sources, serpentine waveguide, TWT

I. Introduction

Conventional sources of sub-millimeter wavelength radiation, such as the TWT and BWO, require very small single mode electrodynamic systems, in which propagation of intense electron beams is a very complicated problem. Many attempts at building such devices have failed because of beam interception. Meanwhile, at present there are several sub-millimeter wavelength sources on the basis of serpentine waveguides [1-3], which are basically TWT amplifiers. We describe such a source design for 75 GHz.

II. Concept of a 75 GHz Oscillator

A 75 GHz frequency tunable source with kW-level radiation using serpentine rectangular waveguide with wide wall a=3.1 mm, as in the standard WR-12 waveguide that has frequency range 60-90 GHz is described. We intend to achieve frequency tuning from 65-85 GHz using a maximal applied voltage U=25 kV that corresponds to a relative electron velocity β=0.30184. During the minimal half microwave period $\tau=f_{max}/2$=5.882 ps the electrons' path is 0.544 mm. Because of this, we choose for the narrow wall of the waveguide b = 0.5 mm. To travel a distance b = 0.5 mm for the same time τ of interaction in the same phase of the decelerated electric field electrons must change their velocity at different frequencies, which can be achieved by changing the applied voltage (Table 1). Such dependence $f(\beta)$ is likely similar to that in a BWO.

This work supported by RDMR-WSS Redstone Arsenal Contract Phase II STTR A11A-001-0471 via TechFlow Scientific, Albuquerque, New Mexico.

We choose period d of the serpentine waveguide to correspond to central frequency f_0=75 GHz from the condition that electrons will be at the same phase passing through an integer number n of periods, $d=n\beta\lambda$ (here λ is the wavelength of the operating wave). We use a periodic magnetic focusing system to guide the electrons. The minimum thickness of the neodymium ring is about Δ_*=0.8 mm (www.apexmagnets.com); therefore, accounting for the thickness Δ of the waveguide, the serpentine period must be greater than $d>b+2\Delta+\Delta_*$; that is, n = 3, d = 3 mm. The dependence $f(\beta)$ is summarized in Table 1.

TABLE I. Dependence of Frequency on Applied Voltage

f (GHz)	65	75	85
β	0.2167	0.25	0.3018
U (kV)	12.43	16.76	25.0

We choose the diameter of the holes for electron propagation as in [1], $2R_h$ = 0.7 mm. Such holes weakly change the dispersion characteristics of the serpentine rectangular waveguide $h=2\pi/\lambda_w=2\pi/\lambda\beta_{ph}=[(2\pi/\lambda)^2-(\pi/a)^2]^{0.5}$ (here λ_w is the guide wavelength and β_{ph} is the phase velocity related to the light speed of the operating TE_{01}-wave). Above all, we can use data from [1] that shows the current of electrons passing through such a hole is 0.2 A when the applied voltage is 21.5 kV. The length of this waveguide at the one period of the serpentine (from one hole to next) must be $L_d=(2m+1)\lambda_w/2$ (for integer m) in order to provide π phase shift (in this case an electron appears in the next hole in the same phase as in the previous one). Relations for d and L_d provide synchronism of electrons with the electric field. Naturally $L_d>d$. Since $\beta_{ph}=\lambda_w/\lambda$=1.3088, λ_w=5.2353 mm, we find the minimal L_d=13.088 mm (m = 2) that consists of two straight parts with each length 1.832 mm and one bend with radius $d/2$=1.5 mm and length $\pi d=9.425$ mm. The total number of periods will be found by optimizing the output power in computer simulations.

In order to achieve kW-level radiation we plan to place many such serpentine waveguides placed around a given radius, forming a peculiar kind of electrodynamic system, and to use multi-spike cathode. At the opposite end all waveguides extend up to the standard narrow dimension 1.55 mm (after passing electrons through the last hole) and open onto a coaxial transmission line, in which co-phase radiation from the open waveguides excites the symmetric TM_{01}-mode.

References

[1] G. Dohler, D. Gagne, D. Gallagher, and R. Moats, "Serpentine Waveguide TWT," *IEEE Intl. Electron Dev. Meeting* (Washington, DC, Dec. 6-9, 1987), 455-458.

[2] C.D. Joye *et al.,* "Demonstration of a High Power, Wideband 220 GHz Serpentine Waveguide Amplifier Fabricated by UV-LIGA," *Proc. IVEC 2013* (Paris, France, May 21-23, 2103), 1-2.

ID 020

Measurement of the Stochastic Electromagnetic Field Coupling into a Double Wire Transmission Line

Mathias Magdowski, Ihsan Ullah, and Ralf Vick
Chair of Electromagnetic Compatibility, Institute for Medical Engineering
Otto-von-Guericke-University
Magdeburg, Saxony-Anhalt, Germany
Email: mathias.magdowski@ovgu.de

***Abstract*—Measurements of the field coupling to double wire transmission lines have been carried out in a mode-stirred chamber. The coupled voltage at one end of the line was measured by amplitude and phase via a balun for different frequencies and line lengths using an oscilloscope. The other line end was open-circuited. For comparison with simulations, the average field strength was determined using field probes. The measurements were done for different stirrer positions and the results were analyzed statistically.**

***Keywords*—electromagnetic coupling; immunity testing; reverberation chambers; statistical distributions; transmission lines**

I. Introduction

Closed-form formulas for the stochastic field-to-wire coupling [1] were published and shall be experimentally validated.

II. Measurement Setup and Results

The setup is shown in Fig. 1. Eight mechanical line lengths between 10 cm and 150 cm were analyzed. The electrical line lengths were determined from the minima of the input reflection coefficient. The wire diameter was $d_0 = 0.8\,\mathrm{mm}$, the wire separation $2h = 32\,\mathrm{mm}$. According to this the characteristic impedance is $Z_\mathrm{c} = 525.5\,\Omega$ and transmission line theory is valid up to $\approx 3\,\mathrm{GHz}$. The line beginning is terminated with $100\,\Omega$ via the balun, the end is left open. 36 stirrer positions and 801 frequencies between 200 MHz and 1 GHz were measured.

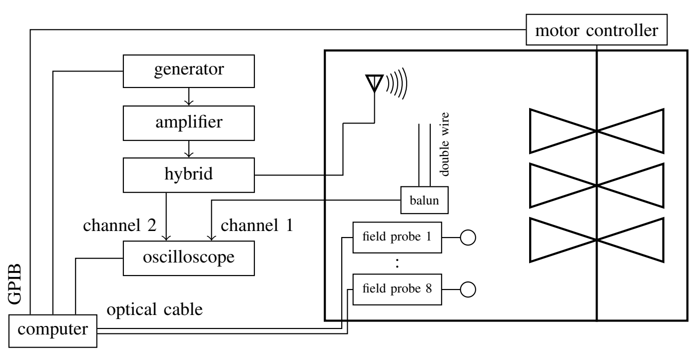

Figure 1. Schematic of the measurement setup in a reverberation chamber.

The average magnitude of the coupled voltage is shown in Fig. 2 as a function of the frequency and in Fig. 3 as a function of the line length. The voltage was normalized to the chamber constant E_0 [2] and h to get a dimensionless quantity. In Fig. 2 the transmission line resonances are clearly visible. In Fig. 3 a critical line length of a quarter of the wavelength is observed, at which the coupling reaches a first maximum. Fig. 4 presents the statistical distribution of the mean normalized voltage magnitude.

For immunity tests especially the distribution of the maximum or rather the maximum-to-average ratio is interesting, which was calculated according to [3]. Here this ratio is ≈ 2.3.

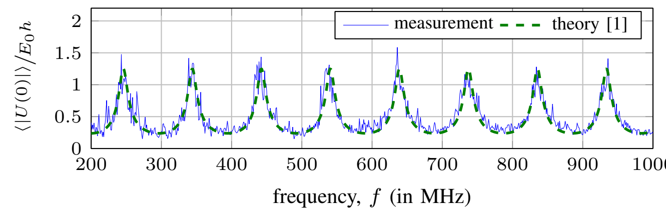

Figure 2. Normalized average magnitude of the coupled voltage at the beginning of the line as a function of the frequency for a line length of 150 cm.

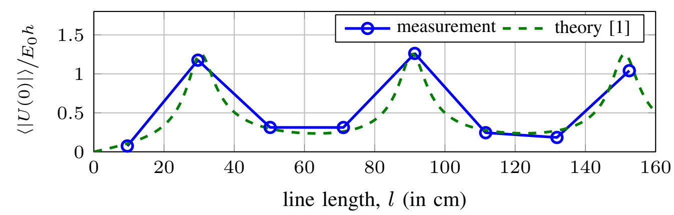

Figure 3. Normalized average magnitude of the coupled voltage at the beginning of the line as a function of the line length at a frequency of 248 MHz.

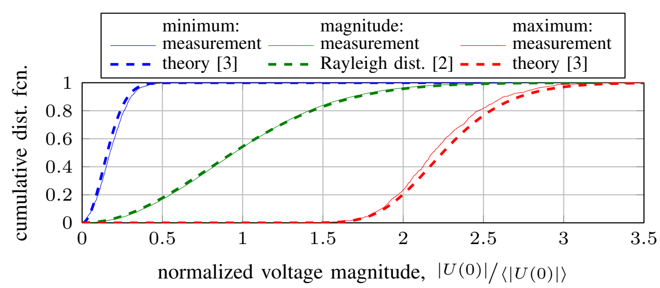

Figure 4. Cumulative distribution function of the magnitude of the coupled voltage at the beginning of the 150 cm long line normalized to the mean value.

III. Conclusion

In general a good agreement between the theoretical and experimental results could be observed.

References

[1] M. Magdowski and R. Vick, "Closed-form formulas for the stochastic electromagnetic field coupling to a transmission line with arbitrary loads," *IEEE Trans. Electromagn. Compat.*, vol. 54, no. 5, pp. 1147 – 1152, Oct. 2012.

[2] D. A. Hill, *Electromagnetic Fields in Cavities: Deterministic and Statistical Theories*, 1st ed., ser. IEEE Press Series on Electromagnetic Wave Theory. Piscataway, NJ: IEEE Press, Oct. 2009, chapter 7.

[3] J. Galambos, *The Asymptotic Theory of Extreme Order Statistics*, 1st ed., ser. Wiley Series in Probability and Statistics – Applied Probability and Statistics Section. New York, USA: Wiley, May 1978.

A New Configuration of Axial Vircator with Reflectors to Maximize the Power Efficiency

S. Champeaux, Ph. Gouard

CEA,DAM, DIF
F-91297 Arpajon, France
stephanie.champeaux@cea.fr

R. Cousin
CST AG
Bad Nauheimer Str. 19
D-64289 Darmstadt, Germany

J. Larour
LPP, Ecole Polytechnique
F-91128 Palaiseau, France

***Abstract*— The classical architecture of an axial Vircator is modified by introducing reflectors in the cylindrical waveguide. Behaviour of this new type of vircator is numerically analyzed using CST particle Studio® PIC 3D simulations. Decreasing reflectors radius is shown to be crucial in maximizing the power conversion efficiency. This new design enables to deliver up to 2 GW output power in S-band on TM_{01} mode only with a total efficiency close to 21%.**

Keywords-component; High power microwave, virtual cathode oscillator, Particle-in-cell, open drift tube

I. Introduction

Virtual cathode oscillators (so-called Vircator designs) are one of the most important classes of High-Power Microwave (HPM) generators. Axial Vircators are rather simple microwave (MW) devices which consist of two parts: a diode responsible for an electron beam emission, followed beyond the anode by a cylindrical waveguide in charge of shaping MW fields. Their operation requires an electron beam current exceeding the space charge limiting current in order that a virtual cathode (VK) builds up beyond the anode at a distance from the real cathode roughly twice the anode-cathode spacing d_{AK}. The electron cloud oscillation, both in location and potential, generates a powerful MW emission. Appreciated for their conceptual simplicity and robustness, Vircators unfortunately exhibit low power conversion efficiency (~ 1%). To overcome this severe drawback, reflectors consisting of thin anodic foils are introduced in the cylindrical waveguide [1].

II. Axial Vircators With Reflectors

The axial Vircator under consideration is designed to operate in S-band, delivering a MW emission in TM_{01} mode. The electrons are emitted from a 4.5 cm radius cathode. Beyond the anode, the beam propagates through a cylindrical waveguide of radius R_G = 7.6 cm. The d_{AK} spacing is equal to 2.1 cm. The applied diode voltage is about 500 kV with a rise time of 5 ns. This design gives an input power of roughly 9.5 GW.

Following [1], 5 reflectors of 6-cm radius are placed in the waveguide. A spacing of 6 cm separates two successive reflectors. Reflectors are thin anodic foils 100 % transparent for the electrons and totally reflecting electromagnetic waves. As a result, a virtual cathode formation process gets duplicated beyond each reflector where MW created by VKs are trapped in pseudo-cavities. The power conversion efficiency is found maximum, roughly 13 %, when 3 reflectors are used. The averaged ouput power is about 1.26 GW and transmitted in the TM_{01} mode at 2.88 GHz (Figure 1). Adding more reflectors in the device weakens performances since the MW emission can also propagate in the TE_{11} mode at 1.4 GHz, creating a mode competition with the TM_{01} mode excited.

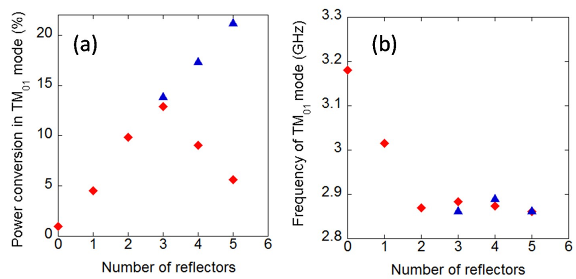

Figure 1. Power conversion efficiency in TM_{01} mode (%) (a) operating frequency in TM_{01} mode (b): comparison between devices with 6-cm constant radius reflectors (red diamonds) and devices with reflectors of decreasing radii (blue triangle).

To further increase the device performances when using more than two reflectors, it is shown that, despite [1], the reflectors radii have to be decreased below the threshold of $0.75R_G$, as claimed in [2]. Following [2], the radii of the third, fourth and fifth reflectors are respectively reduced down to 50, 50 and 40 mm. Figure 1 illustrates the increasing power conversion efficiency while the operating frequency remains roughly unchanged.

III. Conclusion

Compared to conventional axial Vircators, this novel architecture, based on a series of virtual cathodes, located in the center of adjacent pseudo-cavities, achieves higher output powers. A power conversion efficiency up to 21% is obtained with 5 reflectors of decreasing radii, yielding an averaged power of 2 GW at 2.86 GHz in TM_{01} mode only.

References

[1] J.-L. Faure, and Ph. Gouard, "Microwave generating device with oscillating virtual cathode," European patent EP1815492, 2006

[2] S. Champeaux, and Ph. Gouard, "Générateur de microondes à cathode virtuelle oscillante et à réflecteurs ouverts," French patent B120329FRA,2014

The Power Wave Theory of Antennas and Some of its Implications

Everett G Farr

Farr Fields, LC
Albuquerque, NM USA
egfarr@gmail.com

***Abstract*— We introduce here a simple theory of antenna radiation and scattering that fully extends into the time domain a number of standard antenna terms, including gain, realized gain, antenna pattern, beamwidth, scattering cross section, and radar cross section. Power wave theory applies to linear reciprocal antennas of all feed impedances and feed types, including waveguide feeds. We identify receiving and transmitting impulse responses, and prove that they always have a simple relationship to each other. The approach provides a uniquely useful method of characterizing radiation from and coupling into a complex system, using the same parameters in transmission and reception.**

Keywords-power wave theory; antennas; gain; time domain; impulse response

I. INTRODUCTION

We address here the problem of characterizing antenna performance in the time domain. Currently, no standard terms have been defined in the antenna definitions standard [1], which becomes a challenge, for example, when buyers and sellers of wideband antennas need to discuss antenna specifications. In this work, we cast the antenna equations into a particularly simple form. This allows us to very naturally extend into the time domain a collection of commonly used antenna terms, including gain, realized gain, antenna pattern, beamwidth, radar cross section, and scattering cross section. Since complex systems may be considered poor or unintentional antennas, this approach provides a uniquely useful method of describing radiation from and coupling into a complex system. Parts of this paper appeared in [2].

II. ANTENNA IMPULSE RESPONSE

Let us define far-field antenna performance on boresight for dominant polarization using the parameters defined in Figure 1. This resembles a two-port network, in which Port 2 is a virtual port or radiation port. We define a collection of power waves as

$$
\begin{aligned}
\tilde{\Pi}_{src} &= \frac{\tilde{V}_{src}}{\sqrt{Z_{o1}}} && = \text{source power wave} \\
\tilde{\Pi}_{rec} &= \frac{\tilde{V}_{rec}}{\sqrt{Z_{o1}}} && = \text{received power wave} \\
\tilde{\Sigma}_{inc} &= \frac{\tilde{E}_{inc}}{\sqrt{Z_{o2}}} && = \text{incident power flux density wave} \\
\tilde{Y}_{rad} &= \frac{r\,\tilde{E}_{rad}}{\sqrt{Z_{o2}}} e^{\gamma r} && = \text{radiated radiation intensity wave}
\end{aligned}
\quad , \tag{1}
$$

where $\gamma = s/v = jk$, $s = j\omega$, $k = \omega/v = 2\pi f/v$ is the propagation constant in the surrounding medium, and v is the velocity of propagation in the medium. Furthermore, Z_{o1} is the real reference impedance of the input port, Z_{o2} is the real impedance of the surrounding medium, and $\tilde{Z}_{in}$ is the complex impedance looking into the antenna. A tilde indicates a frequency domain quantity. Note that Π, Y, and Σ are Greek versions of P, U, and S, which are commonly used symbols for power, radiation intensity, and power flux density, respectively

With these definitions, we can now define a Generalized Antenna Scattering Matrix (GASM), which is a complete far-field characterization of any linear reciprocal antenna embedded in a lossless medium. First, we treat the special case of dominant polarization on boresight. The antenna equations are expressed compactly as

$$
\begin{bmatrix} \tilde{\Pi}_{rec} \\ \tilde{Y}_{rad} \end{bmatrix} = \begin{bmatrix} \tilde{\Gamma} & \tilde{h} \\ s\,\tilde{h}/(2\pi v) & \tilde{\ell} \end{bmatrix} \begin{bmatrix} \tilde{\Pi}_{src} \\ \tilde{\Sigma}_{inc} \end{bmatrix}, \tag{2}
$$

The proof that these equations are consistent is contained in [5]. In the time domain, this takes the form

$$
\begin{bmatrix} \Pi_{rec}(t) \\ Y_{rad}(t) \end{bmatrix} = \begin{bmatrix} \Gamma(t) & h(t) \\ h'(t)/(2\pi v) & \ell(t) \end{bmatrix} \circ\!\!\!\!\bullet \begin{bmatrix} \Pi_{src}(t) \\ \Sigma_{inc}(t) \end{bmatrix}, \tag{3}
$$

where the "$\circ\!\!\!\!\bullet$" operator is a matrix-product convolution operator. Here, $h(t)$ is the antenna impulse response. This can be extended to both polarizations and to arbitrary angles of incidence and observation, as shown in [2].

With this formulation, one can define a transient antenna pattern and beamwidth with respect to a specified norm in the time domain. Mutual coupling can be defined in antenna arrays. Complex systems may be treated as poor antennas, so they may be described with the same parameters.

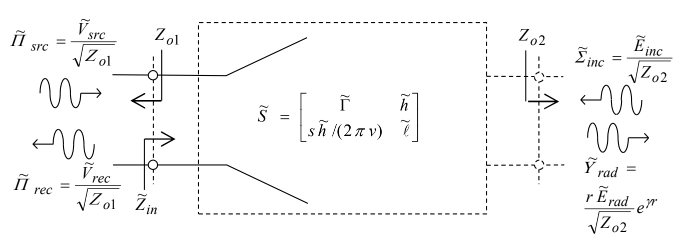

Figure 1. The Generalized Antenna Scattering Matrix (GASM), on boresight, for dominant polarization.

REFERENCES

[1] IEEE, *IEEE Standard Definitions of Terms for Antennas*, IEEE Std. 145-1993, Institute for Electrical and Electronics Engineering, Inc., New York, March 1993.

[2] E. G. Farr, "A Power Wave Theory of Antennas (With Corrections)," Sensor and Simulation Note 564, May 2013.

Response of an Electrical and Communication Raceway to HPEM Transient Field Illumination

N. Mora, C. Romero, F. Vega, F. Rachidi
Electromagnetic Compatibility Laboratory
Swiss Federal Institute of Technology in Lausanne (EPFL)
Lausanne, Switzerland
nicolas.mora@epfl.ch

M. Rubinstein
Institute for Information and Communication Technologies
University of Applied Sciences and Arts Western Switzerland
Yverdon, Switzerland

P. Bertholet, M. Nyffeler
Federal Department of Defence
Armasuisse
Thun, Switzerland

***Abstract*— We present measurements of currents and voltages in power, telephone, and Ethernet cablings of a commercial raceway induced by a transient HPEM field.**

Keywords- IEMI; HPEM; GTEM Cell

I. Introduction

An efficient hardening of infrastructures against intentional electromagnetic interferences (IEMI) requires the characterization of the expected disturbances at the equipment to be protected.

The main objective of the tests reported in this contribution was to characterize the voltages and currents induced by a HPEM transient field inside the power, telephone, and Ethernet cablings of a commercial raceway.

II. Experimental Setup

A 200-cm long test raceway containing several power, network, and telephone cables typical of an office environment was built. Three different types of Ethernet cables were used for the network cabling: Category 7 S/FTP cable (C7), Category 6 SF/UTP cable (C6-S), and Category 6 U/UTP cable (C6-U). Category 5 was not included since most new installations are expected to use category 6 or higher. The raceway was illuminated inside the GTEM Cell of Armasuisse (20 kV/m peak and 100 ps risetime), and induced common mode currents and differential mode voltages in the lines were measured. The measured signals were relayed with a fiberoptic link to a Lecroy SDA1000 oscilloscope located in the measurement cabin outside the GTEM cell. In order to test the effect of having a grazing or parallel E field polarization, the tests were made with the raceway in horizontal or vertical positions.

III. Obtained Data

More than 100 measurements were performed for the induced currents and voltages. Figure 1 shows an example of an induced current waveform measured in the Ethernet C6-S cable. Table I shows the range of the measured peak values of the induced currents and voltages for each type of cabling.

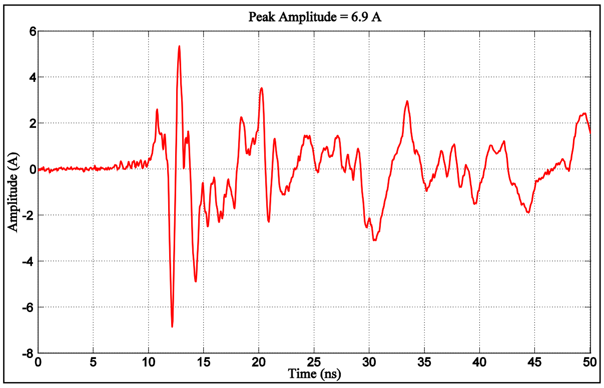

Figure 1. Example of a current waveform measured in the Ethernet C6-S cable.

TABLE I. Measured Range for the Induced Current and Voltage Peaks

Network	Induced Current range (A)	Induced Voltage Range (V)
LV power cabling	2.1-8.5	122-474
Telephone cabling	1.7-9.8	40-298
Ethernet C7 cabling	4-6.8	13-34
Ethernet C6-S cabling	4.4-6.8	10-49
Ethernet C6-U cabling	2.2-5.6	91-107

IV. Conclusions

It is found in general that the effect of the considered disturbances highly depends on the equipment connected to the lines. Ethernet equipment may be compromised due to the low voltage requirements in the communication protocols of network cards. The signals induced in the telephone and power lines are not likely to harm the connected equipment since the induced levels are in the same order of the working levels.

This study is financially supported by the Swisselectric Research and the European Community's 7th Framework Programme under the grant agreement 285257, STRUCTURES (Strategies for the improvement of critical infrastructure resilience to electromagnetic Attacks).

Analysis of the Propagation of High Frequency Disturbances along Low-Voltage Test Raceway

N. Mora[1], C.Kasmi[2,3], F. Rachidi[1], M. Darces[3], M. Hélier[3], M. Rubinstein[4]
[1] EMC Lab, Swiss Federal Institute of Technology in Lausanne (EPFL), Lausanne, Switzerland
[2] Wireless security Lab, French Network and Information Security Agency (ANSSI), Paris, France
[3] Sorbonne Universités, UPMC Univ. Paris 06, UR2, L2E, F-75005, Paris, France
[4] IICT, University of Applied Sciences and Arts Western Switzerland, Yverdon, Switzerland

***Abstract*—The propagation of high frequency disturbances along a low-voltage power mockup is assessed through experiments and numerical simulations with MTL models up to 200MHz.**

Keywords- IEMI; MTL modeling; low-voltage power network

I. Introduction

This paper discusses the experimental and modeling procedures that were used in the assessment of the propagation of high frequency disturbances along a low-voltage power raceway. The transfer functions between the power sockets of the raceway were modeled using (i) CST Cable Studio, and (ii) the CRIPTE code [1] up to 200 MHz.

Preliminary results of this study in which the magnitudes of the transfer functions were measured with a Spectrum Analyzer and validated through MTL models have been presented in [2]. In this work, the validation of the phase measurements is included and the total time domain response is recovered by using an inverse Fourier transform of the transfer functions.

II. Experimental Setup

A schematic diagram illustrating one of the injection tests performed with the low-voltage power raceway is shown in Figure 1. The impulse responses were measured by injecting a rectangular impulse into socket AC1 and measuring the output voltage with an oscilloscope in the other sockets.

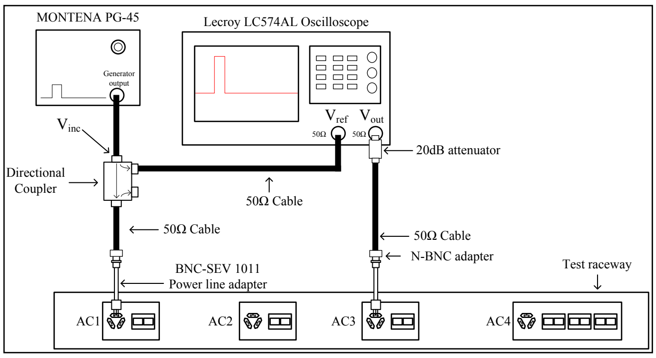

Figure 1. Schematic diagram of the experimental setup.

This study is financially supported by the Swisselectric Research and the European Community's 7th Framework Programme under the grant agreement 285257, STRUCTURES (Strategies for the improvement of critical infrastructure resilience to electromagnetic Attacks).

III. Results

The obtained simulation results are in fair agreement with the experimental data and reproduce the overall characteristics of the measured transfer functions and impulse responses. However, due to the uncertainty of the cable lengths and dielectric parameters of the PVC, the predicted resonance frequencies do not always match with the measured ones.

An example of the impulse response results obtained from measurements and numerical simulations with CRIPTE and CST is presented in Figure 2. Both tools produce waveforms that are in fair agreement with the measured results. It can be seen that the peak voltage predicted by CRIPTE is about 15% lower than that predicted by CST, which matches the experimental value. This discrepancy might be attributed to the presence of a highly non-uniform cabling in the junction box of the raceway that are modeled with approximate cross-sections in both tools. The correct delay between the input and the output waveforms shows that the permittivity of the insulators was correctly chosen.

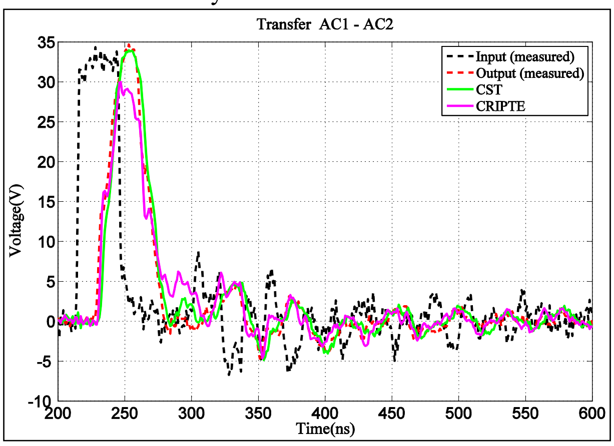

Figure 2. Example of a comparison between the measurement and simulation results obtained with CRIPTE and CST CS.

REFERENCES

[1] P. D. J-P. Parmantier, "Topology Based Modeling of Very Large Systems," in *Modern Radio Science*, O. U. P. J. Hamelin, Ed., ed, 1996, pp. 151-177.

[2] N. Mora, C. Kasmi, F. Rachidi, M. Darces, and M. Helier, "Modeling of the propagation along low voltage power networks for IEMI studies," in *Electromagnetics in Advanced Applications (ICEAA), 2013 International Conference on*, 2013, pp. 436-439.

IEMI Immunity Test Methods for Equipment and Systems

Anthony Wraight, Ministry of Defence, London, England
Mats Bäckström, Saab Aeronautics, Linköping, Sweden
Richard Hoad, QinetiQ, Farnborough, England
William Radasky, Metatech, Goleta, CA, USA
Frank Sabath, WIS, Munster, Germany
Edl Schamiloglu, University of New Mexico, Albuquerque, NM, USA

***Abstract*— This paper describes a standard being developed by the International Electrotechnical Commission (IEC) Sub Committee 77C (SC 77C) concerning test methods for the evaluation of equipment and systems against Intentional Electromagnetic Interference (IEMI) environments.**

Keywords-IEMI; assessment methods; test methods; equipment; systems.

I. INTRODUCTION

The use of electromagnetic sources to generate Intentional Electromagnetic Interference (IEMI) is of increasing concern as the reliance of society on technology increases significantly. Many technical papers have been published that show the effects of IEMI are cause for concern and are summarized in [1]. The effects of IEMI on equipment can be similar to the effects caused by High Power Electromagnetic (HPEM) environments such as High Intensity Radiated Fields (HIRF) generated by Radio and Radar systems, Lightning Electromagnetic (LEMP) fields and Electrostatic Discharge (ESD). Some of these HPEM environments have similar characteristics to those sources used to cause IEMI but are unintentional EMI sources; i.e. non-malicious. However, it is possible to use information regarding qualification of equipment and systems to these environments to inform the likely response to IEMI (i.e. malicious use of EMI sources).

This paper describes a new technical standard being developed by the IEC SC 77C which covers IEMI test methods for electronic equipment and systems. This standard will be published as IEC 61000-4-36 in 2015.

II. INTENTIONAL ELECTROMAGNETIC INTERFERENCE

The IEC defines IEMI within IEC 61000-2-13 [2] as ‘Intentional malicious generation of electromagnetic energy introducing noise or signals into electric and electronic systems, thus disrupting, confusing or damaging these systems for terrorist or criminal purposes’. Within this definition it is possible to also include jammers, which are designed to overload antenna receiver circuits (front doors) by operating at or close to the victim receiver frequency of operation. Jammers typically require low power to operate due to the fact that receivers are designed to operate at very low power levels (nW or less).

III. IEMI TEST LEVEL DERIVATION

IEC 61000-4-36 provides a thorough discussion of IEMI environments and relates these to both capability groups and deployment scenarios (a typical deployment scenario is shown in Figure 1). The capability groups considered include novice, skilled and specialist and the deployment scenario considers IEMI sources varying from those that are man portable to those that are air delivered.

For each capability group, the range of various types of IEMI sources likely to be technically available to the group is discussed along with an estimation of the E-field•range (E•r) product. Further to this, an Example Protection Level (EPL) is defined for a given scenario which allows the user of the standard to choose a total EPL (expressed in dB) taking into consideration range between the source and the victim, path loss and any barrier attenuation. These EPL are then related to test levels applicable for each IEMI source type (Hyperband, Mesoband, Hypoband) along with other important parameters (when relevant) such as rise-time, pulse width, pulse repetition frequency, pulse length, center frequency. Test levels are provided for both radiated and conducted scenarios.

IV. INFORMATIVE ANNEXES

IEC 61000-4-36 includes a number of informative annexes that provides the user with useful information regarding testing electronic equipment and systems against IEMI environments. The annexes include:

- Failure Mechanisms and Performance Criteria
- Developments in IEMI Source Environments
- Interaction with Buildings
- Relation between plane wave immunity testing and immunity testing in a reverberation chamber
- Complex Waveform Injection – Test Method
- Significance of Test Methodology Margins
- Intentional EMI – The Issue of Jammers

REFERENCES

[1] Threat of Electromagnetic Terrorism, Lessons learned from documented IEMI attacks, F Sabath, EUROEM 2012, July 2012, http://www.researchgate.net/publication/230815457_Plenary_Presentation_Threat_of_electromagnetic_terrorism/file/d912f504d9d4f9fa50.pdf

[2] IEC 61000-2-13 Electromagnetic compatibility (EMC) - Part 2-13: Environment - High-power electromagnetic (HPEM) environments - Radiated and conducted

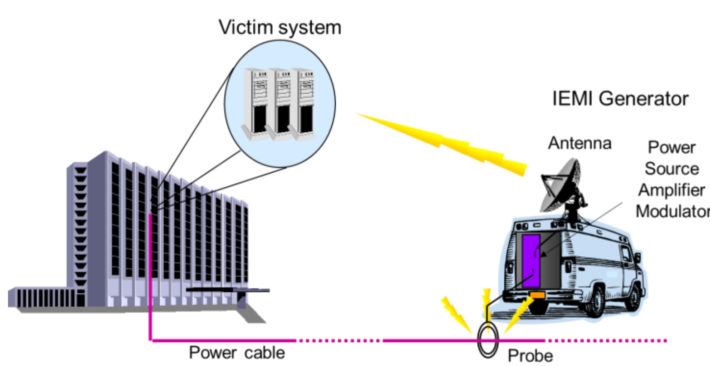

Figure 1. Example of Radiated and Conducted IEMI Interaction with a Building

Microstrip transducer for UWB EMP characterization

K. Yu. Sakharov, V. A. Turkin, O. V. Mikheev, M. I. Dobrotvorsky, A.V. Sukhov
All-Russian Research Institute for Optical and Physical Measurements (VNIIOFI)
Moscow, Russia
m12@vniiofi.ru

***Abstract* – The microstrip transducers for UWB EMP characterization have been described. The microstrip transducers have a step transient response and it means that their output signal replicates the E-field waveform. The rise time of transient response is up to 8 ps at the time window duration of order 3-5 ns.**

***Keywords* – HPEM measurement, microstrip line, E-field, transducer, UWB, EMP**

I. Introduction

In the 1980–90's researchers at VNIIOFI suggested using the microstrip lines for the measurement of EMP waveform parameters. They developed the theory of the microstrip transducers (Russian acronym – IPPL), carried out the experimental investigations and worked out the production technology [1-3]. More than 20 years the Russian leading test laboratories apply the microstrip transducers to determine the EMP waveform parameters in the different HPEM simulators.

II. Design and Characteristics

The incident electromagnetic field excites the traveling TEM-wave propagation along non-symmetrical strip line. The design and external view of IPPL are presented in Fig. 1: the dielectric base *2* with thickness *d* and relative dielectric constant ε > 1 separates the potential electrode *1* and grounded electrode *3* of the microstrip line. The ends of the microstrip line are loaded on the matched impedances $Z_1 = Z_2 = 50$ Ohm.

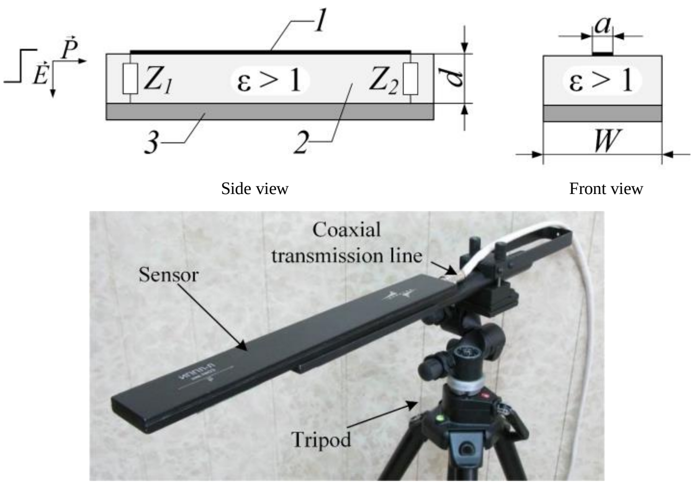

Figure 1. IPPL design and external view

The main advantage of IPPL is its step transient response. This means that *the sensor output signal replicates the waveform of the radiated pulsed electric field*. There is need not an integration of sensor output signal (as in D-dot and B-dot sensors). Consequently, the measurement error decreases and the measurement procedure is essentially simplified.

The signal pick-off is realized from the beginning of the microstrip line and it means that unwanted interference on the coaxial transmission line comes to the recorder after the wanted measuring signal. This solution increases accuracy of measurement. The high-frequency losses in the coaxial line could be compensated with the change of the strip line geometry without the broadband deterioration (for example, with the change of *a* width of the potential electrode in Fig. 1).

The IPPL bandwidth is determined with the *d* fit of the microstrip line. At present the values of rise time of transient response $t_r \approx$ 8-10 ps are reached (pass band upper-frequency F = 35-40 GHz). The t_w time window duration of the transducer is determined with the strip line length and in practice it is 3-5 ns. The oscillograms of step signal recorded by the IPPL are presented in Fig. 2 (the rise time of radiated standard step EMP is t_{rad} = 15 ps [4]). Taking in account rise time of oscilloscope t_{osc} = 7 ps and using root sum of squares approximation, the IPPL's rise time of transient response is

$$t_r = \sqrt{t_f^2 - t_{rad}^2 - t_{osc}^2} = \sqrt{18{,}5^2 - 15^2 - 7^2} = 8{,}3\,\text{ps},$$

where t_f = 18,5 ps is pulse rise time measured by IPPL.

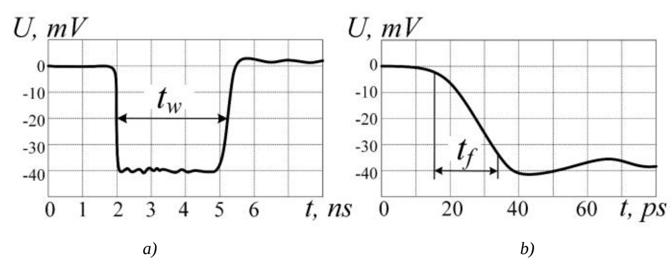

Figure 2. Standard step signal recorded by IPPL:
a) time window, *b)* initial part

The IPPL calibration is realized with the National Primary Special Standard of the unit of electric and magnetic field strength [4].

References

[1] S. A. Podosenov, A. A. Sokolov "Linear Two-Wire Transmission Line Coupling to an External Electromagnetic Field. Part I: Theory", *IEEE Transactions on Electromagnetic Compatibility*, vol. 37, No 4, pp. 559-566, Nov. 1995.

[2] S. A. Podosenov, K. Yu. Sakharov, Ya. G. Svekis, A. A. Sokolov "Linear Two-Wire Transmission Line Coupling to an External Electromagnetic Field. Part II: Specific cases, Experiment", *IEEE Transactions on Electromagnetic Compatibility*, vol. 37, No 4, pp. 566-574, Nov. 1995.

[3] M. I. Dobrotvorsky, K. Yu. Sakharov, V. A. Turkin, A. I. Aleshko, V. N. Dnischenko "Measuring Instruments of Powerful UWB EMP Parameters", *Proc. of Ultrawideband and Ultrashort Impulse Signals, The Third International Conference (Sevastopol, Ukraine)*, pp. 373-375, 2006.

[4] K. Yu. Sakharov, O. V. Mikheev. V. A. Turkin, "National Standard of Russian Federation for reproduction and transmission of unit sizes of pulse electric and magnetic intensities in ultrawide band range", *Proc. of EUROEM-2012 conference (Toulouse, France)*, p. 90, 2012.

Impulse Response and IEMI Susceptibility of Commensurate-Line Filters

Mirjana Stojilović, Marcos Rubinstein
Institute for Information and Communication Technologies
University of Applied Sciences Western Switzerland
Yverdon-les-Bains, Switzerland
mirjana.stojilovic@heig-vd.ch

Antonije Djordjević
School of Electrical Engineering
University of Belgrade
Belgrade, Serbia
edjordja@etf.rs

***Abstract*—In this paper we analyze the relation between the impulse responses of microwave filters with periodic spurious passbands obtained under ideal and realistic conditions. For the latter, we show analytically that increasing the number of passbands taken into account, the impulse response approaches a sequence of delta functions. We conclude that considering the spurious passbands is necessary when evaluating vulnerability to IEMI, because a significant portion of the energy can penetrate into the system through these passbands.**

Keywords-impulse response; microwave filters; spurious passbands

I. Introduction

An exact evaluation of the impulse response (IR) is possible only theoretically, on simplified models of real devices. Under realistic conditions of limited spectrum (or, equivalently, finite duration of excitation pulses) the obtained IR may be inaccurate and may leave out important information. We refer to this IR as quasi-impulse response (QIR). Despite these limitations, the QIR is used in many applications: to evaluate the applicability of microwave filters for radars, in analyzing pulse compression, to eliminate reflections in antenna measurements, etc.

The aim of this paper is to investigate QIR properties for devices whose frequency-domain parameters exhibit a periodic variation, such as commensurate-line filters. In addition to its main passband, such a filter has a sequence of spurious passbands, which are often neglected in computations and measurements. However, they are weak points of any system that uses these filters, as IEMI energy can penetrate the system through the spurious passbands.

The QIR can be evaluated in two ways. One way is to perform computations or measurements in the time domain. The other way is to obtain results in the frequency domain first, and then implement the inverse Fourier transform to obtain the time-domain response. Clearly, the QIR depends on the bandwidth; here we analyze this dependency.

II. Impulse Response

We derive a mathematical relation between the QIR and the exact IR for band-pass filters. To that purpose, we assume a periodic network function $S(f)$ of period f_0. The central frequency of the filter is $f_0/2$. The IR, $s(t)$, is the inverse Fourier transform of $S(f)$ covering the complete spectrum. If, however, we consider only the main passband, we obtain:

$$s_1(t) = \int_{-f_0}^{f_0} S(f)\exp(2\pi \mathrm{j} f t)\,\mathrm{d}f\ . \qquad (1)$$

We refer to the impulse response $s_1(t)$ as the first-order QIR (QIR1). Similarly, by taking n periods of $S(f)$, where $n = 2, 3, \ldots$, we obtain the n-th order QIR (QIRn),

$$s_n(t) = \int_{-nf_0}^{nf_0} S(f)\exp(2\pi \mathrm{j} f t)\,\mathrm{d}f\ . \qquad (2)$$

When $n \to \infty$, $s_n(t)$ yields $s(t)$, which is a sequence of delta impulses. All responses have similar envelopes, but the energy of the response $s_n(t)$ is proportional to n. Therefore, significant IEMI energy can penetrate through the spurious passbands.

III. Experimental Verification

We verify the theoretical predictions on an interdigital filter designed for medium-power UHF TV transmitters. To evaluate the scattering parameters, we perform both modeling and measurements, obtaining excellent agreement of the results. Fig. 1 shows the computed quasi-impulse responses QIR1 and QIR4, which confirm the theoretical predictions.

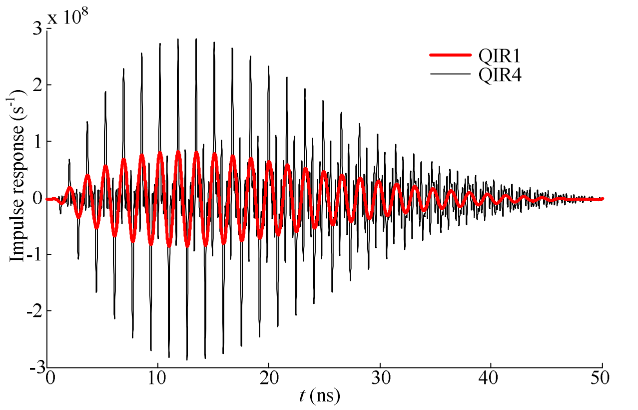

Figure 1. QIR1 and QIR4 for scattering parameter s_{21} of an interdigital filter.

The research leading to these results was supported in part by the Project STRUCTURES, co-funded by the European Union Seventh Framework Programme under grant agreement no. 285257, and by the Serbian Ministry of Education, Science, and Technological Development under grant TR32005.

ID 028

Measurement of Lightning Currents at the Säntis Tower in Switzerland

Mario Paolone[1], Davide Pavanello[2], Farhad Rachidi[3], Marcos Rubinstein[4]

1 Swiss Federal Institute of Technology, DESL, Lausanne, Switzerland, Mario.Paolone@epfl.ch

2 University of Applied Sciences of Western Switzerland, Sion, Switzerland, Davide Pavanello, Davide.Pavanello@hevs.ch

2 Swiss Federal Institute of Technology, EMC Lab., Lausanne, Switzerland, Farhad.Rachidi@epfl.ch

3 University of Applied Sciences of Western Switzerland, IICT, Yverdon, Switzerland, Marcos.Rubinstein@heig-vd.ch

***Abstract*— We describe the instrumentation of the Säntis Tower in Switzerland to measure lightning currents and lightning current derivatives. A summary of the obtained data during the first 18 months of operation is also presented.**

Keywords-lightning; lightning current; instrumented tower; upward discharge; negative lightning; positive lightning; bipolar lightning.

I. THE SÄNTIS TOWER

The 124-m tall Säntis Tower (Fig. 1) is located on the top of Mount Säntis (2502-m above sea level), in the northeast of Switzerland. The tower that serves mainly as a telecommunications tower and a climate station, is by far the most frequently struck structure in Switzerland [1].

Fig. 1 – Säntis Tower

Lightning current waveforms and their time-derivatives are measured at two different heights (24-m and 82-m AGL) using Rogowski coils and multigap B-dot sensors [2]. The analog outputs of the sensors are relayed to a digitizing system by means of optical fiber links. The system allows an over-the-Internet remote maintenance, monitoring and control. More details on the measurements sensors and instrumentation system can be found in [1] and [2].

This work has been carried out within the framework of the European COST Action P18. Financial support from the Swiss Office for Education and Research SER (Project No. C07.0037) and the Swiss National Science Foundation (Projects No. 200021-122457 and 200021_147058) are acknowledged.

In 2013-2014, a certain number of updates were made to the overall measuring system, including the replacement of National Instruments PCI digitizers by PXI systems, and the update of the data acquisition software.

II. OBTAINED DATA

Since the instrumentation of the tower (May 19, 2010) until January 1, 2014, more than 350 flashes were successfully recorded at the Säntis tower. A total of 200 flashes recorded during the first 18 months of operation of the tower were recently analysed [3,4]. All of them were apparently of upward type, including 30 positive flashes.

An example of a current waveform associated with a positive flash is presented in Fig. 2 [4]. The peak current is 93 kA and the transferred charge to ground is about 405 C.

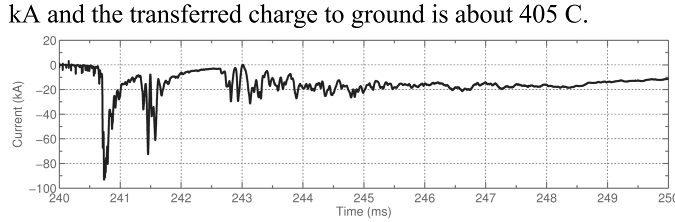

Fig. 2 - Example of a current waveform associated with a positive flash that occurred on August 3, 2011 at 11:51. Adapted from [4].

REFERENCES

[1] C. Romero, M. Paolone, M. Rubinstein, F. Rachidi, A. Rubinstein, G. Diendorfer, W. Schulz, B. Daout, A. Kaelin, P. Zweiacker, "A System for the Measurements of Lightning Currents at the Säntis Tower," *Electric Power System Research Journal,* vol. 82, pp. 34-43, 2012.

[2] C. Romero, A. Mediano, A. Rubinstein, F. Rachidi, M. Rubinstein, A. Paolone, P. Zweiacker, N. Mora, D. Pavanello, and B. Daout, "Measurement of Lightning Currents Using a Combination of Rogowski Coils and B-Dot Sensors," *Journal of Lightning Research,* vol. 4, pp. 71-77, 2012.

[3] C. Romero, F. Rachidi, A. Paolone, and M. Rubinstein, "Statistical Distributions of Lightning Current Parameters Based on the Data Collected at the Säntis Tower in 2010 and 2011," *IEEE Transactions on Power Delivery,* vol. 28, pp. 1804-1812, 2013.

[4] C. Romero, F. Rachidi, M. Rubinstein, M. Paolone, V. A. Rakov, and D. Pavanello, "Positive Lightning Flashes Recorded on the Säntis Tower in 2010 and 2011," *Journal of Geophysical Research,* vol. 118, pp. 12'879-12'892, 2013.

Frequency tunable L-band HPM Coaxial Backward Wave Oscillator

E.M. Totmeninov, I.V. Pegel, V.V. Rostov, R.V. Tsygankov
Siberian Branch, Russian Academy of Sciences
Institute of High Current Electronics, HCEI SB RAS
Tomsk, Russia
totm@lfe.hcei.tsc.ru

***Abstract*— Results are presented of theoretical and experimental investigations L-band relativistic backward wave oscillator based on coaxial waveguide (CRBWO). The possibility was shown in the experiment the oscillator carrier frequency tuning ranging from 1.23 to 1.31 GHz that corresponded to 6 % relative frequency variation at -3 dB level relative to 290-MW microwave peak power maximum within the range.**

Keywords- high power microwave (HPM), backward wave oscillator, modulating reflector, coaxial waveguide

I. Introduction

RBWO based on coaxial slow-wave structure (SWS) is considered as advantageous oscillator for producing high power microwaves pulses in frequency band ranging from 1 to 2 GHz [1]. This oscillator has more small size of its electrodynamic system as well as rather short microwave oscillation transient time [1] in contrast to well-known RBWO based on circular waveguide including cutoff neck [2] or modulating reflector [3]. This paper reports on results concerning the investigation of modified CRBWO the electrodynamic system of which included modulating slot.

II. Designe of Oscillator and Mode Competition Investigation

The design of oscillator consists of tubular explosive emission cathode, quarter-wave modulating slot, SWS based on coaxial waveguide, compact TEM to H_{11} circular waveguide mode convertor and solenoid for transportation electron beam along interaction space. The quarter-wave modulating slot is located at the entrance of SWS in the smooth part of coaxial waveguide. The slot basic functions are backward wave reflection to collector end of the oscillator and electron beam preliminary modulation by z-component of electric field of the TEM-mode in the slot region.

The design of CRBWO electrodynamic system was optimized using the axis symmetric (2.5-D) version of PIC-code KARAT at operation TEM-mode, 300-keV electron energy and about 1-GHz carrier frequency. The results of the simulation are as follows: the oscillator efficiency, the microwave peak power and the carrier frequency were about 30 %, 200 MW and 1.2 GHz, respectively. It was shown that substantial transient time of the oscillations decreasing (down to 20 ns) with respect to usual RBWO [2,3] was caused by increasing coupling resistance between the electron beam and the TEM-wave electromagnetic field synchronous component up to about 10 Ohm.

The mode competition was investigated theoretically. It was shown that start current of non-symmetric TE_{m1}-modes is lower than that one for TEM-mode. Primary excitation of non-symmetric modes was proved in numerical simulation with 3-D version of PIC-code KARAT.

III. Experimental Results

For depressing non-symmetric modes the longitudinal splits were made in the inner conductor of coaxial SWS of oscillator. As a result L-band CRBWO with efficiency of 30 % and peak microwave power of 290 MW was realized in experiment at operation TEM-mode and carrier frequency of 1.23 GHz. The microwave pulse length was about 30 ns. Mechanical fine frequency tuning from 1.23 to 1.31 GHz was shown in the experiment by changing drift distance between modulating slot and SWS.

References

[1] Xingjun Ge, Huihuang Zhong, Jun Zhang, and Baoliang Qian "A high efficient relativistic backward wave oscillator with coaxialnonuniform slow-wave structure and depth-tunable extractor," Phys. of Plasmas. 2013. 20. 023105.

[2] N.F Kovalev, M.I. Petelin, M.D. Raizer, A.V. Smorgonsky, and L.U. Tsopp "Generation of high-power electromagnetic radiation pulses by a relativistic electron flow," Pis'ma Zh. Tekh. Fiz., V. 18, No. 4, pp. 232-235 (1973).

[3] S. D. Korovin, I. K. Kurkan, V. V. Rostov and E.M. Totmeninov "Relativistic Backward Wave Oscillator With a Discrete Resonance Reflector", *Radiophysics and Quantum Electronics*, vol. 42, (no 12), p. 1047-1054, (1999).

Repetitively Pulsed High Power Microwave Cherenkov Oscillators

E.M. Totmeninov, A.V. Gunin, A.I. Klimov, V.V. Rostov
Siberian Branch, Russian Academy of Sciences
Institute of High Current Electronics, HCEI SB RAS
Tomsk, Russia
totm@lfe.hcei.tsc.ru

***Abstract*—Results of experimental investigations are presented of relativistic backward wave oscillators with resonance reflector (RBWO-RR) using external guiding magnetic field as well as Cherenkov microwave oscillators without guiding magnetic field. Both kinds of the oscillators were driven by repetitively pulsed "SINUS" nanosecond electron accelerators.**

Keywords-high power microwave (HPM), backward wave oscillator, resonance reflector, relativistic Cherenkov oscillator, solid cylindrical electron beam, velvet-covered cathode, fiber carbon cathode

I. Introduction

Repetitively pulsed high power microwave oscillators are of the most interest for practical applications It is very important to decrease the total set power consumption devices. One of the ways is decreasing or eliminating power consumption for producing quasi-constant magnetic field guiding electron beam along the oscillator electrodynamic system. The development and investigation of microwave oscillators with tunable output microwave radiation parameters are of interest as well.

II. Oscillators Based on RBWO-RR

X-band RBWO-RR with efficiency of 21 % using guiding magnetic field as low as 0.6 T was investigated in the experiment [1]. At repetition rate of 100 Hz microwave peak power was 0.5 GW with a pulse width of 12 ns. The solenoid power consumption was about 20 kW.

In [2] mechanical pulse-to-pulse fine carrier frequency tuning was obtained of 50-Hz repetitively pulsed S-band RBWO-RR using magnetic field as low as 0.4 T. The frequency tuning bandwidth was of 10 % corresponded to -3 dB level relative to maximum 2.5-GW microwave peak power within the band. Maximum peak efficiency was 20 %.

1 to10-sec batches with 100-Hz pulse repetition rate were produced in experiment with X-band RBWO-RR operated at 0.4-T guiding magnetic field. The oscillator efficiency was about 30 % corresponded to microwave peak power of 0.32 GW. The microwave pulse length was 90 ns.

The experimental model was realized of X-band 100-Hz pulse-periodic oscillator [3] the design of which included two-section solenoid produced ~ 2-T guiding magnetic field. The oscillator microwave peak power was 0.2 GW corresponded to efficiency of 0.25%. Smooth tuning of the output microwave pulse length from 25 to 34 ns was obtained as a result of changing magnetic field lines configuration.

III. Oscillators Based On Cherenkov Microwave Oscillator Without a Guiding Magnetic Field

4-GHz relativistic Cherenkov oscillator without an external magnetic field has been realized operated in repetitively pulsed mode. The electron beam of the oscillator was generated in the diode with velvet-covered [4,5] cathode or fiber carbon cathode.

The oscillator efficiency was 15 % corresponded to about 2.0 GW of microwave peak power at electron energy of 1.1 MeV in a 2-sec batch under 10-Hz repetitively pulsed operation. The lifetime of the velvet-covered cathode was about 3000 pulses.

At 0.5-MeV electron energy in a 2-sec 30-Hz batch mode the oscillator efficiency was 8 % corresponded to microwave peak power of 0.21 GW. The lifetime of the velvet-covered cathode can exceed 11000 pulses and the lifetime of fiber carbon cathode exceeds 100 000 pulses.

References

[1] S.D. Korovin, I.K. Kurkan, V.V. Rostov, et. al., "Relativistic Backward Wave Oscillator With a Discrete Resonance Reflector", *Radiophysics and Quantum Electronics*, vol. 42, no 12, p. 1047-1054, 1999.

[2] E.M. Totmeninov, A.I. Klimov, I.K. Kurkan, S.D. Polevin, V.V. Rostov "Repetitively Pulsed Relativistic BWO With Enchanced Mechanical Tunability," IEEE Trans. Plasma Sci, vol. 36, no. 5 (Part 3), pp. 2609-2612, 2008.

[3] E.M. Totmeninov, A.V. Gunin, A.I. Klimov, V.V. Rostov, A.S. Stepchenko, P.V. Vykhodtsev, A.H. Mahir "X-Band Relativistic BWO-RR With Controlled Microwave Pulse Duration," IEEE Trans. Plasma Sci., vol. 40, no. 6 (Part 1), pp. 1590-1593, 2012.

[4] E.M. Totmeninov; S.A. Kitsanov; P.V. Vykhodtsev "Repetitively Pulsed Relativistic Cherenkov Microwave Oscillator Without a Guiding Magnetic Field," IEEE Trans. Plasma Sci., vol. 39, no. 4 (Part 2), pp. 1150-1153, 2011.

[5] E.M. Totmeninov; S.A. Kitsanov; P.V. Vykhodtsev "Experimental Investigation of the S-band Relativistic Cherenkov Microwave Oscillator without a Guiding Magnetic Field at the Repetitively Pulsed Modes," Proc. 8th Inter. Workshop Strong Microwaves and Terahertz Waves: Sources and Application, Nizhny Novgorod, pp. 134-135, July 2011.

ID 032

Compact High Voltage Pulse Generator Based on Magnetic-Core Tesla Transformer

Jin-Ho Shin
Replex Co., Ltd.
HPEM Application Laboratory
Seoul, Republic of Korea
hpett@replex.co.kr

Dong-Gi Youn
Replex Co., Ltd.
Chief Executive Officer
Seoul, Republic of Korea
ceo@replex.co.kr

Abstract— This paper presents a compact and portable high voltage pulse generator based on magnetic-core Tesla transformer for driving an UWB high power electromagnetic source. In order to optimize the performance of the high voltage pulse generator, a novel open-loop cylindrical magnetic-core using the quad-division lamination structure is proposed and manufactured. The designed high voltage pulse generator using the proposed magnetic core has a battery-powered operation and compact size of 280mm × 150mm in length and diameter, respectively. The high voltage pulse generator can produce a voltage pulse waveform with peak voltage of 450kV, a rise time of 1.5ns, and pulse duration of 2.5ns at the 800V input voltage.

Keywords-component; high power electromagnetics; high voltage pulse generator; Tesla transformer

I. INTRODUCTION

Recently, the vulnerability of electronic devices to high power electromagnetic (HPEM) threats have been studied widely [1]. Ultra-wideband (UWB) HPEM source capable of producing output power in the gigawatts range allows real susceptibility investigation of electronic devices as well as their protection and hardening against HPEM threats [2]. In the future, UWB HPEM source tends to be higher pulse repetition rate, compact and portable size for the efficient testing in a variety of conditions.

The magnetic-core Tesla transformer is suitable for compact size and high repetition rate because it has high efficiency and only one spark-gap switch. The most commonly known generators based on the magnetic-core Tesla transformer are SINUS and RADAN series. In this paper, a novel magnetic-core using the quad-division lamination structure is proposed. The high voltage pulse generator using the proposed magnetic-core is evaluated.

II. Development of High Voltage Pulse Generator Based on Magnetic-core Tesla Transformer

A. Design and Construction of high voltage pulse generator

Table I lists electrical parameters of the designed Tesla transformer.

TABLE I. Electrical Parameters of the Tesla Transformer

Parameters	Values	Parameters	Values
L_1	237nH	R_1	0.1mΩ
L_1	133mH	R_2	200Ω
C_1	25uF	R_{k1}	17mΩ
C_2	40pF	L_{k1}	40nH

In table I, C_1 and R_1 are the capacitance and resistance of primary circuit except parasitic element. The corresponding elements of secondary side are marked up as C_2 and R_2. R_{k1} and L_{k1} represent stray inductance and a stray resistance of the primary circuit, respectively.

The high voltage pulse generator is shown in Fig. 1. The generator has 280mm length and 150mm diameter.

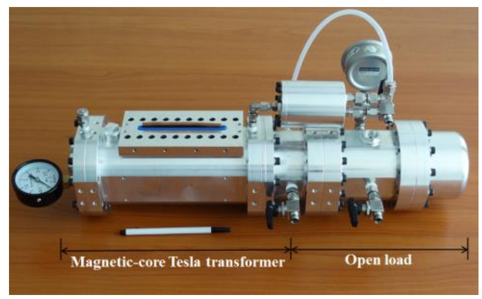

Figure 1. Photograph of high voltage pulse generator with open dummy load

B. Test Results

At 800V charging voltage of C_1, the output pulse of C_2 is nearly 450kV in peak voltage with charging time of 2μs. The voltage gain of the transformer is 563 and the energy conversion efficiency is about 50%.

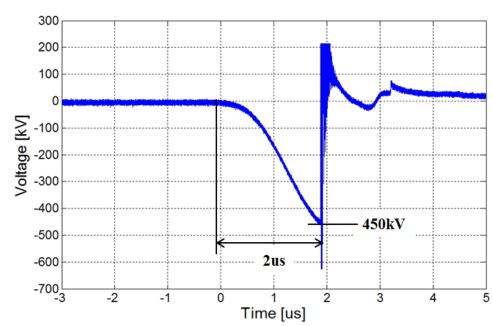

Figure 2. Output voltage waveform of secondary capacitor

REFERENCES

[1] F. Sabath, D. Nitsch, M. Jung, T.H.G.G. Weise, "Design and Setup of a Short Pulse Simulator for Susceptibility Investigations, IEEE Transaction on plasma science, vol. 30, no.5, pp.1722-1727, Oct. 2002.

[2] L. Pecastaing, A. Silvestre de Ferron, M. Rivaletto, "Compact Self-loaded Marx Generator with Integrated Pulse-forming Line for an Ultra-wideband Source", Journal of the Korean Physical Society, vol. 59, no.6, pp.3463-3467, Dec. 2011.

CHAOS CONTROL IN TRANSMISSION LINES COUPLED TO NONLINEAR CIRCUITS

Dr. Ioana Triandaf

Naval Research Laboratory
Code 6792
Washington, DC 20375
Email: ioana.triandaf@nrl.navy.mil

Abstract - **In a transmission line oscillator a linear wave travels along a piece of cable, and interacts with terminating electrical components. We present a simple model of a two-conductor transmission lines, connected to a transistor. Loss of signal integrity may manifest itself as chaotic behavior. In a real circuit, such chaotic signals, could be transmitted into the primary circuitry and disrupt or possibly damage the device. A chaos control method is presented that achieves chaos suppression by small perturbations of the resistance at one of the boundaries of the transmission line.**

Index Terms— Chaos, transmission line, Telegrapher's equation, chaos control.

1. INTRODUCTION

The effect of the transmission line on the signal integrity is a critical aspect of high-speed digital system performance. Interconnections between electronic devices may behave as transmission lines and one would like to reduce signal losses and distortions in order to ensure the correct operation of electronic circuits.

In what follows we give an exampled of signal distortion due to chaotic behavior, which occurs when the transmission line is coupled with a transistor. We show how this chaotic behavior can be controlled.

2. THE NONLINEAR DYNAMICAL SYSTEM

It is known [1] that the voltage $v = v(x,t)$ and the current $i = i(x,t)$ along a two-conductor transmission line are modelled by the Telegrapher's equations:

$$\partial v/\partial x = -L\partial i/\partial t, \;\; \partial i/\partial x = -C\partial v/\partial t \;, 0 < x < 1, t \geq 0 \quad (1)$$

where L and C are the inductance and the capacitance per unit line length, respectively. For our system we impose intial conditions and the following boundary conditions [2]:

$$v(0,t) = 0, \qquad v(1,t) = \alpha i(1,t) - \beta i^3(1,t) \qquad t \geq 0 \qquad (2)$$

where α and β are parameters. These boundary conditions correspond to having a transistor attached to the far end of the transmission line. A source is attached at the near end. We vary α and keep $\beta = 1$. As α varies periodic patterns of the solution change into complex patterns which become chaotic. In Fig.1a) we show the chaotic solution of Eq. (1), at a fixed spatial point, and note that chaos is pervasive for $0 < x < 1$.

This spatial chaotic solution can be controlled using a boundary control method [4]. Boundary control of chaos is done by applying perturbations in the parameter α at $x = 1$. Using a Poincare map approach, the parameter perturbations are applied when the solution at the boundary reaches a maximum. These perturbations are calculated proportional to the distance to the desired state which is multiplied by a gain factor derived by a local linearization of the solution about the orbit to be stabilized [3]. As a result of applying the boundary control, a high-period orbit is obtained. The periodic solution at a fixed spatial point is shown in Fig.1b). The stabilization performed at the boundary achieves control over the entire spatial domain since for hyperbolic equations the solution remains constant along characteristic curves emerging from the boundary.

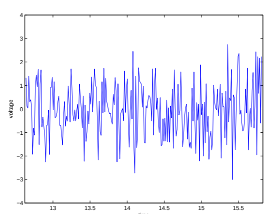

Fig. 1 a) Chaotic voltage as a function of time sampled at $x = 0.8$

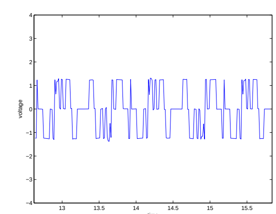

Fig.1 b) Controlled voltage as a function of time sampled at $x = 0.8$

3. REFERENCES

1. Clayton R. Paul, "Analysis of Multiconductor Transmission Lines", IEEE Press, Wiley, 2007.
2. Goong Chen et al. "Chaotic Vibrations of the One-Dimensional Wave Equation Due to a Self-Excitation Boundary Condition, Part I", Trans. of the American Mathematical Society, Vol. 350, Number 11, Nov 1998, pages 4265-4311.
3. Edward Ott, Celso Grebogi and James A. Yorke, "Controlling chaos", Phys. Rev. Lett. 64, 1196 (1990).
4. Ioana Triandaf, Ira B. Schwartz,"Karhunen-Loeve mode control of chaos in a reaction-diffusion process", Phys. Rev. E 56, 204 (1997).

The author gratefully acknowledges the support of the Office of Naval Research.

Ultimate Broadband High Power Microwaves

Andrew S. Podgorski, Fellow IEEE
ASR Technologies Inc.
Ottawa, Ontario K1H 5G6, Canada
a.podgorski@ieee.org
www.asrtechnologiesinc.com

Abstract— **This paper describes High Power Microwave (HPM) research of combining GW peak power to achieve MV/m radiated E-fields in the range of air and vacuum breakdown and frequency range of, but not limited to, 1 to 50 GHz. Multiplicity of spatially dispersed, independently triggered GW power sources, broadband and/or narrowband, supplying power to multiplicity of broadband radiators/antennas allow achieving power levels up to or exceeding ionization. The time of triggering of each generator and the generated pulses spectral content is selected to permit varying the radiated E-field and energy to achieve the highest levels at the point of power delivery. The TW antenna arrays, generating MV/m E-field can be used for verification of protection against ultimate microwave weapons. The broadband character of the radiators/antennas and the ultimate peak power density ensures the highest probability of protection of very large systems.**

Keywords-component; HPM, broadband terawatt electromagnetics, immunity testing, HPM weapons, plasma studies.

I. Introduction

Development of high power sources led to achieving GW peak power levels at microwave frequencies [1]. Initial use of narrowband GW generators resulted in inefficient coupling of the EM energy to target, undermining the effectiveness of the HPM as weapons. To address this issue, early on the broadband single GW generators were utilized eliminating need for large power supplies, shortening the test time and reducing the cost of the facilities [2]. However, application of solitary broadband GW generator left a question - what if multiple generators are used in the HPM weapons. Broadband Composite Threat [3] showed that if TW peak power, limited only by air or vacuum breakdown is reached, the HPM threat could be significantly increased. To achieve the TW radiated power, the GW power from individual generators had to be added using broadband antenna arrays. Since all broadband antennas were not electrically enclosed [4], to reach the highest gain, maximum frequency of operation and suitability for high power array assembling new antenna had to be developed. Design was narrowed to distributed hybrid consisting of a broadband TEM parallel plate antenna and a narrowband microwave horn creating an electrically enclosed broadband TEM-horn antenna [5,6].

In designing of broadband HPM array the power density and breakdown E-field strength along the energy path from the generator to the target is a limiting factor at points of highest power density i.e. close to generator or at focusing points. To assure very high peak power, coaxial single polarization antennas were used in the design of broadband spatially distributed antenna arrays with each adjacent antenna having different polarization. In broadband antenna arrays use of flat face design, normally associated with narrowband arrays, is possible but this precludes advantageous illumination that occurs when each broadband antenna fires pulses at different time and directs them to different areas. As per Ref. 7, multi-antenna arrays are configured into flat, concave and convex face curvatures. The illumination of a single target is achieved using a concave array while the convex arrays is used for uniform illumination of many targets or large objects with each antenna radiating into a different section of the object. For reference see MIL-STD-464C where 2 x 2 m adjacent areas of a single target are illuminated separately [8]. This paper addresses broadband antenna arrays capable of generating and radiating TW peak power pulses with the E-field levels exceeding the air and vacuum breakdown limits. The issues paramount to achieve such E-fields i.e. use of high antenna gain of at least 16 dB, use of new concave arrays and independently triggered generators will be addressed in the presentation.

References

[1] S. H. Gold and G.S. Nusinovich, "Review of high-power microwave source research", Rev. Sci. Instrumentation 68 (11), Nov. 1997, pp. 3945-3974.

[2] W. D. Prather, C. E. Baum, R. J. Torres, F. Sabath, D. Nitsch, "Survey of Worldwide High-Power Wideband Capabilities", IEEE Trans. on EMC, Vol. 46, Nov 3, Aug. 2004, pp 335-344.

[3] A. S. Podgorski, "Composite Electromagnetic Pulse Threat", Proc. IEEE Int. Symposium on EMC, Washington DC, Aug. 21-23, 1990, pp. 224-227.

[4] B. Cadilhon and el., "Ultra Wideband Antennas for High Pulsed Power Applications" - Chapter 15, INTECH EUROPE Open Science, "Ultra Wideband Communications: Novel Trends - Antennas and Propagation", Edited by: M. Matin, Aug. 09, 2011, pp. 277-306.

[5] A. S. Podgorski, US Patent No. 6,075,495, "Broadband TEM-horn antenna", June 13, 2000.

[6] A. S. Podgorski, "100 GHz Broadband High Power Antennas", Ultra-Wideband Short-Pulse Electromagnetics 7, Chapter 33, Springer, Germany, 2006, pp 297-305.

[7] A. S. Podgorski, US Patent No. 6,295,032 B1, "Broadband horn antennas and electromagnetic field test facilities", Sep. 25, 2001.

[8] MIL-STD-464C, "Electromagnetic environmental effects requirements for systems", US Department of Defense, Dec. 1, 2010.

Design of an Ultra Wide Band Dipole Antenna for High Power Electromagnetics

Taehyun Lim
Hanwha Corporation
Gumi, Republic of Korea
Scrape@hanwha.com

Jongwon Lee
Agency for Defense Development
Daejeon, Republic of Korea
Jwlee@add.re.kr

***Abstract*— It is important to design the proper antenna in ultra wide band (UWB) systems for effect analysis. We design the UWB antenna of 200MHz frequency bandwidth by using electromagnetic programs such as CST and FEKO. Marx generator is applied to the proposed antenna to complete the UWB system. Measurement data agree with the simulation results.**

***Keywords* — Ultra wide band (UWB), Dipole antenna, Far voltage, Integrated Antenna Source (IAS) system**

I. Introduction

Integrated antenna source (IAS) systems have been researched as an important issue of ultra wide band (UWB) systems [1]. While the main study of IAS system is focused on the high voltage power supply, we here study a spark gap antenna to efficiently control the radiated pulse property. We first develop the UWB system so as to show a specific frequency bandwidth of 200MHz. We then experimentally and numerically validate the UWB system.

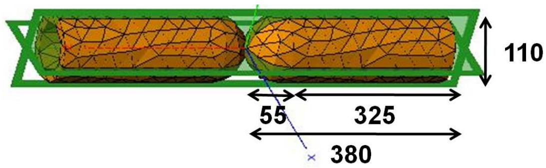

Figure 1. Design of UWB dipole antenna (unit:*mm*)

II. Design and Validation

The center frequency of dipole antennas can be derived as:

$$\text{frequency} = \text{speed of light} / \lambda \qquad (1)$$

where λ is the wavelength. Thus, to design 200MHz frequency, λ is 1.5m. From $\lambda/4$ dipole theory, the required dipole length is about 0.38m. Based on this background, we design the dipole-shaped antenna as shown in figure 1. The antenna has 380mm length and 110mm diameter. To reduce the oscillation of signal, the ratio of the diameter to the length is determined by using electromagnetic simulations. In addition, to eliminate the unexpected breakdown, we trim the head of dipoles as in the figure 1 and case the antenna with charging by nitrogen gas.

We applied a Marx generator to the proposed antenna to verify the performance of the antenna system. Electric fields radiated from the dipole antenna are measured by using D-dot (Prodyn AD-80[2]) sensors. Figure 2 indicates the measured signal in time domain. The peak to peak electric fields is 140kV. Figure 3 shows the signals in frequency domain. Three lines represent the measured data, the computed signal in FEKO, and the computed signal in CST, respectively.

The measured frequency of peak electric fields appears at

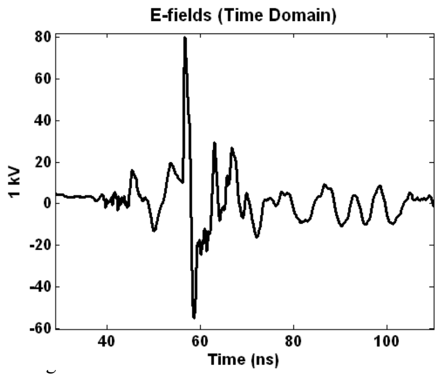

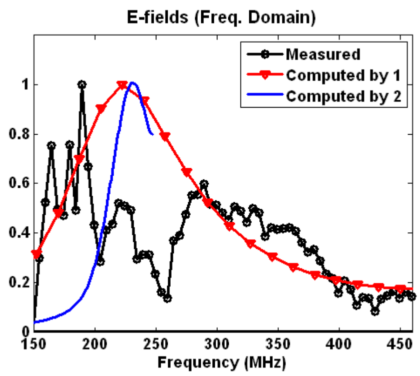

Figure 3. Fields waveforms in frequency domain

190MHz. Although the measured frequency is lower than those of simulations, this difference can be from the slight fabrication error of 20mm distortion. Therefore, the measured data agree with the simulation results. The figure also shows the secondary peak in the wavelength of 0.8~1.2m. This may be caused by the path consists of Marx generator, dipole part, and the connecting cable since the wavelength of this unexpected antenna is similar to that of the secondary peak.

III. Conclusion

A UWB system is developed to have a specific center frequency. We design the specific antenna by electromagnetic simulations. We then combine a Marx generator with the antenna. The frequency bandwidth of the developed UWB system is validated by numerical and experimental results.

References

[1] J. Ryu and J. Lee, "An Integrated Antenna-Source System of Very High Ultra Wide-Band Gain for Radiating High-Power Wide-Band Pulses", *IEEE Trans. Plasma Science*, vol.40, no.4, pp.1019-1026

[2] PRODYN, http://www.prodyntech.com

ID 037

Detection of railway signalling jamming signals using the EVM method

S. Mili, V. Deniau, D. Sodoyer, M. Heddebaut
Univ. Lille Nord de France, IFSTTAR
Villeneuve d'Ascq, France
souheir.mili@ifsttar.fr

***Abstract*—GSM-Railway is the ground to train radio communication system currently under deployment along the European railway infrastructure. 150.000 km of railway track are foreseen to be covered in Europe in the coming years. The system is designed to ensure different communication services between ground and trains and is replacing progressively various old analogue radio equipment. It is one of the components of the "Euroradio" system, managing voice and signalling data. As a component of a critical infrastructure, GSM-R is a potential target for intentional electromagnetic interference. Indeed, malicious attacks can generate and propagate electromagnetic energy into the GSM-R frequency bands with the objective to impact the whole railway system. This paper presents a methodology based on the error vector magnitude parameter enabling to detect the presence of jamming signals at the receiver. This early detection can then be used by the railway system to appropriately react.**

Keywords-component; GSM-R; EM jammer; Error Vector Magnitude; EM detection.

I. INTRODUCTION

The GSM-R protocol fully complies with the EIRENE railway specifications [1]. Considering the physical layer, GSM-R should provide radio coverage of at least 95% of time on over 95% of the required area. Moreover, the received power by ground or train receivers should be kept in the range -95 dBm to -30 dBm, whatever is the train distance to the nearest ground Base Transceiver Stations. These values, especially the lowest one, indicate that even low-power jammers could possibly interfere with the exchanged railway signalling information.

II. METHOD OVERVIEW AND EXPERIMENTAL RESULTS

Common radio frequency bands are used all over Europe. These allocated frequency bands are 876 MHz to 880 MHz for the uplink, i.e. train to ground communication and 921 MHz to 925 MHz for the downlink, i.e. ground to train. A GMSK standard modulation is used with a normalized bandwidth time product (BT_b) of 0.3. We consider these characteristics to investigate a suitable detection process based on the Error Vector Magnitude (EVM) method. The objective is to quickly detect incoming jamming signals.

A. GSM-R communication chain model

A communication chain is modeled, transmitting GSM-R bursts of 148 bits using a GMSK generator and, superimposing an AWGN noise. We then recover the data using a GMSK demodulator. Disturbances are injected using a wideband CW signal covering a larger frequency band than the allocated GSM-R ones. Signals are extracted and processed.

"SECRET" project European Community's Framework Program FP7/2007-2013 under grant agreement number "285136".

B. EVM Detection process

We consider the quadratic specificity of the communication and particularly the EVM parameter. EVM is normally used to evaluate the quality of modulation [2] but, in our study, we use it as an indicator of the presence of jamming signals. The EVM is calculated using the constellation data of both the normal, i.e. non-jammed communication and of the jammed communication as expressed:

$$EVM = |y_i - s_i| \Rightarrow \begin{cases} y_i = \sqrt{I_y{}^2 + Q_y{}^2} \\ s_i = \sqrt{I_s{}^2 + Q_s{}^2} \end{cases} \qquad (1)$$

where y_i represents the signal in the normal condition and s_i represents the signal in the jammed condition for I and Q in-phase and quadratic data respectively.

C. Experimental measurement

A GSM-R radio communication is established using laboratory equipment. A communication analyzer is used. On demand, an available hand held jammer is switched on. Fig. 1 represents on the left side the EVM values when no jammer is applied (S/B is set to 20 dB). On the right side, the jammer is applied, 10 dB below the GSM-R received signal level. We conclude than the EVM method detects this specific low-power jamming condition.

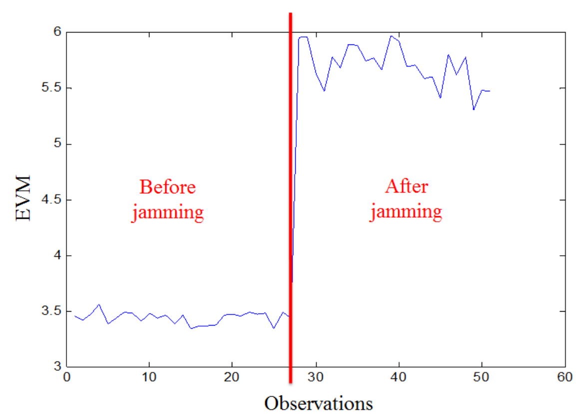

Figure 1. EVM of normal and disturbed conditions.

III. Conclusion

Among the existing detection methods, the EVM method seems a good candidate to implement jamming detection equipment in the receiving chain. This detection information can then be used in order to get a proper system reaction.

REFERENCES

[1] UIC Project EIRENE, «Functional Requirements Specification,» 2006.

[2] T.L. Jensen and T. Larsen, "Robust Computation of Error Vector Magnitude for Wireless Standards," IEEE Trans. on Communications, vol. 61, n° 2, pp. 648-657, 2013.

The threat of Intentional Electromagnetic Interference (IEMI) against modern critical infrastructures: Awareness and Protection

Stylianos C. Panagiotou
National Center for Scientific Research "Demokritos"
Institute of Informatics and Telecommunications
Integrated Systems Laboratory
Athens, Greece
email: stelios.panagiotou@iit.demokritos.gr

Stelios C. A. Thomopoulos
National Center for Scientific Research "Demokritos"
Institute of Informatics and Telecommunications
Integrated Systems Laboratory
Athens, Greece
email: scat@iit.demokritos.gr

Abstract— **The issue of intentional electromagnetic interference (IEMI) attacks against modern critical infrastructures is addressed. A description of how an IEMI attack is implemented and the categories of the relevant radio frequency weapons are provided and the effects of an IEMI incident on a targeted system are thoroughly examined. Moreover, techniques associated with electromagnetic interference mitigation and protection, as well as their advantages and disadvantages, are presented along with examples of how these techniques can be tailored to effectively address the particular consequences derived from IEMI events. Novel protection methods are proposed.**

Keywords- electromagnetic interference, radio frequency weapons; high power microwave; infrastructure protection; hardening measures; shielding; filtering; surge protective devices;

I. INTRODUCTION

IEMI, also known as Electromagnetic Terrorism, is the intentional, malicious generation of electromagnetic energy, introducing noise or signals into electric and electronic systems, thus disrupting, confusing or damaging these systems for terrorist or criminal purposes. IEMI can also be considered as a cyber attack since it corrupts data and damages critical data assets. Moreover, there is a worldwide trend to include IEMI to the broader category denoted as cyber threats.

A definition combining cyber and IEMI is following:

- **Cyber EMI attack** is any deliberate action involving the use of electromagnetic energy to control the domain characterized by the use of and the electromagnetic spectrum to store, modify, and/or exchange data via networked systems and associated physical infrastructures.
- **Cyber EMI protection** is the passive and/or active means taken to protect electronics and/or access to the electromagnetic spectrum from any effects of friendly or enemy employment of cyber EMI that degrades, neutralizes, or destroys ability to store, modify, and/or exchange data via networked systems and associated physical infrastructures.

Two factors determine in general the vulnerability of a target:

1. Coupling modes possible between the interfering source and the targeted equipment (front door or back door coupling)
2. The level of energy coupled that will damage or destroy a particular target.

The effects of IEMI on a system are taken into account in this work, including (in order of decreasing severity):

- permanent physical damage,
- permanent function failure,
- temporary upset (with operator intervention),
- performance reduction,
- temporary upset (without operator intervention).

II. PROTECTION MEASURES AGAINST IEMI

Protection methods against IEMI have been surveyed in this work, including:

- Organizational practices (e.g. physical keep-out perimeters),
- Use of T-R limiters in radar and antenna systems,
- Controlling the directivity pattern of an antenna so that nulls are created along the directions of the interfering incoming signals (e.g. exploitation of smart antennas),
- Use of frequency selective surfaces on the radome to limit the out of band energy reaching the antenna,
- Electromagnetic Shielding,
- Earthing and Grounding topologies
- Use of circuit protection technologies (limiting with surge protective devices and filtering),

Furthermore novel hardening architectures are introduced.

This work is supported by the "HIPOW" EU research project ("Protection of Critical Infrastructures against High Power Microwave Threats" HIPOW-FP7-SEC-2011-284802).

HPEM Tests of Communication Devices

Ch. Adami, M. Joester, M. Suhrke, H.J. Taenzer
Electromagnetic Effects and Threats
Fraunhofer Institute for Technological Trend Analysis INT
Euskirchen, Germany
michael.suhrke@int.fraunhofer.de

***Abstract*—Intentional Electromagnetic Interference (IEMI) can be used to support illegal activities ranging from robbery up to terroristic attacks. The general idea is to use High Power Electromagnetics (HPEM) beyond the Electromagnetic Compatibility (EMC) immunity of handheld communication devices to compromise their functionality. In particular, smart phones and tablets could be in focus of such an attack as those devices are increasingly used to control and communicate in critical infrastructures. Fraunhofer INT did HPEM vulnerability tests with a selection of smart phones and tablets showing disturbances in a wide frequency range.**

HPEM; IEMI; Electromagnetic Threat; smart phones; tablets; communication systems

I. Introduction

Smart phones and tablets more and more find their way into the control of critical infrastructures. HPEM tests of mobile phones in the past showed a high vulnerability against HPEM fields [1]. The new technology offers more frequency bands for communication, Wi-Fi and touch sensitive displays, why they are more susceptible to HPEM. Fraunhofer INT conducted HPEM vulnerability tests of eight smart phones and four tablets.

II. Testing

A. Test Objects

Fraunhofer INT conducted vulnerability tests of four low-cost smart phones with 240 x 320 pixel displays, four devices from the mid-range price segment with 1280 x 720 pixel and four tablets with 7 inch and 10 inch displays. All devices run with Android system software except one Blackberry and one with Windows Phone 8.

B. Test Setup

The tests were set up in the TEM waveguide of Fraunhofer INT with a frequency range from 150 MHz to 3.4 GHz. A GSM/UMTS connection with the smart phones was not possible during the tests. The Wi-Fi connection of the smart phones was used to establish a mobile radio connection. A Wi-Fi network with two Wi-Fi routers was installed inside the shielded test facility whereupon router #1 functioned as the access point (DHCP server) and router #2 as in bridge mode to check the Wireless Distribution System during the tests. The connections between the routers and the PCs outside of the shielded hall were fiber optic cables together with media converters.

The first two smart phones were tested in two different setups corresponding to different operation modes of the smart phones.

In setup #1 the smart phone had a Wi-Fi connection with the Wi-Fi network inside the shielded hall. The front side of the smart phones with the internal camera was oriented to the waveguide input and the camera signal was transferred out of the shielded hall via the Wi-Fi connection. In setup #2 a video was played on the DUT during HPEM field application. Both smart phone displays were monitored with an RF hardened camera.

III. Test Results

The tests in both setups #1 and #2 show that HPEM can disturb smart phones and tablets in a broad frequency range. The RF field triggered unwanted operations on the touch sensitive display. The Wi-Fi data transfer was interrupted in a broad frequency range, also outside the Wi-Fi spectrum. In some cases the transfer had to be started all over again. During the tests one DUT has been broken.

Fig. 1 gives an overview of normalized susceptibility thresholds for two smart phones. The failure frequencies vary from 280 MHz to 2.46 GHz.

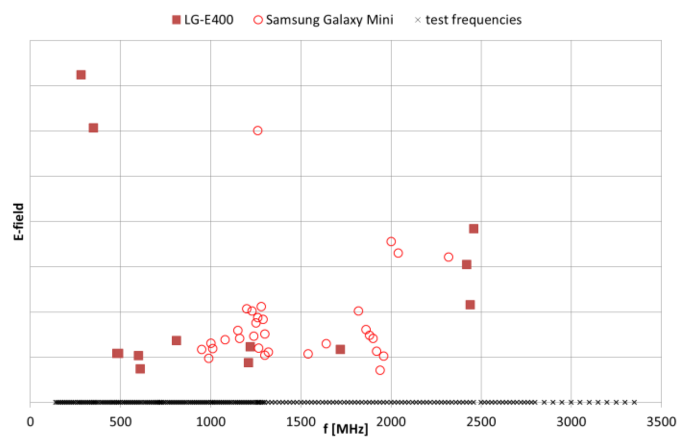

Figure 1. Susceptibility threshold of two smart phones.

References

[1] Braun, Ch. and Schmidt, H.-U., " Effects of microwave irradiation on modern Telecom devices - failure thresholds of five mobile phones " AMEREM 2002, Annapolis, 2002.

HPEM Tests of Security Systems

Ch. Adami, M. Joester, M. Suhrke, H.J. Taenzer
Electromagnetic Effects and Threats
Fraunhofer Institute for Technological Trend Analysis INT
Euskirchen, Germany
michael.joester@int.fraunhofer.de

***Abstract*—Intentional Electromagnetic Interference (IEMI) can be used to support illegal activities ranging from robbery to terroristic attacks. The general idea is to use High Power Electro-magnetics (HPEM) beyond the Electromagnetic Compatibility (EMC) immunity of electronic protection systems to impair its safety level. In particular, surveillance and alarm systems could be in focus of such an attack. Fraunhofer INT did HPEM vulnerability tests with an alarm system. The results allow to discuss possible scenarios.**

HPEM; IEMI; Electromagnetic Threat; Alarm System; Surveillance System; HPM Testing

I. Introduction

Surveillance and alarm systems are the key tools used for property protection, where the area is large or the observation is automated during night and holidays. An attack with IEMI could be used to disable this functionality directly or indirectly by the “human factor”. Fraunhofer INT performed HPM tests to investigate the behavior of an alarm system during pulsed high power RF application.

II. Testing

A. Test Method

Tests were done using the Fraunhofer INT open TEM waveguide in combination with RF pulsed power oscillators in the range of 10 kW to 35 kW and 1 µs/1 kHz pulse modulation. The frequency range is 150 MHz up to 3450 MHz.

B. Test Object

An easy to purchase alarm system set with the German security quality label ‘VdS’ has been selected for the tests. There are additional EMC immunity requirements related to this label [1]. The set consists of a central unit, a control panel, an outdoor alarm device, two IR motion sensors, five windows/door relay sensors, and a key switch. The test setup is completed with a wireless extension unit and one relay sensor to test a wireless alarm system path, too.

C. Test Setup

The system has been grouped into a Device Under Test (DUT) with the central unit and the wireless extension unit and a group of sensors, actuators, and operating devices (Fig. 1). The cable harness in between is app. 2 meters with 1.5 meters in a straight length according to automotive EMC test setups. All wire lengths in the cable harness are realized to represent long lines in a real cabling layout. The cable is the original screened one sold by the alarm system manufacturer.

Figure 1. Test setup fixed on rigid foam with groups and cable harness.

The system wiring configuration is the example described in the manual and all installation details have been done exactly following that document. A notable detail is that there is no description how to handle the cable shielding. Consequently, it hasn’t been connected in the setup.

III. Test Results

The alarm system shows two effect groups. Functional state B (blue marks in Fig. 2) is mainly a permanently glowing flash LED of the alarm unit and LCD turn off during RF exposure. It does not affect the alarm functionality and is therefore acceptable. Functional state D (red marks) is a delayed reaction of the IR motion sensors on RF amplitude changes leading to alarm release, which is not acceptable in terms of operation purpose.

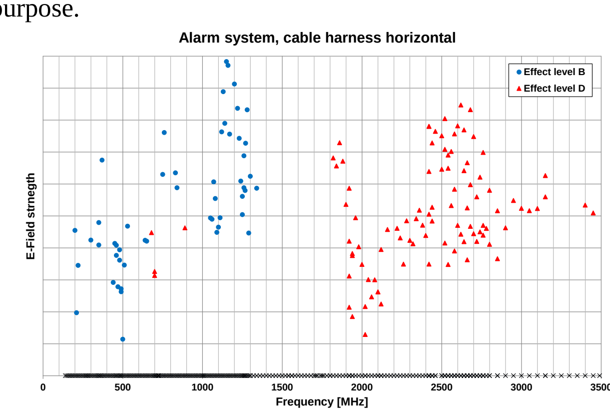

Figure 2. Susceptibility threshold of alarm system.

As the alarm can be released easily in a broad range from 2 GHz to 3 GHz (red marks in Fig. 2), HPM could be used gain access to a facility. In a fictive scenario repeated hidden HPM alarm activation might misguide the operator to disarm the alarm system.

References

[1] VdS Guidelines for Control and Indicating Equipment (CIE), “Control and Indicating Equipment (CIE) of classes B and C, Requirements,” VdS 2252en, Edition: 2003-12. Link: http://vds.de/en/quick-links/vds-guidelines/

Influence of LLS Detection Efficiency on the Measured Distribution of Interstroke Intervals

Mohammad Azadifar[1], Mirjana Stojilović[2], Marcos Rubinstein[2], Farhad Rachidi[1]

1 Swiss Federal Institute of Technology, EMC Lab., Lausanne, Switzerland, Farhad.Rachidi@epfl.ch
2 University of Applied Sciences Western Switzerland, Yverdon, Switzerland, Marcos.Rubinstein@heig-vd.ch

***Abstract*—Interstroke intervals can be estimated from Lightning Location Systems (LLS) data. We present here a methodology to assess the effect of an imperfect stroke detection efficiency on the measured statistical distribution of the interstroke intervals.**

Keywords-lightning location; lightning parameters

I. INTRODUCTION

Numerous studies have investigated the remote estimation of lightning parameters from LLS data [1-3]. In this paper, we propose a methodology to study the effect of the imperfect stroke-detection efficiency of lightning location systems on the statistical distribution of interstroke intervals.

II. METHODOLOGY

The methodology can be summarized as follows. Use a computer to generate a control dataset composed of flashes with the same stroke-multiplicity and interstroke-interval statistical-distributions as those observed in experimental measurements. Out of the control dataset, select a subset at random to simulate the imperfect detection efficiency of an LLS. Finally, compare the statistical distribution of the interstroke intervals of the subset to that of the original dataset.

The following steps describe the methodology.

1. Select a histogram of measured multiplicities [4] and call $n_{\mathrm{hys}}(m)$ the number of flashes of multiplicity m.
2. To obtain a large enough dataset for the interstroke intervals, select a positive integer q and calculate the number of m-stroke flashes $n_{\mathrm{s}}(m)$ as

$$n_s(m) = q n_{hys}(m). \tag{1}$$

The value of q is selected so that the interstroke dataset in point 5 below passes a lognormality test.

3. Calculate the total number of flashes in the control set as,

$$N = \sum_{m=1}^{m_{\max}} n_{\mathrm{s}}(m) \tag{2}$$

where $m_{\max}$ is the maximum multiplicity in the histogram.

4. Calculate the total number of strokes in the set as

$$n_{\mathrm{total}} = \sum_{m=1}^{m_{\max}} m \cdot n_{\mathrm{s}}(m) \tag{3}$$

and the total number of interstroke intervals as

$$r = \sum_{m=1}^{m_{\max}} (m-1) \cdot n_{\mathrm{s}}(m) \tag{4}$$

5. Generate a set of r interstroke intervals Δt_i belonging to a lognormal distribution with geometrical mean and standard deviation similar to those reported in the literature based on continuous measurements (not based on LLS data).
6. Generate a table for each stroke in each flash (see Table I).

TABLE I. GENERATED TABLE FOR ALL THE CONSIDERED STROKES

Overall stroke number	Stroke number in flash	Multiplicity	Interstroke interval
1	1	1	N/A
…	…	…	…
$n_{\mathrm{total}} - 1$	$m_{\max} - 1$	$m_{\max}$	Δt_{r}
n_{total}	$m_{\max}$	$m_{\max}$	N/A

7. Assume a LLS stroke detection efficiency of de%. The number of missed strokes can be evaluated as

$$n = \mathrm{abs}\left(n_{\mathrm{total}} \frac{100 - de}{100}\right) \tag{5}$$

8. Generate n random integers from 1 to n_{total}.
9. Based on Table I, create a table of interstroke intervals measured by the considered LLS using the following rules:
   a) If the missed stroke is the first or the last in a flash, delete the corresponding line in the table.
   b) In all other cases, add the interstroke interval of the missed stroke to that of the previous stroke and then delete the line of the missed stroke.
10. Compare the statistical distribution of interstroke intervals from the resulting table to that of the original Table I.

REFERENCES

[1] Cummins K.L. and E.A. Bardo, On the relationship between lightning detection network performance and measured lightning parameters, paper presented at the 1st International Conference on Lightning Physics and Effects, Sao Paulo, Brazil, November 7-11, 2004.

[2] M. Rubinstein, “On the determination of the flash detection efficiency of lightning location systems given their stroke detection efficiency”, Proceedings of the 11th International Zurich Symposium on Electromagnetic Compatibility, March, l995.

[3] F. Rachidi, J.L. Bermudez, M. Rubinstein, V.A. Rakov, "On the estimation of lightning peak currents from measured fields using lightning location systems", Journal of Electrostatics, Vol. 60, pp. 121-129, 2004.

[4] CIGRE Working Group C4.407, "Lightning Parameters for Engineering Applications", Technical Brochure 549, CIGRE, 2013.

Financial support from the Swiss National Science Foundation (Project No. 200021_147058) is acknowledged.

A Multi-Channel Hardware Prototype for IEMI Diagnosis

David Recordon, Mirjana Stojilović, Marcos Rubinstein
University of Applied Sciences Western Switzerland
Yverdon-les-Bains, Switzerland
mirjana.stojilovic@heig-vd.ch
marcos.rubinstein@heig-vd.ch

Loubna Rouiller, Werner Hirschi
Montena Technology SA,
Rossens, Switzerland
loubna.rouiller@montena.com
werner.hirschi@montena.com

***Abstract*—In this paper we present the design of cost-efficient multi-channel hardware for the detection, location, and analysis of intentional electromagnetic interference (IEMI) signals. The system is designed to identify the type of IEMI signal and locate the IEMI source. Preliminary measurements on a single-channel prototype are performed and confirm the suitability of the design.**

Keywords- hardware; intentional EMI; pulse-width modulation;

I. Introduction

Protecting important electronic systems against IEMI is of high importance. One way of protecting is IEMI event (attack) detection. However, this is not always sufficient. Sometimes, it is useful to perform IEMI diagnosis, i.e., to be able to determine the type of the signal or find the location of the IEMI source.

Unlike IEMI detection systems, which can be relatively inexpensive, systems for performing IEMI diagnosis are significantly more complex and thus costly. The reason lies in the nature of IEMI signals: they are typically very short and exhibit very fast rise/fall times. To capture, visualize, and analyze them, one needs a high-speed digitizing channel per EM-field sensor. The price of such a system increases quickly with the number of sensors in use. In this paper we show a cost-efficient hardware-implementation of a modular system for (i) visualization of IEMI signals, (ii) their classification according to the waveshape (continuous wave, damped sinusoid, double exponential) and (iii) the estimation of the location of the IEMI source, based on the time difference of arrival algorithm.

II. System Architecture

Fig. 1 shows a simplified block diagram of a two-channel system. Since the design is modular, additional channels are added simply by replicating the first channel. The IEMI signal is received using a field sensor. Its output is connected to the electronic system by a coaxial cable. At the cable output, a variable attenuation is introduced. This is necessary as IEMI signals have a very high dynamic range. After being attenuated, the signal is fed to the amplitude-measurement circuit and to a 1-bit digitalization module. To decrease the overall system cost, only one of the input signals is relayed for displaying on a high-frequency oscilloscope. Based on the measured signal amplitudes, the FPGA generates selection signals for the switch block, choosing the signal with the higher amplitude for external monitoring. The output of the 1-bit digitalization block is a pulse-width modulated sequence of unit-amplitude impulses, where the duration of the impulses is proportional to the duration of IEMI impulses. The time durations are measured by an FPGA and used to determine the approximate waveshape of the IEMI signal.

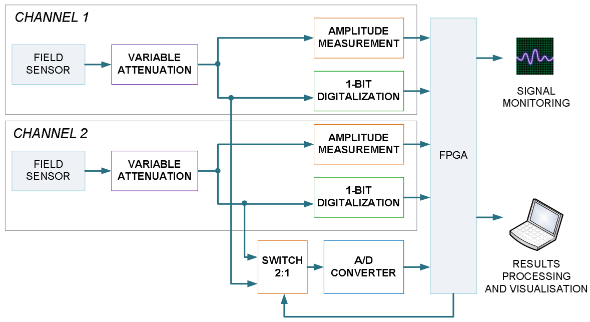

Figure 1. Block architecture of a two-channel system for IEMI diagnosis.

III. Experimental Verification

To verify the correctness of the system design, we used a one-channel prototype. Fig. 2 shows the signal measured at the output of the 1-bit digitalization module when a damped sinusoid excitation is used. The results confirm that the pulse-modulated impulses contain the information on the half-pulse width, needed to identify the signal type. Estimating the location of the IEMI source requires at least four channels and is left for future work.

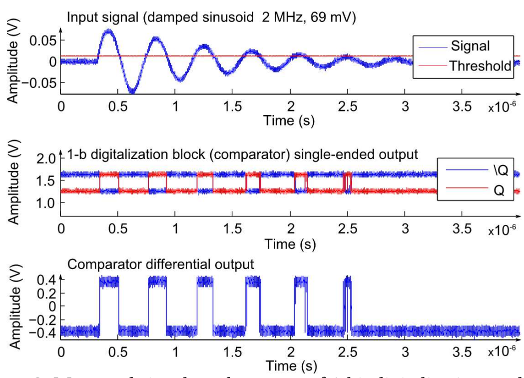

Figure 2. Measured signals at the output of 1-bit digitalization module.

The research leading to these results was supported in part by the Project STRUCTURES, co-funded by the European Union Seventh Framework Programme under grant agreement no. 285257.

Lightning Overvoltages on Shield Wire Lines

Alexandre Piantini, Miltom Shigihara
Institute of Energy and Environment
University of São Paulo
São Paulo – SP, Brazil
Piantini@iee.usp.br

José Ezequiel Ramos
Eletrobrás Distribuição Rondônia / Universidade Federal de Rondônia
Porto Velho - RO, Brazil
jer.pvh@gmail.com

***Abstract*—One of the non-conventional technological alternatives for energy supply to small communities located relatively close to transmission lines is the shield wire scheme (SWS). The three phase SWS adopted in the State of Rondônia, Brazil, consists in the energization of the two shield wires of a 230 kV transmission line, being the ground the third phase. The shield wires are energized at 34.5 kV. Lightning has a great impact on the system performance and in this paper an evaluation is presented on the overvoltages induced on shield wire lines (SWL) by indirect strokes.**

Keywords- lightning; overvoltages; power distribution lines; shield wire lines, shield wire scheme.

I. Introduction

In the Amazon region, the existence of small towns and villages located relatively close to transmission lines, but far from the sub-transmission and electricity distribution systems is not uncommon. The use of conventional medium-voltage lines for providing power supply to these communities is sometimes not feasible due to economic reasons.

A non-conventional and low cost alternative conceived by Iliceto [1, 2], namely the shield wire scheme (SWS), has been applied in the State of Rondônia, Brazil, since 1995. Loads greater than 4 MVA can be supplied with the SWS, and the insertion of this technology in the regional scenario enabled energy to be supplied to more than 40.000 people [3].

The Brazilian experience with the SWS is highly positive, but lightning has a great impact on the system operational performance and is responsible for most of the reported power outages. The effect of the overvoltages resulting from direct strikes to the two SWL systems implemented in Rondônia (SMQ and AQJR) was examined in [4]. This paper evaluates the overvoltages induced by nearby strokes on the SWL SMQ.

II. Results

The average conductor height of the SWL SMQ is 21.5 m, more than twice the height of a typical 34.5 kV line. Although the SWLs are located in regions dominated by pastures, there are tall trees close to some line sections. Such trees provide some shielding to the conductors and reduce the line exposure to direct strokes, but on the other hand lightning may occur very close to the line and therefore induced overvoltages can reach sufficiently high levels to cause insulator flashovers. The critical impulse flashover overvoltages of the SWL, referred to the reference atmospheric conditions, are 278 kV and 281 kV for the positive and negative polarities, respectively.

Fig. 1 indicates that, for the conditions considered, the incidence of lightning to distances (d) shorter than about 200 m from the SWL can cause line flashovers. The calculations were carried out assuming a stroke current with triangular waveshape, amplitude of 30 kA, front time of 2 µs, time to zero of 160 µs and propagation velocity equal to 30 % that of light in free space. The soil resistivity and relative permittivity were assumed equal to 4000 Ω.m and 10, respectively.

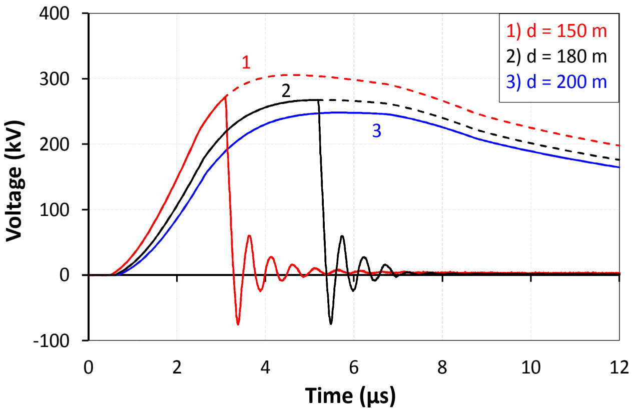

Figure 1. Lightning-induced voltages at the insulator terminals at the point of the SWL closest to the stroke location.

III. Conclusions

Lightning has a significant impact on the performance of SWL systems in regions with high ground flash density.

In comparison with a conventional power distribution line, a SWL is more prone to lightning-caused flashovers. As its conductors are at a higher position, they tend to be struck more times and, additionally, the magnitudes of the lightning-induced voltages by nearby strokes tend to be higher.

References

[1] F. Iliceto, "Lightly loaded long HV transmission lines. Guidelines prepared at the request of the World Bank", Washington D.C., 1982-83.

[2] F. Iliceto, E. Cinieri, L. Casely-Hayford and G. Dokyi. “New concepts on MV distribution from insulated shield wires of HV lines: operation results or an experimental system and applications in Ghana”, IEEE Trans.Power Delivery, vol. 4, n. 4, pp. 2130-44, Oct. 1989.

[3] J. E. Ramos, V. A. Pires, A. Piantini, and A. D´Ajuz, “Experiences with the Energized Shield Wire Line technology in Brazil,” Proc. IX Int. Symposium on Lightning Protection (SIPDA), Foz do Iguaçu, pp. 323-328, Nov. 2007.

[4] J. E. Ramos, V. A. Pires, A. Piantini, P. F. Obase, A. Silva Neto, T. O. Carvalho, and P. R. O. Borges, “Analysis of the Effect of Lightning on the Energized Shield Wire Line Technology,” Proc. XI Int. Symposium on Lightning Protection (SIPDA), Fortaleza, pp. 267-271, Oct. 2011.

ID 044

Analytical and Experimental Studies on a Fast UWB Pulse Generating System

Vijay H Bhosale

LRDE, DRDO, Bangalore, Karnataka, India
imvijayb@yahoo.com

D C Pande

LRDE, DRDO, Bangalore, Karnataka, India,
pande.dc@gmail.com

M. Joy Thomas

IISC, Bangalore, Karnataka, India
jtm@ee.iisc.ernet.in

Abstract— **With the advent of Ultra Wide Band (UWB) technology, several areas of applications have been opened. The UWB based impulse radiating antenna is based on radiation of an intense short duration Electro Magnetic (EM) pulse in a desired direction. Important subsystems of such UWB radar are the short pulse generator or in short 'Pulser' and a high bandwidth high gain antenna. Several researchers have developed and experimented on the UWB pulse generating system and studied the switch characteristics in particular. [1] This paper presents the developmental efforts for a 30 kV sub nanosecond UWB pulse source and a Half Impulse Radiating Antenna (HIRA) based radiating system. One of the basic intentions was to obtain fast rise time and the least jitter. Parametric analysis of simulated HIRA based UWB system with variation of angle between TEM feed transmission lines is carried out. Results of the realized UWB system for optimized rise time and jitter are also presented.**

Keywords- Ultra Wide Band (UWB), Pulser, Half Impulse Radiating Antenna (HIRA), Transverse Electro Magnetic (TEM)

I. INTRODUCTION

In order to obtain the necessary bandwidth consistently, it is essential to realize the UWB system with a fast rise time and least jitter. In the present work, the influence of the switching gas medium and the gas pressure for a range of switching voltages are experimented. It is also necessary to obtain higher field intensities in the far region of the UWB system. Hence in addition to the fast rise time it is also necessary to have a better antenna feed. In the present configuration a tapered conical TEM transmission line fed HIRA antenna is proposed. Radiation performance of the UWB system is a function of the antenna feed geometry. Reflected waves from the antenna see an aperture blockage due to the TEM feed lines. Aperture blockage and hence the far region electric field as a function of the variation of angle between the TEM feed lines wrt antenna axis is studied by modeling. CST simulation was carried out for a double exponential voltage pulse input. Pulser performance was measured for the best rise time & jitter.

II. MODELING, REALIZATION AND THE EXPERIMENTAL RESULTS

The realized UWB system consists of a mineral oil based compact coaxial capacitor and a pressurized gas switch. CST modeling of the HIRA as depicted in Table. 1 shows that for the variation of angle of TEM feed line wrt the vertical from 60° to 30° there is continual improvement in the radiated far electric field. The optimized angle was found to be 30°. The realized UWB system shown in Fig. 1 was experimented with

Table 1 : Effect of feed angle variation on peak radiated field

Distance from Antenna (m)	Peak radiated field at various feed angles wrt antenna axis (V/m)	
	45°	30°
1.5	405	651
3	223	303
4	100	126

various switching gases such as air, N_2 and SF_6 and different pressures to obtain the least rise time and jitter.

Figure 1. HIRA based UWB system, gas switch and test set up developed

Rise time measurements of the pulser output voltage were carried out by measuring the radiated field using a D dot sensor of 1.5GHz bandwidth and a Tektronics 16GHz oscilloscope. As depicted in Table 2, though the rise time was the best in case of pressurized SF_6 gas as switching medium, jitter performance was different at low and high pressures. At low pressures, jitter with N_2 was lower than that of the SF_6 gas as the switching medium.

Table 2 : Rise time performance of the 30kV system

Gas type	Rise time in ps at different gas pressures	
	1.5 bar	3 bar
Dry air	1500	925
N_2	1100	845
SF_6	900	620

III. CONCLUSION

i. Modeling results show that aperture blockage is the least and hence better performance is achieved when feed angle is reduced upto 30°. At angles less than 30° performance doesn't improve rather reduces due to high impedance mismatch.

ii. The best rise time was obtained in the case of switching gas SF_6 at 3 bar. Actual rise time obtained could be still better as the D dot sensor used had a limited bandwidth of 1.5GHz.

iii. Switching jitter is lesser in SF_6 at high pressures but at low pressures it is relatively more than air and N_2 due to the possible scavenging of electrons in the electronegative SF_6.

REFERENCES

[1] Y Chen, et al, " Optimization of a low jitter, 50 kV, 100Hz triggered spark gap with high pressure gas mixtures", IEEE Trans. On Dielectrics and Electrical Insu., Vol.16, No 4 pp. 971-978, 2009.

ID 045

EMC Aspects of the Square Kilometre Array in South Africa

Howard C. Reader

Dept. EE Engineering
University of Stellenbosch, Cape Province, South Africa.
hcreader@sun.ac.za

***Abstract*— The Square Kilometre Array (SKA) will be the most sensitive radio telescope ever built [1]. This paper describes elements of electromagnetic compatibility (EMC) that have been considered in the development of South Africa's SKA site in the northwest of the country. Possible self-generated radio frequency interference (RFI) has to be addressed vigorously at every stage of the project. Specific EMC measures taken relate to the: power provision; site infrastructure, including shielding properties of the processor buildings; telescope interfaces and grounding; pre-build testing of the aforementioned.**

Keywords-EMC, MeerKAT, metrology, Square Kilometre Array

I. INTRODUCTION

The SKA will become the largest radio astronomy telescope in the world [1]. The instrument will be at least 50 times more sensitive than existing systems. The mid-band and telescope arrays will be built in the Karoo of South Africa and the low-band array in the Murchison Valley of Australia. RFI may well prove to be a limiting factor in the science that can be achieved by the three distributed arrays. This paper overviews the general EMC aspects of the Karoo work, but will give specific focus to some of the projects by way of illustration. General references to this can be found in [2], but more detail will be provided in the presentation on: the power provision; the hardening measures of the partially-underground Karoo Array Processor Building (KAPB) – in the throes of construction at the time of writing; the shielding effectiveness (SE) properties of the soil berm arising from the excavation of the KAPB; some of the Karoo Array Telescope (KAT) modeling and measurement; general techniques and equipment.

II. INFRASTRUCTURAL EMC

A. Power provision

An early development to the site was the 22 kV power line which has since been up-rated to 33 kV. The line was designed not to spark. Modeling and measurement findings added to the decision to point the power lines away from the site core. Fig. 1 shows the evolving layout of the core where power lines are underground and hills are used for shielding.

B. Karoo Array Processor Building and Soil Berm

Fig. 2 shows the KAPB at a mid-construction phase. The excavated soil was exploited to form a shielding berm. The earth mat, bond ring conductor, reinforcing connections and cable entry points were carefully designed and checked.

C. Modeling and Metrology

Many of the systems have been the subject of physical scale, analytical and computational modeling. Measurements in both time and frequency domains has been undertaken. Cutting-edge technology in the KAT processing systems has been exploited for the time instruments.

III. CONCLUSION

A brief outline of the EMC aspects of the South African SKA project has been given. The conference presentation will expand on the highlighted topics.

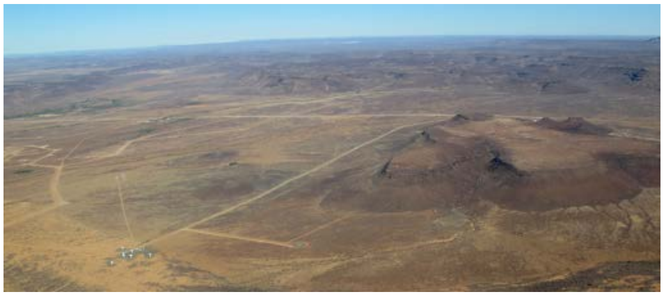

Figure 1. South African SKA site showing the first seven Karoo Array Telescopes (KAT-7), the foundations of some MeerKAT telescopes (mid-left), and the flat topped hill called Losberg. The site base with data processing and power rooms is situated directly behind Losberg.

Figure 2. The mid-phases of the Karoo Array Processor Building (KAPB) construction showing soil berm from earth excavation, some connected reinforcing, the ground level with earth mat and bond-ring conductor.

REFERENCES

[1] P. E. Dewdney, W. Turner, R. Millenaar, R. McCool, J. Lazio, and T. J. Cornwell, "SKA1 system baseline design," SKA-TEL-SKO-DD-001,Rev.1;http://www.skatelescope.org/wp-content/uploads/2013/03 /SKA-TEL-SKO-DD-001-1 BaselineDesign1.pdf

[2] H.C. Reader, "Components of EMC Thinking Relevant to Radio Astronomy Sites", APEMC 2013, Melbourne, Australia, Session TC18-1, ISBN 978-1-9221-0702-2, May 2013, paper 145.

NRF and SKA of South Africa are thanked for support.

Analysis of electromagnetic SE(shielding effectiveness) by the change in receiving and transmitting antenna position

Jeong-Ju Bang, Chang-Su Huh
Department of Electrical Engineering
Inha University
Incheon, Korea

Woo-Chul Park
EMP Assessment Team
Korea Testing & Research Institute
Yongin, Korea

Sun-Mook Hwang
Hanwha Corporation
Gumi, Korea

***Abstract*—In modern society, the threat of HPEM(high-power electromagnetic) is increasing. If the infrastructure and electronic equipments were attacked in HPEM, confusion will occur socially. From the threat of HPEM, to protect facilities that should block high-power electromagnetic and then electromagnetic shielding effectiveness evaluation of facilities is very important. But, when shielding facilities was constructed, to arrange shielding wall adjacently in the exterior concrete structures is general because of the effectiveness of space and construction cost savings. As between shielding wall and conerete structures is narrow, shielding effectiveness measurement is impossible. In this paper, analyze of the effect on shielding effectiveness by change of the receiving and transmitting antenna position. Shielding effectiveness of shielded room wall and honeycomb were measured. Experimental results, standard deviation of shielding effectiveness by changing the position of the antenna is about 3 ~ 5dB.**

Keywords-Shielding Effectiveness; HPEM; High-Power; SE Electromagnetic

I. INTRODUCTION

To construct HPEM shielding facility, First concrete infrastructure was constructed and then, shielded room was constructed inside the concrete buildings. But, effectiveness of space and construction cost savings in the exterior infrastructure adjacently arranging wall of shielding room is usually. For this reason, gap of between shielding facility wall and exterior concrete infrastructure is narrow. So, shielding effectiveness measurement of shielding facility is difficult. For shielding effectiveness test, as enormous construction costs are consumed, occupying gap of between shielding facility wall and exterior concrete infrastructure is difficult. So in narrow state exterior space of shielding facility, plan measuring shielding effectiveness will show impact effectiveness. If the measurement of shielding effectiveness in a small space possible, construction cost will be saved.

II. Experiment setup

MIL-STD test method is shown Figure 1(a). Experiment is in progress to arrange transmitting antenna in the outside shielding room and exchange transmitting-receiving antenna's position.

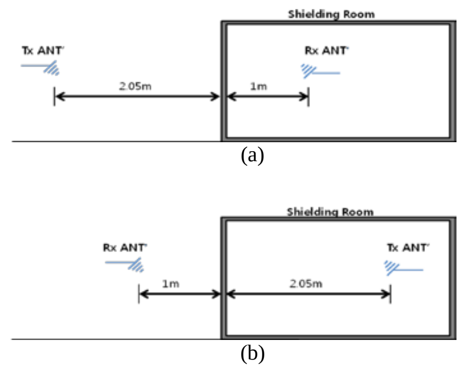

Figure 1. Shielding effectiveness experimental setup. (a)Typical SE test setup (b) Antenna position change setup

III. Experiment result

Standard deviation of specification experimental result is presented in Table. 1. As we measure shielding effectiveness according to position of antenna, from total measurement frequency region. In the case of horizontal polarization, the standard deviation is about 3.1 dB~3.7 dB. In the case of vertical polarization, the standard deviation is about 3.8 dB~4.4 dB. The standard deviation per frequency band is 2.1dB~5.6dB in the horizontal polarization and 1.5dB~6.3dB in the vertical polarization.

TABLE I. Standard deviation According to Tx-Rx Antenna's position.

Shielding wall	Standard deviation	
Frequency	Horizontal	Vertical
Band1 (10kHz~20MHz)	2.3718	2.5799
Band2 (20MHz~100MHz	2.7897	5.8307
Band3 (100MHz~300MHz)	4.1503	4.2312
Band4 (300MHz~1GHz)	3.7328	3.7121
Full Band (10kHz~1GHz)	3.2207	3.9104

The magnitude of standard deviation generated by changing position of antenna is almost similar to that generated by repetitive experiments.

REFERENCES

[1] IEC 61000-1-5, Electromagnetic compatibility (EMC) - Part 1-5 : Genera l - High power electromagnetic (HPEM) effects on civil systems.
[2]MIL-STD-188-125-1, HIGH-ALTITUDE ELECTROMAGNETIC PULSE (HEMP) PROTECTION FOR FIXED GROUND-BASED C4I FACILITIES PERFORMING CRITICAL, TIME-URGENT MISSIONS.

This research was supported by the Standardization program(Project NO. 10042466) of MOTIE(MINISTRY OF TRADE, INDUSTRY & ENERGY)

A High Power Wideband Radiator with a Paraboloidal Reflector Illuminated by an Integrated Antenna-Source

Jiheon Ryu, Jongwon Lee, Jeonghyun Kuk, Jin Soo Choi
The 4th R&D Institute
Agency for Defense Development (ADD)
Daejeon, Republic of Korea
ryujiheon@gmail.com

***Abstract*— This paper presents a high power wideband radiator with a paraboloidal reflector illuminated by an integrated antenna-source (IAS). The reflector is employed to obtain very intensive electric fields because the paraboloidal reflector dramatically increases directivity of the radiated field. The proposed radiator was designed by using a transient analysis of the reflector and an electromagnetic simulation. It is demonstrated by experiments that the proposed radiator has an electric field strength of 52.5 kV/m at a distance of 40 m.**

Keywords-High Power Wideband Radiator, Integrated Antenna-Source, Far Voltage, Paraboloidal Reflector

I. INTRODUCTION

High power wideband radiators (HPWRs) have been investigated for a number of applications such as electromagnetic car stopper, counter improvised-explosive-devices (IEDs). In order to study effects of high power wideband pulses on vehicles and IEDs which are located at a long distance, the radiators with far voltage of megavolt range are required.

In a previous work [1], we developed an autonomous, compact, and robust integrated antenna-source (IAS) system. Because paraboloidal reflectors are capable of achieving high directivity, we apply the paraboloidal reflector as a directive antenna to the IAS. We analyzed the proposed radiator based on a theoretical transient analysis. In addition, the radiated electromagnetic fields are calculated by using an electromagnetic simulation. It was demonstrated by experiments that the far voltage of the radiator is 2.1 MV.

II. DESIGN

Fig. 1 shows the proposed radiator which consists of a high-voltage power supply, a Marx generator, an IAS and a paroboloidal reflector. The transient response of the reflector and the optimum ratio of the focal point to the diameter are analyzed by transient electromagnetic analysis. Based on the analysis, we designed the radiator by an electromagnetic simulation. The diameters of the reflector and the IAS are 1.5 m and 15 cm, respectively.

Fig. 1. Proposed high power wideband radiator.

III. MEASUREMENT

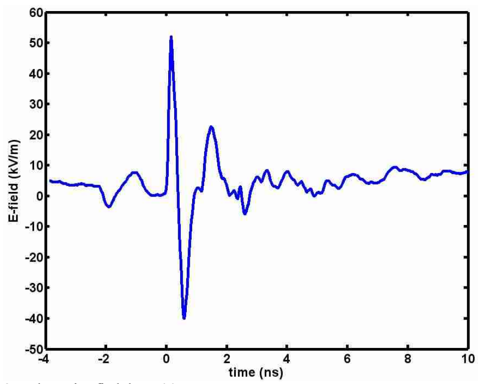

Fig. 2. Electric field at 40 m.

Fig. 2 shows the electric field radiated from the proposed radiator at a distance of 40 m. The peak electric field strength in Fig. 2 is 52.5 kV/m and the peak-to-peak electric field strength of 92 kV/m is obtained from experiments.

REFERENCES

[1] J. Ryu and J. Lee, "An integrated antenna-source system of very high ultra wide-band gain for radiating high-power wide-band pulses," *IEEE Trans. Plasma Sci*., vol. 40, no. 4, pp. 1019–1026, Apr. 2012.

[2] J. Ryu, J. Lee, H. Chin, J.-H. Yeom, H.-T. Kim, H.-O. Kwon, S. H. Han, and J. S. Choi, "A high directive paraboloidal reflector antenna for high far voltage in an ultra wideband source system," *IEEE Trans. Plasma Sci*., vol. 41, no. 8, pp. 2283–2290, Aug. 2013.

JEMS-FDTD and Its Applications in Electromagnetic Scattering and Coupling by Large Complex Object

Li Hanyu, Zhou Haijing
Institute of Applied Physics and Computational Mathematics
Beijing, China

Bao Xianfeng
Software Center for High Performance Numerical Simulation, CAEP
Beijing, China

***Abstract*— A massively parallel electromagnetic field simulation software named JEMS-FDTD (J Electromagnetic Solver-Finite Difference Time Domain) is presented. JEMS-FDTD uses FDTD-related methods to solve the Maxwell equations in time domain. JEMS-FDTD has the capability of solving electric-large problems of thousands wavelengths with hundreds of billions mesh cells, which makes it a suitable tool to simulate electromagnetic scattering and coupling by large complex objects. In this paper, the characteristics of JEMS-FDTD is discussed. As a numerical example, the computation and analyzing of electromagnetic wave scattered and coupled by a building is presented.**

Keywords-computational electromagnetics; FDTD; parallel computation; coupling, scattering

I. INTRODUCTION

The FDTD method [1], which is a simple and direct way to solve the Maxwell equations and easy to implement, has been widely employed to solve various electromagnetic problems for decades. However, FDTD always requires a finer mesh compared to other numerical methods such as MoM, thus limits its application. Recently, as the development of parallel computation technique, FDTD solving electric-large problems becomes possible [2].

II. A BRIEF TO JEMS-FDTD

Despite of the simplicity of parallel FDTD in principle, a high efficiency parallel FDTD program is always difficult to develop because of the complexity and flexibility of parallel computation technique, especially when thousands of processors and hundreds of teraflops of computation performance are involved.

We have been developing a massively parallel electromagnetic field simulation program named JEMS-FDTD since 2008 [3]. JEMS-FDTD is a universal massively parallel electromagnetic field simulation program, which is capable of simulating transient high frequency electromagnetic problems, such as transmitting, propagation, scattering and coupling. JEMS-FDTD adopts FDTD-related methods, including conventional FDTD method, AMR-FDTD. JEMS-FDTD is designed and structured oriented to using thousands of processors with multi-core on HPCs (High Performance Computers), with MPI (Message Passing Interface) and OPENMP (Open Multi-Processing) hybrid-parallel techniques.

Usually, there are two key issues that may constrain the massively parallel computation performance, the load balance and system RAM (Random Access Memory) latency. JEMS-FDTD adopts a four-level hierarchical data structure strategy to deal with these problems. The efficiency test performed on TIANHE-1A super computer shows a high parallel efficiency of >80% of 30000-task parallel computation case (parallel efficiency E is defined by $E = T_s/(T_n\, n)$, where T_s and T_n is the computation time on one processor and n processors respectively. In our test, we considered the efficiency of 600-task parallel computation case is 100%).

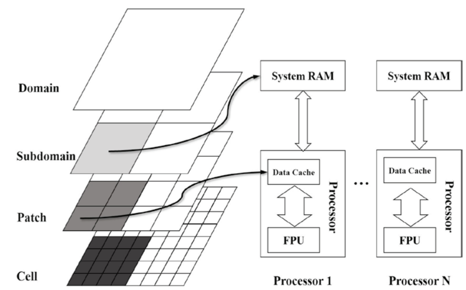

Figure 1. Hierarchical data structure strategy of JEMS-FDTD

III. NUMERICAL EXAMPLES

In this example, the scattering and coupling by a real building is simulated. The dimension of the building is 15m × 7.5m × 13.27m. The electric properties of materials are obtained by field test. The incident wave is set to a wideband pulse from 1 to 3 GHz. A fine mesh of 12.5 billion cells is generated to describe this model. The computation takes approximate 30 hours on 5760 Intel Xeon X5670 2.93GHz processors. The computation result shows good agreement with experiment test.

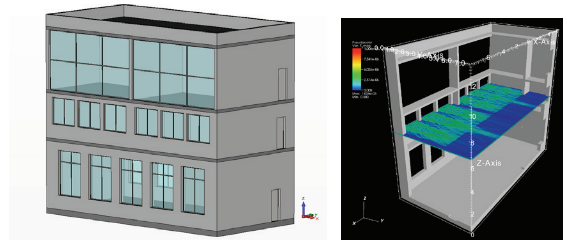

Figure 2. Building model and Electric field distribution on horizontal slice

REFERENCES

[1] K. S. Yee, "Numerical Solution of Initial Boundary Value Problems Involving Maxwell's Equations in Isotropic Media", IEEE Trans. Antennas Propagation, 1966, 17(5):302-307.

[2] V. Varadarajan and R. Mittra, "Finite-Difference Time-Domain (FDTD), Analysis Using Distributed Computing", IEEE Microwave and Guided Wave Letters, Vol.4, No.5, May 1994, pp.144-145.

[3] Li Hanyu, Zhou Haijing, Dong Zhiwei, "Parallel electromagnetic FDTD program design and implementation on JASMIN", 17th International Conference on High Power Particle Beams (BEAMS), July 2008.

Two methods for D-dot sensor designed

Yang Chao[1,2]
1Department of Engineering Physics, Tsinghua University,Beijing,China
2Key Laboratory of Particle & Radiation Imaging(Tsinghua University),Ministry of Education
c-yang13@mails.tinghua.edu.cn

Meng Cui[1,2]
1Department of Engineering Physics,
Tsinghua University,Beijing,China
2Key Laboratory of Particle & Radiation Imaging(Tsinghua University),Ministry of Education
mengcui@mails.tinghua.edu.cn

***Abstract*— With the development of the technology, there are more and more electronic devices around us, forming the complex and harmful electromagnetic environment. Nowadays people pay more attention to the high power electromagnetic environment which can affect the work of the electronical equipment and the health of people, electromagnetic interference covers wide spectrum, ranging from few Hz to few GHz. Therefore, we need some effective method to test electromagnetic field so that we can take the appropriate measurement. According to two methods of measuring transient electric field, we designed two different D-dot transient electric field sensors which have wide bandwidth and good sensitivity**

Keywords- HPEM; D-dot sensor; Bandwidth; TEM cell; Signal recovery

I. INTRODUCTION

We have made two kinds of D-dot sensors, as is shown in Fig.1. The one is monopole antenna, and the other is dipole antenna. The bandwidth of the two D-dot sensors designed is around 1 GHz, The characteristic impedance of the sensors designed is 50Ω. The sensors are available for most of the situation, we make it by ourselves, the volume of the sensors are small and the cost is cheap.

Figure 1. Two kinds of D-dot sensors

The sensors' sensitivity and bandwidth is tested in the TEM cell. The Specific parameters of the two kinds of D-dot sensors are listed in the table.1.

TABLE I. parameters of the two kinds of D-dot

type	Physical height/mm	equivalent capacitance/ pF	equivalent area/cm^2	turning frequency/G Hz
dipole	25	0.367	9.37×10^{-4}	1
monopole	25	3.183	7.72×10^{-3}	1

In the test, Gaussian pulse generator as source and digital oscilloscope which has wide bandwidth were used, as is shown in Fig.2. We use Matlab software to remove interference of the noise and get the original signal. We get the practical bandwidth and sensitivity of the sensors. The later work is to increase the sensor's bandwidth for better application.

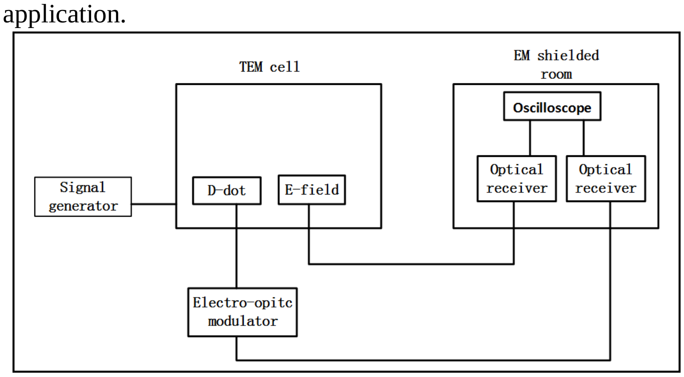

Figure 2. The test system

REFERENCES

[1] De, N. C., et al. "Design and experimental investigation of the asymptotic conical dipole antenna." Electromagnetic Compatibility, IEEE Transactions on 37.2 (1995): 282-285.

[2] Baum, Carl E. "Tiny fast-pulse B-dot and D-dot sensors in dielectric media." Sens. Simulation (2009).

[3] Cui Z, Mao C, Nie X. "E-field sensor design for subnanosecond fast transient." 2012 6th Asia-Pacific Conference on. IEEE(2012): 108-110.

[4] Farr, Everett G., and Joseph S. Hofstra. "An incident field sensor for EMP measurements." IEEE transactions on electromagnetic compatibility 33.2 (1991): 105-112.

ID 051

HPM-Testing of COTS Network Equipment

Go / No Go Test of 19” cabinet in HPM-Simulator SUPRA (Germany)

Markus Nyffeler
armasuisse, Science and Technology
CH-3602 Thun, Switzerland
markus.nyffeler@armasuisse.ch

Armin W. Kaelin
EMProtec GmbH
CH-8340 Hinwil, Switzerland
armin.kaelin@emprotec.ch

***Abstract*— Commercial off the shelf (COTS) equipment is increasingly used in critical infrastructure applications. Mission critical electronics is usually HEMP-protected by expensive shielding and filtering techniques. To understand the effects of newer threats such as IEMI, this work describes a HPM go / no go test. This test investigates the behavior of electronics protected by shielding and filtering components readily available on the market to protect against HEMP. The equipment and some meters of cables which form a loop to monitoring equipment outside the test chamber are exposed to HPM-radiation. The system is permanently monitored while irradiated with different HPM field levels and frequencies.**

Keywords: HPM, HPM-testing, computer network components, IEMI, SUPRA, COTS, 19” EMC enclosure, HEMP-filters

I. Introduction

Many critical infrastructure applications increasingly rely on commercial off the shelf (COTS) electronics rather than using dedicated and especially hardened equipment. Especially in the fast progressing information technology commercial equipment provides the benefits of the latest technology at an unbeatable price. To cope with HEMP and other EM-threats such as IEMI [1] mission critical equipment is usually installed in especially hardened facilities consisting of shielded rooms and special protection filters against conducted threats. In this work we investigate a partial protection concept of computer network components using commercial off the shelf protection components, which are placed in a cabinet. The whole cabinet including the attached wires are irradiated by High-Power Microwaves (HPM).

II. Equipment under Test and Test Setup

A. Equipment under Test

For this test commercial network components were installed in a commercially available 19” cabinet (Schroff®) designed for EMC applications. This cabinet uses a frame, which is fitted with conductive textile EMC gaskets, which link the cover metal sheets in an electrical conducting manner. According to the manufacturer this construction provides a shielding effectiveness of 60 dB up to 1 GHz and 40 dB up to 3 GHz. All cabling attached to the cabinet are protected by commercially available HEMP- and lightning protection components (Meteolabor®) which are installed in a feed-through panel of the cabinet.

B. Test Setup

The equipment under test (EUT) is placed in the anechoic chamber of the German HPM-simulator SUPRA [2] at a distance of 14 m from the antenna (see schematic test-setup in Fig.1). The cabinet and several meters of cables are illuminated by the HPM-radiation in the frequency range from 0.9 to 1.5 GHz. The other ends of the cables are fed through the same types of EMP-filters to a monitoring room outside the anechoic chamber, where the data from the network components are permanently monitored and fed back to the cabinet in a closed loop manner.

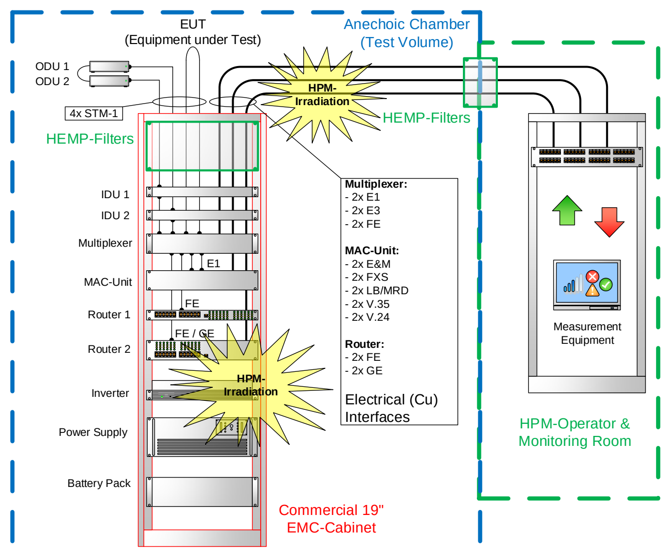

Figure 1: Schematic HPM Test-Setup

III. Results and Conclusions

The protection by commercial components results in a considerably improved immunity of the system against HPM compared to an unshielded setup. No damages occurred during this test. In some configurations various disturbances have been observed. More details will be presented during the conference.

References

[1] Workshop on “Electromagnetic Terrorism and Adverse Effects of High Power Electromagnetic (HPE) Environments”, Proceedings of the 13th International Zurich Symposium and Technical Exhibition on Electromagnetic Compatibility, February 16-18, 1999

[2] IEC/TR 61000-4-35, Technical Report, HPEM-Simulator Compendium, 2009-07, IEC Geneva, Switzerland

---

Work done in collaboration with WIS, Munster, Germany

ID 052

A Compact HEMP Test System based on Movable Electrode

Ke-jie LI, Yan-zhao XIE
State Key Laboratory of Electrical Insulation and Power Equipment
School of Electrical Engineering, Xi'an Jiaotong University
Xi'an, Shaanxi Province, China
kejie.li@hotmail.com

Abstract—A compact HEMP test system was introduced. The core component was a high-voltage pulse generator with a RC circuit. Unlike normal spark gap switches used in other generators[1], however, a movable electrode was built in, which makes it possible to be triggered by means of adjusting the gap distance. The output waveform characterizes 2.5ns rise time, 23ns pulse width and 10kV maximum voltage. With a TEM cell and 50Ω matched load, it can produce 50kV/m electromagnetic field in laboratory.

Keywords—HEMP Generator; EMP; Spark Gap Switch; Movable Electrode;

I. Introduction

There is a need of standard electromagnetic field with known waveform to test small devices. The IEC gives 50kV/m a significant value of HEMP field, which can be simulated with low-height TEM cell in a small place. However, kinds of spark gap switch are indispensable to form a wave front with nanosecond rise time. These switches have dispersion on break down voltage and break over time.

Thus, a switch with a movable electrode was fabricated. The gap distance can be adjusted from outside by a cylinder. The gap is so long that it can hardly self-break down before being triggered. Then the gap was shortened to form a discharge spark, conducting the path and decreasing the inductance.

II. Construction of the Generator

A. Structure of Movable Electrode Switch

In order to move the electrode outside the switch, the cavity was divided into two isolated parts: one is for the switch and another one is for a cylinder which can push its piston forward or backward. The following figure shows the details:

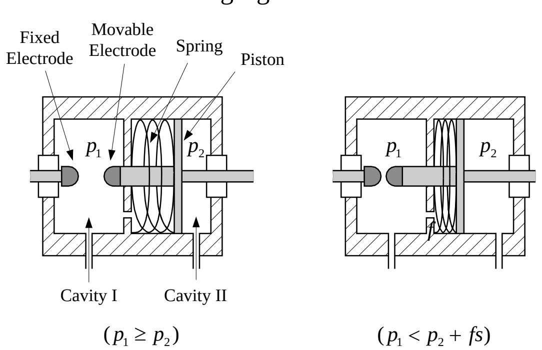

Fig. 1 A fig to show how the movable electrode moves

There are two electrodes in the Cavity I, which has invariant pressure of nitrogen denoted as p_1. The Cavity II, with a piston and spring, is size-changeable. The pressure caused by compressed air, is denoted as p_2. Whenever $p_1 \geq p_2$, the piston is at the end of the right side, making the connected electrode far from another. If the p_2 increases, the piston starts to compress the spring, the electrode moves and as a result, the gap distance decreases. It won't hold too long before the whole gap breaks down.

B. Principle of the Generator

The equivalent circuit of the generator was a typical RLC circuit. When $R > 2\sqrt{\frac{L}{C}}$, the voltage got from the resistor approximates:

$$u_R(t) \approx U_0\left(e^{-\frac{t}{RC}} - e^{-\frac{t}{L/R}}\right) = U_0\left(e^{-\frac{t}{\tau_2}} - e^{-\frac{t}{\tau_1}}\right) \qquad (1)$$

where $\tau_1 = L/R$, $\tau_2 = RC$.

We chose $R = 50\Omega$ and in order to get a double exponential waveform with 2.3ns/25ns, L and C were respectively 56.8nH and 666.7pF, with which the whole circuit were determined.

III. The Measurement and Test of the System

A TEM cell was made to form an EMP field and test the object in it. The size was designed to make the wave impedance 50Ω, which is matched with both sides. In our measurement test, a coaxial attenuator was connected to decay the amplitude of the output pulse, whose input impedance was also used as the load. The setup of the experiment can be seen in Fig. 2.

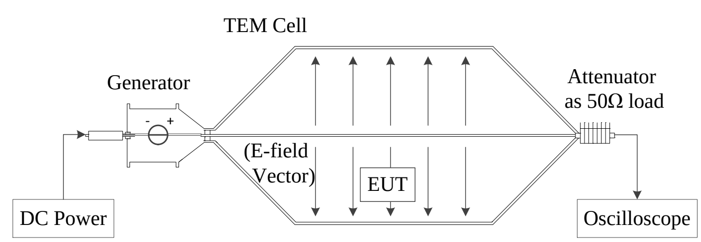

Fig. 2 The setup of the HEMP test system

IV. Conclusion

A HEMP test system was made with kinds of movable electrode switch built in and the compact size and stability was achieved.

References

[1] TAN Jian-wen, SHI Li-hua, LI Yan-xin, ZHANG Li-qun and XIE Yan-zhao, "Development and experimental research on the fast rise time EMP generator", High Power Laser and Particle Beams, Vol.16, No.11, Nov. 2004, pp1434-1436.

ID 053

Comparison of two analytic approaches for the Prediction of EMP Coupling to Multiconductor Transmission Lines

Jun Guo, Yan-zhao Xie, Qing Liu
State Key laboratory of Electrical Insulation and Power Equipment
Electrical Engineering College, Xi'an Jiaotong University
Xi'an, Shannxi, China
gjgjgj@stu.xjtu.edu.cn, yzxie@mail.xjtu.edu.cn, liuqing623nn@163.com.

***Abstract*—The distributed analytical representation and iterative technique (DARIT) Jacobi iteration (Jacobi-DARIT-field) method has been proposed for the calculation of electromagnetic pulse (EMP) radiated field coupling to multiconductor transmission lines (MTLs). More recently, based on the Jacobi-DARIT-field method, the Seidel-DARIT-field method (the DARIT-field method which adopted the Gauss-Seidel Iteration Algorithm) has been developed as well. This paper compares these two methods from the points of view of the accuracy and convergence speed, etc.**

Keywords-analytical solution; Gauss-Seidel iteration; electromagnetic pulse; iterative method; transient analysis; transmission line modeling; waveform relaxation.

I. INTRODUCTION

To predict the effects of EMP coupling to multiconductor transmission lines (MTLs), many researchers have proposed the method of modeling of EMP coupling to MTLs [1]-[2]. In 2013, Y.-Z. Xie, J. Guo and F. Canavero proposed an approach using the distributed analytical representation and iterative technique (DARIT) method which is based on the Waveform Relaxation and Transverse Partitioning (WR-TP) for the response computation between multiconductor transmission lines illuminated by the incident EMP field [1]. Hereafter, this algorithm is named Jacobi iterative method of DARIT-field (Jacobi-DARIT-field). The algorithm can avoid the need for inversing the matrix when solving MTLs equations and leading to high computational efficiency.

Based on the Jacobi-DARIT-field method, another DARIT-field method employing the Gauss-Seidel Iteration Algorithm (Seidel-DARIT-field) has been developed [2]. This paper provides comparison result between these two methods.

II. OUTLINE OF THE TWO METHODS

By applying waveform relaxation techniques [2] to the Telegrapher's equations, we obtain a recursive set of decoupled differential equations in:

$$\frac{dv_i^{(r+1)}(x,s)}{dx} + z'_{ii}(\omega) i_i^{(r+1)}(x) = -\sum_{j=1, j\neq i}^{N} z'_{ij} i_j^{(r+1)}(x,s) + V'_i(x,s)$$

$$\frac{di_i^{(r+1)}(x,s)}{dx} + y'_{ii}(\omega) v_i^{(r+1)}(x) = -\sum_{j=1, j\neq i}^{N} y'_{ij} v_j^{(r+1)}(x,s) + I'_i(x,s) \qquad (1)$$

The algorithm of iteration 1 of the two methods is the same, it only takes the illuminating EMP wave into account. At iteration 2, each line is excited not only by the incoming EMP wave but also by the coupling effects of all the other adjacent lines, this is where the main difference between the two methods happen:

- Jacobi-DARIT-field method handles every line parallelly and updating the state of lines based on the state of lines at the previous iteration.
- Seidel-DARIT-field method handles every line one by one. It update the state of *n*th line based on the state of line 1~n-1 at the present iteration and line n+1~N at the previous iteration.

The details of the two methods are proposed in [1], [2].

III. VALIDATION OF THE PROPOSED ALGORITHM

A validation example is proposed to give a comparison between the two methods. In the example, a symmetrical and lossy three wires with the length of 7.5 cm, height of 2 mm and diameter of 0.2 mm which above the lossy ground is considered. The loads on both sides are 50 Ω. There are three cases in this example with the distance between wires of 6.76 mm, 2.14 mm and 1.50 mm to make the coupling factors (the expression of CF see [1]) equal to 0.05, 0.25 and 0.35, respectively. Fig. 1 shows the frequency response of wire #1 obtained with the two methods and with the conventional one (Chain Parameters Matrix method). The results of the relative errors ε after Iteration 3 and 4 of the two methods are presented in Table I. It can be seen that the results from iteration 3 of Seidel-DARIT-field are more convergent than them from iteration 4 of Jacobi-DARIT-field.

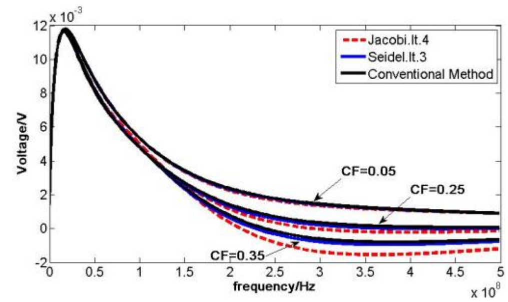

Figure 1. The far-end response of wire 1 with different coupling factors.

TABLE I. RELATIVE ERRORS OF THE EACH METHOD

CF	ε (%)		
	Jacobi.It.3	***Jacobi.It.4***	***Seidel.It.3***
0.05	0.049	0.029	0.012
0.25	0.330	0.198	0.095
0.35	1.000	0.925	0.385

V. CONCLUSION

The validation result shows that Seidel-DARIT-field method has a faster convergence speed than Jacobi-DARIT-field method. However, it is worthy to note that the current Seidel-DARIT-field method is not so convenient for the very large conductors case, which is still an open problem.

REFERENCES

[1] Y. Z. Xie, J. Guo and F. Canavero, ``Analytic iterative solution of electromagnetic pulse coupling to multiconductor transmission lines," IEEE Transactions on Electromagnetic Compatibility, vol.55, no.3, pp.451-466, June 2013.

[2] J. Guo, Y. Z. Xie and F. Canavero, ``Gauss-Seidel Iterative Solution of Electromagnetic Pulse Coupling to 3-Conductor Transmission Lines," submitted to IEEE Transactions on Electromagnetic Compatibility.

Design Of High Current HEMP Filters For Reliability

William H. Turner
Engineering Dept
MPE Ltd
Liverpool, Merseyside, UK
WTurner@MPE.co.uk

David Rimmer
Engineering Dept
MPE Ltd
Liverpool, Merseyside, UK
DRimmer@MPE.co.uk

***Abstract*— Most High Altitude Electromagnetic Pulse (HEMP) protection filters are used in critical infrastructure protection applications and therefore reliability is of paramount importance. This paper covers the key design factors affecting the reliability of these filters with a focus on high current ratings.**

Keywords-High Altitude Electromagnetic Pulse (HEMP); Nuclear Electromagnetic Pulse (NEMP); MIL-STD-188-125; reliability; filters;

I. Introduction

MIL-STD-188-125 is the standard normally used to define performance requirements of HEMP filters for critical infrastructure applications. This requires verification testing of HEMP filters when first installed. However, to ensure continued protection the HEMP filter must also perform without failure or degradation over its entire service lifetime. A good maintenance plan is important to identify any degradation of performance but is not a substitute for reliable filters.

II. Key Design Factors

Key factors affecting reliability of electrical devices derived from MIL-HDBK-217 include operating temperatures of components, and safety margins on voltage and current ratings. With regards to filters, these reliability factors impact on the choice of capacitor and inductor materials, their design and integration into the filter enclosure, and the choice of material for the filter enclosure.

A. *Voltage Safety Margins*

The voltage safety margin has a direct impact on the reliability of capacitors. A large ratio of capacitor test voltage to working voltage reduces electrical stress from voltage transients experienced by the filter over its service life. The use of self-healing capacitor technology further improves reliability allowing the capacitor to recover from minor overvoltage transients. Empirical measurements on filters in service demonstrate the benefit of this approach. Figure (1) shows the measured capacitor parameters of 42 filters after 20 years of continuous service utilising self-healing filter capacitors with a voltage safety margin of greater than 6:1. The plot shows little change in capacitance value after 20 years. There were also no electrical failures of any of the filters in service although some transient suppression varistors had been replaced.

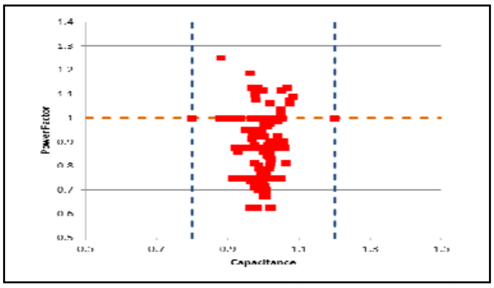

Figure 1. Normalised capacitance of filters after 20yrs of service

B. *Temperature Rise*

Higher temperatures have a negative impact on reliability therefore maintaining cool running of a filter is vital. There will inevitably be greater heat dissipation in high current filters and any shortfalls in the design or manufacture will have exacerbated consequences; one problematic area is enclosure design and material choice where there can be a conflict between shielding performance and eddy current heating effects.

Figure (2) shows the eddy current heating effect on three shielding barriers of different grades of steel with a 1200A conductor passing through. It follows that without careful material selection any filter enclosure could introduce serious eddy current heating to a filter, shortening its service life.

By taking this into account in the design of a 1200A filter, it was possible to reduce the overall case temperature rise above ambient, at full load current, from 30°C to 18°C; this translates to a calculated MTBF improvement from 256,000 hours to 406,000 hours. This will result in significantly improved reliability in service.

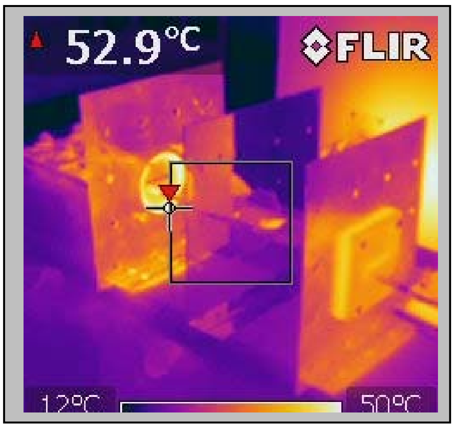

Figure 2. Eddy Current Heating in Steel Barriers

Statistical model for coupling of EM energy through apertures

The random coupling model

Thomas M Antonsen Jr, Steven Anlage, and Edward Ott

IREAP, University of Maryland
College Park, MD USA

Gabriele Gradoni
Faculty of Science
Nottingham University
University Park Nottingham NG7 2RD UK

***Abstract*— A statistical model for the coupling of electromagnetic radiation into enclosures through apertures is presented. The model gives a unified picture bridging deterministic theories of aperture radiation, and statistical models necessary for capturing the properties of irregular shaped enclosures. The enhancement of coupled radiation due to aperture resonances will be emphasized, and general formulas for the statistics of the radiation entering the cavity and reaching an antenna in the cavity will be presented. In the high and low loss cases these formulas have particularly simple forms that can be used to assess coupling in specific cases**

-

Keywords: Aperture, quality factors, voltage statistics

I. INTRODUCTION

The coupling of electromagnetic radiation into enclosures or cavities through apertures both electrically small and large has attracted the interest of electromagnetic community for many years. Full solutions of this problem are particularly complicated because of the mathematical complexity in the solution of the boundary-value problem and because of the sensitivity of the solution to the detail of the enclosure's dimensions, content, and the frequency spectrum of the excitation. These difficulties have motivated the formulation of a statistical description (known as the random coupling model, RCM [1], [2]) of the excitation of cavities, in particular the linear relation between voltages and currents at ports in the cavity, when the ports are treated as electrically small antennas.

The RCM has recently been extended to the case of apertures [3] of arbitrary size. In this treatment the aperture is characterized by an admittance matrix that relates the amplitude of the tangential component of the electrical field in the aperture to the amplitude of the transverse components of magnetic field. Field components are represented as a superposition of basis functions whose amplitudes are voltages and currents related by the admittance matrix. The matrix takes on two generic forms: a radiation admittance that applies to the case in which the aperture faces free space and a cavity admittance that applies when the aperture is backed by a cavity. The cavity admittance is a statistically fluctuating quantity, with properties derived from random matrix theory, that account for the uncertainties in the spectrum and properties of modes of the cavity in question. The cavity is then characterized by the spectral density of modes and an average loss factor.

Coupling to an antenna in the cavity is included in the model by augmenting the admittance matrix of the aperture with the impedance matrix of the antenna, including a load impedance on the antenna. This results in a matrix circuit equation that gives the voltage on the antenna's load in terms of the amplitude of a plane wave incident on the aperture.

A sample plot of power delivered to the load as a function of frequency is shown in Fig. 1. Interestingly, the resonant frequencies of the aperture are not in the range of frequencies displayed in Fig.1. Yet they play a strong role in the large enhancements in coupled power depicted. A general expression describing this effect will be presented.

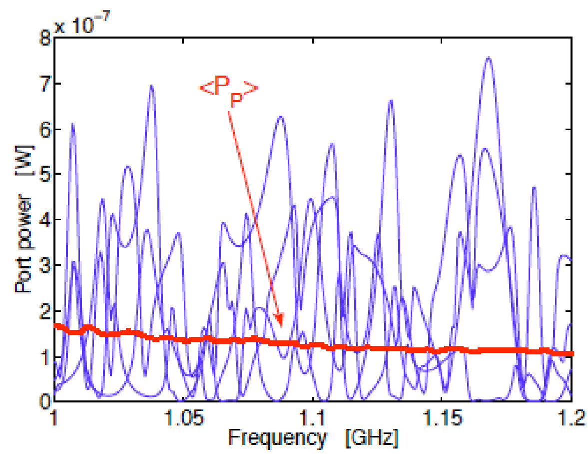

Figure 1. Power coupled through a 25 cm by 2 cm aperture in a cavity wall to a small antenna. Shown in blue are several individual realizations of the cavity, and in red the average over 800 realizations.

REFERENCES

[1] X. Zheng, T. M. Antonsen, and E. Ott, "Statistics of impedance and scattering matrices in chaotic microwave cavities: Single channel case," *Electromagnetics*, vol. 26, p. 3, 2006.
[2] ——, "Statistics of impedance and scattering matrices of chaotic microwave cavities with multiple ports," *Electromagnetics*, vol. 26, p. 33, 2006
[3] G. Gradoni, T. M. Antonsen, E. Ott and S. Anlage, submitted to IEEE Trans EMC.

Supported by the Office of Naval Research

Subnanosecond Pulses for Electrostimulation

Shu Xiao[1,2], Andrei Pakhomov[2], Dongkoo Kang[2], Karl H. Schoenbach[2]

[1]Department of Electrical and Computer Engineering, Old Dominion University, Norfolk, VA, USA

[2]Frank Reidy Research Center for Bioelectrics, Old Dominion University, Norfolk, VA, USA email: sxiao@odu.edu

***Abstract*—Subnanosecond pulses can be delivered with impulse antennas, offering the potential for noninvasive treatment of subcutaneous tissue. The pulse duration, 100–200 ps, makes it possible to focus the radiation on the target efficiently and produces a focal spot of 1-cm^3 in the tissue. We found that very intense electric fields are needed to cause significant cell death, making it difficult to use antennas. Other effects, such as membrane permeabilization or stimulation of action potentials, however require lower electric fields, which makes the approach of pulse delivery with antennas more practical. This paper presents the typical pulse parameters for electrostimulation and discusses possible pulse delivery methods for *in vitro* and *in vivo* models.**

Keywords- subnanosecond pulses, electrostimulation

I. INTRODUCTION

A previous study [1] showed that for the 800-ps pulses and an electric field of 150 kV/cm, approximately 18,000 pulses were required in order to cause 50% B-16 cell death. For a moderate field intensity of 20 kV/cm [2], increasing the pulse repetition rate caused an increase of cell killing partially due to the increase in temperature. A recent experiment on liver cancer cells [3] also confirmed the role of temperature elevation in facilitating cell death.

While cell death may require a large number of high intensity subnanosecond pulses, moderate or mild effects, such as the increase of cell membrane conductance, can be induced with much fewer pulses. In neuroblastoma cells (NG-108) for example [2], after exposure to 1000-2000 pulses, the inflow of current was measured, an indication of increased membrane conductance. The modification of membrane transport processes by subnanosecond pulses suggests the feasibility of stimulating excitable cells.

A whole-cell current clamp recording configuration was used to measure the membrane voltage of the neurons [4]. The selected neurons were patched before subnanosecond pulses were applied. The current varying in a stepwise fashion was injected to the neurons and subsequently subnanosecond pulses were applied (100 pulses within 200 ms) in the course of the constant current.

II. RESULTS

Shown in Fig.1 is a neuron stimulated by subnanosecond pulses. An immediate increase of the membrane potential (depolarization) was observed (Fig.1a), regardless of whether the cell was hyperpolarized or depolarized by the injection current. The increased potential stayed as long as the pulses were applied. But it was within the rising phase, i.e., in the first 30 ms, that the firing of an action potential was recorded. The time it took was somewhat correlated with the membrane potential at the instant of the pulse application. For instance, when the injection current was held steady (-100 pA), the action potential was recorded after 20 pulses. But fewer pulses were needed to induce the action potential if the injection current had already caused depolarization. The neurons may not fire an action potential at all if the cells were hyperpolarized. We note that stimulating with subnanosecond pulses will not cause any damage to the neurons, evidenced by their capability to fire the action potentials repeatedly. Shown in Fig.1b is a neuron stimulated 20 times at 1 Hz under the same pulse conditions, indicating that this method is safe and reliable.

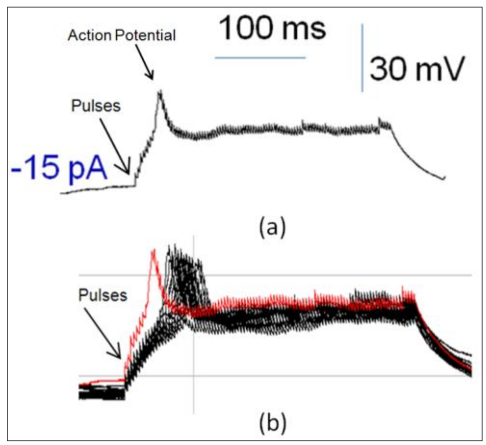

Figure 1. A neuron was stimulated by subnanosecond pulses *in vitro*. a) The neuron was clamped by a constant current (-15 pA) and subnanosecond pulses were applied to induce the depolarization. An action potential was fired approximately 30 ms after applying the subnanosecond pulses; b) Repeated firing of the action potentials at 1 Hz by the same neuron for 20 stimulations in a row.

REFERENCES

[1] K. H. Schoenbach, S. Xiao, R. P. Joshi, J. T. Camp, T. Heeren, J. F. Kolb and S. J. Beebe, "The Effect of Intense Subnanosecond Electrical Pulses on Biological Cells," IEEE Trans. Plasma Science, 36 (2), p.414-422, April, 2008.

[2]S. Xiao, S. Guo, V. Nesin, R. Heller, and K. H. Schoenbach, "Subnanosecond Electric Pulses Cause Membrane Permeabilization and Cell Death," IEEE Trans. Biomedical Engineering, 58(5), 2011.

[3] J. T. Camp, Y. Jing, J. Zhuang, J. F. Kolb, S. J. Beebe, J. Song, R. P. Joshi, S. Xiao, and K. H. Schoenbach, "Cell Death Induced by Subnanosecond Pulsed Electric Fields at Elevated Temperatures," IEEE Trans. Plasma Science, 40(10), p.2334-2347, October, 2012.

[4] S. Xiao, A. Pakhomov, F.Guo, S. Polisetty, and K. H Schoenbach," Neurostimulation Using Subnanosecond Electric Pulses," SPIE Photonics West, Bios, Terahertz and Ultrashort Electromagnetic Pulses for Biomedical Applications, Feb.2-7, 2013, San Francisco, CA, doi:10.1117/12.2003341.

Sponsors: ODU Office of Research, NIH, R21(1R21EB016912-01A1)

Influences of Electrical Pulse Disturbances on Digital Device Operation

Yu. V. Parfenov, B. A. Titov, L.N. Zdoukhov
Russian Academy of Sciences
Joint Institute for High Temperatures
Moscow, Russia
e-mail: Parfenov@ihed.ras.ru

W. A. Radasky
Metatech Corporation
Goleta, California USA
e-mail: wradasky@aol.com

***Abstract*—The method of calculating the parameters and characterizing the degree of pulse electrical disturbances influence on digital devices functioning is considered here. By means of this method, assessments of the consequences of the repetitive pulse disturbance influence on digital devices functioning on such factors as the pulse disturbance waveshape, its duration, its peak, and the mode of coding data being transmitted, etc. were carried out.**

Keywords-IEMI; data transmission; pulse disturbances;

I. Introduction

In the situation of a pulse electromagnetic field incident on a digital device, its case and external circuits are subjected to direct electromagnetic influence. Generally the case is made of metal, serving as a screen decreasing the level of electromagnetic field penetrating into the device. However, the case screening effect is restricted by its imperfections (port-of-entries, joints etc.). These imperfections are the channels for the electromagnetic field penetration into the case. As a rule the internal wiring elements are the main receptors receiving the penetrating field influence. The pulse electrical disturbances, which can lead to the distortions of data circulating among separate digital devices, are being induced in all of them.

The analytical method for calculating the occurrence of error probability in transmitting data packets under the influence of repetitive pulse disturbance has been offered in [1, 2]. Using this method enabled us to solve a range of practical tasks. For example, it can be effective in choosing the optimal values of average signal power-to-repetitive disturbance average power and disturbance repetition frequency-to-data transmission rate ratios, under which the most effective disturbance influence on actual digital devices is noticed. It should be added also, that the method underwent an experimental check, which showed that it adequately reflects the real mechanisms and regularities of repetitive disturbance influence on digital devices [3].

II. Algorithm of Modeling

As opposed to available analytical methods, a numerical method permits us to estimate the concrete consequences of the repetitive pulse disturbance influencing the function of digital devices in dependence on such factors as pulse disturbance waveshape, its duration, its peak value, the mode of coding data being transmitted, etc. For example, the algorithm proposed here provides for the assigning of several coding modes, namely NRZ, RZ, Manchester, four-level and eight-level codes.

The results of the examination of the listed factors' impact on the quantity of the received data packets containing errors caused by the pulse disturbance influence are given in the presentation. In all cases it was assumed that transmission of 1000 packets of 1000 binary bits with a 10^8 bps rate would be performed. The amplitude of the signal being transmitted is equal to 2.5 V.

In the work presented here we have used the so-called "algorithm of the ideal receiver" as described in [4].

III. Influence of Various Factors

In this part of the paper the influence of four different factors are considered in detail:

- The shape of the pulse disturbance waveform
- The duration of the pulse disturbance
- The peak of the pulse disturbance
- The mode of the data coding

IV. Conclusions

The numerical method of assessment of digital devices immunity to repetitive pulse disturbance influence has been offered. It permits us to assess the consequences of the repetitive pulse disturbance influence on digital devices in dependence on such factors as the disturbance waveshape, its duration, its peak value, the mode of data coding, etc. To demonstrate the capability of this method some example calculations have been performed.

References

[1] Kohlberg I., Carter R., "Some theoretical considerations regarding the susceptibility of information systems to unwanted electromagnetic signals," Proc. of the 14th Int. Zurich Symposium on EMC, Zurich, Switzerland, February 20–22, 2001, p. 41–46.

[2] Parfenov Yu., Kohlberg I., Radasky W, Titov B., Zdoukhov L., "The Probabilistic Analysis of Immunity of the Data Transmission Channel to Influence of Periodically Repeating Voltage Pulses," Asia-Pacific EMC Week and Technical Exhibition, Singapore, May 19-23, 2008.

[3] Parfenov Yu., Titov B., Zdoukhov L., Radasky W., "Results of experimental research of IEMI effects on a model of a typical computer network," EMC Workshop, Paris, June 14-15, 2007, CD-ROM, paper #1, 4 pages.

[4] Bernard Sklar, Digital Communications. Fundamentals and Applications, Prentice Hall, PTR, Upper Saddle River, New Jersey 07458, www.phptr.com, 2nd edition, 2001, 1079 pages.

Transmission Cross Section for Apertures and Arrays Calculated Using Time-Domain Simulations

Ronny Gunnarsson and Mats Bäckström
Saab Aeronautics
Saab AB
Linköping, Sweden

***Abstract*—Despite continuing advancements regarding computer technology and simulation software, having access to analytical equations that can be used to reduce the computational burden is still desirable. Transmission cross sections are presented for a number of apertures and arrays in perfectly conducting, and infinitely thin, ground planes. Comparisons are made between results obtained from numerical simulations, analytical equations as well as semi-analytical calculations obtained by combining analytical equations with numerical results.**

Keywords-transmission cross section; time-domain simulation; transmission line model; finite-difference time-domain (FDTD); finite integration technique (FIT)

I. INTRODUCTION

Knowledge of the transmission cross section of apertures and arrays constitutes an important factor in the design and analysis of shielding structures. With the continuing advancements regarding computer technology and simulation software, the shielding performance of increasingly complex apertures can today be studied using accurate full-wave simulations. Having access to analytical equations that can be used to calculate the transmission cross section, or at least reduce the computational burden, is, however, still desirable. In this study the transmission cross section of different types of geometrically simple apertures are presented and comparisons are made between results from numerical simulations, analytical equations and semi-analytical calculations obtained by combining analytical equations with numerical results.

II. TRANSMISSION CROSS SECTION

Using antenna theory an analytical equation can be derived describing the ratio between the transmitted power, P_N, from an array of dipoles and the transmitted power, P_1, from a single dipole [1]. This ratio is given by

$$\frac{P_N}{P_1} = N - 6\sum_{n=1}^{N}(N-n)\left[\frac{\cos nkd}{(nkd)^2} - \frac{\sin nkd}{(nkd)^3}\right] \qquad (1)$$

where N is the number of elements in the array, k is the free-space wavenumber and d is the distance between the dipoles. The validity of (1) was tested by comparing results from a FDTD-simulation on an array consisting of four 40×5 mm^2 sub-apertures separated by 3 mm with semi-analytical results obtained by combining (1) with a FDTD-simulation on a single 40×5 mm^2 aperture, see Fig.1. Apart from an overshoot at first resonance, there is excellent agreement between the semi-analytical results and the “correct” numerical results. The discrepancy at resonance is due to a strong aperture coupling, which is not included in (1). The reduction in simulation time using the semi-analytical approach is approximately proportional to N.

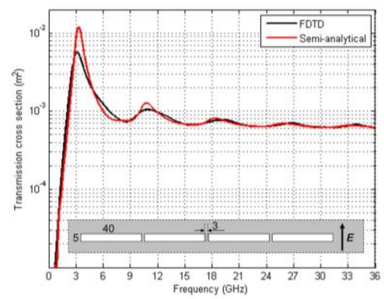

Figure 1. Transmission cross section (m^2) for an array of four sub-apertures of size 40×5 mm^2 and a separation of 3 mm. FDTD-simulation on the entire array (black) and semi-analytical results (red).

The validity of a previously reported transmission line model [2] has been investigated for rectangular apertures with moderately small values on the length-to-width ratio. The transmission line model was found to provide accurate results when the ratio exceeds approximately five. By combining the transmission line model in [2] with (1) an analytical solution is obtained for the transmission cross section. Fig.2 compares the analytical solution with the numerical solution for two linear arrays. Very good agreement is obtained for frequencies up three times the first resonance frequency.

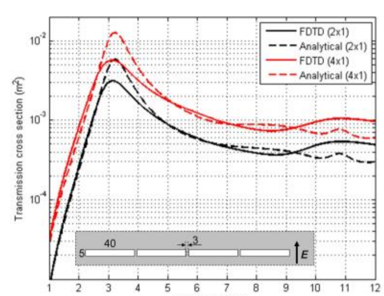

Figure 2. Transmission cross section (m^2) for arrays with two (black) and four sub-apertures (red) of size 40×5 mm^2 and a separation of 3 mm. FDTD-simulations on the entire array (solid) and analytical results (dashed).

REFERENCES

[1] T. Martin, M. Bäckström and J. Lorén, “Semi-Empirical Modeling of Apertures for Shielding Effectiveness Simulations”, IEEE Trans.on EMC, vol. 45, no. 2, May 2003.

[2] Larry K. Warne and Kenneth C. Chen, “A simple transmission line model for narrow slot apertures having depth and losses”, IEEE Trans. on EMC, vol.34, no.3, August 1992, pp.173-182.

Measuring DC Voltage using Acoustic Wave Propagation in $LiNbO_3$

Nishant Patel,[1] Darren Branch,[2] Stefan Cular[1]
[1]Primary Electrical Standards
[2]Biosensors and Nanomaterials
Sandia National Laboratories
Albuquerque, NM 87185 USA

Edl Schamiloglu[3]
[3]Dept. of Electrical and Computer Engineering
University of New Mexico
Albuquerque, NM 87131 USA

***Abstract*—Two different cuts of lithium niobate ($LiNbO_3$) were monitored with an acoustic wave prior, during, and after DC high voltage (HV) was applied to the crystal. The data show that the voltage (256 V to 1,100 V) induced shift in the acoustic wave arrival time scales quadratically for 0º X-cut and linearly for 36º Y-X cut. The amount of voltage induced shift measured ranged from 10 ps-273 ps for 0º X-cut and -2.6 ps to -17.2 ps for 36º Y-X cut. The response difference between the two crystal cuts was attributed to the type of mode propagation in each crystal. Measured DC data is compared to both theory and a 1-D impedance matrix model. This presentation describes progress towards developing a new high voltage sensor.**

Keywords-DC High Voltage, Measuring Instruments, Electrical Measurements, Acoustic Waves, Lithium Niobate

I. Introduction

Performing high voltage (> 10 kV) measurements with a high degree of accuracy typically requires using a voltage divider. Piezoelectric crystals offer advantages for HV sensing, including relative high electric field breakdown voltage and operability over a large frequency range. The presentation focuses on using $LiNbO_3$ as a HV sensing element for direct voltage measurement without dividers or an electrostatic meter.

II. Experimental Setup and Results

In this experiment, an acoustic wave propagated through the crystal and was monitored before, during, and after the HV was applied. Two transducers were controlled by a pulser/receiver system. A time interval counter was used to monitor the difference in the baseline acoustic wave propagation and propagation while a voltage was applied.

The voltage induced shift versus voltage was measured for two crystal cuts using a DC voltage range from 256 V to 1100 V. Figure 1 shows the results for both crystal cuts. The 36º Y-X cut, which propagates a longitudinal mode, showed good agreement with linear piezoelectric theory. For the 0º X cut case, the linear theory breaks down before 640 V. In order to explain the deviation in linear piezoelectric theory for the latter case, a 1-D impedance matrix model in the frequency domain was used to estimate the voltage induced shift in time by inputting a calculated change in length, Δl, due to voltage strain. For calculating strain, a simplified version of the linear piezoelectric constitutive strain relation was used:

$$S_i = d_{ji} E_j \quad (1)$$

where the subscript i ranges from 1 to 6 and j ranges from 1 to 3, S is the strain, d is the piezoelectric constant, and E is the electric field. An inverse transform of the impedance was performed to extract the time response for the matrix model. The simplified equation assumes that the mechanical strain on the crystal is negligible compared to the strain from an applied electric field.[1]

For 36° Y-X $LiNbO_3$, a single d_{ji} term is needed, d_{21}, since only a longitudinal mode is excited at this cut angle. For the 0° X $LiNbO_3$ crystal, both a longitudinal wave and shear wave can be excited. It was found that between 256 V – 512 V, a longitudinal mode with d_{11} term was used to explain the measured data. In the range of 512 V – 768 V, a fraction of both the shear mode and longitudinal mode contribute to the response. For voltages >768 V, both modes fully contribute to the strain.

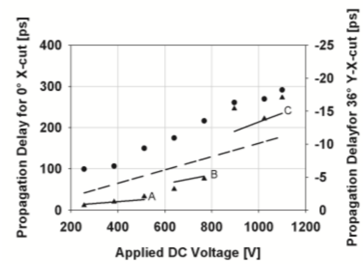

Figure 1: Measured response of 36° Y-X-cut $LiNiBO_3$ (circles, right axis) and 0° X-cut $LiNiBO_3$ (triangles, left axis) for DC voltages of 256 V-1100 V. The solid line segments (left axis) describe the calculated response from 1-D impedance matrix model over the same voltage range. The Δl term was used as the model input. Line A used the d_{11} term to calculate Δl. Line B used 50% of the d_{11} term and 50% of the d_{61} term to calculate Δl. Line C uses the full d_{11} and d_{61} term to calculate Δl. The dashed line (right axis) is the linear piezoelectricity theory used to describe the 36° Y-X-cut $LiNiBO_3$.

III. Conclusion

In summary, DC voltages were measured using a piezoelectric voltage sensor by monitoring acoustic wave propagation time changes with applied voltage. The measured crystal responses are consistent with linear piezoelectric theory for longitudinal mode propagation only. Shear wave propagation adds additional amplification to the response. Measurements using this method can be made with good sensitivity and low noise.

The work was performed at Sandia National Laboratories. Sandia National Laboratories is a multi-program laboratory managed and operated by Sandia Corporation, a wholly owned subsidiary of Lockheed Martin Corporation, for the U.S. DOE's NNSA under contract DE-AC04-94AL85000.

References

1. S. G. Joshi, Review of Scientific Instruments **54** (8), 1012-1016 (1983).

A Comparison of Intentional EMI, Cyber and Physical Threats and Protection

R. Hoad, C. Harper, B. Petit and A. Fernandes
QinetiQ Ltd.
Farnborough, Hampshire, UK
rhoad@qinetiq.com

***Abstract*— Recently QinetiQ has been commissioned to undertake several surveys of Critical National Infrastructure (CNI) sites in the UK and the US to evaluate the risk to the sites from Intentional Electromagnetic Interference (IEMI). This paper summarizes some observations from these surveys and our interactions with CNI owners/operators. This paper also compares and contrasts the IEMI threat with Cyber (computer network attacks) and physical threats.**

Keywords- IEMI, Electromagnetic Compatibility, Critical National Infrastructure, Cyber

I. INTRODUCTION

Intentional Electromagnetic Interference (IEMI) is of growing concern to Critical National Infrastructure (CNI) asset owners/operators, largely because of the recent expansion in the use of embedded electronic systems for control and diagnostic purposes and the growing availability of capable IEMI sources [1]. New legislative drivers such as the SHIELD ACT in the USA [2] and the perceived risk from Cyber threats are forcing CNI asset owners and operators to consider their vulnerability to these relatively new threats.

A definition of Cyberspace is “an operational domain whose distinctive and unique character is framed by the use of electronics and the electromagnetic spectrum to create, store, modify, exchange and exploit information via interconnected information-communication technology (ICT) based systems and their associated infrastructures” [3]. However, mostly the term Cyber is associated with a rather narrow definition of the threat which can be summarized as Computer Network Attack (CNA), whereby both the source of the threat and the target are ICT based. Examples of CNA include; hacking, malicious software (malware), Denial of Service (DoS) and Distributed Dos (DDoS), Botnets, and network intrusion [4].

Physical threats to the CNI are perhaps more familiar and can include, for example; bombing, arson, and theft.

II. OBSERVATIONS

A summary of observations of the difference in threat perception and protection are given in Table 1. These observations are ‘first hand’ and were identified from various Technical Visual Assessments (TVAs) of established functional CNI Sites in the UK and the US and of plans and designs for new sites yet to be built. The TVAs were conducted by QinetiQ in the last 24 months.

This paper explores these differences in a higher level of detail, providing examples where they have been observed.

TABLE I. A SUMMARY OF OBSERVATIONS

Cyber/Physical Threats	**IEMI Threats**
Most Infrastructure providers/operators have an individual(s) responsible for Cyber Security or ‘digital risk’ and Physical Security	Very few infrastructure providers presently acknowledge or recognize the IEMI threat – therefore they do not generally appoint someone to be responsible for IEMI protection
Cyber and Physical threats can affect confidentiality, integrity and availability	IEMI is primarily a threat to the availability of information/capable of denying service
Cyber exploits can be conducted from another continent, outside of one Nation’s legal jurisdiction. Physical threats require physical interaction with the asset	The range of IEMI threat sources can easily exceed the physical perimeter of a CNI asset but do not have the reach of Cyber threats
Cyber is fundamentally a risk to interconnected ICT networks. Physical threats are a risk to physical, tangible assets	IEMI can affect all unprotected electronic devices – not just interconnected ICT networks and can even affect electronic systems used to support physical security
Laws already exist for Cyber-crimes and Cyber Terrorism. Physical acts on a CNI site are covered by standard legal doctrine	Whilst it is illegal to transmit Radio Frequency signals without a license in many countries the act of procuring and using an IEMI source has not been legally tested
The manifestation of a Cyber disturbance can be subtle or severe but it is possible to recover an evidence trail. Physical threats tend to leave physical evidence	IEMI disturbances can leave very little or no physical evidence.
Cyber/Physical Protection	**IEMI Protection**
A wide variety of standards and guides are available to infrastructure designers to improve the physical and Cyber security of new facilities	Whilst design rules and standards exist to protect a new-build facility from IEMI, they are rarely mandated.
Cyber and Physical attack is often detectable – detectors are available and deployed	Whilst IEMI detection concepts are starting to become available, their adoption is uncommon
For Cyber threats, software patches can be used to rapidly mitigate vulnerabilities. Physical threats can be difficult to mitigate rapidly	IEMI threats can be difficult to mitigate rapidly
For Cyber threats Isolation and precise control of network connectivity boundaries (including the human behavioral boundary) massively reduces risk. Physical protection generally employs physical boundary controls	IEMI protection can make use of the physical protection boundary if it is constructed in a way that mitigates IEMI. For example perimeter fences that have good attenuation properties or provide adequate stand-off.

REFERENCES

[1] EU FP7 Security Research Topic SEC-2011.2.2-2 Protection of Critical Infrastructure (structures, platforms and networks) against Electromagnetic (High Power Microwave (HPM)) Attacks http://cordis.europa.eu/search/index.cfm?, 2011

[2] HR 2417, US Congress, '“Secure High-voltage Infrastructure for Electricity from Lethal Damage Act ”or the “SHIELD Act ”, June 18 2013

[3] Kuehl D. (2008), ‘From Cyberspace to Cyberpower: Defining the Problem’, Information Resources Management College/National Defense University, Air Force Symposium 2008: Cyberspace, July 15 – 17 2008, Air University (AU) Maxwell AFB, USA.

[4] Singer P and Friedman A., ‘Cybersecurity and Cyberwar: What Everyone Needs to Know’, 6 February 2014

ID 064

Statistical Mechanics and Chaos Applied to Electromagnetic Compatibility

Ira Kohlberg
Kohlberg Associates, Inc.,
Reston, Virginia 20190 USA
ira.kohlberg@gmail.com

Robert L. Gardner, Consultant
6152 Manchester Park
Alexandria, Virginia 22310 USA
Robert. L. Gardner@verizon.net

Abstract—A large number of excellent papers have been written in the last 50 years to link the "new" field of chaos to established disciplines of classical mechanics and non-conservative dynamical systems on one side, and set theory and stochastic processes on the other side [1-3]. In this paper we show that many of these chaos-related topics can be folded into a roadmap that demonstrates chaos's strong dependence on statistical mechanics when applied to electromagnetic compatibility.

Keywords-component: Chaotic dynamical system, stochastic processes, logistic map, butterfly effect, strange attractor

I. BACKGROUND

It's conjectured that chaos began when Newton's laws of mechanics started to accurately predict the motion of planetary bodies from mutual gravitational attraction. In retrospect this was relatively easy to do for the two-body interaction because not only was the force between them known but one could also be confident that energy was conserved. The predicted orbits were well defined and essentially periodic. Poincare's studies of the three-body problem around 1900 showed the existence of non-periodic orbits and bounded in today's language as a limit cycle connected to a strange attractor. It was also noted that slight differences in initial positions of interacting bodies produced surprisingly huge differences in their orbits —this is one of the cornerstones of chaos theory.

A conclusion from the early studies demonstrated the need for physical models based on statistical mechanics where the focus shifted drastically from a few interacting bodies to gases and fluids. The classic application is Edward Lorenz's 1961 study of weather prediction. His results showed an acute nonlinear sensitivity to initial conditions. There is also similarity between Lorenz's equations and those of the Rossler and Chua systems.

II. APPROACH

In this paper we examine the synergism between the Lorenz, Rossler and Chua systems from the instability viewpoint. In particular we seek to better quantify how long these systems can remain in quasi-equilibrium before bifurcation begins. This issue appears to be of high interest in power electronics and power supplies where sub-harmonic bifurcations can connect a single point to a limit cycle [4]. Chaos behavior can appear in a large number of power electronic circuits such as: regulators, current limiter devices, amplifiers, etc.

III. THEORY

A critical feature of the Lorenz, Rossler, and Chua systems is that they are not necessarily energy conserving, and are solved from of the general autonomous equation

$$(d\vec{x}/dt) = \vec{F}(x^{(1)}(t), x^{(2)}(t), \ldots. x^{(N)}(t))$$

By making a connection with turbulence theory Landau and Lifshitz showed that near a limit cycle the foregoing equation can be represented by only two variables—and ultimately modeled by a Poincare map [3]. Ultimately this leads to the solution of the discrete equation

$$x_{j+1} = f(x_j, \lambda) = 1 - \lambda x_j^2$$

In the foregoing equation j is measured in units of the period and λ is a system dependent parameter determined by the bifurcation conditions and the multiplier μ --the numerical factor by which the frequency changes from the stable condition. At this transition point, x_*, it's required that $x_{j+1} = x_j \equiv x_*$, and $\mu = dx_{j+1}/dx_j$, which then provides the conditions for bifurcation [3]. The foregoing theory, originally applied for turbulence, will be explored to analyze ripple and duty cycle stimulation of sub-harmonics in networks [4]. Related conceptual foundations and limitations of chaos will also be explored.

REFERENCES

[1] R. Brown and L. Chua, (1999) "Clarifying chaos III: Chaotic and Stochastic Processes, Chaotic Resonance, and Number Theory", *Int. J. Bifurcation and Chaos* **9** (5), 785-803

[2] R. L. Devaney, *An Introduction to Chaotic Dynamic Systems*, 2nd Ed, Addison-Wesley 1989

[3] L. D. Landau and E.M. Lifshitz, Fluid Mechanics, 2nd Ed. Pergamon Press, 1987

[4] http://www.smpstech.com/chaos000.htm

Interpreting Radar Signal-to-Clutter-and-Noise-Ratio as a Stochastic Process

Ira Kohlberg
Kohlberg Associates, Inc.,
Reston, Virginia 20190 USA
ira.kohlberg@gmail.com

Robert McMillan
Consultant
St. George Island, Florida 32328 USA
R.Mcmillan@ieee.org

Abstract—This paper illustrates and defines basic stochastic factors required for computing the target and clutter return for non-distributed field objects. It is shown that path-dependent stochastic changes in polarization and random target response can adversely affect the SCNR.

Keywords-component: Non-distributed clutter, stochastic process, SCNR

I. BACKGROUND

Accurately determining the SCNR is a complex problem arising from the electromagnetic interaction between the incident radar signal and the target and/or clutter. As targets and decoys become more sophisticated and complicated it is more risky to rely only on test data. We need to push harder on rigorous theoretical fundamentals if we are required to deal with man-made and non-normal electromagnetic environments. Because of these difficulties semi-empirical formulas based on combining probability theory with experimental data have been of significant value, but may often result in uncertainties in SCNR and ultimately system performance.

II. APPROACH

In this paper we: (1) define basic stochastic factors required for computing the target and clutter return for non-distributed field objects, and (2) show that rigorous application of basic stochastic process techniques and probability theory can accurately account for path-dependent stochastic changes in polarization and random target response that seriously affect the SCNR in a complex electromagnetic environment. By keeping rigorous account of the target and clutter interactions the uncertainties in predicting the SCNR can be minimized. We determine target and clutter return for a point and/or collection of non-distributed objects: the direction of the Poynting vector does not change over the size of the field object (target or clutter) on the macroscopic scale.

III. THEORY

Our starting point assumes that clutter is modeled as a non-random and Memoryless System—the behavior only depends on the current time. Aside from the time delay between the radar and the field point, its radiating power is proportional to the radar power $P_0(t)$. However, targets and clutter may be classified as Systems with Memory which include Linear Time Invariant (LTI) systems. For LTI systems the target/clutter power generated is [1]

$$P_\Theta(t) = \int_{-\infty}^{+\infty} h_\Theta(t-\tau) P_0(\tau) d\tau$$

where $h_\Theta(t)$ is a non-random and linear transfer function, and is adequate for use in the calculation of SCNR. We consider three causes of random effects: (a) propagation path from radar to object, (b) interaction between the incident field and object, and (c) propagation path from object back to radar. For illustrative purposes we consider random propagation effects to be caused by fluctuations in polarization and is represented by a random polarization vector $\vec{\rho}$. If $\vec{u}_z$ is a unit vector in the direction of propagation, the two orthogonal directions of random polarization are $\vec{u}_x$ and $\vec{u}_y$. Assuming that the energy (but not the direction) is constant allows us to write

$$\vec{\rho} = \gamma(l_p \mid \vec{\rho}_0)\vec{u}_x + \left(1-\gamma(l_p \mid \vec{\rho}_0)\right)\vec{u}_y$$

The function $\gamma(l_p \mid \vec{\rho}_0)$ is the conditional probability that polarization is in the $\vec{u}_x$ direction after the wave has travelled a distance l_p starting with polarization: $\vec{\rho} = \vec{\rho}_0$, and $1-\gamma(l_p \mid \vec{\rho}_0)$ is the corresponding conditional probability for the $\vec{u}_y$. The statistical properties of $\vec{\rho}$ are assumed to be known from actual measurements. Using the statistical properties of $\vec{\rho}$ we derive the probability density function of SCNR.

REFERENCES

[1] A. Papoulis, Probability, Random Variables, and Stochastic Processes, McGraw-Hill, 1965
[2] E. Parzen, Modern Probability and Its Applications, John Wiley & Sons, Inc., 1960

ID 067

Calculus of Low Probability-High Consequence Events

Implications for Electromagnetic Hardening Assessment

Edward Toton
Toton LLC
Reston, Virginia 20194 USA
etoton@toton.org

Ira Kohlberg
Kohlberg Associates, Inc.
Reston, Virginia 20190 USA
ira.kohlberg@gmail.com

***Abstract*—We develop a strategy for exploring the relationships between electromagnetic front–and-back door threats, hardening, modeling and testing for systems of all sizes. Real systems can experience hardware and/or logic failure and whose responses may depend critically on design geometry, copy-to-copy variability and stochastic factors. Modeling of the survivability of such systems under such conditions is fraught with risk: a rigorous failure mode analysis cannot be guaranteed to identify all combinations of components and software states that might lead to a critical failure. That is, the *true* probability of survival must always be less than any computed value – and by an unknown amount. We discuss an approach for quantification of survivability bounds that utilizes test results and survived exposures of operational hardware using insights developed by Walley, colorfully illustrated by his "bag of marbles."**

Keywords-survivability; probability; failure; survivability; risk; Bayesian; odds; EMP; hardening

I. Introduction

This paper extends the notion presented by the authors in a previous AMEREM publication (AMEREM, Ottawa, Canada, July 2010) to the problem of quantification of low probability – high consequence events such as critical system failures from hostile electromagnetic environments. We develop a strategy for exploring the relationships between electromagnetic front–and-back door threats, hardening, modeling and testing for systems of all sizes. Real systems can experience hardware and/or logic failure and whose responses may depend critically on design geometry, copy-to-copy variability and stochastic factors. Modeling of the survivability of such systems under such conditions is fraught with risk: a rigorous failure mode analysis cannot be guaranteed to identify all combinations of components and software states that might lead to a critical failure. That is, the *true* probability of survival must always be less than any computed value – and by an unknown amount. A dramatic example of this type of oversight was encountered in the nuclear meltdown at Three Mile Island, precipitated by the formation of an unpredicted hydrogen bubble forcing coolant away from the reactor core [1]. Since we seek quantification of low-probability failures, these unknown system failure modes become critical to the analysis.

II. Approach

We base the strategy for quantification of survivability bounds that utilizes test results and survived exposures of operational hardware on insights developed by Walley, colorfully illustrated by his "bag of marbles" [2]. He asks visitors to his office to guess the probability of drawing a red marble from an opaque bag on his desk; there is no other information about the contents given! The red ball is a clear metaphor for catastrophic system failures. In the absence of information of the nature of such a failure, the Walley questions are: "What is the *highest* probability for a red marble to be drawn for which you are willing to bet that this *will* occur?" and "What is the *lowest* probability for a red marble to be drawn for which you are willing to bet that this *won't* occur?" In the absence of *any* data, these must have the values 0 and 1, respectively. A multivariate analysis with an unknown number of possibilities results in the probability bounds

$$\begin{aligned} P^a &= n_r/(N+s) \\ P^b &= (n_r+s)/(N+s) \\ P^c &= s/(N+s) \end{aligned} \qquad (1)$$

Here, P^a and P^b are the lower and upper bound probabilities for the unknown probability for drawing a red ball or, in our case, encountering an EMP-induced catastrophic system failure, when N draws have been made and n_r red balls drawn. The quantity P^c represents the spread between the lower and upper bounds. The quantity s is a user selected parameter that represents the user's degree of persuasion by the data; Walley suggests that a value of $s=2$ is reasonable. We see immediately from Eq.(1) that meaningful EMP exposures without system failure, i.e., with $n_r=0$, have a lower probability bound of 0 and an upper bound of $P^b = P^c = 1/(1+N/s)$. This shows that repeated survivals forces the upper bound to zero – a reasonable and satisfying quantified behavior.

We have rendered a computational model in [3] based on Walley's concept. This new methodology gives us the opportunity to examine various subsets of threats and tradeoffs between probabilities connected with lethality and survivability, while taking into account the existence of potential unknown EMP-induced catastrophic system failure modes.

References

[1] http://www.nrc.gov/reading-rm/doc-collections/fact-sheets/3mile-isle.html

[2] Walley, P. "Inferences from Multinomial Data: Learning about a Bag of Marbles," J. R. Statist. Soc. B (1996) 58. No. 1, pp. 3-57

[3] E. Toton, M. Frankel, and I. Kohlberg, "High Power Electromagnetic Pulse Characterized as Low Probability-High Consequence Events," AMEREM, Ottawa, Canada, July 2010

Application of UWB Technique for Wall Shielding Measurements

F. Sonnemann, R.H. Stark
Diehl-BGT-Defence GmbH & Co.KG
90552 Roethenbach a d Pegnitz, Germany
frank.sonnemann@diehl-bgt-defence.de

***Abstract*— A measurement method to determine the electromagnetic properties of walls with ultra-wide-band (UWB) radiation technique is presented. The advantage of this method is the possibility to determine shielding effectiveness and dielectric constant of walls without the requirement of a closed shield environment.**

Keywords-UWB; wall shielding; electromagnetic properties

I. Introduction

The standard method for measuring the effectiveness of electromagnetic shielding enclosures is based on a swept-frequency continuous wave (CW) technique in the frequency domain according to IEEE-STD-299. Because the method requires a closed shield environment, its application is only useful when the shielding of the building is complete.

The presented UWB measurement technique in the time domain has the advantage that due to different time delays the penetrated signal through a potential leakage can be separated from the scattered signal around the shield. Therefore, this technique is suitable to determine shielding properties of detached wall segments. The covered frequency range is given by the bandwidth of the radiated UWB pulse.

II. Steel Reinforced Walls

In the following example, the electromagnetic properties of a detached steel reinforced test wall shall be determined. An UWB transmitter and an UWB receiver unit are positioned on both sides of the 50 cm thick wall as shown in Figure 1.

Figure 1. Determination of the electromagnetic properties of a 50 cm thick steel reinforced wall segment with UWB technique

The distance between transmitter and receiver unit was chosen to d_{TR} =1m. The propagation of the pulse through the wall is not only attenuated, but also reduced in velocity. This can be observed by measuring the time difference of the received probe signal at d_{TR} =1m in free space u_{ref} (t) compared to the received signal $u_{wall}(t)$ with wall located between transmitter and receiver (Figure 2). The triggering was equal for both measurements. The time difference amounts to 3.8 ns and corresponds to the propagation time through the steel reinforced wall. The velocity v can be calculated to $v = d_{wall} / \Delta T = 1.32 \times 10^8$ m/s. From this, the relative dielectric constant ε_r of the wall can be calculated to: $\varepsilon_r = (c_0/v)^2 = 5.1$, whereas c_0 is the propagation speed of light.

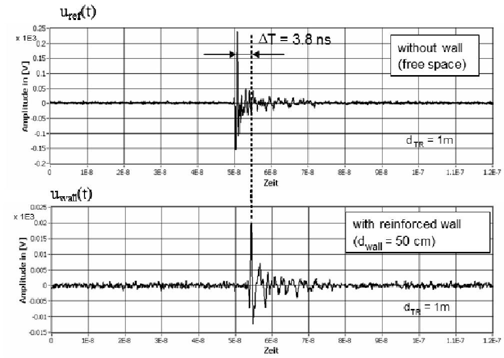

Figure 2. Received UWB probe signals $u_{ref}(t)$ and $u_{wall}(t)$

Figure 3 shows the shielding effectiveness of the wall in the frequency range 0.4 – 1.9 GHz, calculated by SE = FFT{$u_{wall}(t)$} / FFT{$u_{ref}(t)$}. It can be noted that the attenuation increases with frequency which is assumed due to increasing absorption losses of water in the range of 2 GHz [1].

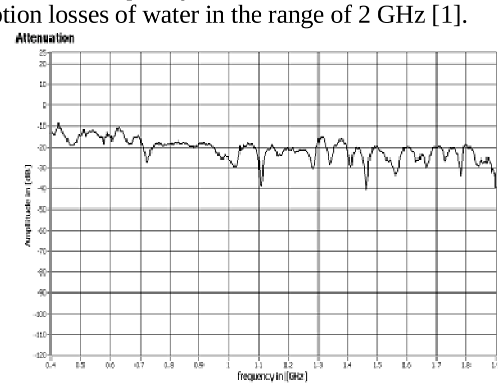

Figure 3. Shielding effectiveness of a 50 cm steel reinforced wall

III. Conclusion

The presented time domain measurement method with time-gating technique is capable to determine the electromagnetic properties of walls and wall segments in their original environment.

References

[1] T. Frenzel, J. Rohde, J. Opfer, “Elektromagnetische Schirmung von Gebäuden“, BSI-Richtlinie, BSI-TR-03209-2, April 2008

Dual Conical Electromagnetic Lens between a Marx Generator and a Helical Antenna

D. V. Giri
Dept. of ECE, Univ of New Mexico
Albuquerque, NM, USA and Pro-Tech,
11-C Orchard Ct, Alamo, CA 94507, USA
Giri@DVGiri.com

Ian D. Smith
L-3 ATI, L-3 Pulse Sciences
2700 Merced Street
San Leandro, CA 94577 USA
Ian.d.Smith@l-3com.com

Abstract— This paper describes the design and performance of an electromagnetic lens to connect a high-power Marx generator to a helical antenna. The Marx generator is in a coaxial geometry and its outer conductor eventually becomes the ground plane of the helical antenna. The helix is fed by the inner conductor through a small hole in the ground plane. The dual conical EM lens described here transports nearly all of the energy from the Marx to the helical antenna in the pass band frequencies of the helix.

Keywords- EM Lens, Helical Antenna, Transient pulse, Marx

I. INTRODUCTION

Baum et al [1] had considered the problem of launching the TEM mode on a coaxial circular cylindrical transmission line at high frequencies, by using a coaxial circular cone as a wave launcher. This can be seen in Figure 1.

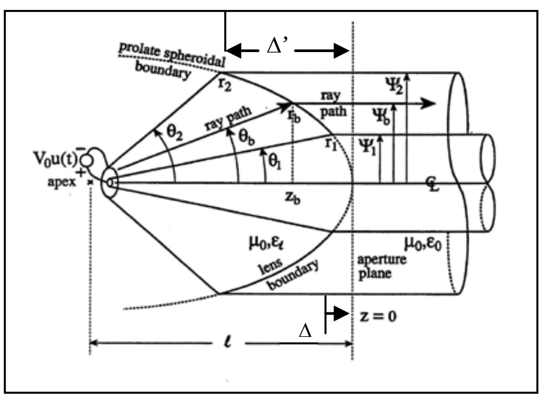

Figure 1. Prolate spheroidal lens with a circular conical transmission line feeding circular coax

The lens medium in Figure 1 can be a uniform isotropic dielectric, such as transformer oil or polyethylene for high-power applications. While the lens is not perfect in that there are small reflections at the lens surface, the high frequency performance has been demonstrated to be quite good for a large range of lens parameters. As has been described in [1], there are seven design parameters of this lens, $\psi_1, \psi_2, \ell, \theta_1, \theta_2, \Delta \; and \; \Delta'$. However, by setting $\psi_2 = 1$, we have six independent parameters and one can write six equations to solve for these parameters and complete the design and assess the lens performance In this paper, the above described lens design has been extended to the case of connecting a Marx generator [2,3] to a helical antenna. The last stage of the Marx with a peaking switch is in oil medium and the helical antenna is in a SF6 medium. The diameters of the Marx and the helical antenna are different and we have designed a dual conical lens for interconnecting the source to the antenna.

.

II DUAL CONCIAL LENS

The EM lens is shown in Figure 2.

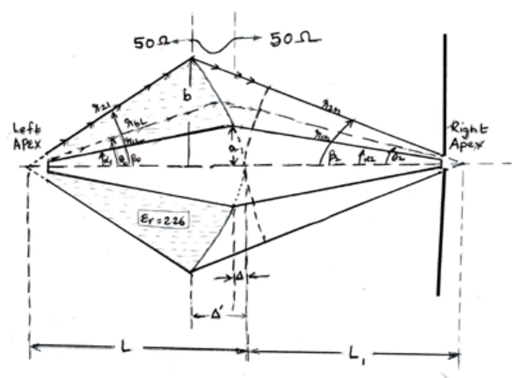

Figure 2. Design parameters of a dual conical lens

The design parameters are: input cone angles (α_1, β_1), output cone angles (α_2, β_2), and five geometrical parameters as seen in Figure 2. $(L, L_1, a, b, \Delta \; and \; \Delta_1)$. As before we can set b =1 and set up 8 equations for the 8 independent unknowns. The equations ensure proper impedances, equal transit times etc. It turns out there many sets of solutions and we have picked the one that minimizes the total length (L + L_1) of the dual conical lens. We have also verified that the solution of our lens reduces to the results in [1], when we make the length L_1 very large. Our lens tapers up and then down, adjusts for the needed dimensions at both ends and also provides for transitioning from oil medium in the input taper to SF6 in the output taper. We will be presenting detailed design and predicted performance which cannot be included here due to length limitation. This lens has been successfully fabricated and used.

REFERENCES

1.C. E. Baum, J. Sadler and A. Stone, A Prolate Spheroidal Uniform isotropic Dielectric Lens Feeding a Circular Coax, Sensor and Simulation Note 335, 12 December 1991.

2. D. Morton, J. Banister, T. DaSilva, J. Levine, T. Naff, I. Smith, H. Sze, T. Warren, D. Giri, C Mora, J. Pavlinko, J. Schleher, C. Baum, "A 2MV, <300ps Risetime, 100Hz, Pulser for Generation of Microwaves," IEEE Pulsed Power Conference 2009.

3.. D. Morton, J. Banister, T. DaSilva, J. Levine, T. Naff, I. Smith, H. Sze, T. Warren, D. Giri, C Mora, J. Pavlinko, J. Schleher, C. Baum, "WBTS HPM A Transportable High-Power Wide-Band Microwave Source," IEEE Pulsed Power Conference 2009.

ID 070

Measurements of Isotropic Absorption Cross Sections of Lossy Structures

A Contribution to the Shielding Effectiveness of Cavities

Bengt Vallhagen, Tony Nilsson
Saab Aeronautics
SAAB AB
Linköping, Sweden
bengt.vallhagen@saabgroup.com

***Abstract*— This paper describes measurements and results from the characterization of COTS absorbers and resistive structures, with respect to the isotropic absorption cross section in an overmoded cavity. The aim of this work is to increase practical and theoretical knowledge in how to increase shielding effectiveness (SE) of a cavity (i.e. avionics bay). The results will be an input to a practical guideline on how to increase the protection level against High Power Microwaves (HPM). Measurements of these materials and structures have been done in a reverberation chamber (RC).**

Keywords - absorption cross section; high power microwaves; shielding; reverberation chamber.

I. INTRODUCTION

The threat from HPM sources has recently entered military standards, such as Mil-Std 464C. Also, in the aircraft industry one is required to harden the system against High Intensity Radiated Fields (HIRF). An increased threat level requires a higher level of protection, i.e. shielding effectiveness (SE) of cavities, such as avionics bays. By introducing lossy materials or resistive structures according to [2] and [3], the quality factor (Q) of the cavity can be decreased, and thus the SE increased. Different types of lossy materials and resistive structures have been systematically investigated, to see which ones will fit our needs best, for different applications. The tested materials consist of both dielectric and magnetically load absorbers. The effects of resistive lattice structures have also been investigated.

II. LOSSY STRUCTURES

A. *The Power Balance Approach*

Based on the power balance approach [1], the determination of the average shielding effectiveness $\langle SE \rangle$ can be derived:

$$\langle SE \rangle = \frac{2\pi \cdot V}{\sigma_a \cdot \lambda \cdot Q} \tag{1}$$

Eq. (1) makes clear that by lowering σ_a (the aperture cross section) or the Q-value in a cavity, $\langle SE \rangle$ will increase. Our current studies aim to lower the Q-value.

B. *Isotropic absorption cross section of lossy structures*

By comparing measurements of Q in an empty reverberation chamber vs. a loaded ditto – Q_{empty} vs. Q_{loaded} – the isotropic absorption cross section $\langle \sigma_{lm} \rangle$ in (2), can be calculated.

$$\langle \sigma_{lm} \rangle = \frac{2\pi \cdot V}{\lambda} \cdot \left(\frac{1}{Q_{loaded}} - \frac{1}{Q_{empty}}\right) \tag{2}$$

The reverberation chamber was loaded with several types of lossy COTS absorbers and resistive structures. One example of a measurement is given in Figure 1.

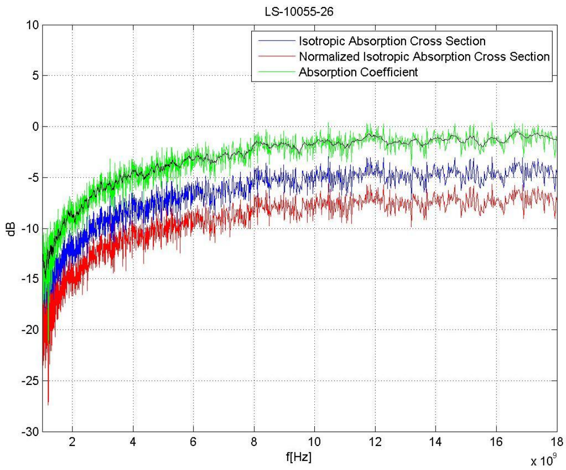

Figure 1. Measurement of absorption cross section, LS-10055-26 absorber from ARC Technologies, Inc.

C. *Applicability*

Adding absorbing materials into avionics bays is a simple way to significantly increase the shielding effectiveness without major design changes.

REFERENCES

[1] M. Bäckström, T. Nilsson and B. Vallhagen, "Guideline for HPM protection and verification based on the method of power balance", submitted to EMC Europe 2014, September 1-4, 2014, Gothenburg, Sweden.

[2] C. E. Baum, "Damping Electromagnetic Resonances in Equipment Cavities", Interaction Note 613, University of New Mexico, 10 June 2010.

[3] C. E. Baum, "Damping Transmission-Line and Cavity Resonances", Phillips Laboratory, Interaction Note 503, 24 May 1994.

Absorption by Non-Radiating Systems

A possible way to generate low frequency components in UWB fields

Joerg Fricke
Dept. of Mechanical Engineering
University of Applied Sciences Muenster
Muenster, NRW, Germany
j.fricke@bkbmail.de

Abstract— **The radiation energy lost by absorption is not always taken into account by superposition of the fields, rendering necessary a deflation or inflation of the incident field. Deflation / inflation of radiation fields can be described only by modified Maxwell equations. By phase-locked deflation / inflation of UWB fields it might be possible to generate low frequency components. Such fields would enable the stimulation of neurons in a better focused way than by using near fields.**

Keywords - absorption, divergence, modified Maxwell equations, UWB, low frequency component, neural stimulation

I. A CASE NOT COVERED BY CLASSICAL THEORY

As a consequence of the two Maxwell equations related to divergence, radiation fields cannot be multiplicatively attenuated. Proofs that non-radiating systems cannot absorb energy are based on this fact. The goal of this paper is to provide a counter-example in form of a simple thought experiment:

A non-conducting, evenly charged spherical shell which oscillates radially does not radiate. Since the power radiated by a charge is the same in all inertial frames the shell remains non-radiating as long as its center moves without acceleration. The center of a nearly harmonically oscillating shell moves uniformly along the axis of a radially polarized monochromatic beam of the same frequency. Suppose the profile of the longitudinal E component of the beam has a flat top. Then the field components of the beam exchange energy with the charged sphere as follows (subscripts L and R refer to longitudinal resp. radial components):

Seen from the rest frame of the shell, $P_{ER} = P_{BR} = P_R = 0$. Since the power gained or lost by the oscillation has to be independent of the frame, this is true in every inertial frame. Due to the oscillation, $F_{BL} \neq 0$. Thus in this frame, conservation of momentum is violated. Seen from the rest frame of the focus, generally $P_{ER} \neq 0$ => $P_{BR} \neq 0$. Since always $P_{BL} + P_{BR} = 0$ => $P_{BL} \neq 0$. If the sphere remains inside the flat portion of the beam profile $F_{EL} \approx 0$ => $P_{EL} \approx 0$ => $P_L \neq 0$. In this frame, energy and momentum are not conserved. Introducing deflation of the beam, F_L becomes radiation pressure and P_L becomes the absorbed power. Magnitude and direction of the power flow depend on the phase relation of oscillation and beam, of course.

All details of this thought experiment including numerical examples will be published in the full presentation, of course. Please note that the equations employed to model the beam are exact solutions of the Maxwell equations [1]. The described effect does neither depend on quantization nor on extremely strong fields but belongs to the domain of classical theory.

II. ADAPTING THE MAXWELL EQUATIONS

In order to enable the deflation or inflation of radiation fields some kind of "free" (i.e. not bound to particles) divergence has to be introduced. The density of this divergence is termed ς_e for the electric field and ς_m for the magnetic field. Due to geometry, the divergence is accompanied by a curl of the magnetic resp. electric field. Therefore, a virtual velocity (as if the fields were moving) is assigned to the divergence in such a way as to yield the continuity equations

$$\nabla \cdot \mathbf{J}_{\varsigma e} = -\partial \varsigma_e / \partial t \quad \text{and} \quad \nabla \cdot \mathbf{J}_{\varsigma m} = -\partial \varsigma_m / \partial t$$

with the current densities $\mathbf{J}_{\varsigma e}$ and $\mathbf{J}_{\varsigma m}$. The modified Maxwell equations thus read

$$\nabla \times \mathbf{E} = -\dot{\mathbf{B}} - \mathbf{J}_{\varsigma m} \tag{1}$$

$$\nabla \times \mathbf{H} = \dot{\mathbf{D}} + \mathbf{J}_{\mathbf{e}} \tag{2}$$

$$\nabla \cdot \mathbf{D} = \rho_e + \varsigma_e \tag{3}$$

$$\nabla \cdot \mathbf{B} = \varsigma_m \tag{4}$$

with $\mathbf{J}_{\mathbf{e}} = \mathbf{J}_{\rho e} + \mathbf{J}_{\varsigma e}$. Of course, parts of the theory have to be adapted resp. complemented (e.g. $\mathbf{B}$ has to be determined by a vector potential and a scalar potential; the spatial distribution of ς_e and ς_m has to be determined).

III. VERIFICATION AND APPLICATION

Directly measuring the divergence or proving the existence of $\mathbf{J}_{\varsigma m}$ by measuring $\nabla \times \mathbf{E}$ during absorption of a monochromatic radiation field seems not to be feasable. An interesting question is whether it is possible to generate a low frequency component in UWB radiation by deflating or inflating half cycle pulses depending on their polarity. To look beyond classical theory: Chopping photons mechanically is known to broaden their spectrum [2]; multiplicatively modulating might as well generate frequency components far below the initial spectrum of polychromatic photons. If so, the LF component in $\nabla \times \mathbf{E}$ would be easy to detect. Presupposing suitable technology, this would enable a medical application: UWB beams resp. localized waves containing an LF component provide a method of non-invasive neural stimulation for diagnostic and therapeutic purposes, focused to a smaller volume than is possible with near fields.

REFERENCES

[1] F. G. Mitri, "Quasi-Gaussian electromagnetic beams", Physical Review A 87, 035804, March 2013

[2] U. Hauser et al., "Time-dependent modulation of the probability amplitude of single photons", Physics Letters, Vol. 49A, No. 1, pp. 57-58, August 1974

Double-Pulse Technique for Defending from Hostile Systems

D. V. Giri
, Pro-Tech
11-C Orchard Court, Alamo, CA 94507
E-mail: Giri@DVGiri.com

Prof. T. T. Wu
Division of Engineering and Applied Sciences
Harvard University, Cambridge, MA 02138

Abstract— In this paper, we have addressed a promising way of defending from a hostile system, using two electromagnetic pulses. The first pulse is a hyperband signal meant to interrogate the target system to determine its vulnerabilities in terms of the frequencies that can penetrate the system. The second pulse is then tailored to contain the electromagnetic energy in the appropriate frequency band in an attempt to disable the hostile system. The possibility of such a double-pulse technique has been raised by many and we have decided to look into this further. In a representative example considered in this paper, we find that a single equation can lead to both external and internal resonances of the target system.

Keywords-Hyperband, narrowband, vulnerabilities, resonances

I. Introduction

A promising way to defend against a hostile system in air, on water or land (ex: an incoming missile, speed boat or a ground vehicle with hostile intention) is to send a powerful electromagnetic pulse to disable the electronic control system [1]. It is the purpose of this paper to discuss one aspect of such a defense. In order to disable the electronics some of the energy of the electromagnetic pulse must penetrate to the interior of the incoming system. If the outer shell of the hostile system is not highly conductive, this penetration can be accomplished with relative ease. Even if the outer shell is metallic, there are unavoidable points of entry consisting of junctions of metallic surfaces, slits around moving surfaces, inadvertent apertures etc, where the electromagnetic pulse can penetrate. Points of Entry (PoEn) for electromagnetic energy can also serve as Points of Exit (PoEx).

Such penetration into the system is more easily accomplished at some frequencies of the electromagnetic pulse than other frequencies. Therefore, the disabling of electronics can be more easily carried out if the pulse can be tailored to contain most of its energy in these frequencies. From this point of view, the defense can be accomplished in two successive stages.

1) We first send a moderately powerful electromagnetic pulse. Over certain frequency ranges, this pulse contains significant energies. We analyze the return signal to determine the frequencies that may have penetrated the target system, which are likely to be the frequencies where the system is vulnerable. It is noted that coupling of certain frequencies into the system is necessary, but may not be sufficient to accomplish the necessary damage. We will discuss this aspect further in the presentation.

2) We send a second pulse to disable the electronics of the system. This second pulse is much more powerful than the first electromagnetic pulse and is tailored to contain as much energy as possible in the frequencies that coupled into the system.

This procedure of using two electromagnetic pulses has another side benefit. It is conceivable that systems of the same type can be individualized so that their responses to electromagnetic pulses are different from each other. Such a discriminating program does not have any effect on the present procedure of using two pulses. The double-pulse defense has been suggested in the past by researchers including the first author of this paper. A general intuitive response has ranged from "this technique is not practical" to "it cannot give the interior resonances". The implied pessimism and finality of the responses has motivated us to look into this problem, in some detail.

II. AIRBORNE TARGET SYSTEM

We have considered a canonical problem representative of the missile defense in this paper. We find that in an idealized case, it is possible to write a single equation that yields both ***exterior*** and ***interior*** resonances. We believe this is a new result opening the door for pursuing this problem. We consider a perfectly conducting cylinder of radius "a" and the same cylinder coated with a reactive surface. The exterior and interior regions are coupled by a scalar parameter α. We find both sets of resonances are given by

$$J_n(ka)\,H_n^{(1)}(ka) = \frac{2\,i}{\alpha\,a} \qquad (1)$$

If there is no coupling between the two regions, the interior resonances are given by the real zeros of the Bessel function and the exterior resonances are given by the complex zeros of the Hankel function. On the other hand, for finite values of α, no matter how large, there is no such factorization, and the interior resonance and the exterior resonance are not separate. We have numerically solved the above equation for the cases of n = 0, 1, 2 and 3 and for $1 \leq a \leq 100$. The numerical results at least for this idealized situation indicate that there is no problem in separating the interior and exterior resonances.

In our two pulse procedure, the return signal from the first Hyperband illumination is analyzed for the resonance mix. We then look for identifying the interior resonances which are likely to be in the fourth quadrant of the complex k plane with small imaginary parts. In the simple problem considered here, there are no difficulties in separating the interior and exterior resonances. This delineation of interior and exterior resonances is likely to hold for the realistic missile return signals. Identification of the interior resonances leads to the more important second-pulse excitation (narrow or moderate band signals) with its energy concentrated in the interior resonance bands.

[1[This presentation is based on Interaction Note 602 of the same title by D.V.Giri and T. T. Wu, which can be downloaded from www.ece.unm.edu/summa/notes

Increasing Peak-Power Field Generation Efficiency in Reverberation Chambers

H. VALLON[1,2], G. DEFRANCE[1],
F. MONSEF[1], A. COZZA[1]

[1] Research Department on Electromagnetism
L2S, UMR8506, CNRS-SUPELEC-
Univ. Paris-Sud
Gif-Sur-Yvette, Essonne, France
henri.vallon@supelec.fr

A-S. CHAUCHAT[2]

[2] THALES Communications and Security
Gennevilliers, Île-de-France, France

***Abstract*— In the present work we compare the efficiency of generating high-intensity fields inside a reverberating chamber in the case where the test volume is driven by continuous waves and when excited by a time-reversed signal. Experimental results are compared to an asymptotic model showing the importance of frequency bandwidth and losses within the chamber.**

Keywords-efficiency; electromagnetic compatibility test; peak-field; reverberation chamber; time-reversal.

I. INTRODUCTION

A reverberating chamber (RC) usually consists of a rectangular test chamber with metal walls and a stirrer that allows one to smooth out the sharp nulls of the field. During immunity tests, the average response of the object to the field is found by integrating the response over multiple stirrer positions. The equipment under test (EUT) is thus exposed to high field levels. For frequencies where the chamber is highly overmoded, the test facility is considered to be a perfectly diffuse system. The electromagnetic environment is then characterized as being isotropic, randomly polarized and uniform. The field arriving at any point in the volume can be described as an infinite sum of plane waves propagating in all directions of the volume with the same probability [1]. In such an environment a statistical approach is more suitable given the field description complexity.

When the RC is driven by a continuous-wave (CW) harmonic signal, only a fraction of the total energy stored within the chamber can be used as aggression on the EUT. When carrying out certain electromagnetic compatibility tests, it would be more useful to be able to choose the incidence angle and to concentrate the field on the EUT. This scenario can be achieved by using time reversal (TR) techniques [2]. In such a case, the RC can be used as a high-intensity field generator.

Based on prior work in the case of energy efficiency [3], we propose an asymptotic model capable of predicting the average improvement brought by time reversal techniques on peak-power field generation. Experimental results have allowed us to check the validity of the model.

II. THEORETICAL MODEL

In a similar way than in [3] we define the peak power generation efficiency as the square-root of the ratio between maximum field according to one direction $\max_t |e_n(t)|^2$ and the peak power injected in the RC, P^{peak} such that,

$$\eta^P = \sqrt{\frac{\max_t |e_n(t)|^2}{P^{peak}}} = \frac{\max_t |e_n(t)|}{A^{peak}} \quad (1)$$

In order to compare the case of standard use of RC's with the case when using time-reversal techniques we derived a simple asymptotical model of the ratio between efficiencies based on the works in [3]:

$$\mathrm{G}^{\mathrm{P}}_{\mathrm{ave}} = \frac{\langle \eta^P_{TR} \rangle}{\langle \eta^P_{CW} \rangle} = \sqrt{\frac{1}{3}\mathrm{G}^{\varepsilon}_{\mathrm{ave}}} \leq \sqrt{\frac{\mathrm{B_t}\overline{\mathrm{Q}}}{6\pi f_c}} \quad (2)$$

where $\langle\ \rangle$ is the ensemble averaged value and $\mathrm{G}^{\varepsilon}_{\mathrm{ave}}$ the asymptotic model developed in [3] with $\mathrm{B_t}$ the bandwidth, $\mathrm{f_c}$ the central frequency and $\overline{\mathrm{Q}}$ the average quality factor.

III. EXPERIMENTAL RESULTS

Experimental data were obtained in a 45 m^3 reverberation chamber. A total of 50 stirrer states and 16 spatial positions for two field polarizations were considered. Measurements were performed for 3 different frequencies. Figure 1 shows the variation of the ratio between model and measurements with respect to the bandwidth. We obtain very good agreement between model and experiments especially when the bandwidth is large.

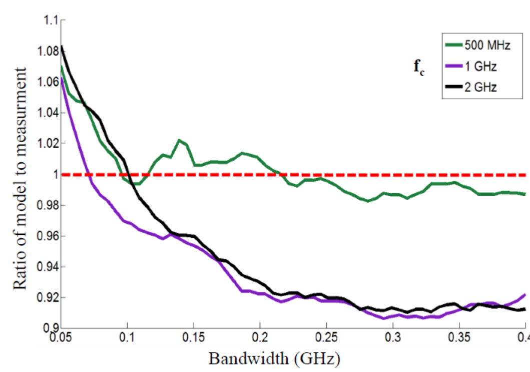

Figure 1. Ratio of model to measurement according to bandwidth for the average efficiency improvement using time reversal.

REFERENCES

[1]D. Hill "Plane wave integral representation for fields in reverberation chambers", IEEE Transactions on Electromagnetic Compatibility, vol. 40, no. 3, August 1998.

[2]G. Lerosey, De Rosny J., Tourin A., A. Derode, Montaldo G., M. Fink "Time Reversal of Electromagnetic Waves" Phys. Rev. Lett., vol. 92,2004.

[3]A. Cozza "Increasing peak-field generation efficiency of reverberation chamber", Electronic Letters, IET, vol. 46, no. 1, 2010.

This work is part of a project financed by THALES.

An Overview of Some Site Specific IEMI Risk Assessment Tools

B. Petit, R. Hoad, A. Fernandes and G. Eastwood
DEW & E3 Capability Group,
QinetiQ Ltd.
Farnborough, Hampshire, UK
bjpetit@qinetiq.com

***Abstract*—.With the reduction in cost and wider availability of Intentional Electromagnetic Interference (IEMI) systems, a greater risk is posed to Critical National Infrastructure (CNI). QinetiQ are working with CNI providers to understand the risk posed to their sites and how to mitigate this risk. This is being done through Technical Visual Assessments of sites to determine the inherent protection and to offer advice on hardening where relevant. QinetiQ have developed a number of tools to aid this work. This paper describes these tools and how they are being applied to help to understand the risk from IEMI to CNI.**

Keywords- IEMI, Electromagnetic Compatibility, Critical National Infrastructure

I. Introduction

With the reduction in cost and wider availability of Intentional Electromagnetic Interference (IEMI) systems including jammers, the risk to Critical National Infrastructure (CNI) has increased. These IEMI systems are becoming more prevalent and pose a risk to the electronic control systems used within CNI, as well as the vital signals that CNI sites need to operate, for example the timing signals received from Global Positioning Systems (GPS) via satellite. If the operation of CNI sites is compromised, the consequences could be drastic and far-reaching. This makes it very important to understand the risk posed by IEMI systems to the sites, as well as how to mitigate and protect against potential effects.

QinetiQ have been working with CNI providers within the UK to assess the sites used to control and operate CNI. Through this work QinetiQ have been able to offer advice on vulnerabilities and how to mitigate the risks.

II. Risk Assessment tools

In order to easily illustrate to CNI owners and operators where the risk from IEMI impinges on the facilities, QinetiQ have developed a risk visualisation tool known as PhoS. The tool accepts a plan view of the site. Details gathered from a Technical Visual Assessment (TVA) of the site such as the specific locations of critical electronic systems (usually control rooms, or other central processing facilities) together with an assessment of the protection (attenuation) of the physical boundaries are entered into the tool and indicated on the plan.

QinetiQ have developed and are continuing to evolve an attenuation database of building façade materials and other physical perimeter materials and have recently been adding to the database with measurement data. QinetiQ have built databases of both the IEMI threat environments and effects criteria.

The risks are assessed by comparing the IEMI ‘threat environment’, which covers a wide parameter space including frequency range and time domain parameters, with the estimated level required to exceed immunity and drive an effect at critical electronic systems.

QinetiQ have focused on the IEMI threat from readily available IEMI source technologies classifying threat actors by technical capability into novice, skilled and specialist groups. QinetiQ have considered both ‘front door’ effectors (jammers) and ‘back door’ effectors in different delivery formats, man-portable, vehicle borne and fixed installation, as well as the possibility of a malicious insider.

The risk boundaries indicated by the tool are based on immunity, upset (50% probability) and damage (50% probability). An example visualisation from the PhoS tool is shown in Figure 1.

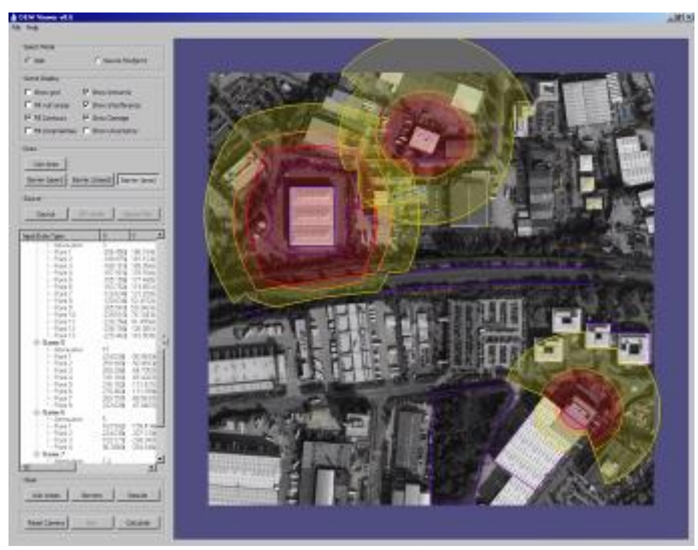

Figure 1 – Example Visualisation from the PhoS Tool

The visualisations produced by the tool have been found to help to easily guide the CNI owner/operator to the magnitude of the risk to a particular facility from IEMI and further indicate where best to include pragmatic protection.

A Review of the Current Status of IEMI Standards for the HIPOW Project

A. Fernandes, C. Harper, R. Hoad and B. Petit
QinetiQ Ltd.
Farnborough, Hampshire, UK
pafernandes@qinetiq.com

***Abstract*— As an essential contribution to the HIPOW project, QinetiQ have recently completed a study to review the latest standards for the protection of Critical National Infrastructure (CNI) against Intentional Electromagnetic Interference (IEMI). This paper specifically discusses the elements of each standard which relate to High Altitude Electromagnetic Pulse (HEMP) or IEMI environments and includes a review of testing and measuring techniques, as well as the simulation of High Power Electromagnetic environments.**

Keywords-IEMI; Electromagnetic; Compatibility; Standards

I. Introduction

As the threat from Intentional Electromagnetic Interference (IEMI) increases, standards have been developed to aid in the endeavour to protect electronic and electrical systems, equipment and installations. For the most part, civilian systems are designed and tested against commercial/civilian standards which provides for a range of Electromagnetic Environments (EMEs) that are less severe but more commonly occurring than those of IEMI. The majority of systems which make up the Critical National Infrastructure (CNI) in Europe are tested and certified against relatively low levels of Radio Frequency (RF) disturbances, potentially leaving a gap through which a successful IEMI attack could be executed.

The main objective of HIPOW is to improve the current European situation regarding awareness of IEMI threats and the adequacy of protection of critical infrastructure against the threat. It attempts to achieve this by: demonstrating to policy makers the seriousness of the deficiencies regarding the current situation; defining and preparing procedures and tools for a risk management regime; preparing a database and a handbook for policy makers and critical infrastructure owners; and promoting an organisational and institutional framework for the future regulation regime. To this end, a review of international civilian and unclassified military standards relevant to this objective has been undertaken.

II. Standards

A. *International Electrotechnical Committee (IEC)*

The IEC has been publishing IEMI-related standards and reports since 1989. This has been led by Sub-Committee (SC) 77C which has 20 current publications to its credit. As is evident, significant efforts have been made to provide guidance on the protection of equipment and systems from the effects of High Altitude Electromagnetic Pulse (HEMP) and IEMI. In our review we conclude that this is the most useful body of guidance for the HIPOW project given the generic or horizontal nature of the advice being pertinent to a very wide range of CNI types and functions.

B. *North Atlantic Treaty Organization (NATO)*

NATO has recently developed Allied Environmental Conditions and Test Publication (AECTP) 250 – a series of nine Leaflets presenting various EME which may influence the design and operation of military systems. The Leaflets considered in this paper are 256 – ‘Nuclear Electromagnetic Pulse (NEMP/EMP)’ – and 257 – ‘High Power Microwave (HPM)’.

C. *United States Department of Defense (US DoD)*

Military Standard 464C – ‘Electromagnetic Environmental Effects, Requirements for Systems’ – is a US DoD publication focused on a wide range of EMEs relevant to military systems. It describes the EME characteristics which are likely to be experienced by systems and provides guidance on minimum performance and test requirements for exposure to such conditions. Importantly, this document defines an HPM ‘threat’ environment.

D. *International Telecommunications Union Telecommunications Standardization Sector (ITU-T)*

Study Group (SG) 5 – ‘Environment and Climate Change’ – of the ITU-T provides guidance for the protection of Fixed Telecommunications systems against the effects of HEMP and IEMI. As a baseline, SG5 uses the basic publications of IEC SC77C to aid in the preparation of its recommendations. Recommendations ITU-T K.78 (HEMP) and ITU-T K.81 (IEMI) are of particular importance and relevance to the Telecommunications functions of CNI.

E. *Institute of Electrical and Electronics Engineers (IEEE)*

With the support of Technical Committee 5, The IEEE Electromagnetic Compatibility Society is in the process of developing Project 1642 – ‘Recommended Practice for Protecting Public Accessible Computer Systems from Intentional EMI’. The purpose of this work is to provide guidance for protecting against IEMI to builders of computer systems which are to be used by or are accessible to the public.

F. *Conseil International des Grands Réseaux Electriques/ Council on Large Electric Systems (CIGRÉ)*

CIGRÉ Working Group C4.206 – ‘Protection of the High Voltage Power Network Control Electronics Against Intentional Electromagnetic Interference’ – has recently produced a brochure which evaluates the threat of IEMI to High Voltage (HV) substations and recommends mitigation methods. This brochure is considered to be an important reference for the Electrical Power network function of CNI which is considered by many to be the most important as it underpins many others.

ID 078

Overview of the French Capabilities in the Field of High-Power Microwaves

Dominique J. SERAFIN
CEA-Centre de Gramat 46500 Gramat, France

E-mail : dominique.serafin@cea.fr

The paper will present an overview of the major French capabilities in the field of high power microwave research. Unique experimental capabilities have been developed at the Gramat research center together with numerical simulation capabilities to support the French HPM research program. The CEA-centre de Gramat is a part of the French Atomic Commission. The intent of the paper is to present the rationale of the development of the key elements from the early days till today. Unclassified examples of research projects will illustrate the HPM activities at Gramat.

HYPERION

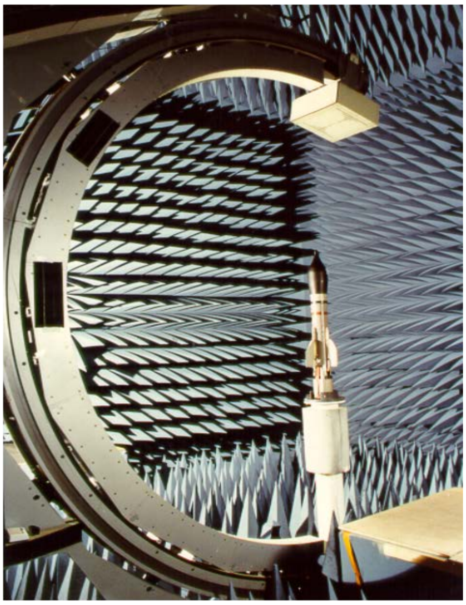

SOCRATE

MELUSINE

Metal Plate Lenses for A High Power Microwave Zoom Antenna

Julie Lawrance
Air Force Research Lab
Albuquerque. NM, USA

Christos Christodoulou
Department of Electrical and Computer Engineering
University of New Mexico
Albuquerque, NM, USA

***Abstract*—A high power microwave antenna with true zoom capability was designed with the use of metal plate lenses. Proof of concept was achieved through experiment as well as simulation. This concept comprises a horn feed antenna and two metal plate lenses. Good agreement was found between experiment and simulation. This antenna provides true zoom capability in the TEM mode with continuously variable diameter pencil beam output and approximately 10% bandwidth.**

I. INTRODUCTION

The metal plate lens was proposed by W.E. Koch in the 1940's [1] but has seen little use since. Some design considerations are presented in [2]. This paper presents results of experiment and simulation exploring application of metal plate lenses to a high power microwave zoom antenna concept. This antenna consists of three elements: a pyramidal horn feed antenna and two appropriately designed metal plate lenses that can be translated along the boresight axis relative to each other and to the feed horn. The output of this antenna system is a variable diameter (TEM) pencil beam output. The bandwidth is on the order of 10%.

The metal plate lens antenna, shown conceptually in (1) is essentially a waveguide array antenna that works only in the TEM mode.

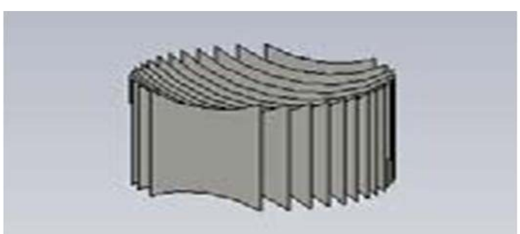

Fig. 1. Conceptual illlustration of metal plate lens.

It consists of an array of parallel metal plates with constant spacing "a". The index of refraction of the structure, n, is less than 1 and is determined by

$$n = \sqrt{1 - (\frac{\lambda}{2a})^2} \tag{1}$$

where λ is the wavelength. The front and back faces of the metal plate array can then be shaped to provide the desired focal length,*f*, according to the lensmaker's equation:

$$\frac{1}{f} = (n-1)\left(\frac{1}{R1} - \frac{1}{R2}\right) \tag{2}$$

Positioning of the lenses to achieve a collimated (pencil beam output) is governed by

$$\frac{1}{f} = \frac{1}{S1} + \frac{1}{S2} \tag{3}$$

where S1 is the distance from the phase center of the pyramidal horn antenna and S2 is the distance from the center of lens 1 to the center of lens 2, as shown in (2).

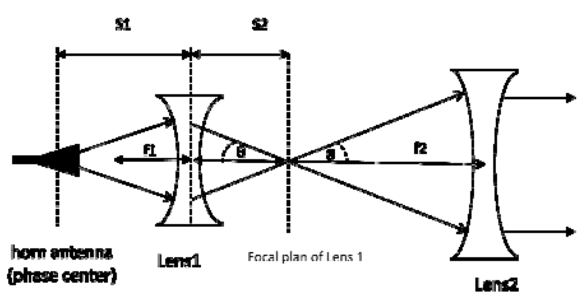

Fig. 2. Zoom antenna concept – broad collimated beam output.

Reducing the diameter of the collimated beam output of the zoom antenna is achieved by repositioning the lenses such that lens one is closer to the phase center of the horn antenna (while still being greater than a focal length, f1, away) and such that lens 2 is again one focal length, f2, from the new location of the focal plane of lens 1. This is illustrated graphically in (3).

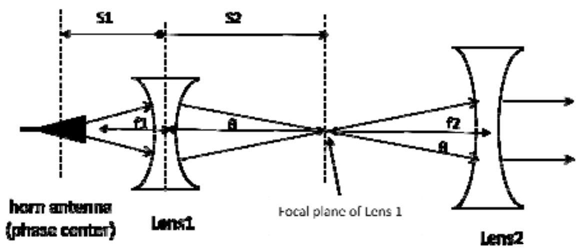

Fig. 3. Zoom antenna concept – narrow collimated beam output.

II. Experimental and Simulated Results

To demonstrate the concept, a pair of 10-GHz metal plate lenses were designed and built: one with a diameter of 40.6 cm and a focal length of 25.4 cm and the other with a diameter of 81.3 cm and a focal length of 139.7 cm. The plate spacing of the lenses was 1.9 cm, resulting in an index of refraction of 0.6. A 15dBi horn antenna was appropriately placed and driven by port 1 of a network analyzer. The lenses were positioned to achieve a collimated beam output. Low power S21 measurements were made with a small receive horn antenna connected to port 2 of the network analyzer across the focal plane of the first lens in the E- and H- planes as well as at the output of the antenna. The entire system (including the horn antenna and both lenses) was simulated and the results showed good agreement.

Point focus, achieved by placing a single lens greater than a focal length from the phase center of the horn antenna is illustrated by the simulated results shown in (4).

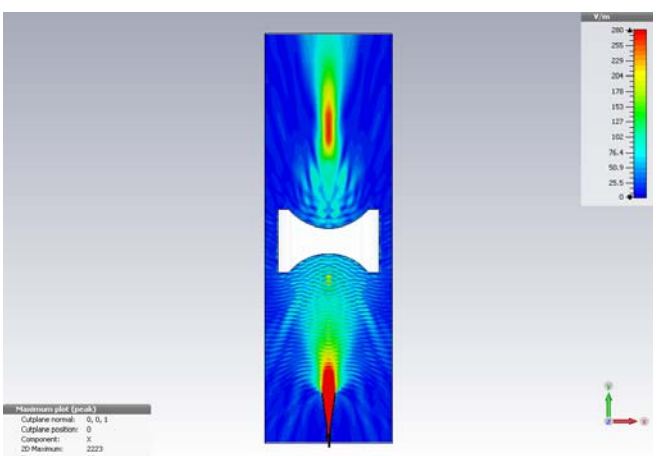

Fig. 4. Focus of TEM beam radiated from a pyramidal horn antenna achieved with a single metal plate lens

The beam is not focused to a single point, but rather to an Airy disc, whose diameter is diffraction limited to greater than a wavelength.

The simulated boresight electric field corresponding to (4) is shown in (5).

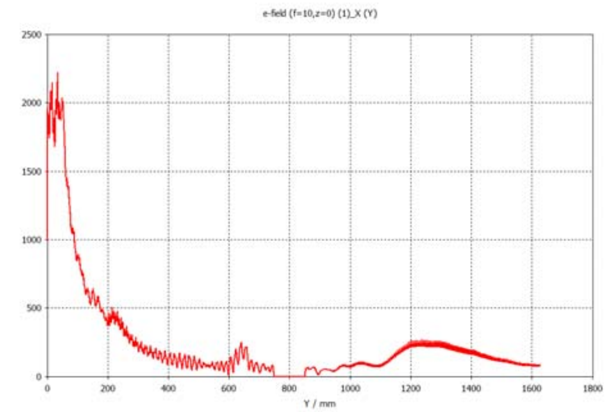

Fig. 5. Simulated boresight electric field (aperture of antenna at y=200mm)

Focus of the beam occurs at approximately y=1200mm; the electric field falls off as 1/r2 as one moves further away from the focal plane. A second metal plate lens, with focal length f', if placed a distance f' from the focal plane of this lens will collimate the beam. The diameter of the collimated beam is then varied by re-positioning the lenses, resulting in a true zoom capability.

Experimental and simulation results indicated focusing of the beam in the focal plane of the first lens to an Airy disc whose diameter is diffraction limited about 1.5*λ. Simulated results also reveal beam collimation when the lenses were correctly positioned relative to each other and relative to the phase center of the horn antenna, as well as variability in the collimated beam diameter.

Experiment and simulation revealed the feasibility of designing, constructing and implementing a high power microwave zoom antenna using metal plate lenses to guide the electromagnetic waves radiated from a horn antenna into a pencil beam output of continuously variable diameter. Air breakdown in the focal plane determines the maximum power handling capability of the system. Analysis reveals an exponential decrease in maximum power with increasing frequency; from several gigwatts at 1 GHz, to almost 40 megawatts at 10 GHz.

References

[1] W.E. Koch, "Metal-Lens Antennas," Proceedings of the I.R.E. (34) 11 , pp. 828–836, November 1946.

[2] C.J. Sletten, Reflector and Lens Antennas: Analysis and Design Using Personal Computers, 1st ed., MA: Artech House, 1988, pp. 262–272.

ID 080

Evaluation of Some New Balun Devices

Hugh H. Pohle
Air Force Research Laboratory
Directed Energy Directorate
HPEM Division (RDHE)
Kirtland AFB, NM 87117
Hugh.pohle@us.af.mil

***Abstract*— Baluns have long been used for by the Electromagnetic measurement community to combine signal outputs from differential sensors (field, current and voltage). Baluns are also extensively used in high speed data transmission; as a result there are several new commercial devices available. These new devices have excellent bandwidth, phase & amplitude match and good CMR. This paper presents the results of an AFRL project to evaluate some of them. Data on more traditional baluns such as made by URS and Prodyn is also included for comparison. Except for low frequencies a 4 port Network Analyzer was used for measurements, this gets around some of the previous problems involved with single ended measurements on baluns.**

Balun, Electromagnetic measurements, antennas,

I. Introduction

In the High Power Electromagnetic measurement word differential field sensors are used to make accurate measurements. A key part of this technique is properly combining the differential out puts into a single ended signal that can be conveniently recorded by a high speed digitizer. This is typical done using a balun device. In principal a balun is quite simple; it invers one of the differential signals on the input and adds it in phase to the other input. If a simple combiner were used the 2 differential signals would add out of phase tend to give no signal at the output. All though a balun is conceptually simple, in practice it is very difficult to make a very broad bandwidth balun because the frequency range of interest requires both lumped element (ferrites) and distributed transmission line topologies. The dividing line between the two techniques is on the order if 1 GHz and EM measurements often span these two ranges. Designing a balun that spans kHz to GHz is a real challenge.

II. Test Articles

Three new state of the art wideband baluns were chosen for evaluation; in addition several baluns from URS and Prodyn were also tested.

TABLE I. Baluns

	Part	Range	CMR	IL dB	Amp B	Ph B
Marki	BAL-0006	200k-6GHz	40dB	7.5	±0.1	±1
Hyper Lab	9402	5M-6GHz	NG*	6.0	±0.1	±2
Pico Sec	5310	4M-6GHz	35dB	7.6	±0.1	±0.5
URS	DMB4	150k-3GHz	28dB	6.4	NG	NG
Prodyn	B1BF	200k-3.5GHz	20dB	8.0	NG	NG
M/C	ZFSC	50M-1GHz	NG	4.7	±0.1	±2

*Not given Amp B, Ph B = Amplitude and phase balance

Octave and multioctave microwave hybrids were also thrown in the mix. Several examples of URS and Prodyn baluns were available; they had all been use for many years so this was an opportunity to looking at ageing effects.

III. Measurements

All measurements were made with Vector Network Analyzers over a frequency range of 100 to 8GHz. At lower frequencies an Agilent 5061B-LF (5 to 3GHz) was used, for higher frequencies a Rohde & Schwarz ZVB8 (300k to 8 GHz) was used. The R&S had the advantage of being a 4 port machine so true differential measurements could be made. Over 300k to 3GHz data was taken by both analyzers to look at differences between single ended and differential measurements.

References

[1] Rohde & Schwartz “Measuring Balanced Components with Vector Network Analyzer ZVB” Application note 1EZ53

FDTD Calculation of LEMP Inside a Reinforced Concrete Building

Akiyoshi Tatematsu
Electric Power Engineering Research Lab.
Central Research Institute of Electric Power Industry
Yokosuka, Kanagawa, Japan

Farhad Rachidi
Electromagnetic Compatibility Laboratory
Swiss Federal Institute of Technology
Lausanne, Switzerland

Marcos Rubinstein
University of Applied Sciences Western Switzerland
Yverdon-les-Bains, Switzerland

***Abstract*—In this paper, using a GPGPU-based three-dimensional finite-difference time-domain (FDTD) simulation code, we calculate lightning electromagnetic fields inside a full-scale reinforced concrete building.**

Keywords-buildings; electromagnetic fields; reinforced concrete; lightning; FDTD method

I. INTRODUCTION

The protection of electronic devices inside a building from lightning electromagnetic pulse (LEMP) effects is based on the concept of lightning protection zones (LPZ) [1], which requires to accurately evaluate lightning electromagnetic fields.

II. CALCULATION MODEL AND RESULTS

A. Calculation Model

Figure 1 shows a calculation model of a five-storey reinforced concrete building, which is composed of thin wires and a lossy dielectric to represent reinforcing bars and concrete, respectively. The conductivity and relative permittivity of the lossy dielectric are set to 0.0052 S/m and 8.6, respectively, which correspond to results at DC obtained by fitting the Debye model to measured results of concrete with a moisture content of 5.5 % [2]. The lightning channel is assumed to be straight and vertical and the transmission line (TL) model is adopted to represent the current distribution. In the direct-strike case, the channel is attached to the corner of the roof; while in the indirect-strike case, the channel is directly attached to the ground surface 30 m away from the building.

B. Calculation Results

Using the subsequent lightning return-stroke current specified in [1], we calculated electric and magnetic fields inside the building model for the direct and indirect strike cases to analyze the effect of the concrete. Figures 2 and 3 show the waveforms of the electric and magnetic fields on the fifth floor for the direct and indirect strikes, respectively. These results confirm that the concrete structure significantly reduces the electric fields. The magnetic field, on the other hand are virtually not affected by the concrete.

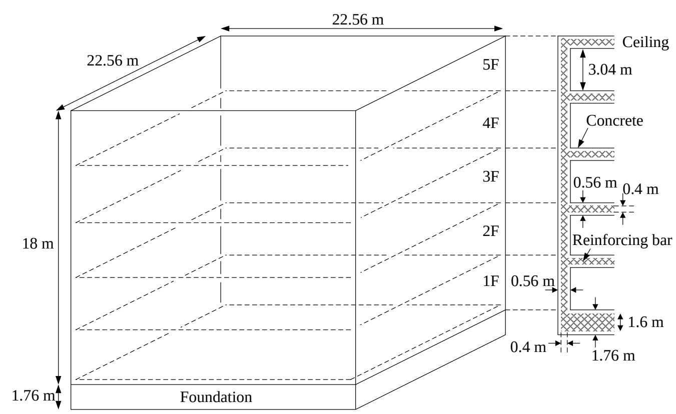

Figure 1. Calculation model of a reinforced concrete building.

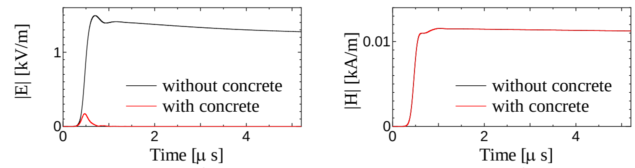

(a) Electric field (b) Magnetic field

Figure 2. Calculated results of electric and magnetic fields on the fifth floor in the case of the direct strike.

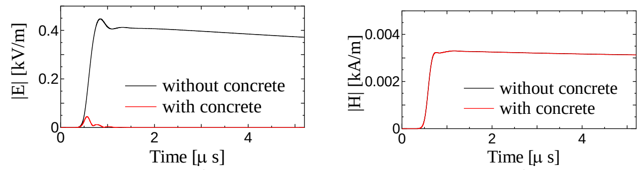

(a) Electric field (b) Magnetic field

Figure 3. Calculated results of electric and magnetic fields on the fifth floor in the case of the indirect strike.

REFERENCES

[1] Protection against lightning. Part 4: Electrical and electronic systems within structures., IEC Standard 62305-4, 2010.

[2] A. Ogunsola and L. Sandrolini, "Modelling shielding properties of concrete," Proc. 17th Int. Zurich Symp. Electromagn. Compat., 2006, pp. 34-37.

Simulation of Indirect Effects of Lightning on Aircraft Engine

P. Aguilera, C. Lair
Snecma
Villaroche, France
paula.aguilera@snecma.fr
cyril.lair@snecma.fr

B. Michielsen, F. Issac
Onera, The French Aerospace Lab, DEMR
Toulouse, France
bastiaan.michielsen@onera.fr
francois.issac@onera.fr

M. Hélier, M. Darces
Sorbonne Universités, UPMC-L2E
F-75005 Paris, France
marc.helier@upmc.fr
muriel.darces@upmc.fr

***Abstract*— This paper presents a new approach for simulating the indirect effects of a lightning impact on an aircraft engine. Based on macro modelling, it performs a model reduction, in a similar way as "stick models", but using a patch support instead. This new macro element allows for fast resolution of the quasi-static lightning injection problem.**

***Keywords*—Lightning Simulation; Macro Modelling; Patch Finite Elements.**

I. Introduction

Numerical simulation plays a major role from the specification to the certification of an aircraft engine regarding lightning indirect effects [1]. On the one hand, 3D solvers, based on the resolution of discretized Maxwell's equations, can be used to predict precisely the constraints to be applied to equipments in a complex system, and therefore be part of lightning certification process. However, they involve heavy tools which are inappropriate for parameters optimization or measurements analysis. On the other hand, much lighter models such as "stick models" have gained a lot of interest [2][3]. Based on the PEEC (Partial Element Equivalent Circuit) method, they have shown to be faster and sufficiently accurate in some aeronautical applications. One drawback though is the poor estimation of the current distribution at higher frequencies as current is constrained to follow the stick path. A new model, based on macro modelling, has been implemented to overcome this problem.

II. Stick model analysis

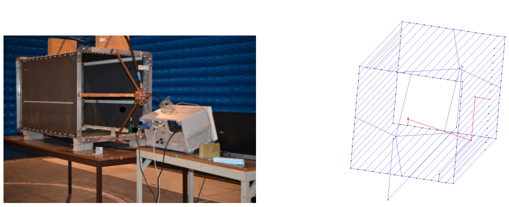

Figure 1. Left: EADS IW composite box. Right: stick model implementation (GiD)

We consider a configuration with a cable inside a composite box (Fig. 1), originating from EADS-IW and simulated in the frame of the French Industry Project called PREFACE [4]. We apply a first model in which the box is meshed with wires the radius of which is determined by the Equal Area Rule (EAR) and with a conductivity extracted from measurements. The simulated current flowing over the cable from a lightning injection differs from measurement beyond 10 kHz, as depicted in Fig. 2.

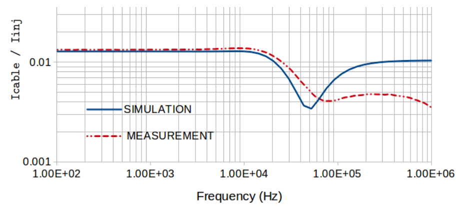

Figure 2. CW analysis of normalized current over a branch of a cable inside the box. continuous: simulation with LiRiC (Onera), dashed: measurement

III. Patch implementation

A new macro finite element has been implemented. Its support, called "patch", results from the segmentation of wires and triangulated surfaces using the Fiedler vector of the corresponding Laplacian matrix.

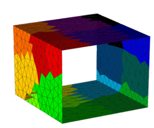

Figure 3. Surface segmentation of the composite box

A quasi-static solution of the lightning injection problem can be approximated using two methods: one takes a static current distribution over the system to represent the macro finite element in the micro element basis and provides a reduced inductance matrix over patches; the other one defines for each patch of the system an adapted number of degrees of freedom. The oral presentation will show the improvement obtained with this new approach.

References

[1] J.-P. Parmantier and al., "Indirect Effects of Lightning on Aircraft and Rotorcraft," *Journal AerospaceLab*, Lightning Hazards to Aircraft and Launchers, Issue 5, pp.20–24, December 2012.
[2] D. Prost and al., "Lightning-Induced Current Simulation Using RL Equivalent Circuit: Application to an Aircraft Subsystem Design," *IEEE Trans. Electromagn. Compat.*, vol. 55, no. 2, pp.378–384, April 2013.
[3] H. Moussa and al., "Lightning Modelling: From 3D To Circuit Approach," *Aerospace EMC*, 2012," Proceedings ESA Workshop on vol., no., pp.1–5, 21-23 May 2012.
[4] J. Ali (2012), "Electromagnetic Modeling of Lightning for Aircraft Applications," Ph.D. Thesis. University of Grenoble, France.

Design and Realization of a High-Voltage Adapter for the Testing of Surge Protective Devices against Intentional Electromagnetic Interferences

P. Bertholet[1], A. Kaelin[2], G. Lugrin[3], N. Mora[3], M. Nyffeler[1], F. Rachidi[3], M. Rubinstein[4]

[1] High-Power Electromagnetic Laboratory, Armasuisse, Spiez, Switzerland

[2] EMProtec, Hinwil, Switzerland

[3] EMC Laboratory, Swiss Federal Inst. of Technology (EPFL), Lausanne, Switzerland

[4] IICT, University of Applied Sciences of Western Switzerland, Yverdon-les-Bains, Switzerland

***Abstract*—We report on the design, realization and experimental test of an adapter for testing of surge protection devices against very fast transients.**

***Keywords*—intentional electromagnetic interference (IEMI); high voltage; surge protective device (SPD)**

I. Introduction

One option for the mitigation of sensitive electronic systems against intentional electromagnetic interference (IEMI) is the use of surge protective devices (SPDs). Testing the response of surge protection devices to IEMI threats is a challenging task (e.g., [1-4]). The expected disturbances can have significant variations in terms of their waveshape and spectral content [5]. They are also often characterized by very high frequency components and amplitudes. Finally, SPDs are generally available for protection against traditional disturbances due to lightning and EMP.

Another practical difficulty in testing SPDs against IEMI pulses stems from the fact that semiconductor-based fast transient generators require a quasi-matched load at their output, a condition hardly realizable when testing SPDs. To cope with this problem, different solutions can be envisioned, such as the use of attenuators [2]. In this paper, we propose the use of a specially-designed coaxial tapered transmission line to adapt a 50-Ohm fast transient generator to the low impedance of a conducting SPD.

II. Design of an adapter

A cross-section of the designed adapter along its length is shown in Fig. 1. It is characterized by a tapered coaxial structure designed in such a way that the characteristic impedance decreases linearely from 50 Ohm to a low impedance. To ensure a good matching also at low frequencies, for which the adapter is electrically small, the internal conductor was made of ten 4.7-Ohm Allen-Bradley resistors.

The design was validated with numerical simulations carried out using CST microwave studio® and the performance of the prototype was tested in the time domain (TDR) and in the frequency domain (VNA).

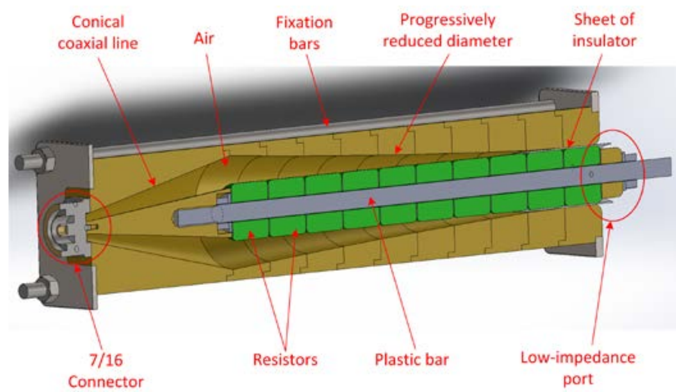

Fig. 1. Cross-section view of the adapter, from the CAD drawings.

The adapter was used to test a few commercially available SPDs.

Acknowledgment

Thanks are due to the staff of EPFL Electromechanical Workshop, especially Pierre-André Pognant, for the realization of the adapter.

References

[1] T. Weber, R. Krzikalla, J.L. ter Haseborg, “Linear and nonlinear filters suppressing UWB pulses”, IEEE Transactions on Electromagnetic Compatibility, Vol. 46, No. 6, pp. 423-430, 2004.

[2] T. Nilsson, “Investigation of Limiters For HPM and UWB Front-door Protection”, Master in Electronic Systems, Linköping University, 2006.

[3] M. Nyffeler, A. W. Kaelin, D. Rolle, P.-F. Bertholet, A. Jaquier, “Behavior of combined Lightning HEMP Protection Devices to HPEM Overvoltage Input Signals”, AMEREM 2010, Ottawa, Canada, July 2010.

[4] E. Savage, W.A. Radasky, “IEMI evaluation of network protectors”, 2013 IEEE Internaional Symposium on EMC, Denver, CO, 2013.

[5] D. V. Giri and F. M. Tesche, "Classification of intentional electromagnetic environments (IEME)," *Electromagnetic Compatibility, IEEE Transactions on,* vol. 46, pp. 322-328, 2004.

This study is financially supported by the Swisselectric-Research and the European Community's Seventh Framework Programme FP7/2007-2013 under grant agreement 285257, STRUCTURES.

Project of compact plasma maser with continuous spectrum within 2 octaves

Svetlana E. ERNYLEVA
Chair of applied physics
Peoples' Friendship University of Russia
Moscow, Russia
ersvev@mail.ru

Oleg T. LOZA, Irina L. BOGDANKEVICH
Plasma physics dept.
A.M.Prokhorov General physics institute RAS
Moscow, Russia
oleg.loza@list.ru

Abstract— **Numerical model shows that plasma relativistic maser can operate as noise amplifier with HPM energy output ratio ~ 10% and emission power of 100 MW during 2 ns. Continuous spectrum within 4 to 16 GHz band may be obtained after ~ 20 repetitive pulses.**

Keywords- microwave; high-power; broadband; plasma

The project is oriented to demonstrate advantages of plasma masers driven by modern generators of high-voltage pulses. The accelerator [1] generates 270-kV pulses with the current 2 kA, about 2 ns long, it may operate with the rep-rate up to 3.5 GHz. Relativistic electron beam (REB) from an explosive cathode propagates in longitudinal magnetic field 2 T, see Fig.1. Plasma is preformed between plasma source and an electrode installed at the cathode by helical support. The helix inductivity prevents a short-cut of the cathode through plasma.

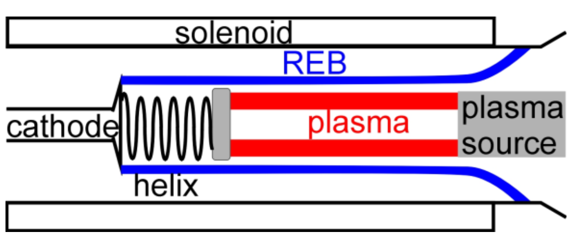

Figure 1. Layout of HPM source

The REB pulse of ~ 2 ns is shorter than time necessary for a distortion to propagate forth and back along the plasma waveguide 20 cm long. The device operates as plasma maser but unlike plasma HPM oscillators [2] it has no feedback, hence, its spectrum does not depend on longitudinal oscillation modes.

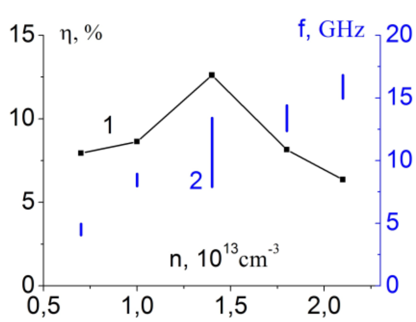

Figure 2 Efficiency η (1) and the frequency f (2) vs plasma concentration n

The main feature of powerful plasma masers is the ability of their emission frequency variation in broad band. Plasma concentration may be set arbitrarily before every pulse, therefore, emission frequency may be changed. Fig.2 shows that emission frequency may be varied within 2 octaves from 4 to 16 GHz, approximately the same band was experimentally demonstrated by rep-rated plasma HPM oscillator [2]. Efficiency ~ 10% of HMP emission provides power up to 100 MW, see Fig.3.

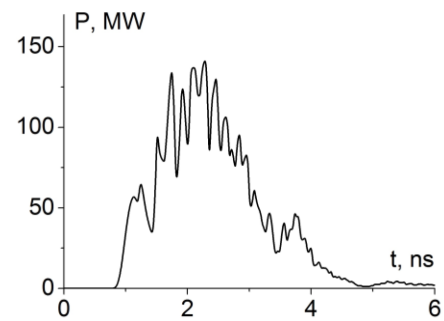

Figure 3. HPM pulse power vs time.

The absence of feedback allows generation of continuous spectrum and plasma variation can change emission frequency. Fig.4 shows that a train of 20 pulses can overlap frequency band from 4 to 16 GHz

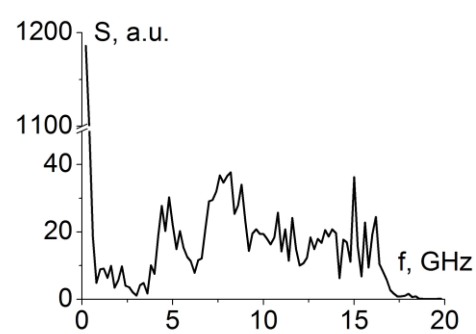

Figure 4. Spectrum of a train of 20 repetitive pulses.

References

[1] D. M. Grishin, V. P. Gubanov, S. D. Korovin, et al. High-Power Subnanosecond 38-GHz Microwave Pulses Generated at a Repetition Rate of up to 3.5 kHz // Technical Phys. Lett. Vol. 28, No. 10, 2002 p. 806

[2] O. T. Loza, I. L. Bogdankevich, D. M. Grishin, et al. Rep-Rated Plasma Relativistic Microwave Oscillator with Tunable Radiation Frequency in Every Pulse // EUROEM 2008, 21-25 July 2008, Lausanne, Switzerland, p.26 // Plasma Phys. Reps., Vol. 34, No. 10, 2008, p. 855.

Supported by Russian Foundation for Basic Research, grants 13-08-00414 and 14-08-31206

Remedying HPM pulse shortening in plasma relativistic microwave oscillators

Svetlana E. ERNYLEVA
Chair of applied physics
Peoples' Friendship
University of Russia
Moscow, Russia
ersvev@mail.ru

Oleg T. LOZA
Plasma physics dept.
A.M.Prokhorov General physics institute RAS
Moscow, Russia
oleg.loza@list.ru

Vladimir P. TARAKANOV
High-current electrophysics dept.
Joint Institute for High Temperatures RAS
Moscow, Russia
karat8tarak@gmail.com

***Abstract*—Numerical modeling of plasma relativistic microwave oscillator revealed reasons for HPM pulse shortening. The proposed method allows to eliminate the cause of this effect and to generate high-power microwave pulses with the duration exceeding 80 ns at power level of 100 MW.**

Keywords- HPM; microwave; high-power; pulse shortening; plasma

The main and insuperable reason for microwave pulse shortening in vacuum HPM oscillators is RF breakdown on the walls of slow-wave structure as a result of proximity to the relativistic electron beam (REB). In plasma masers this reason is not significant because REB is screened by plasma and propagates far from walls, but contrary to this fact, the effect of pulse shortening in plasma HPM devices does exist [1].

The reasons for microwave pulse shortening were found in numerical modeling using 2.5-D version of the KARAT code with PIC-method for electrons and ions. The first reason is a gap that appears between the plasma cylinder and collector [2]. This gap decreases plasma wave reflection coefficient from the collector and may violate the condition for self-excitation. Another reason was found to be more significant, it is the reverse electron flux with the current ~ 1 kA induced by the REB through plasma. This flux interacts with plasma at frequencies other than the REB does. The reverse electron flux hinders plasma from modulation corresponding to the interaction with the REB, reduces plasma wave amplification twice or more and is capable to quench HPM oscillations.

Calculations showed that the electron temperature in plasma grows to 20 keV in the course of the pulse. Such rise of the temperature in itself does not affect the Cherenkov gain but it tends to increase the plasma potential and the reverse electron flux trough plasma. Interaction of these electrons with plasma according to the Cherenkov mechanism takes place at frequencies close to the Langmuir frequency, where the group velocity of the plasma wave vanishes. As a result, plasma does not emit energy and the temperature rises.

The drop in the reflection coefficient of the plasma wave and the gain can be compensated by a multiple lengthening of the beam-plasma interaction area, however, this way has obvious drawbacks. Another method to avoid microwave pulse shortening is shown in Fig. 1. The left border of plasma abuts on an additional electrode connected to a source of negative potential approximately equal to that of the collector. This design prevents electron current throughout plasma.

Fig. 2 shows that unlike conventional plasma HPM oscillator [1], the proposed scheme allows to generate HPM radiation which not terminate. Nevertheless, there remain electron fluxes in plasma which spoil the oscillator. Electrons are emitted from negative (~ 40 kV) collector into positively charged (~ 20 kV) plasma and heats it. Concurrently, the hottest electrons leave plasma overcoming the potential barrier. Therefore, HPM power diminishes to 100 MW but not to zero as it was originally.

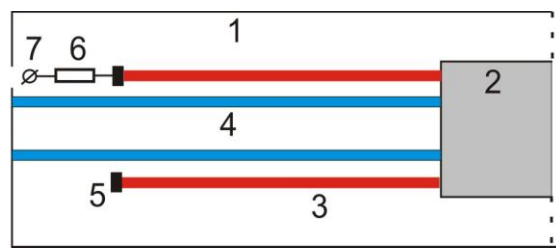

Figure 1. Modified plasma relativistic microwave oscillator: 1 - circular waveguide; 2 – collector; 3 – plasma; 4 – REB; 5 – electrode; 6 – resistor; 7 – source of negative potential.

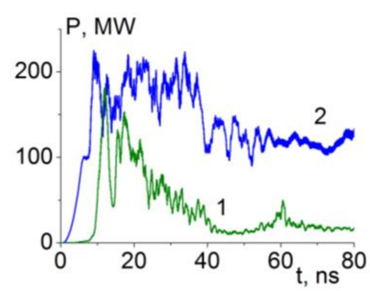

Figure 2. Radiation power vs time: 1 – conventional plasma relativistic microwave oscillator; 2 – modified oscillator.

REFERENCES

[1] O. T. Loza, I. L. Bogdankevich, D. M. Grishin, et al. Rep-Rated Plasma Relativistic Microwave Oscillator with Tunable Radiation Frequency in Every Pulse // EUROEM 2008, 21-25 July 2008, Lausanne, Switzerland, p.26 // Plasma Phys. Reps., Vol. 34, No. 10, 2008, p. 855

[2] I. L. Bogdankevich, O. T. Loza, D.A.Pavlov. Bulletin of the Lebedev phyisics institute, 37(2), 16 (2010)

Development of Electromagnetic Susceptibility Testing of Complex Systems at the Naval Surface Warfare Center, Dahlgren Division

Dr. David C. Stoudt
Senior Director, Naval Capabilities and Readiness
Office of the Deputy Under Secretary of the Navy
for Plans, Policy, Oversight, and Integration
1000 Navy Pentagon, 5E171
Washington, DC 20350
David.Stoudt@navy.mil

Abstract— **The Naval Surface Warfare Center has been involved in electromagnetic susceptibility testing of complex systems for over twenty years. Applications have included electromagnetic compatibility, explosives and ordnance, electromagnetic pulse and high-power radio frequency testing. The challenges of testing complex systems have required the development of a complex testing infrastructure because the only way to approach the problem of predicting failure levels of complex systems is through a combined theoretical and empirical approach. This paper will describe the development of that test support infrastructure from its modest beginnings to its present state.**

Keywords-susceptibility, electromagnetic compatibility, high-power radio frequency

I. INTRODUCTION

The interaction of electromagnetic waves with real systems is very complex and requires an extensive span of capabilities and facilities to perform well-designed experiments. Recent recognition of a variety of electromagnetic threats such as high-altitude electromagnetic pulse, lightning, high-power radio frequency weapons, as well as more traditional high-power transmitters used in such commercial applications as radar and communications, have made the understanding and mitigation of the effects of these sources on electronic control systems vital to the continued proper functioning of our critical infrastructures. Test facilities must represent a variety of interesting systems and must be located so that a variety of high-power sources can be employed to mimic the myriad of proliferated electromagnetic threats. Available analytical tools should include a variety of statistical tools for data analysis and test planning, as well as in the prediction and interpolation of test data. This paper describes the development of such a capability base at the Directed Energy Warfare Office at the Naval Surface Warfare Center (NSWC) in Dahlgren, VA along with some of the theoretical developments used to extend the work to tactical scenarios.

II. APPROACH

The first step in building the capability base was to build a series of test facilities as shown in Figure 1. Those facilities include two multi-story buildings that use common commercial building construction techniques. These buildings are populated with electronic systems, such as computer networks, distributed control systems, communications switches, alarm systems, and Supervisory Control and Data Acquisition (SCADA) systems. In addition to the industrial control systems, actual pumps valves, tanks, and indicators are included to help understand the impact to the industrial process being controlled. The test facilities are located in NSWC-Dahlgren in an area where a variety of fields and impressed currents can be applied in realistic ways. A variety of test planning and data reduction techniques had to be developed to support the understanding of the causes of system and subsystem failure. These tools include statistical and analytical models of various types of system interactions. The point of the analysis is to develop the means to predict system and subsystem failure for a variety of illumination scenarios. Finally, numerical tools and analytical techniques are used to understand the coupling of the fields onto buildings, system cables, and other vulnerable parts of the system.

Figure 1. Open-Air Test Facility at NSWC Dahlgren

Band Pass Filter Limiting Front-Door Coupling of HPEM Threats to Protect K_u-band Satellite Communication System

Werner A. Arriola, Kiho Kim, Ihn Seok Kim
Dept. of Electronics & Radio Engineering
Kyung Hee University
Yongin-si, Gyeonggi-do, South Korea
ihnkim@khu.ac.kr

Tae Heon Jang
Center for Electromagnetic Wave
Korea Testing Laboratory
Ahnsan-si, Gyeonggi-do, South Korea
Thjang1@naver.com

***Abstract*— In this paper, an energy sensitive bandpass filter (ESBPF) is introduced to protect K_u-band satellite communication systems from a front door coupling of high power electromagnetic (HPEM) threats. The ESBPF operates as a BPF at a power level below the maximum permissible power level (MPPL) of the system. However, the circuit works like a variable attenuator at the power level equal to or higher than the MPPL of the system. To increase attenuation and selectivity functions, two cascaded ESBPFs are loaded transversely in a WR-75 waveguide. The development of the circuit model has been started with lumped elements under the condition of 0dBm MPPL of LNA used in the system. Then the model has been simulated, optimized with HFSS, and fabricated. Measurement results show that the ESBPF has insertion loss less than -1.27dB at the power level lower than -2dBm for the frequency range from 11.8 to 12.3GHz. At the power level higher than -2 dBm, the circuit provides different levels of attenuation depending on the input power within the identical frequency band. The insertion loss, which provides isolation characteristics, is larger than -30 dB at the power level of 30 dBm.**

Keywords-Energy sensitive bandpass filter; K_u-band; satellite communication system.

I. Introduction

An energy sensitive band pass filter (ESBPF) has been developed to protect K_u-band satellite systems. After the frequency selective surface (FSS) technique has been reviewed for the structure of the filter circuit [1], [2], where the array of square structure had been used, a single element structure has been selected rather than array, and we modified the structure to mount in a WR-75. A new filter circuit has been mounted on a transverse plane of a WR-75 waveguide. Anti-parallel configuration of the diodes has been applied to operate the circuit without bias. The final circuit has a 63° transmission line section between two adjacent layers.

II. ESBPF Circuit Model and Realization

We have first considered a BPF structure for the frequency range from 11.8-12.3GHz and the equivalent circuit model shown in Figures 1(a) and (b), respectively. The ADS and HFSS simulations for both of the equivalent circuit (Figure 1(b)) and the structure (Figure 1(a)) models without diodes have been tried at the center frequency of 12.5GHz.

To have better selectivity, two layered configuration has been used with a 63° line section between the two, since the 63° section provides two transmission poles, and an anti-parallel Schottky Barrier diode model has been inserted as shown in Figure 1(c) since the diodes provides attenuation control. The two layered ESBPF shown in Figure 2(a), has been simulated with the circuit and structure models shown in Figures 1(c) and 2(a), respectively, by ADS and HFSS simulators based on the dimensions of Wa=20.05mm, Wb=10.525 mm, Ws=5 mm, Ls=2.75 mm, Ss=0.3 mm, Ea=6 mm, gap=0.5 mm on a substrate with ε_r =4.5 and thickness 0.508mm, and distance 7.4mm between two layers for the 63° section as shown in Figures 1(a) and 2(a). After the BPF have been fabricated on the TMM4 substrate, anti-parallel Schottky Barrier diodes, MADS-101318-1197HP, has been mounted across the upper gap of the structure.

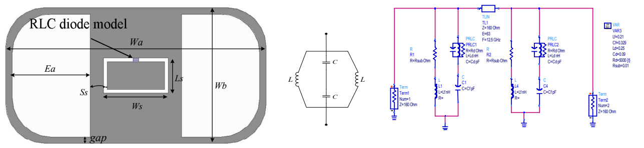

(a) (b) (c)

Figure 1. (a) ESBPF structure. (b) Lumped element equivalent model for the circuit shown in (a). (C) ADS model for two layered ESBPF with anti-parallel Schottky Barrier diodes.

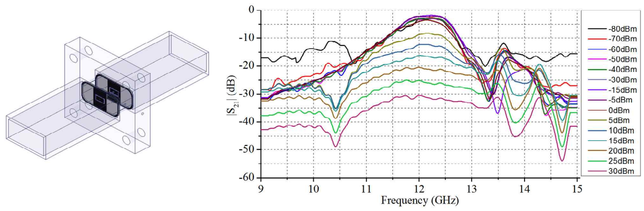

(a) (b)

Figure 2. (a) HFSS simulation structure for the ESBPF using two layers. (b) Measurement results for $|S_{21}|$ of the ESBPF at different input power levels.

At the power level lower than -2dBm, insertion loss less than -1.27dB has been measured when the circuit works like a BPF. Measurement results for different input power levels are shown in Figure 2(b), where the BPF makes the signal attenuate gradually as higher incident power is coupled.

References

[1] G. I. Kiani, K. L. Ford, L. G. Olsson, K. P. Esselle, and C. J. Panagamuwa, "Switchable Frequency Selective Surface for Reconfigurable Electromagnetic Architecture of Buildings", IEEE Transactions on Antennas and Propagation, Vol. 58, No. 2, February 2010.

[2] S. M. Amjadi, and M. Soleimani, "Narrow Band-Pass Waveguide Filter Using Frequency Selective Surfaces Loaded with Surface Mount Capacitors", Int. Conf. on Electromagnetics in Advanced Applications 2007. Pp. 173-176,2007

EM Propagation Measurements and Analysis

H.W.L. Naus, R.R. Wymenga and A.P.M. Zwamborn
Research Group Electronic Defence, Physics and Electronics, TNO, 2509 JG The Hague, Netherlands
rik.naus@tno.nl, roel.wymenga@tno.nl, peter.zwamborn@tno.nl

***Abstract*—This document reports on electromagnetic propagation experiments. The received power has been measured for various distances and frequencies. The acquired data are fitted to simple propagation models, showing satisfactory results.**

***Index Terms*—Antennas, Electromagnetic propagation, Propagation losses**

I. Introduction

Our research addressess the propagation of electromagnetic signals in the frequency region 20 MHz-6 GHz. Measurements haven been performed at a countryside test site in the Netherlands. To analyze the data, some simple radio propagation models have been considered. Such models attempt to predict the received power at a receiver. Given the transmitted power and antenna gains, it is equivalent to determining the propagation loss. The simplest example is the well-known free space loss. However, in practice a large number of phenomena like ground reflections, surface waves, multipath, shadowing and diffraction are present. The environment plays a dominant role. A classic example of a propagation model is the one of Egli for rural environment [1]. More propagation models are discussed in, e.g., [2], [3], [4].

II. Simple EM propagation models

In free space the received electromagnetic power P_R for antenna separation distance d is given by

$$P_R = \left(\frac{\lambda}{4\pi d}\right)^2 G_T G_R P_T, \tag{1}$$

where P_T denotes the transmitted power, λ the wavelength and $G_{T,R}$ the transmitter/receiver antenna gains. Polarization and impedance matching factors [5] are taken to be one, *i.e.*, ideal matching.

The so-called R^n model has been presented in [2]; it effectively means that the factor d^2 in the denominator is replaced by d^n. Thus a different power fall-off in distance is allowed for. We convert to decibels and use the R^n model in the following form

$$P_R(\text{dBm}) = \eta - 10\, n \log d. \tag{2}$$

The parameter η depends on frequency and transmitted power. An alternative phenomenological model explicitly includes the frequency dependence as well:

$$P_R(\text{dBm}) = \alpha \log d + \beta \log f + \gamma, \tag{3}$$

with frequency f and parameters α, β, γ.

This study has been sponsored by the Dutch Ministry of Defence.

III. Experiments and fits

Propagation measurements have been done for distances between transmitter and receiver antenna ranging from 5 to 100 meters. In each frequency band the power has been measured for 500 frequencies. We have also varied the polarization of the receiving antenna.

The measured data haven been analyzed using the proposed models. The first model, the R^n model (2), does fit these data quite well per frequency. This is confirmed by a preliminary statistical analysis. The second model (3) takes the frequency dependence into account by the use of the parameter β. It performs reasonably; in a few cases, however, it fails. No noticeable dependency on the polarization has been observed in the measurements.

As an example, we show results for fitting the R^n model to low-frequency data with horizontal antenna polarization. The left hand side shows the power as function of the distance at 250 MHz only; it is one of fitted subsets. Such a fit is done for each frequency. Herewith we can depict the power as a function of frequency at a fixed distance, here 20 m. The right hand side contains this collected result of the various fits.

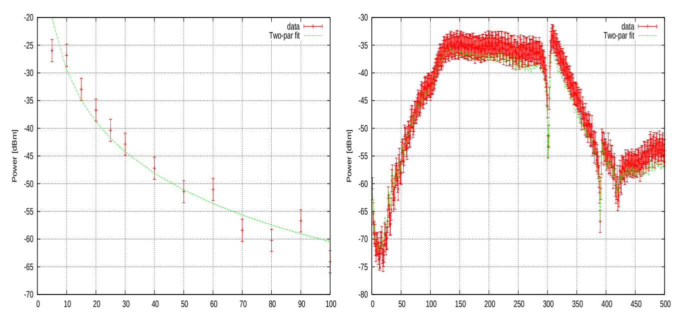

Fig. 1. L.h.s frequency 250 MHz, r.h.s. distance = 20 m

References

[1] J.J. Egli, "Radio propagation above 40 MC over irregular terrain", Proceed. IRE 45 (10), pp. 1383-1391, 1957.

[2] R.A. Poisel, "Modern communications jamming principles and techniques", Artech House, Inc., Norwood, 2004.

[3] K. Craig and M. Willis, "Propagation model development", GRMT Final Report, Annex B, 2007.

[4] N. DeMinco, "Propagation loss prediction considerations for close-in distances and low-antenna height applications", NTIA report TR-07-449, 2007.

[5] P.F. Stenumgaard and K.C. Wiklundh, "An improved method to estimate the impact on digital radio receiver performance of radiated electromagnetic disturbances", IEEE Trans. on Electromagn. Compat., 42 (2), pp. 233-239, 2000.

Therapeutic and Diagnostic Uses of Electromagnetic Energy

D. V. Giri
Dept. of ECE, Univ of New Mexico
Albuquerque, NM, USA and Pro-Tech,
11-C Orchard Ct, Alamo, CA 94507, USA
Giri@DVGiri.com

Jayanti Venkataraman
Department of Electrical Engineering
Rochester Institute of Technology
Rochester, NY 14623 USA
jnvee@rit.edu

Abstract—The electromagnetic (EM) spectrum ranging from DC to Gamma rays and beyond is a vast natural resource that has been very valuable for mankind. With the rapid advances of medical technology, Radio Frequency (RF) techniques are becoming increasingly popular for a variety of applications such as non-invasive diagnosis, continuous monitoring of physiological data, communication between implanted devices, and communication to external devices. In this paper, we review medical uses of EM energy.

Keywords - EM spectrum, therapy, X rays, Gamma rays, ionizing radiation, UWB, FCC.

I. INTRODUCTION

Therapeutic applications of EM energy can be broadly classified into two groups as (1) conventional and (2) emerging therapies. Examples of conventional therapies are: a) hyperthermia (thermal therapy), b) MRI, c) X-ray and d) CT scan. In the emerging category are a) THz Imagery and b) implantable devices. Examining the EM spectrum one can observe a dichotomy at about 10^{15} Hz to delineate non-ionizing and ionizing radiation. At f $=10^{15}$ Hz, the quantum of energy associated with the EM radiation is E = hf ~ 4 eV where 'h' is the Planck's constant. Medical applications are possible at many frequencies such as DC, RF, Microwave, X rays and Gamma rays.

II. EXAMPLE THERAPIES

A. Ionizing Radiation - Gamma Rays, X-Rays and UV

All three of these are ionizing radiation and can cause cancer in high doses. They also have beneficial applications in appropriate and low doses. For Gamma Rays, frequency is 10^{24} Hz, wavelength is 300 femto-m (size of an atom) and the photon energy is 4 BeV. Gamma rays have beneficial applications as well, such as: a) Gamma ray camera in Thallium test of the human heart, b) removing decay-causing bacteria in many food items, and c) screening merchant ship containers at US ports. Regarding X- rays, frequency is 10^{18} to 10^{21} Hz, wavelength is (300pico-m to 300 femto-m) and the photon energy is 4keV to 4MeV. It is an ionizing radiation that can cause cancer in high doses. The beneficial applications are radiography and spectrography. UV radiation frequencies are 10^{15} – 10^{18} Hz, wavelength of 10s to 100's of nm and the photon energy is 4 to 4 keV. While exposure to excessive UV radiation from sun is harmful, beneficial use of UV radiation is water sterilization or removal of pathogens.

B. Non-Ionizing Radiation

Examples of therapeutic uses of microwave radiation are: a) Microwave Balloon Angioplasty (MBA) wherein dipole or helical antenna current can heat the inner plaque surface in an artery [1]. RF ablation in the frequency range of (100 kHz to 10 MHz) is possible to treat arrhythmia caused by abnormal electrical pathways in the human heart. Catheters are threaded to the site and ablation is performed by applying a voltage between the catheter electrode 2 to 3mm and a ground plane 10 cm x 15 cm attached to the patient's back.

C. Emerging Therapies

FCC has classified UWB defined as signals having a percent bandwidth more than 20%, or an absolute bandwidth of at least 500MHz. Characteristics of UWB are: [3.1 to 10.6 GHz] band-width of 7500 MHz. High data rate capability and spectral power density limits (80 nW/MHz) on emission have opened up many technologies including medical applications ex: implantable devices; Wireless Capsule Endoscopy (WCE) is a "camera in a pill" the size of a large vitamin pill is a diagnostic tool. The applications described in this paper and many others will be presented.

D. Noninvasive Therapies

Amongst the most interesting emerging RF technology is a class of noninvasive glucose monitoring techniques. The most notable ones are infrared spectroscopy, optical coherence tomography, Raman spectroscopy, ocular spectroscopy and impedance spectroscopy. Feasibility studies have been shown [2] that an antenna's resonant frequency can track, in real time, changes in glucose concentration, from which glucose levels can be estimated. A recent release, the GlucoTrack uses ultrasound, electromagnetic and thermal techniques. Another noninvasive system is developed by Google, which is a contact lens that measures the glucose level in tears and extracts the data wirelessly.

C. Body Sensor Networks (BSN)

Body sensor networks provide a continuous monitoring of physiological data with an integrated hardware and software platform [3]. Wearable or implanted wireless sensors, gather data and are either locally processed or encrypted and transmitted to a server. BSN has the potential of revolutionizing healthcare. Some examples of continuous monitoring devices that have proved to be very effective are management of acute diabetes with implanted insulin delivery, implanted multi-programmable brain stimulators, implanted cardio-defibrillator for prevention of life threatening events such as sudden cardiac arrest, or arrhythmia.

REFERENCE

[1] R. Habash , "Bioeffects and Therapeutic Applications of Electromagnetic Energy", CRC Press , 2008.
[2] Sidley M. and Venkataraman J., "Feasibility of Blood Glucose Estimation from Real Time Monitoring", Proc. IEEE Ant and Propagation Intl. Sym., Orlando, July 8-12, 2013.
[3] Lo, B. P. L. and Yang, G. "Key Challenges and Current Implementations of Body Sensors" International Workshop on Wearable and Implantable Body Sensor Networks (April 2005)

Evaluation of RF Transfer Functions Between the Outside and the Inside of Building Rooms

EM topology and Power Balance Approaches

I. Junqua – J.P. Parmantier – F. Issac – W. Quenum
ONERA – The French Aerospace Lab, F-31055, Toulouse, France
isabelle.junqua@onera.fr

***Abstract*— This paper focuses on the experimental work led in the context of the European HIPOW project. The objective is to evaluate RF transfer functions between different areas of a building in order to assess EM environment in potential critical rooms in case of external or internal EM source threat. As a first step, an experimental protocol has been developed. Then, EM coupling between different rooms has been evaluated. Finally, transfer functions between the exterior and the interior of the building have been measured and first attempts to demonstrate the application of EM topology to buildings have been carried out.**

Keywords-component; Critical Infrastructures; RF transfer functions; HPM; IEMI

I. Introduction

This paper deals with the experimental evaluation and analysis of electromagnetic (EM) coupling inside buildings or from the outside to the inside of buildings. This work is carried out in the context of the HIPOW European project which intends to improve the current European situation regarding awareness of NEMP/HPM threats and the adequacy of protection of critical infrastructures against EM threats. Here, the objective is to evaluate the transfer functions in a representative building and to analyze how incident EM external or internal fields penetrate and propagate inside different rooms. This work is based on experimental analysis of ONERA's own office building in a frequency range from 300MHz up to 6GHz. Such an evaluation implies the development of an optimized experimental protocol. Then, first electromagnetic topology concepts based on Power Balance can be used to build a quantitative interaction diagram sequence of the problem as in Electromagnetic Topology.

II. Experimental Set-Up

An experimental protocol has been optimized in order to be able to measure transfer functions with a distance up to about 100m from each other (Fig. 1).

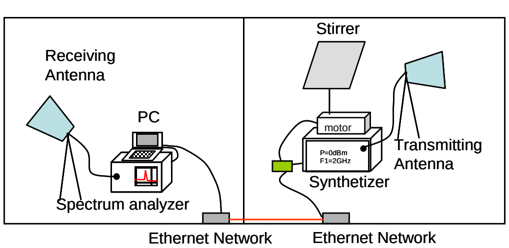

Figure 1. Experimental Set-Up

It is based on mode stirring techniques combined to a set of pre-defined configurations of antennas to take into account imbalanced polarizations (HH, HV and VV). All apparatus are driven by a PC through the internal building Ethernet network.

III. EM Coupling Between Rooms of a Single Building

The first step consisted in measuring EM cross-coupling between one laboratory room (Lab 2) in which the transmitting antenna and synthesizer were installed and several surroundings rooms (offices, corridor and storage rooms) via a receiving antenna connected to a spectrum analyzer. An example of EM resulting cross coupling expressed in dB is given in Fig. 2

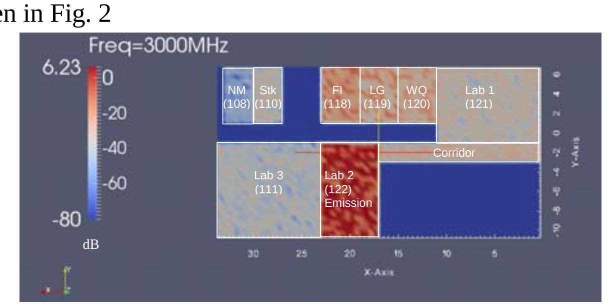

Figure 2. EM cross-coupling between rooms (injection in Lab. 2 room)

IV. EM Coupling Between the Outside and Rooms of the Building

Then, transfer functions from the outside and various rooms of the building have been evaluated. External source was about 50m away from the reception building. As an example, the effect of metallic curtains versus polarizations has been shown. As a final step, applicability of EM topology concepts to EM propagation and penetration in buildings has been successfully demonstrated by analyzing shielding effectiveness with topological network decomposition for different configurations of windows. Various examples and parametric analysis will be given in the oral presentation.

This work has received funding from the European Community's Seventh Framework Program (FP7/2012-2015) under grant agreement number 284802 HIPOW project.

References

[1] HIPOW Description of work. EU project Grant n 284802

[2] "Safety of installations submitted to EM threats", Special Session of EUROEM 2012 – HPEM-TC02-SS1, Toulouse, France, July 2012

.

Microwave Attack Detection System

R. Simniškis, M.Dagys, Ž.Kancleris, and P.Ragulis

Microwave Laboratory of Physical Technology Department
Center for Physical Sciences and Technology
Vilnius, Lithuania
rimantas.simniskis@ftmc.lt

***Abstract*— A microwave attack detecting system on the basis of high power microwave resistive sensor was developed, prototyped and tested in field conditions. The system operates at severe conditions of microwave radiation measures the high power microwave pulse and presents the circular diagram of radiation. It was tested up to several tens of kV/m.**

Keywords-high power microwave; microwave power resistive sensor.

I. Introduction

The modern environment and infrastructure are inseparably related with a plenty of complicated electronic systems and consumable electronic products. Therefore the problems like electromagnetic compatibility, radiation immunity, intentional or accidental electromagnetic attacks are relevant and critical for infrastructure. It is important to register the event of microwave attack, detect the direction of microwave source and measure the radiation level. That enables to assess the risk, value of possible damage and consequence. After the detection and evaluation of microwave attack it is possible to prevent the damage by replacement of most critical components of system, apply the corresponding service measures to prevent the possible accidence and casualties in such critical systems of infrastructure like railway or air traffic control systems.

The application of high power microwave pulse resistive sensors, developed in microwave laboratory, horn antennas and step motor driven antenna actuators, microwave attack detecting system was developed and applied in high power immunity tests in the frame of NATO task group SCI-250 [1] and project HIPOW supported by European community. The exclusive property of the developed system is the capability to operate at very strong radiation, detect the direction of attacking microwave source and measure the radiation in free space from 400 V/m up to 100 and more kV/m in the frequency range of 1-18 GHz.

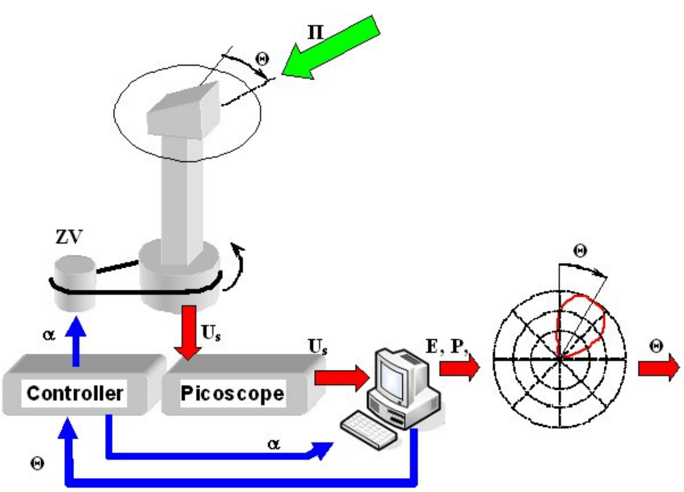

Figure 1. The diagram of microwave attack detecting system.

II. Detecting System

The diagram of structure and operation principle of the developed system is shown in Figure 1. The horn antenna with high power microwave pulse resistive sensor is mounted on actuator which rotates continuously enabling measurement of radiation diagram. The resistive sensor converts the microwave pulse into analog video pulse corresponding to the envelope of microwave pulse. The output signal U_s is captured by digital oscilloscope “Picoscope 630B”. The master computer of the system controls the azimuth angle α of the antenna and picks up the signals, when antenna is rotated. Each signal sample U_{si} corresponds to antenna position α_i. On the basis of the captured signal array, the calibration data of antennas and resistive sensors, the circular radiation diagram of the power density or electric field strength is plotted on the screen. The thresholds of dangerous radiation levels can be set. As a result of the analysis of the radiation diagram the azimuth angle of the radiation source Θ is computed and antenna is directed towards it. The accuracy of Θ evaluation depends on signal level and signal to noise ratio. The mechanical accuracy of antenna actuator is ±1°.

III. Results and Conclusions

The system was tested at field trials. It demonstrated high electromagnetic immunity and uninterruptible operation under radiated electric field conditions up to 30 kV/m. The microwave sensors with horn antennas were tested up to 200 kV/m and demonstrated stable operation. The improvement of radiation direction calculation at noisy signal conditions and application of a few sensors widening frequency range is under development.

The work was supported by Lithuanian Research Council contr.No. MIP-096/2012

References

[1] NATO Yuotube: Suicide bombers and how to beat them, http://www.youtube.com/watch?v=56veH8-KbEM.

Protection of Critical Infrastructures against High Power Microwave Threats - HIPOW

An EU 7th framework project on protection of electronic systems against natural and manmade electromagnetic threats.

Odd Harry Arnesen
Protection and Societal Security Division,
Norwegian Defense Research Establishment (FFI)
PO.box 25, N2027 Kjeller, Norway.
Odd-Harry.Arnesen@ffi.no

***Abstract*— This paper elaborates on the work within the EU FP7 HIPOW project, as well as its objectives and work plan. An update of the progress and key results from the HIPOW project will be presented.**

The concept for HIPOW is to develop a new regulatory and organizational framework for protection against all relevant electromagnetic threats, which includes methodologies, procedures and designated responsibilities, capabilities for risk assessment, testing, protection and emergency preparedness measures. In order to achieve the intended real life impact, this will have to be done so that the final results, or deliverables, are directly applicable to the end users.

The HIPOW consortium consists of 14 partners from 10 european countries.

This paper is intended for the Special Session 2 (SS02) on HPEM-Impacts/Protection on Critical Infrastructure in Europe.

Keywords; EM threats; protection; critical infrastructure.

I. PROTECTION OF CRITICAL INFRASTRUCTURE

The efforts to protect civilian critical infrastructure against possibly harmful effects caused by various transient electromagnetic phenomena have not kept pace with the developments of relevant threats and consequences of system failure. There are several economical and practical reasons for this. Many critical infrastructure owners and operators regard EM threats as relatively obscure compared to other challenges they face. Research on EM susceptibility and hardening has largely been performed within the military sphere, and the results are, more often than not, classified. Private and public entities alike need justification for the resources they spend on protection, and in general seem to focus more on improving performance rather than resilience.

The scientific community does endeavor to provide justification for reasonable levels of protective measures by studying the physical phenomena, and demonstrating effects and consequences. This needs to be done in many ways, and on several levels.

II. OBJECTIVES OF THE HIPOW PROJECT

Our main goal is to improve the European critical infrastructures' overall immunity against the threat from EM radiation like high power microwaves and electro-magnetic pulses by conducting a threat analysis and risk assessment of the occurrence of microwave radiation events and their most likely modalities. And investigate the influence of HPM pulses on civil objects, like buildings, energy units, transport, banks, communication systems, computer networks, computers and electronic units. We need to investigate to what extent the current protection is efficient and identify shortfalls, in order to provide recommendation tools, improved hardening, redundancy architectures etc. for protecting civil objects against EM radiation. Furthermore HIPOW will suggest a organizational regime for risk management and mitigation, and provide recommendations as input to standards organizations. [1]

Reliable detection of potentially harmful EM transients is also a priority, and the project will prepare for EM transient detection and diagnostic systems, also by developing a pulse detector prototype.

Results will be disseminated through unclassified and classified channels, as need be. Our aim is to publish at workshops and meetings with authorized personnel, and disseminate unclassified main results in scientific papers, conferences and newspapers. Our end goal is to publish recommendations as handbooks or other reference material, directly available and applicable to our end users.

III. RECENT ACTIVITIES

The project is now in its second year, with work on threat analysis, current mitigation techniques as well as analysis on the political and legal framework. A scenario based risk and cost analysis is also in progress. HIPOW conducted a large full threat trials campaign in September 2013.

REFERENCES

[1] The HIPOW Project proposal. EU project grant nr. 284802.

Numerical Validation of the Absorption of Ferrite Material in NEMP applications

Marc Sallin and Bertrand Daout
montena technology
Rossens, Switzerland
marc.sallin@montena.com
bertrand.daout@montena.com

Felix Vega
Departamento de Ingeniería Eléctrica y Electrónica
Universidad Nacional de Colombia, Bogotá D.C.
jfvegas@unal.edu.co

***Abstract*— The goal of the present work is to perform a numerical validation of the absorption characteristics of frequency dependent ferrite tiles surrounded by metallic walls. In particular, we are interested in the absorption performance of the ferrite when illuminated by Nuclear ElectroMagnetic Pulse (NEMP) fields generated using a bounded wave antenna inside an anechoic chamber.**

Ferrite; NEMP; Debye Model; FDTD; Complex Permeability

I. INTRODUCTION

There is a clear tendency in both commercial and military EMC laboratories to install pulsed electromagnetic test systems inside anechoic chambers. The reasons are obvious: (1) protect the environment against the generated high amplitude test fields and (2) take advantage of the available free volume, continuous ground plane and test monitoring equipment. In the particular case of a bounded wave antenna installed inside an anechoic chamber, special care needs to be taken in order to choose the maximum antenna size (determining the test object size) that fits in a given chamber, without the signal in the working volume being affected by the neighboring walls. In this context, FDTD electromagnetic wave simulations using Debye models for magnetic materials can be used to predict the effect of existing ferrite tiles. It is also well adapted for the optimization of the parameters of the ferrite tiles (permeability, depth of the ferrite tile, depth of the dielectric layer between the ferrite and the metallic wall).

II. THEORY

The parameter dominating the absorption of electromagnetic waves in ferrites is the magnetic loss. In analogy with the electric losses in conductors, the magnetic losses are linked to the magnetic conductivity which is a function of the imaginary part of the complex permeability and of the frequency.

Due to its strong dispersive character, the complex permeability of ferrites $\tilde{\mu}_r(f)$ can be described in the frequency domain using a one-pole Debye model as follows:

$$\tilde{\mu}_r(f) = \left(1 + \frac{a_1(\mu_{r1} - 1)}{1 + \mathrm{j}2\pi f\tau_1}\right)\mu_0 \qquad (1)$$

where: μ_{r1} is the static relative permeability of the pole, a_1 is amplitude of the pole, τ_1 is the relaxation time of the pole and f is the frequency.

III. RESULTS

The reflection of electromagnetic waves from ferrites whose permeability corresponds to Equation (1) was evaluated using an FDTD based electromagnetic simulation tool [1]. The results of the simulations were contrasted with theoretical calculations and with experimental results reported in the literature.

A first series of validations were performed in the frequency domain. The experimental setups reported in reference [2] where reproduced by simulation and the results were compared. The frequency range was defined between 30 MHz and 1 GHz. The influence of the depth of the ferrite material, the depth of the dielectric spacing between the ferrite and the surrounding wall and the angle of incidence of the wave were studied.

Following this, a second set of simulations studying the reflection of time-domain signals was performed. The simulation of a real case, consisting on a 1.8 m high bounded wave antenna inside a small anechoic chamber, is worth noting. Preliminary results can be seen in Figure 1 where the effect of the ferrite tiles on the reflection of the electric field can be observed.

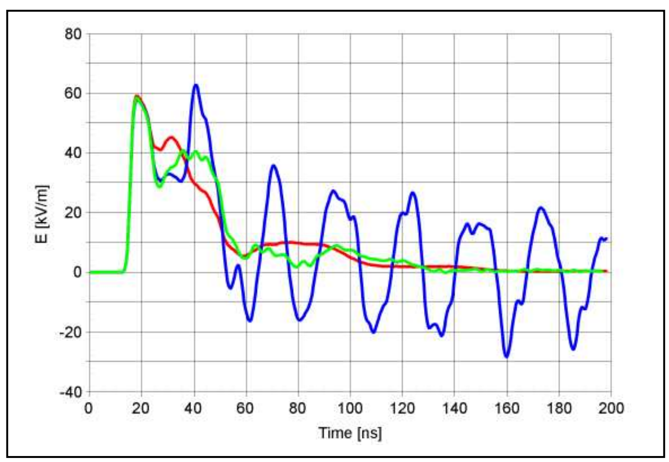

Figure 1. Comparison of the vertical component of the electric field in the test zone of a bounded wave antenna located: (red) in free-field, (blue) in a small sized fully metallic shielded room, (green) in the same shielded room with ferrite tiles covered walls.

REFERENCES

[1] SPEAG, SemcadX Reference Guide, 2013.
[2] C. L. Holloway, R.R. Delyser, R. F. German, P. McKenna, and M. Kanda, “Comparison of Electromagnetic Absorber Used in Anechoic and Semi-Anechoic Chambers for Emissions and Immunity Testing of Digital Devices” IEEE Transactions on Electromagnetic Compatibility, Vol. 39, No. 1, February 1997.

Instruction Dependent Upset of a Microcontroller

David M. French, Tim Clarke
Directed Energy Directorate
Air Force Research Laboratory
Albuquerque, NM, USA

Kyle Gordon
Electrical Engineering and Computer Science
University of Michigan
Ann Arbor, MI, USA

***Abstract*— Direct injection experiments have been carried out on a microcontroller in order to determine upset dependencies of digital electronic systems. The microcontroller provides a platform to examine the effects of direct injection timing, frequency, and pulse duration on a digital system with known programming and a known operational state. Results indicate that in addition to a dependence on frequency and pulse width of the direct injection signal, different programming instructions demonstrate different upset thresholds.**

Keywords-IEMI, Upset, Digital Electronics, HPM

I. Introduction

There has been significant research into the effects of RF signals at the device level [1] as well as at the circuit and chip level [2], while more recently the RF Effects MURI [3] provided significant advances in understanding and predicting RF effects. A microcontroller, being a simple but complete computer on a single chip and thus representing an intermediate level of complexity between an individual CMOS device and a complete digital system, is an ideal device to use as a test-bed in attempting to understand and predict RF effects on digital electronic systems [4]. In addition, earlier research on quantifying the susceptibility of microcontrollers to RF pulses [5] suggested that carefully timed RF pulses relative to clock signals could yield useful information about the underlying mechanisms of RF interference.

II. Experimental System

A. *Experimental method*

Our experimental approach was to mount the microcontroller on an evaluation board, both for ease of programming and to provide convenient connections for RF injection. A function generator provides an external clock signal to the microcontroller. By providing the clock and knowing specifics of the programing the instruction being carried out at each clock cycle is known. A delay generator is used to gate a direct injection RF signal with a user-specified amplitude at a predetermined time into microcontroller XTAL1 signal line, along with the external clock signal from the function generator.

For the majority of experiments, the microcontroller is programmed to execute a counter, and we monitored the outputs to determine the state of the microcontroller. For each suite of experiments, we performed the RF injection and recorded the response of the microcontroller. Specifically, we monitored the output of the counter, and documented whether or not the RF pulse resulted in an upset. At each voltage we repeated the experiment a specified number of times, and made use of a Bayesian approach to convert the binary data (effect/no effect) into a continuous probability of effect curve. We then summarized the curve for each location by the voltage associated with a 50% probability of upset (which we refer as the threshold voltage), together with a 95% confidence interval (strictly a Bayesian credible interval). The model we have developed suggests a number of experimental investigations.

B. *Experimental Results*

Data have been taken to examine the upset threshold dependence on frequency, pulse duration, and instruction state. The most interesting of these is the dependence on the instruction being carried out by the microcontroller at the time of injection.

Data taken to date indicates that the upset threshold varies with the software being executed. Further work is being conducted on a variety of assembly instructions including bitwise operations, data exchange, and branching instructions. Significant progress has been made in programming the MCU, allowing injection of RF while it is responding to interrupts and adhering to the watchdog timer.

This work was sponsored by AFOSR.

References

[1] Estep, N.A. High Power Microwave (HPM) and Ionizing Radiation Effects on CMOS Devices. Master's Thesis, Air Force Institute of Technology, Mar 2010.

[2] Laurin, J., S. G. Zaky and K. G. Balmain. On the Prediction of Digital Circuit Susceptibility to Radiated EMI. IEEE Transactions on Electromagnetic Compatibility, Vol. 37 No 4, 528-535, 1995.

[3] Granatstein, V. L. Effects of High Power Microwave and Chaos in 21st Century Analog and Digital Electronics. MURI Final Performance Report, AFOSR Grant Number F496200110374, 2007.

[4] Clarke, T. J., Dietz, D. and D. French. Modeling of Radio-Frequency Effects on a Microcontroller. Proceedings of ICEAA Conference, Torino Italy, 2012

[5] Wendsche, S., R. Vick and E. Habiger. Modeling and Testing of Immunity of Computerized Equipment to Fast Electrical Transients. IEEE Transactions on Electromagnetic Compatibility, Vol. 41 No 4, 452-459, 1999.

ID 097

Development of a HEMP and IEMI Protection and Testing Guide using IEC SC 77C

William A. Radasky

Metatech Corporation
Goleta, California USA
wradasky@aol.com

***Abstract*— IEC SC 77C has been developing standards and reports dealing with the protection of the civil infrastructures against the threats of High-altitude Electromagnetic Pulse (HEMP) and Intentional Electromagnetic Interference (IEMI) for more than 20 years. While many of these publications deal with hardening measures and testing of facilities, there is no comprehensive single document to describe how to develop and test a hardened facility. IEC SC 77C plans to begin that effort in 2014, and this paper will describe the plans.**

Keywords-IEC, IEMI, HPEM, Standards, Critical Infrastructures

I. INTRODUCTION

Work began in the International Electrotechnical Commission (IEC) in 1989 to develop standardized electromagnetic environments, protection techniques, and test methods applicable for civil society to protect critical equipment and systems from the electromagnetic threat created by a detonation of a high-altitude nuclear burst (known today as HEMP). The work expanded from a working group under TC 77 to a full subcommittee SC 77C in 1992. Later in 1999 the work was expanded to deal with the threat of electromagnetic weapons, now known as intentional electromagnetic interference (IEMI). Figure 1 below indicates graphically the status of publications in SC 77C before 2013 (in black) and the newest projects (in orange) that are active in 2014.

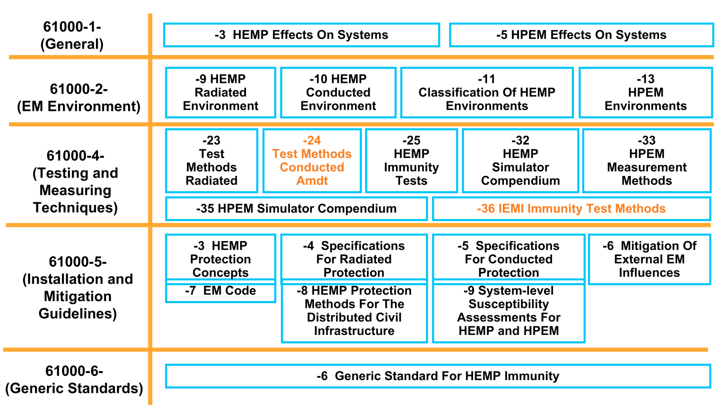

Figure 1. Publications developed by IEC SC 77C.

II. CATEGORIES OF PUBLICATIONS

The 20 publications prepared thus far in IEC SC 77C are split into two main categories – HEMP and IEMI (which is occasionally referred to as HPEM). There are some publications that deal with both areas. This paper will review the 20 publications and describe those papers that provide protection methods for HEMP and IEMI and those that provide test techniques that are required to ensure that the protection methods are properly achieved.

For this one page paper we will only list below only the publications developed thus far that deal with HEMP testing, but the presentation will identify which publications contain relevant information for protecting and testing critical civil facilities from both of these high power electromagnetic threats.

III. LIST OF IEC SC 77C TESTING PUBLICATIONS

IEC/TR 61000-1-3 (2002-06): The effects of high-altitude EMP (HEMP) on civil equipment and systems.

IEC/TR 61000-1-5 (2004-11): High power electromagnetic (HPEM) effects on civil systems.

IEC 61000-4-23 (2000-10): Test methods for protective devices for HEMP and other radiated disturbances.

IEC 61000-4-24 (1997-02): Test methods for protective devices for HEMP conducted disturbance.

IEC 61000-4-25 Ed. 1 Amd. 1 (2012-05): HEMP immunity test methods for equipment and systems.

IEC/TR 61000-4-32 (2002-10): High-altitude electromagnetic pulse (HEMP) simulator compendium.

IEC 61000-4-33 (2005-09): Measurement methods for high power-transient parameters.

IEC/TR 61000-4-35 (2009-07): High-power electromagnetic (HPEM) simulator compendium.

IEC/TS 61000-5-9 (2009-07): System-level susceptibility assessments for HEMP and HPEM.

IEC 61000-6-6 (2003-04): Generic standards – HEMP immunity for indoor equipment.

IV. SUMMARY

This paper will describe the key protection and test aspects found within the 20 publications produced thus far by IEC SC 77C. The objective of the new project in IEC SC 77C is to provide in a single document a complete hardening and testing guide for critical infrastructure facilities to be protected from both HEMP and IEMI.

ID 098

Statistical Distribution of the Induced Voltage in Two Coupled Wave-chaotic Cavities

Xin Li, Cui Meng, Yinong Liu, Jun Zheng
Key Laboratory of Particle & Radiation Imaging, Ministry of Education, Tsinghua University Beijing, China, 100084

Edl Schamiloglu
Department of Electrical and computer Engineering
University of New Mexico, Albuquerque, MSC01 1100, USA

Sameer D. Hemmaday
TechFlow Scientific-A Division of Techflow Inc.
2155 Louisian Blvd.NE, Suite 3200, Albuquerque, NM 87110

***Abstract*— According to the BLT EM topology, a large complicated system can be systematically broken into a topological network on which the BLT equation is implemented to compute the induced voltage or current. In this paper, the BLT equation is applied to a network of two wave-chaotic cavities that connected by a transmission line when excited at the source port. The statistical distribution of the induced voltage calculated by BLT equation will be presented, which is in good agreement with that by others methods.**

Key words- BLT equation, wave chaos, induced voltage

I. INTRODUCTION

The well-known BLT EM topology was formulated by Drs. C. Baum, T. K. Liu and F. M. Tesche in 1978 to analyzing the RF coupling into large complicated enclosures such as aircrafts, ships and buildings [1]. In this paper, a simple network including two wave-chaotic cavities connected by a cable (see fig.1) is chosen to implement the BLT equation and the statistics of the induced voltage will be presented as well as compared with that computed by other methods.

II. EXPERIMENTS

Fig. 1 is the schematic diagram of the experiment setup. Each cavity is a real computer box and excited by two ports. The mode stirrer comprises a central copper shaft and two orthogonally-oriented blades coated with aluminum foil. First, measure the scattering matrix of each box, denoted by $\boldsymbol{S_{1\text{-}2}}$ and $\boldsymbol{S_{3\text{-}4}}$ respectively. By rotating the shaft for 250 different positions, at each position, the scattering matrix is measured from 4GHz to 15GHz in 11001 equally space steps. Second, connect port 2 and port 3 with a 1m coaxial cable and measure the ensemble of the scattering matrix between port 1 and port 4, denoted by $\boldsymbol{S_{1\text{-}4}}$. In addition, the scattering properties of the cable is measured, denoted by $\boldsymbol{S_c}$.

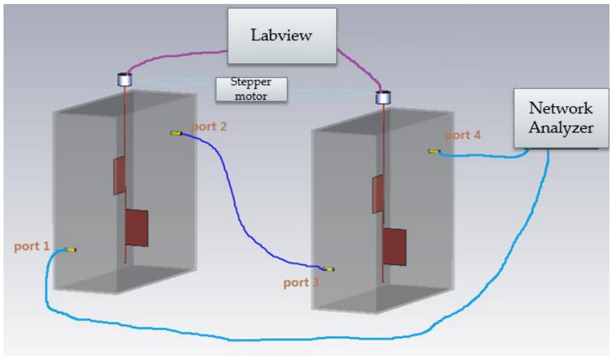

Figure 1. Schematic diagram of the experiment setup

III. DATA ANALYSIS

Assuming that the excitation at port 1 is a voltage source with a flat spectrum of 1V, when the port 2 and port 3 are connected, three methods are used to calculate the induced voltage V_4 at port 4: a) compute V_4 by the directly measured $\boldsymbol{S_{1\text{-}4}}$; b) calculate the scattering properties between port1 and port4 from $\boldsymbol{S_{1\text{-}2}}$, $\boldsymbol{S_{3\text{-}4}}$ and $\boldsymbol{S_c}$ by electrical network theory to compute V_4; c) apply the BLT equation.

Randomly selecting a frequency range, making the probability density function (PDF) of V_4 for all the positions, it's found that the PDFs of V_4 calculated from the above three ways are in good agreement. Fig. 2 presents the PDFs in 6GHz-7GHz. Fig.3 shows the PDFs for the full test frequency range from 4GHz to 15GHz.

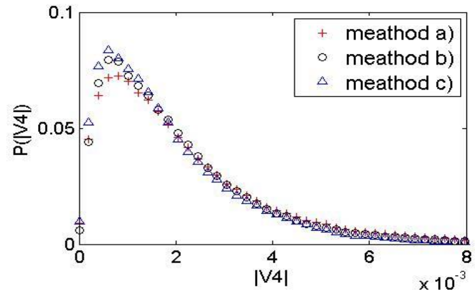

Figure 2. PDFs of induced voltages in 6GHz-7GHz

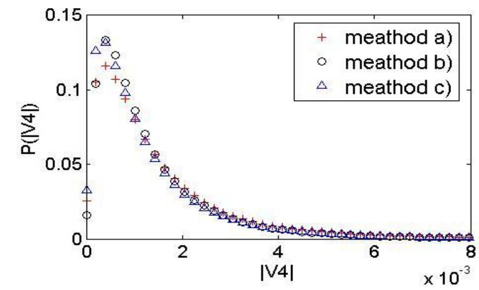

Figure 3. PDFs of induced voltages in 4GHz-15GHz

IV. CONCLUSION

It's concluded that the BLT can be applied to calculate the induced voltage on a topological network of wave-chaotic cavities. By cooperating with the random coupling model which characterizes the statistical fluctuation of the scattering matrix of a wave-chaotic cavity, it's expected to make statistical prediction of the induced voltage at target point within a large complicated system when exposed to HPM radiation.

REFERENCES:

[1]. Baum, C.E., T.K. Liu and F.H. Tesche, on the analysis of general multiconductor transmission-line networks. Interaction Note 350, 1978.

Pulsed Radio Frequencies Using a Photoconductive Semiconductor Switch

Timothy S. Wolfe, John S. Cetnar, Eric S. Moore, Roger Burchett, Andrew J. Terzuoli
Institute of Electrical and Electronics Engineers (IEEE)
Dayton, Ohio, USA
a.j.terzuoli@ieee.org

***Abstract* — Successful integration of Photo-Conductive Semiconductor Switches (PCSS) into existing pulsed Radio Frequency (RF) systems may yield higher switching speeds and power performance than current conventional system architectures, and realize significant size/weight reduction. Despite this, the feasibility of using PCSS technology to replace spark gap switches in pulsed power generators within a microwave system remains an area in need of investigation. This paper presents a comparison of an existing nominal system design to theoretical modified designs utilizing PCSS technology, via computer simulations based on existing data.**

Keywords: pulsed power; RF; microwave; EMP, EMC, semiconductor, switching, solid-state, photoconductive

I. INTRODUCTION

Photoconductive Semiconductor Switches (PCSS) are solid-state transistor devices triggered into an *on* state from a normally *off* state by optical illumination [1]. They are typically made from semiconductor materials with wide bandgaps, which provide high electric field breakdown strength. This enables PCSS devices to be used in high voltage applications. III-V compound semiconductors such as GaN and semi-insulating GaAs constitute the primary material choices of interest for this paper [2]. By modulating the conductivity of these devices with a laser, the high voltage switching characteristics of traditional spark gaps may be reproduced or exceeded.

II. METHODS

A. Modeling the Control Design

A commercial off-the-shelf (COTS) high voltage RF pulse generator was modeled using CST Design Studio and Microwave Studio, a Finite Element Method (FEM) software package. The results from the computer model simulation were compared to known real-world results.

B. Designing PCSS Modifications

The Semiconductor module of COMSOL Multiphysics, another COTS FEM software package, are used to accurately model and assist in designing a theoretical prototype switch, using a III-V nitride based device. Doping levels and device architectures are explored. Designs deemed feasible are modeled as equivalent lumped element circuits.

C. Modeling and Comparison of Modified Designs

The lumped circuit equivalences of the new prototype switches are put into the original design's CST model and compared to the original performance of the design. Successive iterations and additional modifications to the design are implemented as necessary to explore the possibilities of PCSS devices in an indicative system, as well as what necessary alterations must be made to integrate the new technology. In addition, alternative antenna designs and alternative sources of pulsed power are explored in conjunction with the new capabilities of the solid-state switch. A complete systems engineering approach is used in order to accurately compare the theoretical system to the original. Measurement data from prior characterizations was used to supplement these findings.

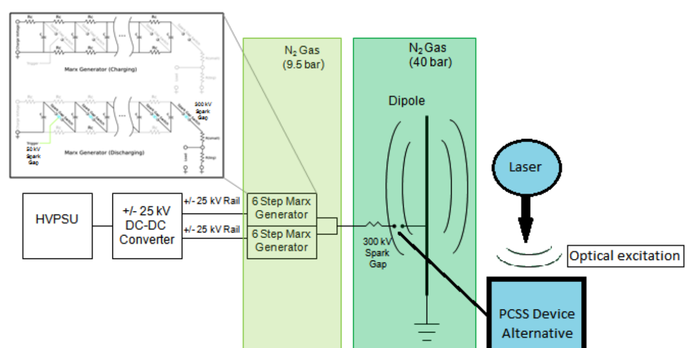

Figure 1. Original system and proposed modification

REFERENCES

[1] Nunnally, William "High-Power Microwave Generation using Optically Activated Semi-conductor switches" *IEEE Transaction of Electron Devices*. Pp. 2439-2447 Vol. 32 Num. 12
[2] Ishida, M.; Ueda, T; Tanaka, T.; Ueda, D. "GaN on Si Technologies for Power Switching Devices" *IEEE Transaction of Electron Devices*. Pp. 3053-3059 Vol. 60 Num. 10

Transmission and Reflection of Microwave Radiation from Novel Window Panes

P. Ragulis, Ž. Kancleris and R. Simniškis
Microwave Laboratory of Physical Technology Department
Centre for Physical Sciences and Technology
Vilnius, Lithuania
rpaulius@pfi.lt

***Abstract*— Measurements of microwave reflection and transmission in a frequency range 2.6-12.5 GHz have been performed on samples of double and triple novel window panes. Thin metal layer properties were taken into account performing modeling of reflection and transmission of microwaves through the window with a help of finite-difference time-domain method.**

Keywords-microwave transmission and reflection measurements; window panes; coated window glass.

I. Introduction

Double or triple window panes are widely used in house building and restoration. They reduce heat leakage, improve acoustical isolation, control sun energy pass into a building. In recent years the coating of glass with different metal thin layers was introduced [1]. These layers usually deposited on a surface of glass using magnetron sputtering under vacuum or controlled atmosphere. The coating demonstrates low emissivity and serves, from one hand, as a reflector of far infrared radiation characteristic to the warmth appeared from the house heating. From the other hand, the layer reflects a large amount of solar energy [1]. Metallic layer deposited on the glass should influence the transmission of microwave radiation as well but we did not find the description of such investigation in the literature. It is worth to mention that the investigations presented here were motivated by the non-planed measurement of attenuation of a newly installed window in the building, which was used for onsite measurements during 7th EU framework project "HIPOW" tests in Norway in summer 2013. It was found that behind the window the microwave pulse at 5.7 GHz was attenuated by 23 dB. In this paper we present the results of more detailed investigation of reflection and transmission of microwaves through double or triple pane window samples in the frequency range 2.6-12.5 GHz. The modeling of the interaction of electromagnetic wave with window was also performed using finite-difference time-domain (FDTD) method.

II. Experimental Setup and Measurement Results

Measurements of reflected and transmitted wave through the window panes have been performed in frequency range 2.6-12.5 GHz in a semi anechoic chamber. Horn antennas were used for the illumination of the sample and for the measurement of transmitted and reflected waves. Dimensions of the window samples were 20×30 cm^2. As microwave source Agilent PSG analog signal generator E8257D was used. Transmitted and reflected power was measured by Rohde & Schwarz average power sensors.

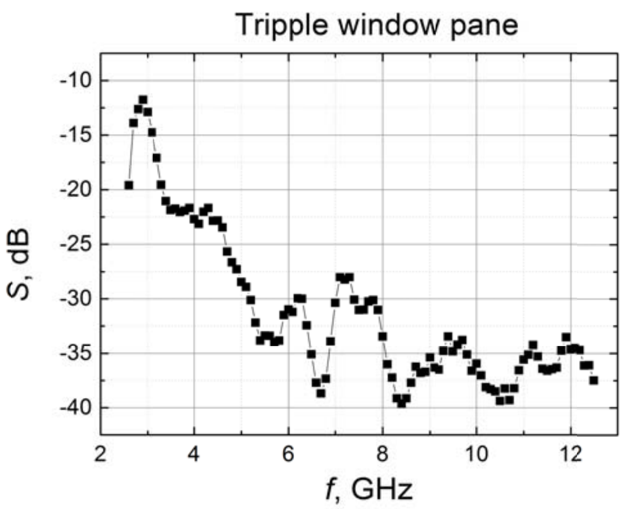

Figure 1. Dependence of microwave transmission through a triple window pane on frequency.

Typical measurement result of transmitted power through a triple window is shown in Figure 1. It is seen that attenuation of microwave signal increases with frequency reaching value of roughly -40 dB in a high frequency range. Even at a low frequency attenuation is more than 10 dB. Sufficiently large values of attenuation of microwaves by the novel window panes should be taken into account when considering a protection of infrastructure against microwave threats.

Modeling of transmission and reflection characteristics of the window panes has been performed using FDTD method. The properties of a thin metal layer deposited on the glass surface were taken into account in the modeling using method proposed in [2].

References

[1] Saint-Gobain home page: http://uk.saint-gobain-glass.com/

[2] Ž. Kancleris, G. Šlekas, and A. Matulis, Modeling of Two-Dimensional Electron Gas Sheet in FDTD Method, IEEE Tr. Antennas and Propagation, Vol. 61, No. 2, pp.994-996, February 2013.

.

This work was supported in part by 7th EU project HIPOW.

Measurement System of Electric Field Strength in Free Space with Flat Frequency Response

P. Ragulis, Ž. Kancleris, R. Simniškis and M. Dagys
Microwave Laboratory of Physical Technology Department
Centre for Physical Sciences and Technology
Vilnius, Lithuania
rpaulius@pfi.lt

***Abstract*— A system for the measurement of electric field strength in free space was developed. It consists of a resistive sensor connected to a wide band horn antenna and matched load. The characteristics of the resistive sensor were chosen enabling the compensation of frequency response of the overall measurement system. It was implemented in WRD250 double ridge waveguide covering frequency range 2.6 – 7.8 GHz.**

Keywords-resistive sensor; high power microwaves; horn antenna.

I. INTRODUCTION

A resistive sensor (RS) is a device based on electron heating effect in semiconductors. It found applications for high power microwave (HPM) pulse measurements [1]. Some advantages of the RS can be mentioned when comparing it with a semiconductor diode, which is also sometimes used for HPM pulse measurement. The RS measures HPM pulses directly, is overload resistant and demonstrates perfect long-term stability [1]. The RS is usually mounted in a rectangular waveguide and this confine the frequency range where particular device can be employed. It is possible to widen this frequency range more than two times by employing a double ridge waveguide for the RS implementation. Connecting the developed RS to a wide band horn antenna, electric field strength measurements in free space can be performed, broadening application of the sensor in electromagnetic susceptibility experiments.

In this work, a measurement system was developed for the measurement of microwave pulse electric field strength in free space. It is comprised of the RS mounted in a double ridged waveguide WRD250 connected to a wide band horn antenna and matched load. The pass band of the system is from 2.6 to 7.8 GHz. The layout of the sensing elements differs from the cross waveguide type RS earlier investigated in this frequency band [2]. The RS was made of two sensing elements, which are separated from each other. This configuration was chosen since it allows us to achieve smaller sensitivity variation on frequency.

II. SENSITIVITY OF THE MEASUREMENT SYSTEM

In order to measure the electric field strength in free space, the RS should be connected to the horn antenna. Sensitivity of such measurement system can be written down as follows:

$$\chi = \zeta \cdot S_{eff} \ , \tag{1}$$

where S_{eff} is an effective area of the wide band horn antenna and ζ is sensitivity of the RS when measuring microwave power in a double ridged waveguide.

The effective area of the horn antenna, in turn, depends on a gain of the antenna and wavelength of the electromagnetic wave. Therefore, accounting for the dependence of the antenna gain on frequency, when choosing the dimensions and specific resistance of the sensing elements of the RS, the system for electric field measurement in free space can be designed, the sensitivity of which is independent of frequency.

In this work we demonstrated such approach for the RS implemented in WRD250 waveguide. Simulation and experimental results are shown in Figure 1. From experimental results it is seen that the sensitivity variation within ±21.3% in the frequency band of the WRD250 waveguide can be achieved. It is very promising result for the system of the electric field measurement in free space in a wide frequency range. Similar system for the measurement in a frequency range 0.8-2 GHz is under development.

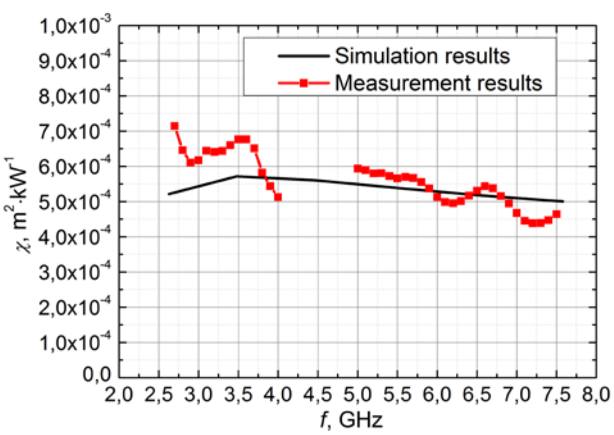

Figure 1. Dependence of the sensitivity on frequency for the measurement system comprised from the RS implemented in waveguide WRD250, horn antenna and matched load.

REFERENCES

[1] M. Dagys, Ž. Kancleris, R. Simniškis, E. Schamiloglu, F.J. Agee, IEEE Antennas & Propagation M., 43, 64 (2001).

[2] Ž. Kancleris, P. Ragulis, R. Simniškis, and M. Dagys, Lithuanian Journal Phys., Vol. 53, No. 2, pp. 99–103 (2013).

This work was in part supported by 7th EU program HIPOW.

Solution of the Fields in a Coaxial Switched Oscillator

Felix Vega
Electrical Engineering Department
Universidad Nacional de Colombia
Bogota, Colombia
jfvegas@unal.edu.co

Farhad Rachidi
Electromagnetic Compatibility Laboratory
Swiss Federal Institute of Technology in Lausanne (EPFL)
Lausanne, Switzerland
farhad.rachidi@epfl.ch

***Abstract*—We present a new design for the electrodes of coaxial switched oscillators using a 3D curvilinear system. The Laplace Equation is solved in the curvilinear space and analytical expressions are derived for the electrostatic field distribution.**

Keywords- Switched Oscillator; Conformal electrodes

I. Coaxial Switched Oscillator

The overall geometry of a coaxial switched oscillator (SWO) is depicted in Figure 1. It is composed of a charged transmission line (coaxial in this case) connected to a higher impedance antenna at one end and to a closing, self-breaking switch gas at the opposite end.

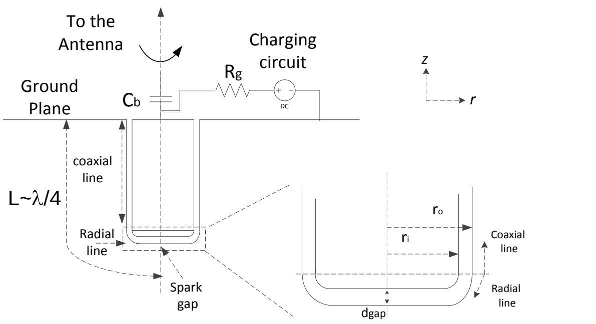

Figure 1. Quarter wave coaxial switched oscillator (SWO). Notice the presence of the electrodes at the bottom end of the coaxial line.

II. Electrodes Profile

We propose to generate the electrodes of the spark gap using two conformal surfaces in a curvilinear orthogonal space, generated from a 2-D transformation called Inverse Prolate Spheroid (IPS), proposed by Moon and Spencer ([1], page 67).

The IPS profile ensures a maximum electric field on the axis of symmetry, and a monotonical decrease when moving towards the coaxial transmission line.

The IPS coordinate (u, v, w) has the following relationship with the Cartesian coordinate system: (1)

$$x = a\frac{\sinh(u)\sin(v)\cos(w)}{\cosh^2(u)-\sin^2(v)} \quad y = a\frac{\sinh(u)\sin(v)\sin(w)}{\cosh^2(u)-\sin^2(v)} \quad z = a\frac{\cosh(u)\cos(v)}{\cosh^2(u)-\sin^2(v)} \qquad (2)$$

where: $a>0$ is a constant and (u,v,w) are defined in the range: $0 \le u < +\infty$; $0 \le v \le \pi$; $0 \le w \le 2\pi$.

A 3D representation of the curvilinear system is shown in Figure 2. It can be seen that the surface u=*constant* forms an inverted prolate spheroid of revolution, while the surface v=*constant* forms an inverted double sheet hyperboloid of revolution and the surface w=*constant* forms a plane.

The electrodes are formed taking two u=*constant* surfaces (u=u_2 and u=u_1) connected to the outer and inner conductors of the coaxial transmission line of the SWO.

Laplace Equation is r-separable in this system. The solution of the electrostatic potential is of the form:

$$V(u,v,w) = \frac{V_1}{k_1}\log\left(k_3\coth\left(\frac{u}{2}\right)\right)\sqrt{\frac{\cosh^2(u)-\sin^2(v)}{k_2^2-\sin^2(v)}} \qquad (3)$$

where k_1, k_2 and k_3 are constants obtained from the boundary conditions of the problem and $V(u_1,v,w)=V_1$ and $V(u_2,v,w)=0$.

Applying the equation for the gradient in the ISP system gives the following expressions for the electric field

$$E_u(u,v,w) = \frac{V_1\sqrt{\Omega}\left(\log\left(\frac{\coth(u/2)}{\coth(u_2/2)}\right)\sinh(2u) - 2\cosh(u)\coth(u) + 2\operatorname{csch}(u)\sin(v)^2\right)}{ak_1\sqrt{\cosh(2u)-\cos(2v)}\sqrt{\cos(2v)+\cosh(2u_1)}} \qquad (4)$$

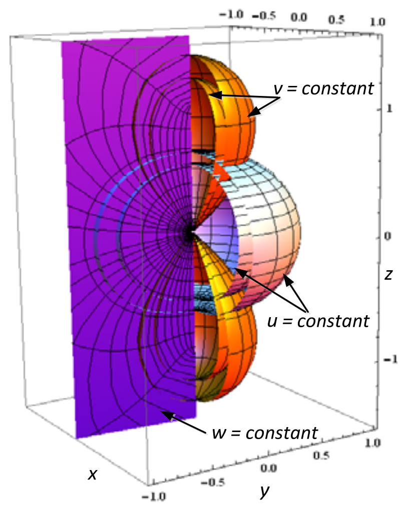

Figure 2. Constant surfaces in the Inverse Prolate Spheroidal coordinate system. The surfaces were generated with parameter a=1. Notice the surfaces corresponding to u-set and v-set.

III. Conclusions

Analytical solution for the electrostatic field distribution in the interelectrodic space of a coaxial SWO was obtained. The derived equation can be used during the design phase of the spark gap. Furthermore, the derived expression allows deriving an analytical solution for the characteristic impedance of the SWO's radial transmission line.

References

[1] P. Moon and D. E. Spencer, Field Theory Handbook: Including Coordinate Systems, Differential Equations and Their Solutions 2ed.: Springer-Verlag, 1971.

Numerical Calculation of the Fields on the Aperture Plane of an Impulse Radiation Antenna

Felix Vega
Electrical Engineering Department
Universidad Nacional de Colombia
Bogota, Colombia
jfvegas@unal.edu.co

Nicolas Mora and Farhad Rachidi
Electromagnetic Compatibility Laboratory
Swiss Federal Institute of Technology in Lausanne (EPFL)
Lausanne, Switzerland
nicolas.mora@epfl.ch, farhad.rachidi@epfl.ch

***Abstract*—A numerical procedure for the calculation of the fields on the aperture plane of an Impulse Radiating Antenna in the frequency domain is presented. The procedure avoids the calculation of the derivative of the inverse of the Jacobi SN function.**

Keywords- Impulse Radiating Antenna; inverse Jacobi SN function

I. INTRODUCTION

The electric and magnetic fields of the main pulse radiated by an Impulse Radiating Antenna ($E_{MP}(x,y,z)$, $H_{MP}(x,y,z)$) can be calculated in the frequency domain by integrating the electric field tangential to the aperture of the reflector $E_A'(x',y')$, weighted by the Green's function, as follows [1]:

$$\vec{H}_{MP}(x,y,z)=\oint_S \nabla'\left(G(r-r')\right)\times\vec{E}_A'(x',y')\,dy'dx'$$
$$\vec{E}_{MP}(x,y,z)=-j\frac{\mu}{\varepsilon\omega}\nabla\times\vec{H}_{MP};\ |r-r'|=\sqrt{(x-x')^2+(y-y')^2+(z-F)^2} \tag{1}$$

where $G(r\text{-}r')$ is the Green's function, F is the focal distance of the IRA and the primed variables are the source coordinates on the aperture of the reflector. The origin of the *x, y,* and *z* coordinates is the focal point of the antenna and the *z* axis is perpendicular to the aperture plane of the antenna. Note that we do not make any far-field approximation, as in the approach presented in [2].

A pair of feeders collinear with the *x'* axis produce the following tangential electric field in the aperture [3]:

$$E_A(x',y')=E_{Ax}(x',y')+iE_{Ay}(x',y')=-\frac{1}{K(m)}\left(\frac{\partial u}{\partial x'}-i\frac{\partial u}{\partial y'}\right) \tag{2}$$

where $u(z')=\mathrm{Re}\left\{sn^{-1}\left(\frac{x'+iy}{b_0m^{0.25}},m\right)\right\}$ and sn^{-1} is the inverse of the Jacobi *sn* function, $z'=x'+iy'$, $b_0=D/2$, D is the diameter of the dish, $K(m)$ is the elliptic integral of the first kind, and m is a constant obtained from $Z_c=120\pi K(m)/K(1-m)$; where Z_c is the input impedance of the antenna.

Very few mathematical software tools have implemented the $sn^{-1}(z)$ function (e.g,. Mathematica). In this paper we propose an alternative numerical procedure for the calculation of the derivatives of the sn^{-1} function.

II. METHOD

The derivation starts with the following identity [4]:

$$sn^{-1}\left(\frac{x}{b},\frac{b^2}{a^2}\right)=\int_0^x f(t)dt=\int_0^x\frac{adt}{\sqrt{\left(a^2-t^2\right)\left(b^2-t^2\right)}} \tag{3}$$

from which Equation can be transformed into:

$$E_{Ax}'(x',y')=\frac{-1}{K(m)}\mathrm{Re}\left(\frac{\partial}{\partial x'}\left(\int_0^{z'}f(t)dt\right)\right)\quad E_{Ay}'(x',y')=\frac{1}{K(m)}\mathrm{Re}\left(\frac{\partial}{\partial y'}\left(\int_0^{z'}f(t)dt\right)\right) \tag{4}$$

The integration path on the complex plane is arbitrary, as the function $f(t)$ is analytical.

After some mathematical manipulations and taking into account that on the aperture plane $\|z'\|<D/2$, Eq. yields:

$$E_{Ax}'(x'+iy')=\frac{b_0}{K(m)m^{0.25}}\frac{\cos(\Theta)}{\left(\left(4x'^2y'^2+(b_1^2+x'^2-y'^2)^2\right)\left(4x'^2y'^2+\left(\frac{b_1^2}{m}+x'^2-y'^2\right)^2\right)\right)^{1/4}}$$
$$E_{Ay}'(x'+iy')=-\frac{b_0}{K(m)m^{0.25}}\frac{\sin(\Theta)}{\left(\left(4x'^2y'^2+(b_1^2+x'^2-y'^2)^2\right)\left(4x'^2y'^2+\left(\frac{b_1^2}{m}+x'^2-y'^2\right)^2\right)\right)^{1/4}} \tag{5}$$
$$\Theta=0.5Arg\left(\left(b_1^2+(x'+iy')^2\right)\left(\frac{b_1^2}{m}+(x'+iy')^2\right)\right)$$

As an example, Fig. 1 shows the stream lines of the aperture plane fields of a four-arm IRA with D=1 m, F=0.33 m and Z_c=100 Ω, obtained using combination and rotations of the vector field in Equation (5). Fig.2 shows the application of the Equation (5) to the calculation of the radiation pattern obtained using Equation (1) at a distance r=100D, for two signals f= 10 c/D, f=5c/D and amplitudes V=1 Volt.

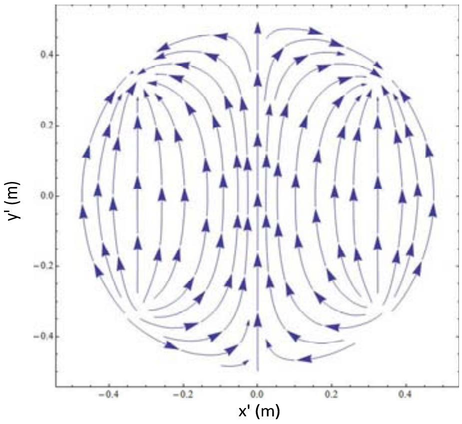

Fig. 1 Fields on the aperture plane of a 4-arm IRA with D = 1 m, Z_c=100 Ω. Notice the arms at and +–45°and +–135°

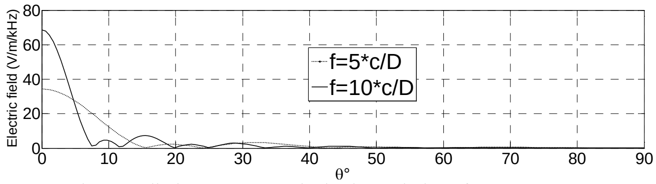

Fig. 2 Radiation pattern on the horizontal plane for a 4-arm IRA

REFERENCES

[1] J. Van Bladel, Electromagnetic fields vol. 2: Wiley Intersience, 2007.
[2] K. Sunitha, et al., "Radiation Patterns of a Reflector Type of Impulse Radiating Antenna (IRA) Relating Time and Frequency Domains," Sensor and Simulation Notes 545, 2009.
[3] Farr. E.G and C. E. Baum, "Prepulse Associated with the TEM Feed of an Impulse Radiating Antenna," Sensor and Simulation Notes, vol. 337, pp. -, 1992.
[4] M. Abramowitz and I. Stegun, Handbook of mathematical functions: National Bureau of Standards, 1972.

ID 105

An Array of Metamatieral-Inspired Antennas for High Power Applications

Eric S. Ramon, J. Scott Tyo, and Richard W. Ziolkowski
College of Optical Sciences
University of Arizona
Tucson, Arizona, United States
Email: eramon@email.arizona.edu

***Abstract*—Metamaterial-inspired antennas leverage techniques that can make an electrically small antenna (ESA), that would typically be an inefficient radiator, achieve radiation efficiencies of greater than 90%. Using an array of such antennas, to distribute the input field over many elements, can be an effective method to create a very low profile antenna array for HPM applications. In this paper we specifically explore using an array of magnetic EZ antennas to act as a mode converter and efficiently radiate energy produced by a 12-cavity relativistic magnetron operating in the TE_{61} mode.**

***Index Terms*—array, metamaterial, magnetron, high efficiency antenna, electrically small antenna.**

I. Introduction and Background

The EZ antenna is an electrically small, magnetic dipole antenna. The EZ antenna consists of a small semi-loop antenna over a ground plane. This driven element is then surrounded by a capacitively loaded loop (CLL) element that is located in the near-field of the semi-loop antenna [1], [2].

To couple the guided TE_{61} mode of the circular waveguide, which is produced by a relativistic magnetron, to the coaxial input of the EZ antenna we modified a design for a high power cavity feed presented in [3] that was designed for GW levels of power. Our waveguide removes the bottom section of the outer conductor and the structure is fed with a circular waveguide, the same as the output of the magnetron. A cross section of the model used in CST simulations of the array is shown in Fig. 1a and a zoomed in section of the probe is shown in Fig. 1b. This probe is used to extract the energy from the cavity and couple it a coaxial output that leads to an antenna. The power handling abilities of the cavity with the probes will be discussed further in the presentation. In Fig. 1b the EZ antenna that is used to radiate the energy extracted from the cavity is seen at top of the outer conductor of the cavity.

The probe used to extract the energy from the cavity modify the fields in the cavity and lead to potential breakdown, and will in turn limit the power handling capabilities of the system.

II. Simulation Results

The waveguide and the EZ antenna were separately tuned via CST simulations to have a resonant frequency near $2.52\,GHz$, which corresponds to one of the frequencies at which the magnetron source we are using to drive the system operates. The two structures were tuned such that the $|S_{11}|$ value at the resonant frequency was minimized. Then the structures were combined using CST's Design Studio software package to simulate the total structures performance. The resulting $|S_{11}|$ values for the combined system are shown in Fig. 2.

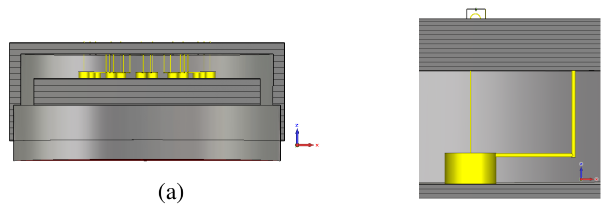

(a) (b)

Figure 1: (a) Cross section of the waveguide used to couple the TE_{61} mode from a circular waveguide to an array of EZ antennas and (b) a zoomed in section of the output probe that extracts energy from the cavity and couples it to the coaxial output

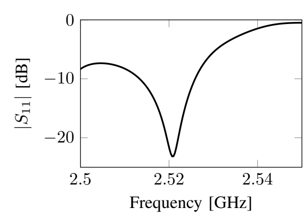

Figure 2: $|S_{11}|$ parameter versus frequency for the total array system

References

[1] R. W. Ziolkowski, "Applications of metamaterials to realize efficient electrically small antennas," in *Proc. IEEE Int. Workshop on Antenna Technology: Small Antennas and Novel Metamaterials*, March 2005, pp. 7–9.

[2] A. Erentok and R. W. Ziolkowski, "Metamaterial-inspired efficient electrically small antennas," *IEEE Trans. Antennas Propag.*, vol. 56, no. 3, pp. 691–707, March 2008.

[3] X.-Q. Li, Q.-X. Liu, X.-J. Wu, L. Zhao, J.-Q. Zhnag, and Z.-Q. Zhang, "A gw level high-power radial line helical array antenna," *IEEE Trans. Antennas Propag.*, vol. 56, pp. 2943–2948, September 2008.

Metamatieral-Inspired Magnetic EZ Antenna for High Power Microwave Applications

Eric S. Ramon, J. Scott Tyo, and Richard W. Ziolkowski
College of Optical Sciences
University of Arizona
Tucson, Arizona, United States
Email: eramon@email.arizona.edu

Michael C. Skipper and Michael D. Abdalla
ASR Corporation
Albuquerque, New Mexico, United States

***Abstract*—Metamaterial-inspired antennas leverage techniques that can make an electrically small antenna (ESA), that would typically be an inefficient radiator, achieve radiation efficiencies of greater than 90%. Driving one of these antennas with a high power microwave (HPM) source, such as a quarter-wave, coaxial standing-wave oscillator (SWO), one can create a HPM system that has a very low profile above the source due to the ESA. In this paper we will discuss results from CST simulations of one of these HPM systems using a magnetic EZ antenna as the radiating element.**

***Index Terms*—high power microwave, MATRIX, metamaterial, electrically small antenna.**

I. Background and Introduction

The source works by charging the low-impedance transmission line to a high potential and then discharging it through a self-breakdown switch on axis. This sets up a standing wave that delivers a small amount of microwave energy to the high-impedance load, which in this case is the antenna. The nearly-open circuit at the load and and the nearly-short circuit at the switch end result in a resonance that has a period that is four-times the round-trip transit time of the oscillator [1].

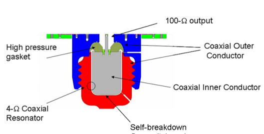

(a)

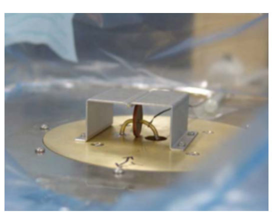

(b)

Figure 1: (a) Cross section diagram of the SWO and (b) the built prototype of the EZ antenna

The EZ antenna, which is pictured in Fig. 1b, is an electrically small, magnetic dipole antenna. The EZ antenna consists of an electrically small semi-loop antenna over a ground plane. This driven element is then surrounded by a capacitively loaded loop (CLL) element that is located in the near-field of the semi-loop antenna. This near-field element acts as a resonant parasitic element, which is conjugate matched to the impedance of the semi-loop antenna that causes their respective reactances to cancel and gives the antenna a purely real input impedance at the resonant frequency [2], [3]. In Fig. 1b there is a solid disk capacitor at the top of the semi-loop antenna, this is necessary to electrically isolate the SWO from the ground plane during the charging phase.

II. Simulation Results

In CST we simulated the performance of the EZ antenna and the SWO separately at first to tune their individual resonances. With the EZ antenna being driven by a $100\,\Omega$ coaxial cable the antenna was tuned to minimize the $|S_{11}|$ near $500\,MHz$. This tells us the antenna has an input impedance of near $100\,\Omega$, which will lead to the SWO having $Q \cong 20$.

Once the systems were individually tuned they were coupled together, as seen in Fig. 2a. The electric field of this combination was monitored $1\,m$ from the antenna in the broadside direction and the spectrum is shown in Fig. 2b for a charge voltage of $10\,kV$ of the SWO. The peak electric field value is near $500\,MHz$ as expected. In addition to these simulated CST results high power test data from a prototype system will be presented.

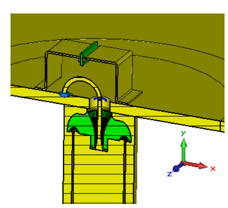

(a)

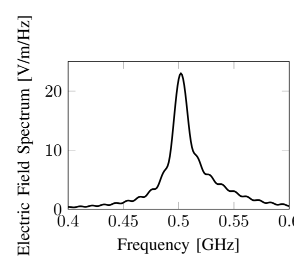

(b)

Figure 2: (a) CST model of the SWO coupled to the EZ antenna and (b) the electric field spectrum measure $1\,m$ from the antenna in the broadside direction

References

[1] C. E. Baum, "Switched oscillators," Circuit and Electromagnetic System Design Notes, Air Force Research Laboratory, Tech. Rep. 45, 2000.

[2] R. W. Ziolkowski, "Applications of metamaterials to realize efficient electrically small antennas," in *Proc. IEEE Int. Workshop on Antenna Technology: Small Antennas and Novel Metamaterials*, March 2005, pp. 7–9.

[3] A. Erentok and R. W. Ziolkowski, "Metamatrieral-inspired efficient electrically small antennas," *IEEE Trans. Antennas Propag.*, vol. 56, no. 3, pp. 691–707, March 2008.

Numerical synthesis and realization of broadband loaded monopole antennae

C.D. de Haan
IP2-solutions B.V.
Leende, NB, The Netherlands
c.dehaan@ip2-solutions.nl

A. Brettschneider, A.P.M. Zwamborn
Research Group Electronic Defence
TNO
The Hague, ZH, The Netherlands
alwin.brettschneider@tno.nl
peter.zwamborn@tno.nl

***Abstract* — This paper presents the successful synthesis and practical realization of a robust design of broadband loaded wire monopole antennae with matching networks. The loads consist of parallel LRC–circuits. For synthesis we use an efficient Galerkin MoM computational technique in combination with an evolved PSO algorithm to maximize frequency bandwidth and optimize the radiation pattern in the horizontal plane.**

The numerical electromagnetic model considers all ideal conductors or L, C and R components, that differ from reality. At first the antenna was built as closely as possible according to the numerical design. Thereafter the components and configuration have been changed and optimized with preservation of the return loss.

Antennae having bandwidth ratios of 12:1 or more, with measured VSWR less than 3.5 and calculated system gain greater than -5 dBi, are discussed and presented.

Keywords-component: Loaded monopole, Broadband VHF antenna, Particle Swarm Optimization, MoM

I. Introduction

Loaded monopole antennas for broadband applications have been investigated previously [1,2]. This paper investigates the design and realization of an antenna system comprising of a loaded monopole and a matching network, optimized by using a stochastic optimization algorithm, known as Particle Swarm Optimization (PSO) [3], to obtain broad bandwidth and a desired radiation pattern. The antenna is intended to be used for ground to ground communication on a vehicle. Preservation of sufficient gain in the horizontal plane is desired. Radiation upwards will reduce that gain and has to be minimized. During the practical realization special attention has been paid to preserve the radiation in the horizontal plane.

Optimization goals

- Requirement for return loss < -5.1 dB over frequency band of 30 to 450 MHz
- VSWR < 3.5 over frequency band of 30 to 450 MHz
- Gain > -5 dBi in the horizontal plane over frequency band of 30 to 450 MHz

II. Fabrication of the Loaded Monopole

The antenna is constructed using the following system parts

A. Antenna pole

Copper pipe connected with plastic spacers

B. *LRC Gaps*

Metal oxide resistors with an inductor wrapped around the pole, capacitors and the resistors (see figure 1)

C. Antenna foot

The antenna foot is of polyurethane and is mounted on a metallic plate connected with plastic screws

D. Transformer 1:4

The transformer below the foot is a Guanella-type 1:4 transmission-line transformer (unun) constructed of two copper pipes of 8 mm diameter. One pipe of the transformer is equipped with ferrite rings to reduce the outside currents

Figure 1. Example of a realized gap and foot.

III. Conclusions

Any practical realization of a numerically designed antenna does involve special attention to assure that mechanical and electro-technical constraints are incorporated in the numerical design parameters. During the presentation, these constraints and consequences in the design procedure will be elucidated. Finally, the successful design will be presented and measurement results will be shown and discussed.

This research is sponsored by the Dutch Ministry of Defense.

References

[1] Design and realization of GA-Optimized wire monopole and matching network with 20:1 bandwidth, S.D. Rogers, March 2003, IEEE AP vol. 51 no 3

[2] Design of Electrically Loaded Wire Antennas Using Genetic Algorithms, IEEE transactions on antennas and propagation, Vol. 44, NO. 5, May 1996, Alona Boag

[3] Efficient Computation techniques for Galerkin MOM antenna design, Design of a loaded monopole by using an evolved PSO algorithm, Cecillia Marasini, PhD thesis Eindhoven University of Technology, 2008.

First Thoughts on a Standard for Future HPEM Immunity Tests

Lars Ole Fichte, Marcus Stiemer
Helmut-Schmidt-University,
Faculty of Electric Engineering

Hamburg, Germany
lo.fichte@hsu-hh.de

Stefan Potthast, Frank Sabath
Bundeswehr Reseach Institute
for Protective Technologies
and NBC Protection
Munster, Germany
frank.sabath@ieee.org

Christian Adami, Gerd Suhrke
Fraunhofer Institute for
Technological Trend Analysis INT

Euskirchen, Germany
christian.adami@int.fraunhofer.de

***Abstract*— Since high power electromagnetic (HPEM) threats to electric devices had been emerging, various attempts were made to classify the threat parameters and to settle on a standard for testing devices. Today, additional sources of high power interference signals are available, with a wide range of bandwidths and frequency coverage. This paper will provide first ideas to tackle the problem of classifying those new threats, and propose new test procedures that cover he whole range of threats with a reasonable number of tests.**

Keywords- HPEM standardization, HPEM sources

I. Introduction

For a first classification of new threats, we follow [1], dividing the possible threat range into four classes according to their characteristic bandwidths: Narrow-, Meso-, Sub-Hyper-, and Hyperband. We propose to classify Sub-Hyper- and Hyperband as one class and to add the nuclear electromagnetic pulse (NEMP) as a single category due to its unique characteristics.

Since we discuss immunity testing in this paper, our goal is to expose a device under test (DUT) to a worst-case environment, e.g., a high power microwave (HPM) signal with a center frequency which can couple into the DUT, a damped sinus signal, an ultra wide band pulse, and a NEMP. After passing an immunity test with adequate threat levels, the DUT can be admitted to work in the real world.

To guarantee an effective test, a minimum field level must be defined. Based on statistical analysis of the susceptibility of electronic devices we estimate the minimum field level needed for disturbance of a DUT at approximately 20 kV/m. An exception must be made for narrowband HPM signals (with interference visible at 10 kV/m), see below.

Alternatively, the maximum field magnitude that available sources can generate at the locus of the DUT was estimated, under the assumption that bulky, powerful threat systems (e.g., JOLT [2]) cannot be operated unnoticed at close distances, whereas low-power miniature systems (e.g., can sources [3]) can be deployed close to the DUT.

Again, a realistic estimation results in a magnitude of 25 kV/m, approximately. The parameters for this estimation and, even more important, additional safety margins to guarantee a robust test are still under intense discussion.

II. Parameters for Threat Classes

A. High Power Microwave Signals

Sinusoidal and quasi-sinusoidal signals can be characterized by center frequency f_C, magnitude ($\approx$10 kV/m) and damping factor. The chosen f_C will decisively effect the coupling.

B. Damped Sinus (DS) Signals

DS signals combine a high power density with limited bandwidths; DUTs will be damaged by the injected power. Additional coupling paths (e.g., through attached power and data cables) should be taken into account. Since tunable DS sources are not yet available, we propose to define a threat corridor in frequency domain from 100 - 1000 MHz, that can be covered with a broadband source at fixed center frequency.

C. Nuclear Electromagnetic Pulses

Several immunity test procedures deal with NEMPs already. The main difference to the other threats discussed here is the higher power and energy content of the signal.

D. Ultra Wideband (UWB) Signals

For characterizing UWB signals, we assume that this class can be defined by a double exponential pulse. Assuming that a critical UWB pulse, compared to a NEMP, contains the same energy with a ten times larger bandwidth, the rise time t_{rise} is the most important parameter for a standard UWB pulse:

$$t_{\text{rise, UWB}} \leq 250 \text{ ps}, \text{ and } t_{\text{rise, UWB}} \leq 0{,}1 \;\, t_{\text{rise, NEMP}} .$$

III. Discussion

Since this vast range of possible threats a priori allows for many possible classifications, we wish to engage in an active discussion of our approach.

References

[1] D. V. Giri and F. M. Tesche, “Classification of Intentional Electromagnetic Environments (IEMI),” IEEE Transactions on EMC, Vol. 46, No.3., August 2004

[2] D. V. Giri, W. L. Baker, W. D. Prather, J. M. Lehr, J. P. O'Laughlin, I. D. Smith, R. Altes, J. Fockler, D. P. McLemore, M. D. Abdalla, and M. C. Skipper, “JOLT: a highly directive, very intensive, impulse-like radiator,” Proc. IEEE 92 :1096 – 1109 (2004)

[3] D. Manson, “IEMI Susceptibity investigations and classification of civilian systems and equipment,” Uppsala 2008

History of the EMP Note Series

The Road to High-Power Electromagnetics

Dr. Robert L. Gardner, Consultant
Alexandria, VA 22310, USA
Robert.L.Gardner@Verizon.net

Dr. Leigh A. Gardner
Assistant Professor
London School of Economics and Political Science,
London, UK
l.a.gardner@lse.ac.uk

Abstract— **This paper documents the expansion of research on the nuclear electromagnetic pulse to a much more diverse range of topics including lightning, high-power microwave devices and effects, electromagnetic effects on electronics as well as various forms of electromagnetic pulse. The expansion of the discipline took place alongside the internationalization of the cohort of researchers. This case provides an example of the movement of military research into the public domain since the 1960s. Two sources are used to track these trends: 1) the titles and authors of the Notes on EMP and Related Subjects beginning in 1964, and 2) the proceedings of the Nuclear Electromagnetic Meetings from 1978. The analysis stresses the importance of the Notes as an informal mechanism for the communication of research findings.**

Keywords-EMP Note Series, EMP, High-Power Electromagnetics

I. TRENDS

In [1] we examined the various NEM, AMEREM and EUROEM publications and examined some of the trends in subject matter at these meetings over the years. Starting in 1992, there was a large increase in non-US participation. There was also a shift in the emphasis from EMP to other facets of high-power electromagnetics (HPEM) like HPM. The Notes provide additional data to examine those and more personal trends among the various authors. These trends are meant to form a foundation and motivation for future note authors.

II. WHAT IS A NOTE?

The Note series on EMP and related subjects was established in 1964 by Dr. Ralph Partridge of Los Alamos Scientific Laboratory. Editorship of the Notes shortly passed to Dr. Carl Baum of Air Force Weapons Laboratory. The aim of the Note series was to provide an informal means of disseminating research findings before the long process of publication, enabling faster communication between EMP researchers in the United States and Britain. Notes did not contain final research findings but rather sets of ideas at the mid-point of the workflow of scientific ideas outlined below:

1. Memos – Raw notes and ideas – not usually published
2. Presentation at work-in-progress conferences like NEM or URSI
3. Notes – Collection of ideas to form a finished but still evolving product
4. Presentation at Conferences designed for finished work like IEEE AP-S or ICEAA.
5. Transactions (IEEE or other peer reviewed journal)
6. Books or hardware

III. MILESTONE NOTES

There were a number of Notes that were of historical significance. The first Note was by Ralph Partridge at Los Alamos and described requirements for an EMP Simulator. Carl Baum expanded on that theme with a number of Notes through Sensor and Simulator Note 143 that stated the requirements for ATLAS-1 or TRESTLE. In this case, the final product of the theoretical work was a large wooden simulator that stands as a monument today to EMP simulation and in a large sense to the scientists of the Cold War.

Substantial basic electromagnetic interaction was key to understanding the effects of EMP and other electromagnetic threats to systems. Many of the early Notes dealt with cable coupling. Much of that early work was formalized in Interaction Note 88 that first described the Singularity Expansion Method. Note 88 was followed by Notes by Drs. R. Latham, L. Marin, and F. Tesche on various theoretical attributes of SEM. Award winning papers, by Marin and Tesche, based on this work were later published in IEEE AP-S Transactions. We will discuss these and other milestone notes during the presentation.

REFERENCE

[1] L. A. Gardner, R. L. Gardner and Carl E. Baum, “The Internationalization of the Electromagnetics Meetings and Related Activities of the SUMMA Foundation”, Proceedings of the 2011 IEEE International Symposium on Antennas and Propagation and USNC/URSI National Radio Science Meeting, Spokane WA USA, 2011.

The Influence of the Static Magnetic Field on the State of Chromatin and Viability of Human Cells

Eugeny R. Stepchenkov[1], Ilya V. Saenko[2]
Biological Faculty of V.N. Karazin Kharkiv National University
Kharkiv, Ukraine
[1] stepchenkov2609@gmail.com
[2] saenkoilya@hotmail.com

Yuriy G. Shckorbatov
Dep. of Genetics, Institute of Biology, V.N. Karazin National Unisersity
Kharkiv, Ukraine
shckor@univer.kharkov.ua

***Abstract*— The influence of static magnetic field (SMF, 25 mT) on human buccal epithelium cells was investigated. Cells were obtained from two donors before experiment (this operation is absolutely bloodless and painless) and placed in buffer solution. The cells were exposed to SMF during 1, 3, 5, 10, 15, and 20 minutes. After the exposure cells were stained by orcein to investigate the process of chromatin condensation (heterochromatinization); or were stained by acridine orange and ethidium bromide to investigate the viability of cells. The data obtained indicate the increase of heterochromatin granules quantity (HGQ) per one cell nucleus after the cell exposure. The number of viable cells decreased after the cell exposure to SMF as indicates by the test for cell viability. The revealed cell reaction of heterochromatinization after SMF exposure indicates the stress reaction of cell to SMF. The data obtained are discussed in connection to the phenomenon of the regulation of the activity of cell nucleus by SMF.**

Keywords-chromatin; heterochromatin; buccal epithelium; orcein; ethidium bromide; acridine orange

I. INTRODUCTION

The public attention to the action of anthropogenic electromagnetic fields (EMFs) is connected with medical consequences of applying of the EMFs sources in communication and electronic media, technology, science, transport, and other spheres [1]. According to the recommendations of the International Commission on Non-Ionizing Radiation Protection (ICNIRP) the occupational exposure of head and trunk to SMF shoud not exeed intensity of 2 T, but for the specific work applications exposure up to 8 T can be permitted [2]. The widespread opinion is that the electric field component of electromagnetic radiation induces most of the biological effects of EMFs [3], but our investigations indicate that the biological activity of the magnetic component of electromagnetic field only slightly inferior the electrical component [4].

II. MATERIALS AND METHODS

A. Cells

Experiments were done on cells of buccal epithelium (cheek mucosa) of two donors – A and B (men) of 18 years old. The cells were collected before experiment and placed in 3,03 mM phosphate buffer (pH=7,0) supplied with 2,89 mM $CaCl_2$.

B. Cell Exposure and Staining

Cells were exposed to SMF (25 mT) for 1, 3, 5, 10, 15, and 20 minutes. After exposure cells were stained by orcein (2%) for determination of heterochromatin granules quantity (HGQ) per one cell nucleus. The HGQ was calculated as mean value of 90 (30x3) cell nuclei for every variant of experiment. To investigate the viability, cells were stained by acridine orange in concentration of 17 μg/ml for 10 min, and by ethidium bromide in concentration of 33 μg/ml for 5 min. The percentage of damaged cells was determined in 1400 (100x4x3) cells in each experiment.

III. RESULTS AND DISCUSSION

The data obtained indicate the significant increase of HGQ after cell exposure to SMF. The most pronounced changes were detected after the 15 minutes of cell exposure to SMF. The increase of HGQ indicates the increase of chromatin condensation which is as a rule connected with decrease of nuclear functional activity. The analysis of the percentage of damaged cells by the acridine orange and ethidium bromide revealed that SMF induced the percentage of damaged cells. The damage of cells gradually increases with exposure time increasing. The cells of different donors revealed the some peculiarities in the measured parameters, but the general regularities in cell reaction to SMF were the same. The data obtained are discussed in connection to the mechanisms of cell reaction to action of electromagnetic factors.

REFERENCES

[1] B. B. Levitt, H. Lai, “Biological effects from exposure to electromagnetic radiation emitted by cell tower base stations and other antenna arrays.” Environ. Rev., vol. 18, pp. 369–395, 2010.

[2] International Commission on Non-Ionizing Radiation Protection, “Guidelines on limits of exposure to static magnetic fields.” Health Physics, vol. 96(4), pp.504-514, 2009.

[3] C.A.L. Bassett, “Beneficial Effects of Electromagnetic Fields.” Journal of Cellular Biochemistry, vol. 51, pp. 387-393, 1993.

[4] G.B. Skamrova, M.P. Yevstigneev, A.N. Trushkin, Y.G. Shckorbatov, “Effect of electric and magnetic component of the electromagnetic field on the membrane permeability and chromatin state in the cell nuclei of human buccal epithelium.” Proceedings of the V.I. Vernadsky Taurica National University. Series "Biology, Chemistry", vol. 25 (3), pp. 187-195, 2012 (article in Russian).

ID 112

Discharge Model of a Spark Gap Peaking Switch

Mrunal Parekh, Sachin Umbarkar, H. A. Manglvedekar
Veermata Jijabai Technological Institute
VJTI-Siemens High Voltage Lab, Mumbai, 400019 India
mrunal.elec@gmail.com

***Abstract*—Ultra-fast breakdown in gaseous or liquid dielectric serves as the basis for generation of short duration high voltage pulse in pulsed power systems. In [1 and 2] electro-dynamic model of high pressure spark gap peaking switch was discussed. Theoretical investigations leading to mathematical model of gas discharges could certainly help the understanding of the physics involved. Gas breakdown is essentially a threshold process which is consequence of the steep dependence of the ionization rate. In this paper mathematical discharge development in a gaseous spark gap switch which is subjected to 300 kV, 3 nanosecond rise time pulse has been carried out. Rate of change of volume charge density in the gaseous region is found out and this will determine at what time the rate of volume charge density has exceeded or equal to ionization charge density for the gas. This will lead us to the value of breakdown delay or the rise time of the output pulse across the connected load. Towards these objective continuity equations for positive ions, negative ions and electrons (coupled with gauss's law) are solved in conjunction with Poisson's equation.**

Keywords: Gas Discharges, Spark gap switch

I. SOLUTION TECHNIQUE

An electrical discharge modeling is a complex problem as multiple physics are involved in the same. The approach used in this paper is Finite element to solve Poisson's equation and continuity equation simultaneously. Transient solver of Ansoft Maxwell is used in conjunction with AC conduction solver. Consistent boundary conditions have been applied to the model. The potential to the plane electrode is set to ground. The point electrode potential is defined as a sinusoid having 3 ns rise time. The top bottom and side walls have been assigned to zero normal displacement field components. The simulation is run for 5 ns and volume charge density is calculated for time steps defined.

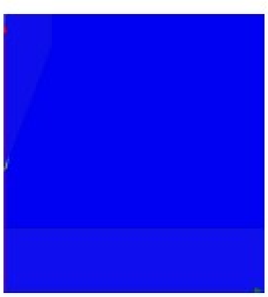

(a) 0.5ns

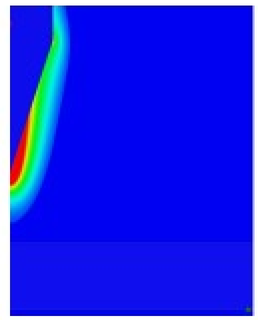

(b) 3ns

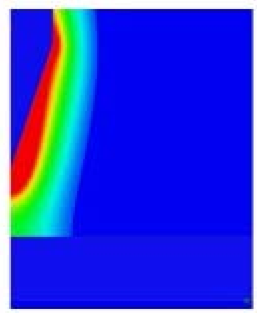

(c) 5ns

Figure 1.(a), (b), (c), Shows the development of charges at different time instants

REFERENCES

[1] Parekh M.G., Bindu S, Mangalvedekar H .A., "Electromagnetic modeling of high pressure spar k gap peaking switch" 16t h E ML 2012,Beijing,China.

[2] Bindu S, Mangalvedekar H .A., Parekh M.G., "Electro-dynamic simulation of high voltage peaking switch" I EE E transaction on plasma science., vol. 40, Issue 11,page s3093-3099.

[3] "Gas discharge physics" by Yuri P Raizer, Springer Verlag Publication

EM Coupling to a Transmission Line Located Symmetrically inside a Cylinder

Ronald Rambousky

Bundeswehr Research Institute for Protective Technologies and NBS Protection (WIS)
Munster, Germany
ronald.rambousky@ieee.org

Sergey Tkachenko and Jürgen Nitsch

Chair of Electromagnetic Compatibility
Otto-von-Guericke University Magdeburg
Magdeburg, Germany
Sergey.Tkachenko@ovgu.de ,
Juergen.Nitsch@ovgu.de

***Abstract*—In this paper we outline an exact analytical solution for the current induced by an arbitrary exciting field in a loaded transmission line with symmetric geometry inside a cylindrical resonator.**

Keywords- cylindrical cavity, Green's function, transmission line

I. Introduction

Investigations of the coupling of high-frequency electromagnetic fields caused by intentional electromagnetic interferences to linear structures placed in cavity-like structures (racks, cases, housings, fuselage of aircraft, etc.) becomes an actual topic. Existing numerical methods (as MoM, TLM, etc.) allow considering specific cases only, but do not describe the general physical picture of interaction. Thus, the analytical description of the interaction of high-frequency fields with wire structures in cavities has become a topic of interest.

To solve this problem several methods can be offered. The approximate methods are based, as is usual in theoretical physics, on the use of small parameters. One group of such methods, Method of Small Antenna, uses the smallness of the dimension of the wiring structure in comparison to the wavelength [1]. Another small parameter that can be used to solve the coupling problem for long electrical objects inside a resonator is the thickness of the wire compared to other geometrical parameters of the problem (wavelength, height of the wire above ground, etc.) [2]. However, the approximate methods have some restrictions (dimension of the scatterer, accounting of a few resonator modes, etc.). It is of great interest to develop exact methods which can be used to check numerical codes, time – domain calculations using numerical inverse Fourier transforms, statistical investigations, etc. As usual in theoretical physics, an exact solution for the system "transmission line in resonator" can be found for systems with high symmetry, when the wire and cavity have the same symmetry. In our paper [3] a thin loaded wire inside a rectangular resonator was considered. The wire is led parallely to four walls of the resonator and connects two opposite ones. This system allows an exact analytical solution by spatial Fourier transformation for any kind of excitation. This method [3] is quite general and can be applied to symmetrical wires inside right cylinders of general form. The most practical case is the right circular cylinder, which has many practical applications in EMC, e.g., for electronic equipment in aircraft or other aerial vehicles.

II. Description of Obtained Results

In this paper we consider a wire, which is lead parallely to the cylindrical axis and connects both caps of the cylinder. Due to the same (transfer) symmetry of the wire and cavity in the z-direction, this configuration allows an exact analytical solution by a Fourier transformation for every kind of excitation (distributed, lumped) and with arbitrary loads. To do that a hybrid representation of the cylindrical cavity Green's function was used. Moreover, during the investigation of the exact equations for the induced current, one can separate the term, which corresponds to the transmission line approximation (TL) and then evaluate the effects of different resonances.

It was shown, that the analytical method demonstrates an excellent agreement of the results with those obtained by direct numerical calculations (PROTHEUS). At the same time, the TL approximation yields wrong results near cylinder resonances (see Fig.1).

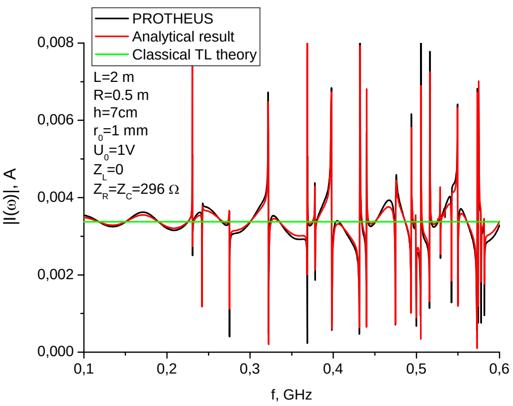

Figure 1: Current at the right matched terminal (Z_R=Z_C=296 Ω) induced in the symmetrical wire inside the cylinder by a lumped source U_0=1V at the left terminal. The length of the cylinder L=2m, the radius R=0.5 m, the distance between wire and wall of the cylinder h=7 cm.

References

[1] S. Tkachenko, F. Gronwald, H.-G. Krauthäuser, J. Nitsch, "High-frequency electromagnetic coupling to small antennas in rectangular resonator", Int. Conf. Electromagn. Adv. Appl. (ICEAA), 2009, pp.74-78.

[2] S. Tkachenko, J. Nitsch, R. Vick, "HF coupling to a transmission line inside a rectangular cavity", URSI Int. Symp. on Electromagn. Theor., Berlin, Germany, Aug. 16-19, pp. 5-8.

[3] S. Tkachenko, J. Nitsch and R. Rambousky, "Electromagnetic field coupling to transmission lines inside rectangular resonators", Interaction Notes, Note 623, 30 June 2011.

Probabilistic Modelling and an EM-Compatibility Calculus

B.L. Michielsen and Jean-Philippe Parmantier
Onera, DEMR
Toulouse, France
Bastiaan.Michielsen@Onera.fr

***Abstract*— We define the ElectroMagnetic Compatibility of a system quantitively as the probability that the states of a system are within the margins of its operational model. We show that under rather weak conditions, such a compatibility coefficient allows one to judge on the consequences of substituting system parts by replacement parts comparing only their respective compatibility coefficients.**

***Keywords*— ElectroMagnetic Compatibility, Stochastic environments, Component Obsolescence, Compatibility Calculus, Compatibility Algebra**

I. Introduction

ElectroMagnetic Compatibility is usually defined in a qualitative way and the proper operation of a system is judged on the basis of experiments or computations of certain cases believed to be critical and/or representative. In this paper, we develop a "compatibility calculus" based on a quantative, probabilistic, definition of ElectroMagnetic Compatibility of sub-systems. The essential property we want this calculus to have is that the overall compatibility of a system with its environment can be evaluated by combining the compatibility coefficients of its parts. Although, the complexity of the non-localisable electromagnetic interactions makes that the complete calculus remains rather complicated, there is one property which is of much practical use and allows one to make quick comparisons where obsolete components are to be replaced by new ones. In such cases, there is a simple rule that overall compatibility of the system does not diminish when the compatibility coefficients do not diminish. This implies, that the compaibility coefficient of a subsystem has an individual meaning as a measure of its quality (see Fig. 1).

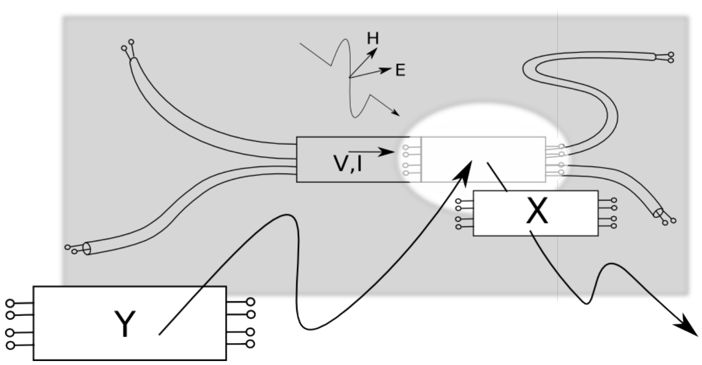

Figure 1. Replacing component X by a component Y with equal or higher compatibility coefficient, will not degrade the compatibility of the system as a whole

II. Stochastic closure of sub-system propositions

In order to test the functionality of a (sub-)system one needs a closure relation representing the (sub-)systems operational environment. As the operational environment is never deterministically controlled, the closure model is of a probabilistic nature. The states of closed system are therefore stochastic processes on every level of the assembling hierarchy. The designer of a sub-system obtains the appropriate stochastic environment from the designer of the embedding system and, using the nominal functionalities of the components of his design, he computes the stochastic environments of the various components, which he passes on to the designers of the respective components, and so on and so forth. This is the top-down specification phase. Now any realisation of a sub-system can be tested with the given stochastic closure applying to the sub-system. If the sub-systems stochastic states would match perfectly with the stochastic states defining the operational model, it would be indistinguishable from the nominal functioning and we cannot hope to get a better realisation. This situation should correspond to maximal compatibility because the states of the system are such as they appear with the nominal system.

III. Application

We will show the results of a compatibility coefficient computation for an interconnect system in an electromagnetic environment with noise sources. We first compute the stochastic environment of a chosen sub-system X. The electromagnetic noise in the environment of the complete system is represented by a covariance operator corresponding to a stochastic plane wave. Using a complete electromagnetic hybrid model for multiport systems, we can explicitly compute the noise sources in the environment and uncertainties in the wanted port-excitations of the chosen sub-system (see [1]). From the stochastic states of the complete nominal system, we use the standard deviations of the port voltages and currents as representing the operational margins, i.e., we say that if a sub-system realisation has voltages within a distance of one standard deviation from the nominal state the system is within spec.'s. (Alternative definitions of what it means to operate within the spec.'s will be presented as well). We then compare the computed compatibility coefficients of various sub-system realisations to the over-all performance.

References

[1] B. L. Michielsen. Probabilistic modelling of stochastic interactions between electromagnetic fields and systems. *Comptes Rendus de l'Académie des Sciences: Physique*, 7:543–559, August 2006.

Application of Singularity Expansion Method (SEM) to Long Transmission Lines

S.Tkachenko, F. Middelstaedt, J.Nitsch, R.Vick
Chair of Electromagnetic Compatibility
Otto-von-Guericke University Magdeburg
Magdeburg, Germany
Sergey.Tkachenko@ovgu.de

G.Lugrin and F.Rachidi
EMC Laboratory
Swiss Federal Institute of Technology
Lausanne, Switzerland
Farhad.Rachidi@epfl.ch

***Abstract*—This work deals with the calculation of the first layer SEM poles of a long finite transmission line above a conducting ground excited by high frequency electromagnetic fields. This set of poles yields the main contribution to the susceptibility of the transmission line to external excitations. For canonical cases of an open-circuit wire and a horizontal wire short-circuited by vertical risers, SEM poles are obtained in explicit form. The comparison of the results of the SEM approach with those of numerical simulation gives a good agreement.**

Keywords- SEM; transmission lines; time domain; pulse response

I. Introduction

Transmission lines play an important role in EMC. They serve for the transmission of desired signals between electronic devices of different kinds. On the other hand, they can be subject to different kinds of electromagnetic interferences. Induced overvoltages are often the reason for the failure of electronic devices. Different numerical methods (such as MoM, FDTD, etc.) can be adopted to calculate induced currents and voltages but they are not very helpful to gain insight into the physics of the coupling phenomena, especially when they are calculated in time domain.

In contrast, the analytical Singularity Expansion Method (SEM) [1] represents the scattering object as a set of oscillators, helpful to understand the underlying physics of the coupling phenomena, both, in the frequency domain and in the time domain. Recently, this method has attracted an increased interest [2, 3] in connection with the definition of the complex eigen frequencies of a finite straight wire for target identification.

In a recent paper [4], SEM was applied to the analysis of loaded transmission lines above a conducting ground, using classical Transmission Line (TL) theory. In particular, it was shown that as a result of the action of a finite sinus-like pulse, transients in the system can greatly exceed the steady-state oscillations, and this effect can cause failures of the electronic components in the early stages of such an exposure. Of course, TL approximation does not describe radiation effects, which can be important for high frequencies, when the wavelength is comparable with the height of the line.

II. Description of Obtained Results

In this work, we consider a long loaded line above a perfect conducting ground with arbitrary terminals illuminated by an incident high frequency plane wave [5, 6]. To obtain the frequency domain solution for the induced current in the main, central part of the wire, the co-called asymptotic approach [7] is used. The zeros of the denominator of this expression yield the SEM poles of the first layer. This set of poles yields the main contribution to the susceptibility of the transmission line to an external pulse excitation in time domain. Furthermore, SEM poles are obtained in an explicit form for two canonical cases: (i) an open-circuit wire, and (ii) a horizontal wire short-circuited by vertical risers. The obtained results using the proposed SEM approach are compared with those obtained using NEC (Numerical Electromagnetics Code) simulations and a good agreement is found.

Using the SEM poles, the time response function can be expressed in an explicit form, which has shown to be in good agreement with the results of numerical simulations obtained by an inverse Fourier transformation of NEC results. Two interesting physical effects were observed: radiation damping of the induced current and the domination of transient oscillation for a high-frequency sinusoidal excitation.

References

[1] C.E. Baum, "The Singularity Expansion Method in Electromagnetics", D.V.Giri and F.M. Tesche (editors), Lulu Enterprises 2012.

[2] F.M. Tesche and D.V. Giri, "On the natural oscillation frequencies of a straight wire", Interaction Notes, Note 621, June 2011.

[3] J.M.Myer, S.S.Sandler and T.T.Wu, "Electro-magnetic resonances of a straight wire", IEEE Trans. Ant. Prop., Vol. 59, Jan.2011, pp.129-134

[4] J. Nitsch, S. Tkachenko, R. Vick, F. Rachidi, D. Poljak, „Coupling of Pulsed EM Fields to TL", 2012 Int. Symp. on EMC (Rome 2012).

[5] S.Tkachenko, J.Nitsch, R.Vick, F.Rachidi, D.Poljak, "Singularity expansion method (SEM) for long terminated transmission lines", 2013 Int. Conf. on EM in Adv. Appl. (ICEAA), Torino, 2013.

[6] S.Tkachenko, F.Middelstaedt, J.Nitsch, R.Vick, G.Lugrin, F. Rachidi, "High–Frequency Electromagnetic Field Coupling to a Long Finite Line with Vertical Risers", accepted for GA URSI2014 Beijing.

[7] F.Rachidi, S.Tkachenko (editors), "EM Field Interaction with TL. From Classical Theory to HF Radiation Effects", WIT Press 2008. Ch. 4 and 5.

A Statistical Approach to Analyze the Risk of HPEM Attacks on Electronic Systems

Torsten Teichert, Lars Ole Fichte, Marcus Stiemer
Helmut-Schmidt-University,
Faculty of Electric Engineering
Hamburg, Germany
torsten.teichert@hsu-hh.de

Stefan Potthast, Frank Sabath
Bundeswehr Reseach Institute for Protective Technologies and NBC Protection
Munster, Germany
frank.sabath@ieee.org

***Abstract*—** Risk analysis of complex electronic systems against radiated interferences is an evident part of the design phase, especially in modern military environments, and is vital for later operation. Since affordable high power electromagnetic (HPEM) sources become more and more available, risk analysis against such threats has to keep pace with these changing circumstances. In this paper a method consisting of computational electromagnetic (CEM) simulations combined with statistical methods based on [1],[2] will be presented. The novel method is then applied to a generic missile.

***Keywords*— HPEM sources, statistical methods, numerical simulation**

I. Introduction

As electromagnetic compatibility (EMC) problems are cost drivers for engineering projects, a trade-off between risk reduction and depth of analysis has to be found. Ideally, a worst-case-scenario is estimated, but, since an electronic system consists of many parts that respond differently on an electromagnetic (EM) interference (EMI) and interact in a complicated way, it is crucial that typically a whole class of critical scenarios has to be considered, whose parameters are a priori unknown. To overcome this problem, a statistical framework has been derived in [1] based on a statistical model of the whole EMI at system level. The risk analysis is performed by a Monte-Carlo-simulation of this model. Aiming at a reduction of the system and, thus, of simulation time, we propose an alternative version, where only the electronic system is statistically modeled as in [1], but the interfering EM field is computed via CEM simulations. The basic idea is employing the reciprocity theorem, to obtain a guess for parameters of critical scenarios after the vulnerable points of the system under consideration (SuC) have been identified with the help of the statistical model. The methodology is exemplarily applied to a generic missile as a SuC. An alternative approach to reduction of costs would be the use of a reverberation chamber, which is also beneficial to figure out thresholds for critical scenarios, but information about cause and effects which lead to an interference is lost.

II. Analytic Procedure

The threat environment and the electronic system are individually analyzed. The electronic system is then statistically modeled as described in [1], while the EMI is treated via CEM simulation. The link between the two different sub-models is established by an application of the reciprocity theorem.

A. Analysis of electromagnetic interference

As a first step, the EM environment is described. In the example SuC, the radiating source is located on the ground, the SuC is airborne, and there is a line of sight between source and SuC. Different source types may be taken into account.

B. EMI propagation

Based on the knowledge of the source type and the distance to object, the coupling paths into the SuC are analyzed. In this special case, there is an intended EMI (IEMI) source radiating directly on the target. No walls or zone models are considered. The target is decomposed into several volumes, which are partly filled with dielectric material and interconnected via a cable harness. Moreover, it is assumed that the SuC has no retroactive effect on the incident field.

C. System characteristics

To identify the most vulnerable points of the SuC, a statistical model according to [1] is constructed. To this end, the inner conditions of the systems are observed and a fault tree analysis is performed. With this model, the mission critical states of the system are identified.

D. CEM-Simulation of an inverse problem

In this step, broadband sources are placed at the vulnerable components of the system and the resulting field is computed with a CEM simulation to identify the SuC's points of weak shielding. From the resulting field pattern the critical parameters of the IEMI are identified. This procedure leads to all critical scenarios, if the system can be assumed sufficiently close to a linear one. If not, an iterative improvement of the guess is possible.

E. EM-Simulation of the native problem

Finally, a CEM simulation with the critical IEMI-parameters identified in the preceding step is performed and the electronic system is set in the resulting state. For additional reduction of costs, the correlation matrix for the representative parameters can additionally be taken into account to deduce the system state from the IEMI parameters.

III. Conclusion

Risk analysis on the system level basically requires a statistical paradigm such as elaborated in [1]. A hybrid version linking a statistical model for the electronic system and a CEM simulation for the IEMI as proposed in this paper is may be more efficient, since the parameter space for a Monte-Carlo-simulation is drastically reduced. Moreover, a reduction of probabilistic parameters increases certainty.

References

[1] Genender, E.; Garbe, H.; Sabath, F., "Probabilistic Risk Analysis Technique of Intentional Electromagnetic Interference at System Level," IEEE Transactions on Electromagnetic Compatibility, vol.56, no.1, pp.200-207, Feb. 2014

[2] Genender, E., „Risikoanalyse von Systemen bei elektromagnetischer Störbeaufschlagung," Shaker-Verlag, 2012

The ARROW Project

Modelling of Lightning Indirect Effects on Composite Aircraft equipped with Current Return Networks

A. Mori, M. Bandinelli, G. Sammarone
IDS - Ingegneria Dei Sistemi S.p.A. Pisa, Italy
a.mori,@idscorporation.com

F. Vipiana, M. A. Echeverri Bautista
DET, Politecnico di Torino, Torino, Italy
francesca.vipiana@polito.it

J.P. Parmantier, S. Bertuol, I. Junqua
ONERA – The French Aerospace Lab, F-31055, Toulouse, France
jean-philippe.parmantier@onera.fr

G. Antonini, D. Romano
DIIIE, Università degli Studi dell'Aquila, L'Aquila, Italy
giulio.antonini@univaq.it

J. Genoulaz, T. Lebreton
Labinal Power Systems, Toulouse, France
jerome.genoulaz@safran-engineering.com

***Abstract*— The ARROW project (Aircraft lightning thReat Reduction thrOugh Wiring optimization) is a research project, funded by the European Community in the framework of the CleanSky program. The project aims at the development of an accurate and reliable modelling method of the indirect effects of lightning on cable-harness configurations installed aboard aircraft of today's technology, including composite materials and current return networks. The proposed numerical methodology links a three-dimensional full wave electromagnetic solver with a MLTN, which allows design as well as optimization of the wiring itself. This contribution reports about the modelling procedure, the mathematical formulation and some validation results of the developed numerical code.**

Keywords - Electromagnetic modelling, Indirect effects of lightning, Method of Moments, Multiconductor Transmission Lines.

I. Introduction

Modelling of the effect of lightning on cables installed on an aircraft can lead to challenging problems, due to the complexity of the environment and due to the necessity of modelling all the involved electromagnetic phenomena (ohmic losses, skin effect, reactive and radiative coupling, …). Even if it is theoretically possible to carry out an electromagnetic analysis on a model comprising the structures and the wires present in an aircraft, a hybrid field-to-wire coupling procedure [1] can advantageously be employed in order to lighten the models and to make easier parametric analysis on the internal cabling.

In such a hybrid procedure, the 3D EM model of the structural parts is solved through a full wave method without explicitly considering the cables. The Multiconductor Transmission Network analysis (MTLN) is then carried out, by considering a distributed excitation term given by the incident electric field produced by the structural parts onto cable routes. In case of non-fully low-impedance metallic structures (e.g. composite fuselages and/or aircraft equipped with a current return network), the application of such a hybrid method must be validated specifically in the low frequency part for lightning problems. Briefly summarizing, the impedance of current paths on structures and common mode voltages induced by the lightning current on to the non perfectly conducting surface have to be considered; finally, the interaction between the cables and the aircraft (i.e. the p.u.l. [C], [L] parameters) is not evaluated anymore by referring to a return path directly located under the cable. In the following we briefly list the main characteristics of the procedure, and we show a small example of application. A more detailed description of the methods employed in the modelling procedure and examples of its application will be presented at the time of the conference.

II. Characteristics of the Modelling Procedure

The modelling procedure is going to be integrated in the electromagnetic CAE Tool E-MIND [2], devoted to support the user in all the phases of the lightning threat analysis, from the input data import to the advanced output data post processing. The main functions implemented by the integrated tool are briefly summarized in the following:

1. Import of the platform geometry and material properties from CAD and the cable Harness representation from Harness Design Electric CAD;
2. Three-dimensional frequency domain Method of Moments full wave electromagnetic solver (MultiResolution and S-PEEC) reliable from the very-low frequency range;
3. MTLN solver able to consider a not perfect ground by means of a common mode impedance and/or a common mode voltage;

A pictorial representation of analysis environment is shown in Figure 1.

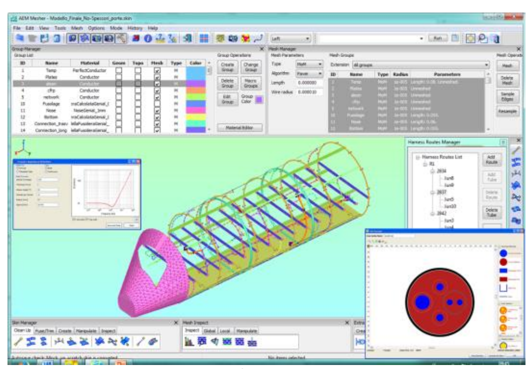

Figure 1. Pictorial representation of analysis environment. Mock up structure built by DEMLAB (Labinal Power Systems)

References

[1] A.K. Agrawal et al "Transient Response of Multiconductor Transmission Lines Excited by a Nonuniform Electromagnetic Field", IEEE Trans. On Electromagnetic Compatibility, Vol. n. 22, 1980.

[2] E-MIND Electromagnetic Multicode Integrated Design Framework, https://www.idscorporation.com/aeronautical/

ID 119

An Incubator Combined with TEM-cell for Cellular Electromagnetic Effects Study

Xiao-Yun LU
Xi'an Jiaotong University,
School of Life Science and Technology
Xi'an 710049, Shaanxi, China
Luxy05@mail.xjtu.edu.cn

Ke-jie LI, Yan-zhao XIE
Xi'an Jiaotong University,
School of Electrical Engineering
Xi'an 710049, Shaanxi, China

Abstract**—**Biological effects of electromagnetic radiation are drawing increasing attentions nowadays. Because of the individual differences and the position status variability, animal based bio-electromagnetics studies showed contradictory results and it's hard to illustrate the instant cellular response. To facilitate the cell based molecular mechanism study of EMF bio-effects, an integrated system combined a cell incubator with a TEM-cell was developed which shows a very good performance.

I. INTRODUCTION

Nowadays, people are exposed to many kinds of electromagnetic fields, such as the continuous waves (CW) and electromagnetic transients near the pulsed power equipments, which can affect different systems of living organisms [1]. Therefore, the biological effects of electromagnetic radiation, which is really an interdisciplinary area, are drawing increasing attentions from both physicists and biologists.

The study of EMF bio-effects could be carried out based on the whole animal exposure experiment or based on the in vitro cultured cells. The animal based study could demonstrate the integrated effects of the whole body responded to an EMF, but because of the animal individual differences and the position status variability during the electromagnetic radiation, the measured results are not entirely consistent, or with big deviations [2]. The cell based study could avoid the position status variability of animal experiment and the calculation of EMF bio distribution. Moreover, it could demonstrate the rapid response of cell and reveal the possible molecular mechanism under a given parameter combination of EMF[3].

While *in vitro* cell cultivation requires standard culture conditions such as temperature of 37℃ and 95% humidified environment with 5% CO_2. Change of the temperature or the pH of medium could activate or inhibit many cell signaling pathway and result in the cell behavior alternation. Therefore, maintain the standard cultivation environment during EMF treatment is of great importance to obtain the precise results for cell based study.

II. STRUCTURE OF CELL INCUBATOR

To establish the identical culture condition of the cells with or without electromagnetic radiation, the interior of the modified incubator was divided into an upper part (with normal culture environment) and a lower part (equipped with a TEM-cell cavity) (figure 1). A signal generator (continuous wave or pulse) is connected to the TEM-cell by cable connectors. The transverse electromagnetic (TEM) wave could be guided traveling through the TEM-cell, and as a result, the cells inside TEM-cell would be illuminated by a pretty uniform EMF.

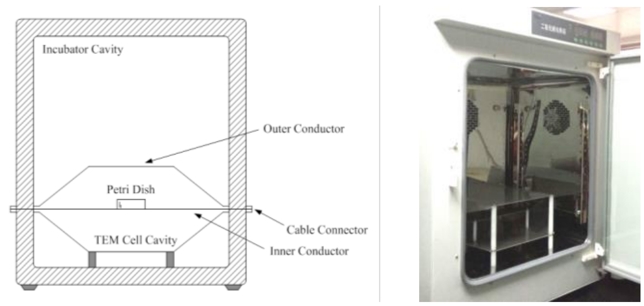

Figure 1. The structure and the photo of the modified cell incubator

The inner conductor and outer conductor are seperated by insulators. A 50 ohm resistor with low inductance is terminated at the end to match the wave impedance of the TEM-cell. Some sealing technologies were adopted when designing the incubator to avoid the gas escape from the TEM-cell.

The strength of electric field inside the TEM-cell can be calculated as $E=V/h$, while V is the applied voltage to the TEM-cell and h is the half height of the TEM-cell.

The newly fabricated incubator has been running stably for a long period and some preliminary results will be presented soon.

III. CONCLUSION

A specific cell incubator has been developed for the research of electromagnetic field bio-effects. In this incubator, the electromagnetic field illumination and cell culture could be achieved simultaneously, which could be easier to illustrate the relations between the cells' response and the given EMF. This is the fundamental to enhance the reproducibility and reliability of EMF bioeffects study and is of great importance to illustrate the molecular mechanism of EMF bioeffects at the cellular level.

REFERENCES

[1] F. A. Mohamed, et al., "Study of the Cardiovascular Effects of Exposure to Electromagnetic Field," Life Science Journal-Acta Zhengzhou University Overseas Edition, vol. 8, pp. 260-U209, 2011.

[2] O. Eser, et al., "The Effect of Electromagnetic Radiation on the Rat Brain: An Experimental Study," Turkish Neurosurgery, vol. 23, pp. 707-715, Nov 2013.

[3] O. V. Kruglik, et al., "Effect of microwave electromagnetic radiation (UHF EMR) on tumor cell viability in experiment," Doklady Biochemistry and Biophysics, vol. 449, pp. 66-68, Mar 2013.

Dielectric Probe for Fully Vectorial Analysis of Electric Field

Gwenaël Gaborit
IMEP-LAHC
Université de Savoie
73 376 Le Bourget-du-Lac Cedex, France
gwenael.gaborit@univ-savoie.fr

Pierre Jarrige, Frédéric Lecoche, Jean Dahdah, and Lionel Duvillaret
Kapteos R&D
73 376 Le Bourget-du-Lac Cedex, France
lionel.duvillaret@kapteos.com

***Abstract*— This paper describes the achievements of electric field characterization performed with an electro-optic probe. The millimeter sized sensor allows the mapping of the field vector components as well as their temporal evolution. The very low invasive measurement is ensured over an ultra wide bandwidth (30 Hz – 18 GHz) and offers a dynamics exceeding 120 dB.**

Keyword: Electric field measurements, Electro-optics, Vectorial analysis, UWB, HPEM.

I. Introduction

The exhaustive analysis of the electric (E) field is required for many applications such as antenna radiation pattern, electromagnetic compatibility, on chip diagnostic or even in bioelectromagnetism. The rigorous E-field characterization implies that each component of the field vector have to be actually known as a function of the time in the considered volume of interest. Among the numerous techniques allowing the E-field assessment (*e.g.* antenna, bolomoter, infrared thermography, ...), only passive antennas and electro-optic (EO) probes provide a linear response, which is furthermore selective to the field vector components. Although metallic sensors are mainly used thanks to their high sensitivity and their technological readiness level, they remain quite invasive and frequency bandwidth limited. Pigtailed EO probes are developed since the beginning of the century. They offer an intrinsic bandwidth covering more than 9 decades of frequency and are fully dielectric. Moreover, the response of such transducers can lead to the simultaneous measurement of several field vector components [1]. Finally, EO technique is applicable in severe environments (temperature variations, *in situ* characterization in fluids or plasmas, partial or total discharges).

II. Electro-Optic Sensor

The EO probes are based on the Pockels effect which operates in non-centrosymetric crystals. This EO effect linearly links the refractive indices variations δn of the crystal to the electric field vector $\vec{E}$ [2]:

$$\delta n = \vec{K} . \vec{E} \tag{1}$$

This latter equation involves the sensitivity vector $\vec{K}$ depending on the crystal transducer and its orientation relatively to the laser beam which probes the E-field induced δn. While The modulus of $\vec{K}$ gives the sensitivity, its direction defines the component of $\vec{E}$ which will be probed. In the particular case of isotropic crystal (<111> cutted), two sensitivity vectors $\vec{K}_x$ and $\vec{K}_y$ allows the simultaneous and balanced measurement of the transverse components E_x and E_y. The two informations are carried out via the induced polarization state modulation (PSM) of the laser beam crossing the crystal. The PSM is treated and analyzed with a servo-controlled optoelectronic instrument ensuring a reliable measurement whatever the temperature environment is. The EO probe itself consists in a smart optical arrangement including the crystal, a gradient index lens and a waveplate. This sensor is fully dielectric and millimeter sized (see Fig.1a). The performances of the EO unit are as follow: a minimum detectable field of 0.1 $V.m^{-1}.H^{-1/2}$, a dynamics exceeding 120 dB, a bandwidth spreading up to 18 GHz, a selectivity greater than 50 dB and a spatial resolution of 1 x 1 x 5 mm^3. Current improvements concern the sensitivity enhancement (down to 1 $mV.m^{-1}.H^{-1/2}$) and the simultaneous analysis of the three components of the E-field achieved with a single EO probe. Some vectorial field mappings will be presented during the conference.

III. Electric Field Vector Characterization

As an example of the EO probe potentialities, Fig.1b illustrates the polarimetric measurement of the E-field associated to an electrical discharge. This results demonstrates that the field behaviour is not only oscillatory but also rotational during the ionization process.

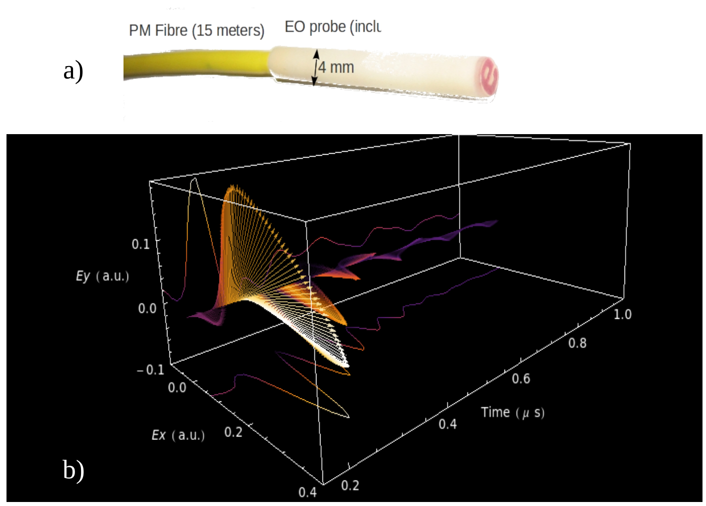

Figure 1. a) Picture of a multilayer dielectric coated EO probe. b) Transient evolution of the transverse electric field vector, associated to an electrical discharge. The single shot measurement is performed with the probe located in the vicinity of the discharge path.

References

[1] G. Gaborit *et al*, “Vectorial electric field measurement using isotropic electro-optic crystals,” Appl. Phys. Lett., vol. 90, 24, pp. 241118, 2007.

[2] L. Duvillaret *et al*, “Electro-optic sensors for electric field measurements. II. Choice of the crystals and complete optimization of their orientation”, JOSA B, vol. 19, 11, pp. 2704-2715, 2002

Nonlinear Time Reversal in a Semi-Reverberant Complex Enclosure

Sun Hong, Victor Mendez, Walter Wall, Tim Andreadis
Tactical Electronic Warfare Division
Naval Research Laboratory
Washington, DC 20375, USA
sun.hong@nrl.navy.mil

Trystan Koch, Steven Anlage
Department of Physics
University of Maryland
College Park, 20742, USA

Abstract— Here we present nonlinear time reversal (NLTR) applied in a complex, semi-reverberant enclosure containing a passive nonlinear circuit. NLTR utilizes the nonlinear response generated at the nonlinear circuit due to an incident pulse. When this nonlinear response is extracted from the overall response, time-reversed and retransmitted into the enclosure, the signal will focus at the location of the nonlinear circuit. This technique provides a way to efficiently deliver short electromagnetic pulses at electronic devices without any prior measurement or knowledge about the environment.

Keywords – time reversal; nonlinear dynamics; HPEM; multipath; harmonic generation

I. Introduction

Time reversal (TR) techniques have shown to be effective in focusing short pulses in rich scattering, multipath environments [1]. In order to apply TR in such environments, the impulse (short pulse) response (IR) between the source antenna(s) and a target location is needed. When the IR is time-reversed and retransmitted into the environment, the waves experience the same multipath while the signal contains a reversed delay profile. This essentially "undoes" the multipath delays, coherently adding the pulses from the multipath components at the target to form a short pulse resembling the original impulse. Such temporal compression and spatial focusing may enable efficient delivery of high power RF pulses to a specific target location within a complex enclosure.

However, in many real-world applications we wish to focus a pulse at a location from which it is impractical or impossible to send an initial impulse. A recent demonstration has shown that an RF pulse can be focused at a target containing nonlinear circuit (i.e. electronic device) without actually sending an impulse from it [2]. That is, the nonlinear excitation due to an incident short pulse sent from a distance can be used as an initial "impulse". This technique, hereafter referred to as nonlinear time reversal (NLTR), therefore could be an efficient way to obtain the IR needed for TR focusing.

In this presentation, we apply NLTR in a semi-reverberant enclosure with open apertures containing a passive discrete nonlinear circuit. Unlike the previous demonstration, which consisted of a closed reverberant enclosure [2], the apparatus used in this experiment better represents a real-life structure. Furthermore, we evaluate the utility of this approach by comparing the peak power levels of the signal at the target location using NLTR waveforms vs. normal RF pulses.

Approved for Public Release, Distribution Unlimited
The views expressed are those of the author and do not reflect the official policy or position of the Department of Defense or the U.S. Government

II. NLTR Experiment

In our experiment, a passive harmonic generator was used as a discrete nonlinear circuit inside an enclosure. The NLTR procedure is illustrated in Fig.1. Various RF frequencies were used to represent different electrical sizes of the enclosure.

We compare the peak power levels of the signals at the target location resulting from NLTR waveforms and normal RF pulses (i.e. short and long pulses). An example is shown in Fig. 2. The NLTR waveforms in general increases the peak power on the target indicating that this approach can be used to more efficiently deliver short pulses to a nonlinear target.

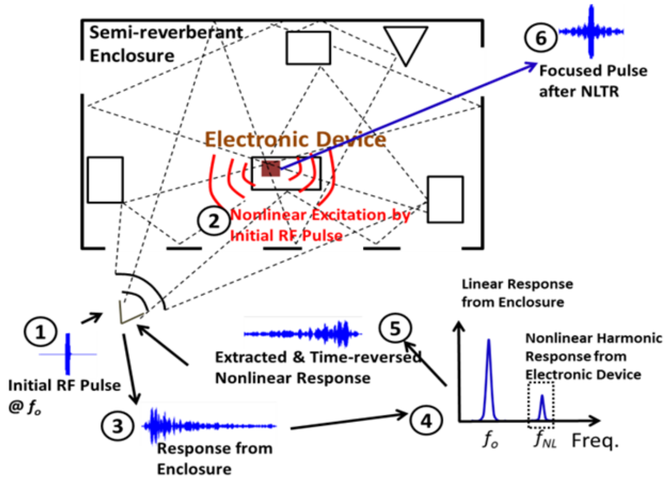

Fig. 1. NLTR experiment procedure

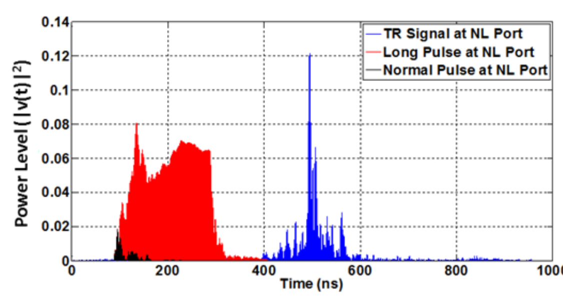

Fig. 2 Signal delivered at target location using NLTR waveform (blue), long CW-like RF pulse (red), and short RF pulse (black)

References

[1] G. Lerosey, J. de Rosny, A. Tourin, A. Derode, G. Montaldo and M. Fink, "Time reversal of electromagnetic waves," Phys. Rev. Lett., vol. 92, pp. 1939041-1939043, May. 2004.

[2] M. Frazier, B. Taddese, T. Antonsen and S. Anlage, "Nonlinear Time Reversal in a Wave Chaotic System," Phys. Rev. Lett., vol. 110, pp.0639021-0639025, Feb. 2013.

Characterization of Building Used for HPM Testing

Narrow band measurements in different parts of building

Jostein Godø
National Centre for Protection of Buildings
Norwegian Defence Estates Agency
Oslo, Norway
jostein.godo@forsvarsbygg.no

Odd Harry Arnesen
Protection and societal security dept.
Norwegian Defence Research Establishment
Kjeller, Norway
odd-harry.arnesen@ffi.no

***Abstract*— During a field trial a computer network and alarm systems were installed in a building, while different HPM sources were used on the outside of the building to radiate the electronic systems inside. No efforts were made to protect the building, and all the tested equipment was placed in a room at the outer wall. This paper will focus on potential protection by placing the equipment in other places in the building**

Keywords-Shielding; attenuation; protection; building

I. INTRODUCTION

Critical infrastructure may be installed in buildings which have not been planned for protection against IEMI. There could be a variety of reasons for this lack of protection; like costs, no defined threat at time of planning, etc. In some cases facilities which was not planned with protection, could still provide considerable shielding.

II. DESCRIPTION OF SITUATION

Studies have been done to investigate shielding effects in normal building materials in laboratories [1] and some measurements have been done on actual buildings. [2] These measurements have shown diverging levels of attenuation. A great variety of parameters can affect the result.

Given an attack on a certain building, the IEMI hazard could be dependent on location in the building. Multiple walls and floor separations may provide considerable attenuation.

III. MEASUREMENTS

Before the field trial, measurements were done to investigate attenuation in the room where tested equipment was installed. Afterwards, we wanted to investigate protection in different locations in the building.

A simple way to estimate the shielding of a building with moderate attenuation is to use already existing electromagnetic environment. [3] Most areas are covered by transmitters for FM radio, TV and cellular phones. Measuring field strength of these signals in different parts of the building was done as a first investigation to locate best location for critical installations.

Further tests were done with a narrow band source in different locations on the outside, and field strength was measured at different location on the inside for each position for the outside source.

REFERENCES

[1] W. C. Stone, "NIST Construction Automation Program Report No. 3 Electromagnetic Signal Attenuation in Construction Materials" Building and Fire Research Laboratory, National Institute of Standards and Technology, Gaitthersburg, Maryland 20899, October 1997.

[2] C. D. Taylor et al, "Measurements of RF Propagation into Concrete Structures over the Frequency Range 100 MHz to 3 GHz" Wireless Personal Communications, The Springer International Series in Engineering and Computer Science Volume 377, pp 131-144, 1997.

[3] E. B. Savage et al, "An Alternative EM Shielding Effectiveness Measurement Method for Buildings" Asia-Pacific Electromagnetic Compatibility Conference, APEMC 2010, Beijing, China, April 13, 2010.

Jamming Signal Immunity Tests on GSM-R Communications Compared to EMC Basic Standards

Véronique Beauvois
ACE
University of Liège
Liège, Belgium
v.beauvois@ulg.ac.be

Michele Fontana, Flavio G. Canavero
Dipartimento di Elettronica
Politecnico di Torin
Torino, Italy
{michele.fontana,þavio.canavero}@polito.it

Virginie Deniau
IFSTTAR
Univ Lille Nord de France
Villeneuve dôAscq, France
virginie.deniau@ifsttar.fr

***Abstract*ð This paper presents the work being done in SECRET project (European Program FP7/2007-2013 under grant agreement number ñ285136ò) to strengthen the European rail network against the potential jamming of the railway communications. Standardized immunity tests, currently conducted on communication equipment in the presence of electromagnetic (EM) interferences are presented. It then presents the tests carried out in SECRET to assess the resistance of railway communication systems face the signals generated by telecommunication jammers.**

Keywords-component; railway; electromagnetic attack; GSM-R; immunity

I. Introduction

The evolution of railways with higher speed and capacity, ERTMS and centralized management, automatic actions, sensors and antennas, GSM-R communications makes the railway network more and more vulnerable and an attractive target for EM attacks. A European consortium was then built in order to assess the real risks concerning EM attacks, identify areas for strengthening the railway network and develop detection solution and to design a resilient architecture.

II. Interfering Signals

After an analysis of the different EM attack devices, 14 attack devices has been selected and classified according to their power level, the waveform and the bandwidth of the interfering signal. Most of these devices are designed to disturb radio communication systems as GSM, TETRA, Wi-Fi,... From this extensive study the signals can be classified as modulated or unmodulated continuous waves, carrierless signals, pulsesé or can be formed by combination of those basic signals. However, the most accessible jammers emit signals that sweep the frequency band of the system to jam. The jamming signal successively covers each channel and come back in the channel with a fixed time interval.

III. Immunity Standards and Tests

A. Immunity standards

Current immunity standards (Railway, ETSI EMC and immunity basic standards) and the associated waveshapes have been studied in order to check that the selected EM attack signals are already included or not. However, basic immunity standards are based on useful signals and their spurious as the EM attacks are intentional signals. As our main concern is the communication, the applicable product standards are ETSI standards series EN 301 489-x for radio equipments and services (e.g. EN 301 489-7 for GSM and DSC mobile equipments) [1]. These product standards are referring to basic immunity standards EN 61000-4-x series. The most significant is EN 61000-4-3 concerning radio frequency fields between 80 MHz and 1 GHz, and 1.4 GHz and 2.7 GHz AM modulated 1 kHz80%, considering exclusion bands around the transceiver nominal frequency. These standards do not reproduce the specific time characteristics of the jamming signal.

B. Immunity tests on GSM-R to jamming waveshapes

The test set-up proposed to study the impact of jamming signals on railway communications is described in Fig. 1 [2]. Our study concentrates on the following characteristics of the signals: (1) frequency in or out of band, (2) number of periods, (3) interval without signal to emulate the sweeping. Two typical waveshapes are illustrated in Fig. 2.

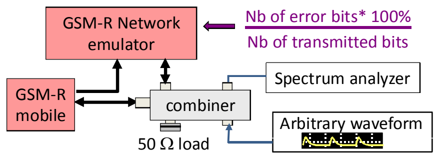

Figure 1. Immunity test set-up.

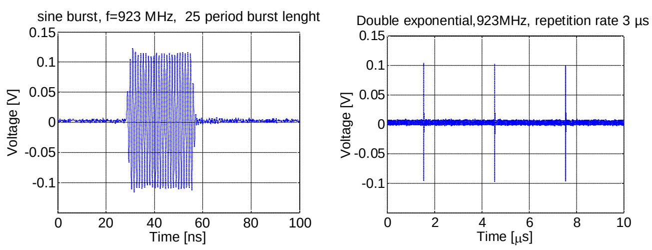

Figure 2. Immunity waveshapes – Sine Burst vs. Double exponential burst.

IV. Conclusions

The results will be presented during Amerem 2014 in order to highlight the main impacting parameters on the railway communications.

References

[1] EN 301 489 series of ETSI standards.

[2] S. Dudoyer, V. Deniau, R. Adriano, M. Slimen, J. Rioult, B. Meyniel, M. Berbineau, ñStudy of the Susceptibility of the GSM-R Communications Face to the Electromagnetic Interferences of the Rail Environment,ò EMC, IEEE Trans. on, vol. 54, n°3, pp. 667ï676, June 2012.

Creating Double Negative Index Metallic Materials for HPM Applications

H. S. Faraji, G. Atmatzakis, M. F. Su, and C. G. Christodoulou

Electrical and Computer Engineering Department, University of New Mexico
Albuquerque, NM, USA
hsfaraji@ece.unm.edu

***Abstract*— In this paper we introduce a new metamaterial unit-cell we name "Complementary Zia Metamaterial (C-Zia)". A Zia structure is a metamaterial unit cell structure which is based on inductive and capacitive regions similar to the well-known split-ring resonators (SRR) but it provides a greater design flexibility and frequency tunability. Also Zia metamaterial was adapted to show bianisotropic, chiral, and biaxial behavior. C-Zia structure is a complementary form of a previously published Zia structure, which is completely metallic and easy to mount. As such it is expected to be more compatible with high power microwave applications, in which traditional SRRs and other forms cannot be used due to dielectric breakdown.**

Keywords: Metamaterial; Zia; HPM

I. INTRODUCTION

Metamaterials are periodic arrays of subwavelength structures which provide an electromagnetic response not typically available in nature. They exhibit many interesting properties for high power microwave (HPM) applications, such as (i) the ability to get dielectric properties out of all-metallic structures, (ii) enablement of operational characteristics not attainable with conventional matarials, and (iii) reduction of physical component sizes.

Some well-known metamaterial structures are split-ring resonators (SRRs) and electric coupled resonators (ELCs). They typically possess a resonant response to the incident electric or magnetic fields and accordingly provide an effective permittivity or permeability. The resonance is closely tied into the few structural parameters of the metamaterial, such as gap widths and ring radii. This, combined with ad-hoc design rules and use of subcomponents made of dielectrics, render such metamaterials impractical in HPM applications.

A recent study in metamaterials research [1] resulted in a new type of structure dubbed the Zia metamaterial. This structure is all-metallic and has more degrees of freedom for tunability compared to other types metamaterial structures. More importantly, the study applied group theory concepts to metamaterials research to come up with Zia-based designs that effectively exhibit biaxial, bianisotropic and chiral material properties. Conventional Zia structures need a dielectric substrate in order to be mechanically mountable. This is a disadvantage for HPM applications, because dielectrics tend to build charge and break down in such environments. In this paper we introduce a complementary form of the Zia structure ("C-Zia") to address this issue. Preliminary results show that a "C-Zia" structure can couple into incident electric and magnetic fields simultaneously to provide concurrent effective negative permittivity and permeability. Such double behavior is not observed in other types of structures such as SRRs without ancillary structures such as rods, strips, or a waveguide.

II. RESULTS

The single-layer-thick C-Zia structure is shown in Fig. 1 (r_w = 0.2mm, r_{ir} = 4mm, r_h = 2mm and fg = 0.1mm). Fig. 2 shows the retrieved permeability and permittivity of the structure. There is a frequency range between 19.1 GHz to 20 GHz in which both permittivity and permeability are negative, hence a "metamaterial" behavior is observed.

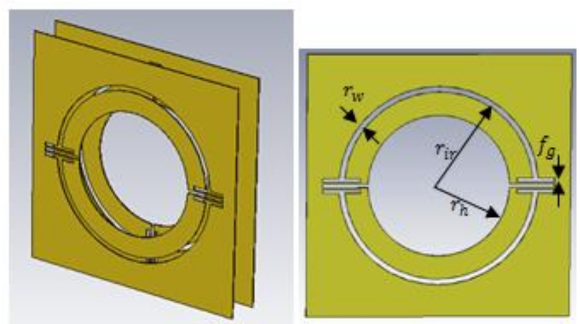

Figure 1. C-Zia unit cell

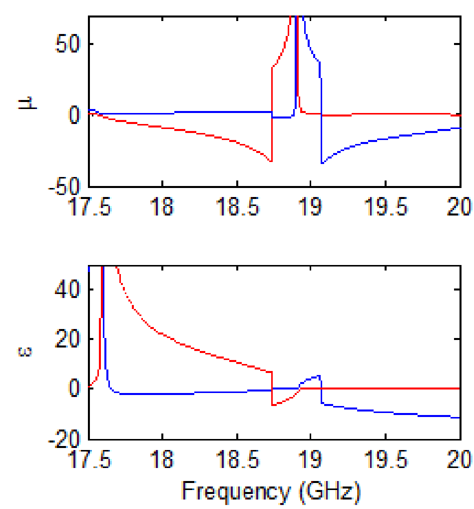

Figure 2. C-Zia magnetic permeability and electric permittivity (real part in blue and imaginary part in red)

REFERENCES

[1] C. M. Reinke, T. M. De la Mata Luque, M. F. Su, M. B. Sinclair, and I. El-Kady, "Group-theory approach to tailored electromagnetic properties of metamaterials:An inverse-problem solution," *Physical Review E* **83**, 066603, 2011.

EMP Protection and Testing of HF Systems An Overview

Walter J. Scott
Analytic & Advisory Services
TASC, Inc.
Lorton, Virginia, USA

Michael R. Rooney
Survivability Assessments Branch
Defense Threat Reduction Agency
Ft. Belvoir, Virginia, USA

***Abstract*—High Frequency (HF) communications are widely used for government, military and civilian infrastructure applications including emergency services. Survivable HF communications systems must be able to function after subjection to High Power Electromagnetic (HPEM) threats such as lightning and nuclear EMP. This paper presents an overview of a systematic method that can be used to Electromagnetic Pulse (EMP) harden and test typical unhardened HF transceiver systems. It begins with a basic analytical approach for determining the EMP-induced voltages and currents in HF antennas from an unclassified 50kV/m EMP environment[1]. These EMP-induced currents are usually sufficient to cause damage to HF equipment, so the next step in achieving a survivable system is to select a protection scheme that is capable of shunting these large currents to an Earth grounding point. There are many protection selection and implementation considerations that must be carefully dealt with in order to avoid adverse affects to normal HF transmit and receive functions, and even to avoid damage to the protective devices by the HF system itself. Finally there is a need to test the system in a high fidelity, threat-level EMP simulator to assess the performance of the hardening design and, for certain applications, to verify compliance with regulatory standards. For example, certain US military HF systems must meet the pass/fail requirements in MIL-STD-188-125-1[2] or MIL-STD-188-125-2[3].**

Keywords-HPEM, HF, system, EMP, hardening, testing, standards, antenna

I. INTRODUCTION

The paper begins with a discussion of the nuclear EMP threat waveform and employs the concept of antenna effective aperture and simple antenna reception equations to calculate the received power from the EMP waveform by the HF antenna's effective aperture. To simplify the analysis, local field reflections are ignored and a matched condition between the antenna and its load is assumed. The antenna manufacturer's literature can be consulted to provide the antenna's gain vs. frequency plot and, since HF antennas operate in the same bandwidth as an EMP, the flat part of the antenna spectrum may be used to specify antenna gain. With the foregoing data, the voltage at the antenna terminals can be calculated and used in the system hardening design.

II. HF SYSTEM HARDENING

Basic antenna equations are used to determine the antenna terminal voltage and current when it is illuminated by an EMP threat waveform. Using Thevenin's Theorem the open circuit voltage and short circuit current are found; short circuit current is then used as the worse-case current that the antenna protection scheme must shunt to Earth ground. An examination of the time history profile of the current indicates

that a device is needed with very low capacitance to handle the initial fast leading edge transition of the current waveform, and it also must be capable of diverting currents on the order of thousands of amperes. Consulting the product literature on fast, high current surge arresters indicates that a Gas Discharge Tube (GDT) is best suited for this application. Several GDT options available from one manufacturer are discussed in detail. The second part of the paper is concerned with hardening the electronics equipment: the transceiver, power amplifier, equalizer (flattener) and other typical HF system components. A brief discussion on shielded cabinets and point of entry treatments completes the hardening design.

III. HARDNESS VALIDATION

The final part of the paper discusses ways to validate the effectiveness of the hardening design through testing the hardened HF system in a threat-level EMP simulator. Measurement points in the system are identified and testing for compliance to certain military EMP protection standards is described. An example system will be described.

REFERENCES

[1] MIL-STD-464 Electromagnetic Environmental Effects Requirements For Systems, December 2010

[2] MIL-STD-188-125-1 High-Altitude Electromagnetic Pulse (HEMP) Protection For Ground-Based C^4I Facilities Performing Critical, Time-Urgent Missions, Part 1 Fixed Facilities, 17 July 1998

[3] MIL-STD-188-125-2 High-Altitude Electromagnetic Pulse (HEMP) Protection for Ground-Based C^4I Facilities Performing Critical, Time-Urgent Missions, Part 2 Transportable Systems, 3 March 1999

Miniaturization of TEM Horn Antenna Using Spherical Modes Analysis

Mohamed A. Elmansouri and Dejan S. Filipovic
Department of Electrical, Computer, and Energy Engineering
University of Colorado, Boulder, CO 80309-0425, USA
Mohamed.Elmansouri@colorado.edu, dejan@colorado.edu

Abstract— **An approach to miniaturize a TEM horn antenna while maintaining and even improving its frequency/time performance is presented. The proposed approach is based on combining a TEM horn with a rectangular loop antenna in order to excite the two fundamental spherical modes (TE_{m1} and TM_{m1}) which improves the antenna's performance at the low frequency end. The spherical modes expansion technique is used to investigate the characteristics of the excited modes and a simple current perturbation approach is utilized to achieve the desired combination of fundamental modes as well the higher order modes to lower the antenna's turn-on frequency and improve its radiation characteristics.**

Keywords- Miniaturization; Spherical modes; TEM horn

I. Introduction

TEM horn antenna (see Fig.1(a)) can operate over very wide bandwidth with low dispersion characteristics and high (CW and Pulsed) power handling capability which makes it an excellent candidate for directed energy weapons and electronic attack systems. However, a persistent issue is its size especially for UHF and VHF operation. Different techniques have been considered to miniaturize TEM horns including material, resistive and ferrite loading. Material-based miniaturizations need to be very carefully executed due to the excess loss and weight. Resistive and ferrite loading approaches reduce the antenna's efficiency due to the power losses. Another interesting miniaturization approach is to combine a TEM horn with dissimilar antennas that operate over different frequency bands like in the case of K-antenna [1]. By adding a configuration that radiates the fundamental spherical TE mode (i.e. loop antenna) to TEM horn, then the combination of the two modes (horn has fundamental TM mode) below the horn's turn-on frequency will not only miniaturize the antenna (lower turn-on frequency) but also improve its gain. The main challenge is to excite the desired modes' with certain magnitude and phase values. In this paper, a combined loop and TEM horn antenna is studied and spherical modes expansion approach [2] is used to analyze the radiated fields in terms of the spherical mode spectrum. The tuning of the desired modes (magnitude, phase, and turn-on frequency) is achieved by adding the perturbation slots to the combined antenna.

II. Results and Discussion

Shown in Fig. 1(b) is an exponential TEM horn combined with a loop. The $5\times5.5\times2.5\text{cm}^3$ combined antenna is modeled over an infinite ground plane using method of moments (MoM) and finite elements method (FEM) implemented in FEKO and HFSS; respectively. As seen in Fig. 2(a), the two different full wave models predict that the combined aperture has better match over significantly wider bandwidth compared to a conventional TEM horn. The turn-on frequency for VSWR < 2 reduced from 3GHz almost down to 1.1GHz. Improved VSWR and gain is observed at the low end and around 2GHz for the slotted topology shown in the inset of Fig. 2(b). To understand the physics of the observed performance and possibly even improve its reach, the spherical mode analysis is used. The relative power levels of the combined antenna's fundamental modes are shown in Fig.3. TE_{11}/ TE_{-11} modes are tuned at low frequencies due to the slots leading to a desired combination with TM_{01} and TM_{02} modes. The destructive interference between modes TM_{01} and TM_{02} (due to the phase difference) around 2 GHz is causing the observed drop in the gain of the combined antenna. As seen, the perturbation of the currents due to the slotting also tunes the phase difference between these two modes and improves the performance. The shape and size of the used slots are obtained after detailed numerical studies of the antenna's current distributions.

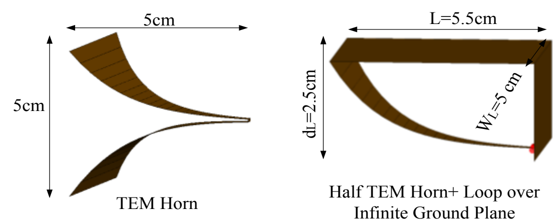

Figure 1. (a-left) TEM horn and (b-right) combined TEM horn-loop.

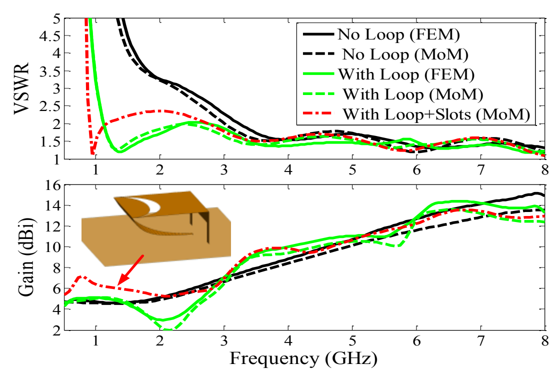

Figure 2. (a-top) VSWR and (b-bottom) gain performances.

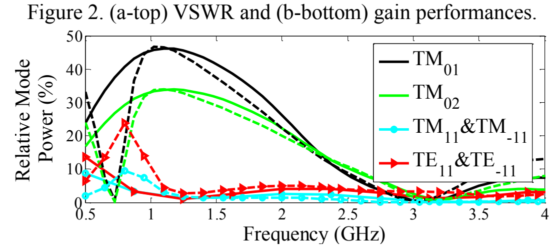

Figure 3. Spherical modes spectrum (solid) no slots (dashed) with slots.

References

[1] V. I. Koshelev, Y. I. Buyanov, Y. A. Andreev, V. V. Plisko, and K. N. Sukhushin, "Ultrawideband radiators of high-power pulses," in Proc. Pulsed Power Plasma Sci., pp. 1661–1664, Jun. 2001.

[2] J. E. Hansen *et al., Spherical Near-Field Antenna Measurements*, ser. London, U.K.: Peter Peregrinus, 1988, vol. 26.

ID 127

OCEAN-LAND INTERFACES

Two Alternative Treatments for Geomagnetic Storms and a Synthesis

James L. Gilbert

Metatech Corporation
Goleta, CA, USA
james.gilbert@metatechcorp.com

***Abstract*— In this presentation, we review two models for calculating the enhancement of geomagnetically-induced electric fields near land-ocean boundaries. The first is a model which requires the solution of an integral equation at each frequency, and the second is a simplified model that only requires Fourier transforms. The mechanism responsible for the differing results is determined, and it is suggested that one of the features of the integral equation model be included in the simplified model. This modification can be made without reducing the computational advantages of the second model.**

Keywords- Geomagnetically induced current, GIC, magnetic storms, Geomagnetic induction.

I. INTRODUCTION

At the edge of the ocean, the abrupt change in surface conductivity between the landward side and the seaward side can enhance the geomagnetically-induced electric field on the landward side. This is important for calculations of the response of electric power systems, which often have electrical generating plants near the seashore for cooling purposes In this paper we will compare an integral equation technique and a simplified Fourier transform approach. The major difficulty with the first approach is that it requires the use of integral equations; the major difficulty with the second approach is the neglect of diffusion of magnetic fields from the landward side beneath the ocean. We will propose a technique that modifies the procedure in [2] to include this term.

II. MODELS

A. Integral equation technique

An integral equation was developed in reference [1] for the horizontal electric field near the land-ocean boundary.

$$\left.\begin{array}{ll} H_0 & x \le 0 \\ H_0\,\mathrm{sech}(k_1 d) - Z_1^{-1} E_i \tanh(k_1 d) & x > 0 \end{array}\right\} = \frac{\sigma_0}{\pi}\int_{-\infty}^{\infty} dx' K_0(k_0|x-x'|)\,E_i(x') \tag{1}$$

where H_0 is the uniform applied magnetic field, E_i is the electric field at the surface of the ground, x is the distance oceanward from the boundary, k_1 is the wavenumber in the ocean, k_0 is the wavenumber in the ground of conductivity σ_0, Z_1 is the wave impedance in the ocean and d is the local depth.

B. Fourier transform technique

In reference [2], a simplified technique was developed that avoided the need for solving an integral equation by using the field diffusing through the ocean to the surface of the ground

$$\left.\begin{array}{ll} H_0 & x \le 0 \\ \dfrac{H_0}{\cosh(k_1 d) + (Z_0 / Z_1)\sinh(k_1 d)} & x > 0 \end{array}\right\} = \frac{\sigma_0}{\pi}\int_{-\infty}^{\infty} dx' K_0(k_0|x-x'|)\,E_i(x') \tag{2}$$

As the LHS of the equation was completely specified and the kernel on the RHS could be inverted in Fourier space.

III. COMPARISON AND A MODIFICATION

Figure 1 shows a comparison of the two techniques. The difference is due to the lack in the Fourier transform technique of the landward magnetic field diffusing outward beneath the ocean.

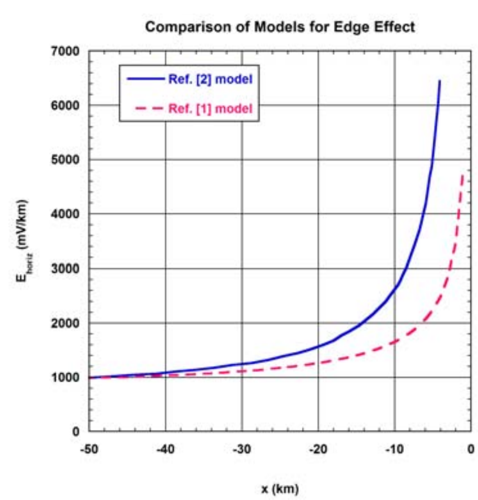

Figure 1. Comparison of techniques.

The Fourier technique may be corrected by adding this diffused field in the left hand side of equation 2. Examples will be shown.

REFERENCES

[1] J. L. Gilbert, "Modeling the effect of the ocean-land interface on induced electric fields during geomagnetic storms" in Space Weather, vol. 3, no 4. S04A03, doi: 10.1029/2004SW000120, 2005.

[2] R. Pirjola, "Practical Model Applicable to Investigating the Coast Effect on the Geoelectric Field in Connection with Studies of Geomagnetically Induced Currents," Advances in Applied Physics, vol. 1, no. 1, pp 9-28, 2013.

Analysis of 20 Stages, 64 J, 300 kV, Marx Generator UWB System

Sachin Umbarkar[1], Mrunal Parekh[1], Archana Sharma[2], H.A.Manglvedekar[1]
[1]Veermata Jijabai Technological Institute, VJTI-Siemens High Voltage Lab, Mumbai, 400019 India
[2]Accelerator and Pulse Power Division, Bhabha Atomic Research Center, Trombay, Mumbai-85, India
sachin.b.umbarkar@gmail.com

***Abstract*— this paper gives the analysis of 20 stages, 64 J, 300 kV Marx generator for UWB application. The output pulse of Marx is sharpen by peaking stage and radiated by two types of antenna. Nanosecond pulse was fed to 1.5 meter length half transverse electromagnetic (HTEM) horn type antenna. Radiated field are observed at azimuthal angle and at various distances from the antenna. Design characterisation of the antenna was done using wavelet transform as the tool gives frequency components of the radiated pulse. The modelling and transient analysis of HTEM antenna and Impulse radiating antenna was done in computer simulation technology (CST) - microwave studio software.**

Keywords- Antenna, impulse, Marx generator, wavelet transform

I. INTRODUCTION

The impulse radiating systems are the important in the field of electromagnetic testing of electronic equipment, image processing, and in ultra-wideband radar technology. It also has wide range of application in the electronic war fair. To get the higher detection range, we need to have higher effective radiated power. This could be obtained from the UWB source consisting of RLC circuit with very low inductance producing low rise time pulses. In this paper, we characterize the compact 20 stages, 64 J, 300 kV Marx generator connected to the impulse radiating antenna to convert it into UWB system. This Marx generator has inbuilt peaking stage connected to the last stage of Marx circuit.

II. UWB SYSTEM

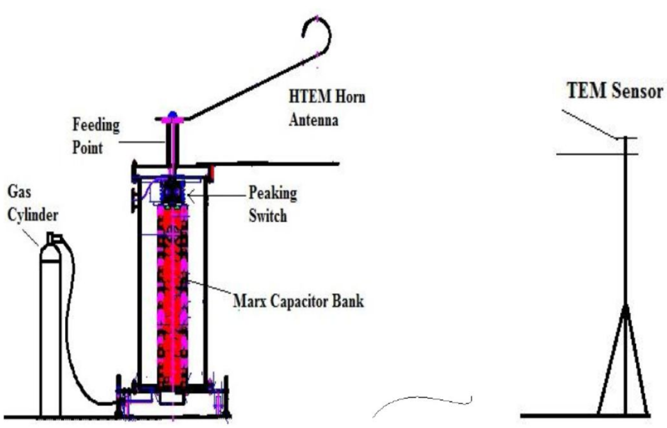

Figure 2 Schematic Diagram

III. RESULTS

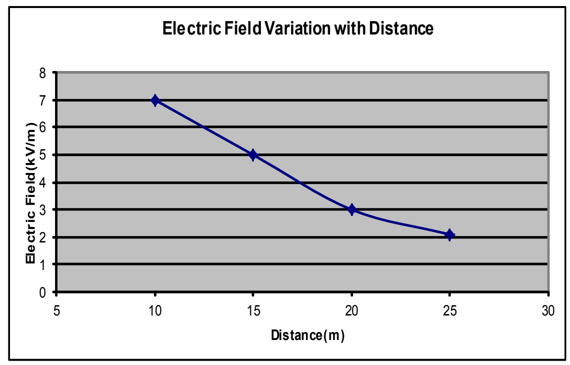

Figure 2 Far field

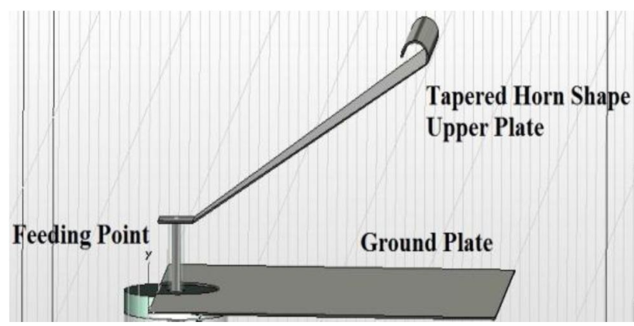

Figure 3 CST model

REFERENCES

1. C. E. Baum et al., JOLT: A highly directive, very intensive, impulse-like radiator, in *Sensor and Simulation Notes,* Note 480, Nov. 10, 2003.
2. R. Todd Lee and Glenn S. Smith, "A Design Study for the Basic TEM Horn Antenna" *IEEE Antennas and Propagation Magazine*, Vol. 46, No. 1, February 2004.
3. [3] S.V. Tewari, Sachin B. Umbarkar, Ritu A, P C Saroj, A Sharma, K C Mittal, H A Mangalvedekar, "Development and analysis of PFN based Marx generator finite integration technique for an antenna load" IEEE Transaction on Plasma Science, Vol. 41, No.10, OCT. 2013.
4. [4] Sachin B. Umbarkar, S. Bindu, H A Mangalvedekar, Archana Sharama, P C Saroj, K C Mittal, "Analysis of Half TEM Horn Antenna for High Power UWB System", Pulse Power and Plasma Science, Conference June. 2013.

A Technique for Evaluating Electrical Insulation in High Frequency/High Voltage Applications

Clayborne D. Taylor, Jr.
Electrical and Computer Engineering
Mississippi State University
Mississippi State, MS, USA
cdt4@ece.msstate.edu

Clayborne D. Taylor, Sr.
Professor Emeritus
Electrical and Computer Engineering
Mississippi State University
Mississippi State, MS, USA

***Abstract*— During fabrication electrical insulation, imperfections that lower the insulation quality cause non-linear responses when energized at high voltages. The non-linear response, generally known as partial discharge (PD) and described by patterns of current pulses, is seen at a broad band of frequencies. The PD pulse shape is approximated by a Gaussian distribution and is directly measured revealing a pulse width less than 1 ns. Patterns of the PD current pulses can help in evaluating the quality of electrical insulation systems. Due to the nature of insulation systems designed to withstand the forces of high power systems, measurement of Gaussian current pulses is quickly degraded at higher frequencies. Traditional methods of low-bandwidth PD measurement do not apply where high bandwidth, high power sources are required. A novel approach is presented that uses a wavelets-based estimator with lower bandwidth multi-channel measurement.**

Keywords: partial discharge, high frequency pulse patterns, wavelet decomposition

I. INTRODUCTION

Precise measurement of partial discharge (PD) is a difficult problem for high bandwidth power sources. PD pulses for gas voids have a steep rise (sub-nanosecond) and short width (typically <10 ns). This shape and bandwidth is based on the size and density of the charge trap, and the electrical properties of the material that the discharge energy must propagate through. Finally, the PD energy may be very close to the electrical noise level of the physical environment.

II. MEASUREMENT SYSTEM

Measurement of current pulse signals shown in Fig. 1 is performed using a 1 GS/s Digital Storage Oscilloscope to capture a pulse train of 10 total square pulses.

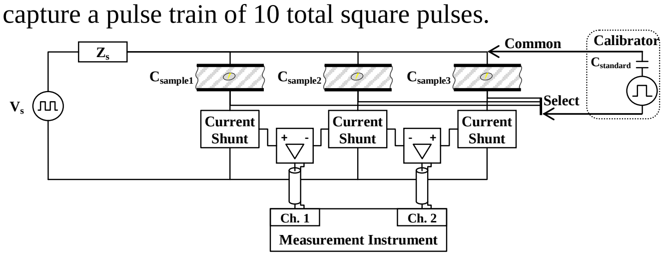

Figure 1. Multi-channel PD measurement system.

III. METHOD OF ESTIMATION

A. Wavelet Transformation

Decomposition of signal data is performed using the Daubechies 4 coefficients with 3 levels of decomposition of a signal that is down-sampled to 300 MHz. Signal estimation threshold for wavelet coefficients was selected at 300% of the coefficient noise level.

B. Algorithm of Estimator

Two channels from the measurement system are transformed with wavelets for proper estimation of pulse patterns. For the estimator, the channel voltage is determined from the first order wavelet detail and the PD coefficients in (1). These PD coefficients are directly correlated to the physical PD phase location and magnitude.

$$\tilde{v}_{ch}[n] = v_{c\pm}^{d1}[n] * PD_{\pm}[n] + v_{cx}^{d1}[n] * PD_x[n]. \qquad (1)$$

IV. RESULTS

Current pulse patterns were recorded when pulse train magnitude reached 750 V for 50 ns rise-time and fall-time and total cycle time of 100 µs, 50% duty cycle. At room temperature, the recorded pulse patterns presented in Fig. 3 show results in good agreement with other similar studies at

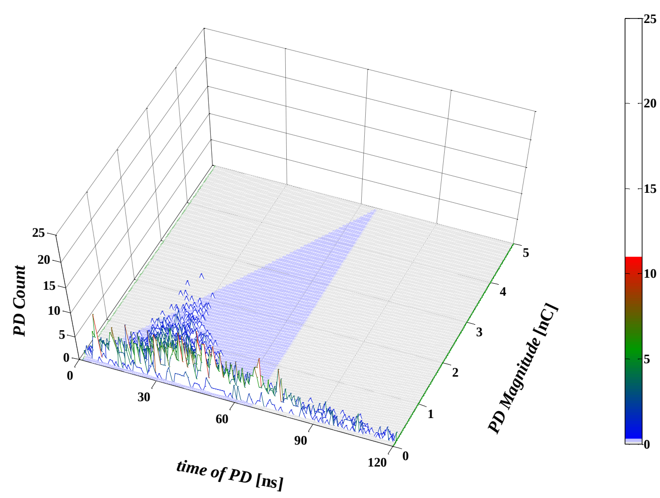

Figure 3. PD Pattern for 750V Magnitude, 10 kHz Square Pulse Train, 20°C.

REFERENCES

[1] S. Grzybowski, C. D. Taylor, S. R. Chalise, "Electrical Degradation Study of Machine Winding Insulation," in Proceedings of the International Conference on High Voltage Engineering (ICHVE'2008), Chongqing, China, 2008.

[2] Kai Zhou, Guangning Wu, Kegang Lei, Jiandong Wu, Jun Liu, "Aging Time Effect on PD Characteristics under Continuous Pulse Voltage," in IEEE International Conference on Solid Dielectrics, 2007, Winchester, UK, 2007, p. 616 – 618.

.

ID 131

Attenuation of Building used for HPM Testing

Variation with frequency, polarization, position, and window configuration

Ernst Krogager
Joint Research and Test Centre
Danish Defence Acquisition and Logistics Org.
Ballerup, Denmark
krogager@mil.dk

Jostein Godø
National Centre for Protection of Buildings
Norwegian Defence Estates Agency
Oslo, Norway
jostein.godo@forsvarsbygg.no

***Abstract*— Before conducting a series of High Power Microwave (HPM) attack tests against electronic equipment placed inside a building, an estimate of the expected field levels at the test objects was desirable. For this purpose, basic attenuation tests were carried out using a handheld network analyzer over the frequency range 100 MHz to 7 GHz. Prior to the tests, a new window was mounted in the wall facing the road along the building in order to obtain a more realistic test configuration. Measurements were carried out before and after insertion of the window. In this paper, the measurement setup is described, and the main findings of the tests are reported. The measurements revealed a significant attenuation of the new, energy-saving window.**

Keywords-RF attack; attenuation; building materials; windows

I. Introduction

One of the objectives of the EU Consortium HIPOW (Protection of Critical Infrastructures Against High Power Microwave Threats) is to perform practical experimentation by irradiating test objects inside a building using high powered RF (Radio Frequency) sources outside. Prior to performing such tests, estimates of the electromagnetic field coupled into the building are desirable in order to plan the test conditions based on expected effects. The measurements reported here were carried out in August 2013 at a test site in Norway. An old building with concrete walls was used as a representative test environment. In the past, the windows in the wall facing the road were replaced by bricks, but before the HPM experiments a new window was inserted in one of the window positions.

II. Measurement procedures

A. Test Equipment

The basic test setup is seen in Fig. 1 and Fig. 2. An Agilent N9343C Handheld Spectrum Analyzer was used with a network analyzer capability up to 7 GHz. A variety of transmit and receive antennas were used to cover the frequency range from 100 MHz to 7 GHz. Measurements were made in two bands, 100 MHz to 1 GHz and 1 GHz to 7 GHz.

Figure 1. Test equipment outside.

Figure 2. Receiving antenna inside.

Figure 3. Window at 45 degrees.

Figure 4. Window at 90 degrees.

B. Calibration and Normalization

Calibration measurements were performed outside the building in order to establish a reference level corresponding to free-space propagation with compensation for cable losses etc. The distance between the antennas was a few meters, i.e., measurements were made in the near-field zone at the lower frequencies. However, due to the complexity and associated general uncertainty of this type of measurements, the results are considered representative for the purpose. Measurements were carried out for both horizontal and vertical polarization and with the antennas at different positions and heights.

III. Sample results

Examples of obtained results are shown in Fig. 5 and Fig. 6, in which the relative amplitude with open and closed window is shown for the frequency ranges 0.1-1 GHz and 1-6 GHz, respectively. Obviously, the effect of an RF attack depends on the frequency of the source. Moreover, the attenuation depends on the configuration of inventory inside the building and the specific point of observation. In general, the characterization of electromagnetic fields inside buildings is complicated. The same applies to the interpretation of associated experimental data.

References

[1] William C. Stone, "Electromagnetic Signal Attenuation in Construction Materials," NIST Construction Automation Program Report No. 3, Building and Fire Research Laboratory, National Institute of Standards and Technology, Maryland, October 1997.

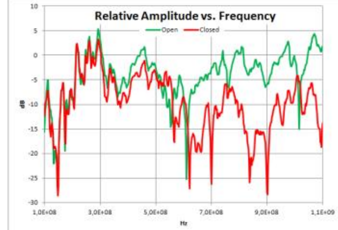

Figure 5. Lower frequencies.

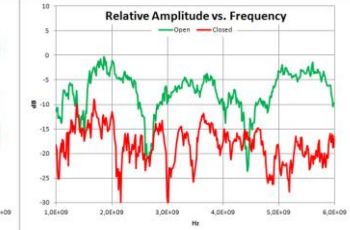

Figure 6. Higher frequencies.

Miniaturized Slotted Waveguide Antennas with Periodic Structures for HPM Applications

Xuyuan Pan and Christos G. Christodoulou
Department of Electrical and Computer Engineering
University of New Mexico
Albuquerque, NM 87131
Email: {xypan, christos}@ece.unm.edu

Mohammed Al-Husseini
Beirut Research and Innovation Center
Lebanese Center for Studies and Research
Beirut 2030 8303, Lebanon
Email: husseini@ieee.org

***Abstract*—This work describes the use of periodic structures for the size reduction of slotted waveguide antennas (SWAs) having slots in either a narrow or a broad waveguide wall. SWAs are attractive for their high-power handling, design simplicity and high efficiency, but their size can grow very large. Periodic structures designed from metamaterial cells or corrugations help compact the size. They offer other advantages, such as better matching at the feed.**

I. Introduction

Slotted waveguide antennas (SWAs) are attractive due to their design simplicity and their significant advantages in terms of high power handling, high efficiency and good reflection coefficient. The size of an SWA is usually large, since it is an array of slots, with constraints on the spacing between adjacent slots. For higher gains and better radiation characteristics, an SWA with more slots is required, meaning an even larger size. Periodic structures, on the other hand, have been extensively researched in the area of antenna engineering, with main applications in gain enhancement, frequency selection, and interference and sidelobe suppression.

In this work, periodic structures based on split-ring resonators (SRRs) and metal corrugations are shown to be very effective in compacting the size of SWAs with slots in either the narrow or broad waveguide walls. They can also be applied for efficient matching at the antenna's feed. Both advantages are important for high-power microwave (HPM) applications.

II. Narrow-wall SWAs Loaded with Metamaterials

Narrow-wall longitudinal-aperture waveguide antennas have drawn increasing attention in HPM applications due to their better power handling ability. However, there exist more constraints on the narrow-wall aperture placement, so size reduction is a major concern for narrow-wall SWA design.

Previous work has been done on narrow-wall SWA designs. An example design achieves a fan-beam radiation pattern with a reflection coefficient less than -30 dB, but has a large size. Upon introducing SRR-based metamaterials inside narrow-wall SWA designs, size reduction is achieved.

An SRR array is inserted into a size-reduced HPB-radiator-loaded SWA, which leads to a further transverse aperture size reduction of about 70%, compared to the conventional case. The new SRR-loaded narrow-wall SWA maintains a fan-beam radiation pattern with high directivity. For high-power handling, the ring arrangement is optimized to maintain a low reflection coefficient and a high radiation efficiency.

III. Broad-wall SWAs with Periodic Structures

Two identical sets of metallic corrugations are added inside an S-band SWA having 10 elliptical slots on one broad-wall and designed for 3 GHz and a sidelobe level (SLL) of less than -30 dB. A first configuration of the corrugations, with optimized number, spacing, and height (height is about $b/1.5$), offers a resonance at a lower frequency, 2.55 GHz instead of 3 GHz. This translates into a reduction in the waveguide length by about 46%. The gain and SLL are almost unchanged. A second corrugation configuration, which differs in the corrugations spacing and height (height now is lower, about $b/4$), keeps the same resonance at 3 GHz but leads to a very low reflection coefficient (-48 dB compared to -18 dB for the non-corrugated version).

With the corrugations, the size reduction was in term of the waveguide length only. Further transversal compactness, that includes smaller a and b values, can be obtained upon the use of a periodic set of metamaterial cells, mainly SRRs. The loading of the SWA by both the corrugations and the SRRs is investigated.

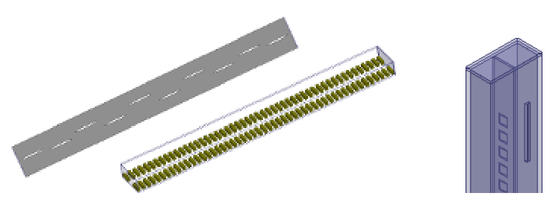

(a) (b)

Fig. 1: Broad-wall SWA with: (a) corrugations (b) SRRs.

IV. Conclusion

This work showed the use of periodic corrugations and SRR-based metamaterials for size reduction of both broad- and narrow-wall SWAs. Better reflection coefficients and high radiation efficiencies can also be achieved. These SWAs loaded with periodic structures are suitable for HPM applications.

Experimental Plan For 70% Efficient Relativistic Magnetron With Diffraction Output (MDO)

Chris Leach, Sarita Prasad, Mikhail Fuks, Jerald Buchenauer, Jeremy McConaha, and Edl Schamiloglu

Department of Electrical and Computer Engineering

The University of New Mexico, MSC01 1100, 1 University of New Mexico,
Albuquerque, NM 87131 USA

***Abstract*— It was demonstrated via MAGIC [1] simulation that a relativistic magnetron with axial diffractive output (MDO) could operate at 70% efficiency [2]. In order to experimentally verify this, UNM's PULSERAD PI-110 electron accelerator was modified to provide a 350 kV, 30 ns flattop pulse with <4 ns rise time [3]. The MDO was characterized with a B-field scan at this voltage, where 6, 4, and 2 cavities are used to excite the downstream microwaves modes to be radiated. Behavior was predicted for a variety of cathode endcaps used to suppress the downstream drift of electrons; these endcaps include spherical, spherical dielectric coated, spherical magnetic, spherical magnetic dielectric coated, and conical. A diagnostic plan was made in order to capture power and microwave pulse shape/length for several potentially co-existing radiated modes using a calorimeter and microwave diagnostics, as well as measuring the microwave diode's voltage and current waveforms via D-dot and Rogowski probes. Finally, a pulsed insulating electromagnet system was recently finished.**

Keywords-magnetron; diffraction; diffractive; MDO; axial; MAGIC

I. Introduction

Preparations for the experimental verification of a 70% efficient MDO are in the final phase at UNM. Following a rebuild and redesign of the PULSERAD PI-110 to provide a 350 kV, 30 ns flattop, <4 ns rise time voltage pulse, a number of peripheral systems were constructed, including a pulsed electromagnet system and a high power microwave calorimeter capable of measuring energy depositions of less than 1 J. A variety of other diagnostics were also put into place. In addition, MAGIC simulations were performed in order to predict the power output with 6, 4, and 2 (of the magnetron's 6 cavities) used to excite the desired output mode and to predict the efficacy of a number of cathode endcaps that are to be used to block leakage current.

II. Experimental Setup

A. Physical system highlights

The PULSERAD PI-110 accelerator's fast rise time is attributed to a low-inductance oil-breakdown switch that separates the pulse forming line from the final transmission line that feeds the magnetron. This will be the first-ever experiment to verify what is observed in simulations, that when the rise time of the applied voltage pulse is less than the cavity fill time for any mode in a vacuum HPM device, there is higher saturated output power. Furthermore, the MDO source will be very compact and quickly output a Gaussian-like antenna profile. This experiment will also be the first test of a variety of cathode endcaps in an MDO system, some which are to be coated with a thin layer of Rexolite dielectric and which are magnetic.

B. Diagnostics

Two D-dot probes will monitor the voltage waves on the PFL and final transmission line. A self-integrating Rogowski coil will monitor the diode current. To measure microwave power, a calorimeter with <1 J sensitivity was built, that would absorb ~70% of the incident power and allow the transmission of a fraction to an open waveguide so that the pulse profile and a time-frequency analysis could be captured and calculated. This open waveguide will also be swept in front of the antenna to calculate an integrated power.

In particular, the calorimeter employs an Arduino Uno microcontroller that measures the change in resistance in a changing volume of ethanol in a 2 mm inner diameter capillary tube, which is output to an LCD display and serial port. The microcontroller uses a nichrome heating coil and PID algorithm to heat the alcohol to just above room temperature and to pre-set the meniscus shape. A calibration coil is used to simulate the deposition of microwave energy.

III. Simulations

Simulations indicate 69% efficiency for an MDO when using 6 cavities to excite a TE_{21} output mode and greater than 50% efficiency when using 4 cavities to excite a TE_{11} Gaussian-like output mode.

References

[1] B. Goplen, L. Ludeking, D. Smithe, and G. Warren, "User-configurable MAGIC for electromagnetic PIC calculations," *Comp. Phys. Commun.*, vol. 87, pp. 54-86 (1995).

[2] M.I. Fuks and E. Schamiloglu, "70% efficient relativistic magnetron with axial extraction of radiation though the horn antenna," *IEEE Trans Plasma Sci.*, vol. 34, 1302-1312 (2010).

[3] S. Prasad, C. Leach, K. Prestwich, C.J. Buchenauer, M. Fuks, E.Schamiloglu, "Experimental demonstration of the output characteristics of the A6 magnetron on Pulserad 110a, a very short rise-time accelerator at UNM," *Vacuum Electronics Conference (IVEC), 2012 IEEE Thirteenth International*, vol., no., pp.495,496, 24-26 April 2012

This work was supported by a grant from ONR Code 30, SAAET.

ID 136

Evaluation of HPEM Effects of Electronic Equipments in Actual Environments

Jin Soo Choi, Jongwon Lee, Jiheon Ryu, Cheonho Kim, Seung Ho Han, and Sung Hoon Hong

The 4th R&D Institute

Agency for Defense Development (ADD)
Daejeon, Republic of Korea
jschoi@add.re.kr

***Abstract*— It is hard to solve the susceptibility of electronic equipments to high power electromagnetics (HPEM) in practical environments due to the complicated parameters such as coupling paths, external interference, and random effects. In this work, we propose the methodology to predict HPEM effects of electronic equipments in the actual building. We first model and simulate the electromagnetic propagation into the building with two stories. We then measure the HPEM susceptibility of electronic equipments in the building structure. The compact high power electromagnetic source developed in ADD is used to validate the HPEM effects.**

Keywords—* *high power electromagnetic effects, actual environment, electronic equipments, susceptibility

I. INTRODUCTION

Electronic equipments are very important to the modern life and military systems. Since the equipments are vulnerable to high power electromagnetic waves, the HPEM effects of the electronics have been researched in past decades. However, due to the unclear parameters such as electromagnetic coupling path and stochastic effects of malfunctions, it is difficult to accurately evaluate HPEM effects in real environments.

To discover the algorithm for HPEM effects of electronic systems in actual environments, we firstly measure the electromagnetic waves penetrated into the actual building with two stories. The system developed by ADD in [1] is used as the HPEM source. The penetrated waves are numerically and experimentally validated. We then analyze the HPEM effects of electronics such as computers, networks, and cameras.

II. SIGNAL PENETRATION

A. 3-D Modeling and Simulation

Fig. 1(a) illustrates the 3-D computer model of the actual building structure. As shown in Fig. 1(b), the distribution of penetrated electric fields is computed by using finite-difference time-domain method.

B. Measurement of Electromagnetic Penetration

We measure the electromagnetic signals simultaneously in various positions like at front windows and at the rooms of the building. Here D-dot sensors are used to obtain pulses from the ultra wideband source. The measured data are compared to the simulation results.

III. EFFECTS OF ELECTRONIC EQUIPMENTS

To validate the HPEM effects of electronics, various computers and network devices are installed at each room in the two-story building. The high power wideband radiators which can generate high electric field are installed outside the building. D-dot sensors and electrically shielded cameras are set up at each observing points. The signals from network devices are regularly transmitted through the optical cable. By using this monitor system, we are able to measure the electric fields and observe HPEM effects of electronic equipments in the remote shielding room. We can also watch the malfunction of network devices.

A number of test results are systematically and statistically analyzed to evaluate the susceptibility of electronic equipments as shown in Fig. 2.

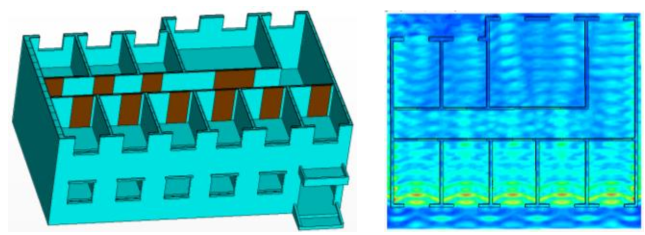

(a) (b)

Figure 1. 3-D modeling and simulation of signal penetration

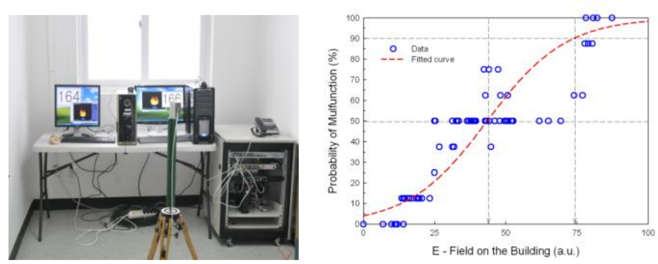

Figure 2. Test Equipments in the Building and results of HPEM tests.

REFERENCES

[1] J. Ryu, J. Lee, H. Chin, J.-H. Yeom, H.-T. Kim, H.-O. Kwon, S. H. Han, and J. S. Choi, “A high directive paraboloidal reflector antenna for high far voltage in an ultra wideband source system,” IEEE Trans. Plasma Sci., vol. 41, no. 8, pp. 2283–2290, Aug. 2013.

High-Power Microwave Weapons' Effects and Failure Analysis Using Sneak Circuit Modeling

Andrew L. Drozd
ANDRO Computational Solutions, LLC
Rome, New York USA
adrozd@androcs.com

Irina Kasperovich
ANDRO Computational Solutions, LLC
Rome, New York USA
ikasperovich@androcs.com

***Abstract*— This paper describes a new knowledge-based toolkit approach for analyzing High-Power Microwave (HPM) weapons' effects failure analysis of large, complex systems due to far-field HPM sources as well as close-in High-Power Electromagnetic (HPEM) interferers. In this approach, hybrid frequency/time-domain analytical and numerical techniques are used to assess electromagnetic interference/vulnerability (EMI/V) to HPM fields incident on electronic equipment locations associated with radio frequency (RF) communications systems, electro-optical/infrared (EO/IR) sensors, Global Positioning Systems (GPS), inertial navigation systems (INS), and processors. In particular, failure effects are traced to individual electronic components or devices to quantify HPM weapons' effects failures for front/back-door critical points of entry (POEs) in the system and then component-level HPM failure effects are ranked. The development of new models are described for characterizing HPM EMI/V at the device level, which are not currently available, and that will result in a new expert system capability for performing efficient *sneak circuit fault-tree* type failure modeling and analysis.**

Keywords- *Numerical Models and Modeling, Applications of Coupling to Structures and Cable, System-level Protection and Testing.*

I. Introduction

Advanced HPM weapon systems and devices are increasingly being deployed by US adversaries for both defensive and offensive purposes. New emerging threats, proliferation and the success of these mechanisms challenge the EMI/V and survivability of the Navy's current inventory and developmental defense systems, subsystems, and components. Some of these concerns are addressed in MIL-STD-464C. However, the effectiveness of HPM devices is difficult to ascertain because, currently, there is no valid method to determine whether any disruption or damage has occurred especially at the component or device level. Also, there is a need to confidently ascertain the level of damage sustained by enemies in the field from US military HPM weapons.

Since HPM damage may not be readily apparent, a combination of internal signal monitoring and post-test disassembly, investigation, and analysis is often necessary to determine specific failure modes. Limited functional monitoring of the system during testing can make this process extremely problematic and potentially cost prohibitive. Therefore, a need exists to develop a comprehensive analysis methodology and simulation process for understanding as well as quantifying HPM failure effects for various electronics and then prioritizing the effects *vis a vis* severity (temporary disruption, performance degradation, and permanent damage).

More specifically, a capability is needed to more accurately pinpoint potential electronics vulnerabilities, failure modes, as well as the probability and type of failure to incident HPM threats. However, a major challenge is the unavailability of EMI/V data on devices, components and pieceparts and the lack of understanding of HPM-induced failure modes and mechanisms. Hence, there exists a need for developing proven methods of extrapolating or relating susceptibility effects and corresponding EMI/V margins for low-level signal interference in computing HPM DDD thresholds.

Furthermore, HPM coupling and interference/destruction mechanisms are stochastic in nature and thus, have a high degree of variability. HPM devices nominally produce a pulse peak power of $\geq$100 MW and the means of delivery can vary dramatically, such as by an individual, via vehicles, or from large ground structures. Some mechanisms generate a single pulse or multiple pulses creating concerns over victim device non-average power (peak power, energy) vulnerability. Coupling or relating internal signal monitoring methods with damage assessed by inspection is essential to applying techniques for coupling the modeling with the actual HPM effects. Unlike kinetic weapon effects, HPM weapon effects can result in signal-induced EMI/V that in turn, may lead to subtle disturbances or possibly physical damage or even destruction. We can examine and somewhat adapt the processes and assessment methodologies developed in kinetic weapon survivability testing, focusing on electronic forensics and failure analysis, in order to devise a tool that will provide the necessary functionality for assessing incident HPM-induced failure effects.

A potential solution to this problem is to combine a system-level modeling/analysis tool with a statistical electromagnetics (EM) analytical approach in conjunction with an automated "sneak circuit" analysis (SCA) tool consistent with the methodology outlined in MIL-STD-785B tailored to the HPM threat. The SCA approach will provide a computer-based system for the identification of sneak paths and failure concerns in switching circuitry in analog or digital design. The statistical EM and SCA methodology would provide a useful means of classifying HPM coupling modes/mechanisms and effects at the system level for both back-door and front-door (antenna aperture) POEs down to the circuit, device or component level. A *Partial Element Equivalent Circuit (PEEC)* tool has also been considered that can provide a basis for frequency-domain and time-domain EMI/V failure analysis.

Analysis of Coupling Effect for Multi-Layered Composite Material with Periodic Structure

Se-Young Hyun, Jin-Kyoung Du, and Jong-Gwan Yook
Dept. of Electrical and Electronic Engineering
Yonsei University
Seoul, Republic of Korea
jgyook@yonsei.ac.kr

Chilsung Jung, and Eung-Jo Kim
The 7th R&D Institute
Agency for Defense Development
Haemi, Chungnam, Republic of Korea

***Abstract*— This paper brings efficient approaches for characterizing electromagnetic coupling into multi-layered composite material with periodic structure. In order to efficiently analyze the coupling effect, analytic method as boundary value solution, periodic structure analysis, and extraction method of material properties are combined together and implemented successfully. The accuracy of the proposed method is verified from the comparison of full-wave simulation result. It is shown that the proposed method is time and cost effective.**

Keywords-composite material; multi-layered structure; periodic structure; extraction;

I. INTRODUCTION

A composite material in aircraft structure is used in the form of a multi-layered structure such as composite material layer with core layer and combined with frequency selective surface (FSS), honeycomb, slot, and etc. These are difficult to define about dielectric properties and its analysis is also not easy because of different types of multi-layered structure. The multi-layered structure which is possible to know its dielectric characteristic of each layer, it can be mathematically performed with analytic method such as boundary value solution and recursive method [1],[2]. However, analytic method has certain limitations for multi-layered composite material with the arbitrary geometries. Limitations of numerical methods used in multi-layered structure, when each layer in the multi-layered structure is changed, mesh in numerical methods should be regenerated for the whole structure.

In this paper, we propose efficient approaches for the electromagnetic coupling into multi-layered composite material with periodic structure.

II. COUPLING EFFECT

Fig.1 shows the flow for analysis of multi-layered composite material with periodic structure. The boundary value solution, periodic structure analysis, and extraction method of effective permittivity and permeability of material are combined together. The accuracy of the proposed method is verified from the comparison of full-wave simulation result. As shown in Fig 2, good agreement was obtained from the full-wave simulation.

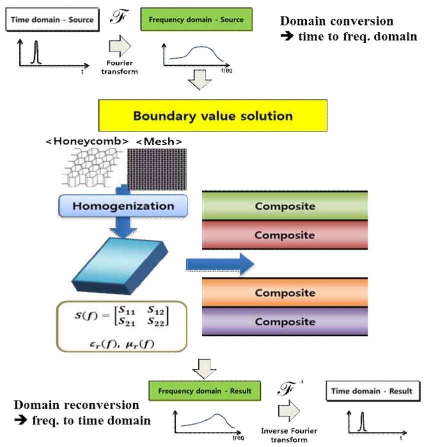

Figure 1. Flow for coupling effect analysis of composite material with periodic structure.

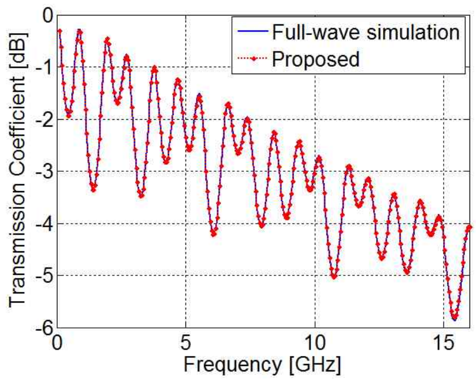

Figure 2. Comparison of proposed method with full-wave simulation.

ACKNOWLEDGEMENT

"This work has been supported by Agency for Defense Development of Republic of Korea under the contract UD130028JD"

REFERENCES

[1] Dennis J. Kozakoff, "Analysis of radome enclosed antennas," Artech House, 1977.

[2] H. Cory and C. Zach, "Wave propagation in metamaterial multi-layered structure," Microwave and Optical Latters, vol. 40, No. 6, pp. 460-465, March 2004.

Lightning Accidents in Colombia

Lightning threats in the Colombian army

Francisco Roman and Felix Vega
Universidad Nacional de Colombia
Electrical and Electronics Department
Bogotá Colombia
fjromanc@unal.edu.co, jfvegas@unal.edu.co

***Abstract*— In this paper we assess the lightning accidents in Colombia, in the specific case of the Colombian National Army. The last eleven years of information indicates that in the Colombian army there is circa an average value of one lightning fatality every month. Knowing that the exposed population of the Colombian army is circa 100.000 soldiers, the number of victims is circa 1,2 per 10.000. This figure is extremely high. Therefore, actions should be taken to save these lives.**

Keywords-component; Lightning, lightning injuries, lightning fatalities in the army, lightning accidents in Colombia.

I. INTRODUCTION

The Direction of Integrity Preservation and Security of the Colombian Army DIPSE (Spanish acronym of Dirección de Preservación de la Integridad y Seguridad del Ejército) has summarized the number of victims of lightning accidents in the last 11 years [1], [2]. Table I LIGHTNING ACCIDENTS IN THE COLOMBIAN ARMY and Fig. 1 show that in the last 11 years 129 soldiers died due to lightning accidents, while 373 were injured for a total number of 502 casualties. From these figures it can be concluded that lightning events produce, as a mean value, 1 fatality every month and 1 injured soldier every day. Additionally, almost 3 soldiers are injured when a soldier died. Referring these numbers to the exposed soldier's population, which is of circa 100.000, every year there are 1,2 wounded soldiers and 4,6 casualties per 10.000 soldiers. These figures are extremely high compared with the 20,7 death rate per million people from 1959-2013 in the USA [3].

II. Lightning threats

The Colombian soldiers are exposed to lightning mainly because they have to patrol rural areas and spend the night hidden among the trees. For this reason they are exposed to indirect lightning discharges which impact the trees and reach their bodies by indirect discharges coming out of the branches. For an example, during the first two week of March 2014, two soldiers were killed by lightning and one was injured. One of the victims got a discharge in his head while was sitting under a very tall tree. In other event, one soldier was impacted by a lightning discharge while was sleeping in his hammock. In December 2013, two more were killed while they were sleeping on the floor in their tents: an indirect lightning current produced a voltage difference between their heads and feet.

III. Conclusions

Lightning discharges are causing a large amount of victims in the Colombian army. To solve this problem the Colombian lightning community is taking actions to protect and save these lives.

TABLE I.LIGHTNING ACCIDENTS IN THE COLOMBIAN ARMY

Ratio I/F is the ratio between injured soldiers and fatalities

Year	Casualties			
	Fatalities	Injured	Total casualties	Ratio I/F
2003	11	36	47	3.3
2004	5	17	22	3.4
2005	12	34	46	2.8
2006	9	41	50	4.6
2007	12	31	43	2.6
2008	19	35	54	1.8
2009	15	39	54	2.6
2010	8	38	46	4.8
2011	16	52	68	3.3
2012	10	29	39	2.9
2013	12	21	33	1.8
Total	129	373	502	2.9
Average	11.7	33.9	45.6	2.9

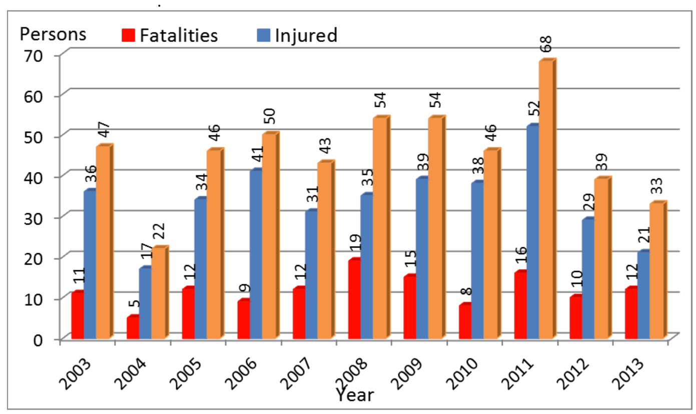

Figure 1. Statistics of lightning accidents in Colombia in the last 11 years. Fatalities is the first column, Injured the second and total the third column.

REFERENCES

[1] Cruz, Carlos; Rentería, Edwin and Román, Francisco. "Statistics of the Colombian National Army Lightning Accidents", International Symposium on Lightning Protection (XII SIPDA), Belo Horizonte, Brazil, October 7-11, 2013

[2] MG j. s. Casas, SP (r) c. m. Farias, CR. c. a. Leon, Boletín, Jefatura de Desarrollo Humano, Dirección de Preservación de la Integridad y Seguridad del Ejército in preparation, March 2014

[3] http://www.lightningsafety.noaa.gov/stats/59-13_State_Ltg_Fatalities.pdf

Coupling Effects According to PCB Orientations

Jin-Kyoung Du, Se-Young Hyun,
and Jong-Gwan Yook
Dept. of Electrical and Electronic Engineering
Yonsei University
Seoul, Republic of Korea
jgyook@yonsei.ac.kr

Jongwon Lee and Jin Soo Choi
Agency of Defense Development
Daejeon, Republic of Korea
jwlee@add.re.kr
jschoi@add.re.kr

***Abstract*— Electromagnetic pulse penetrates into electronic devices and makes influences to PCBs finally. The incident fields generate parallel-plate waveguide resonances of PCB itself and the resonances are coupled through via-hole inducing critic damages. In this paper, the coupling effects are measured according to PCB orientations. Both of vertically and horizontally polarized plane waves are found to generate high coupling effects to PCB at the resonance frequency regardless of the incident angle, except for a front propagation of the horizontally polarized plane wave, which hardly generate resonance modes. Based on this result, PCBs can be located properly inside enclosures considering field distributions nearby to decrease the coupling effects.**

Keywords-Electromagnetic pulse; printed circuit boards; couplings; orientations; polarizations; resonances

I. INTRODUCTION

Electromagnetic pulse (EMP) can make malfunctions or destructions of electric devices which usually have printed circuit boards (PCBs) inside. The penetrated fields may generate different coupling effects to a target PCB according to its orientations, therefore investigation of these coupling phenomena can be helpful to decrease the coupling effects and protect the target PCB against penetrated fields.

Coupling effects to perpendicular and parallel modules of daughter boards from a mother board were studied [1] but EMP is not propagated from adjacent circuit boards but from outside in the form of plane waves. The incident plane wave penetrates to dielectric materials of PCBs and generates parallel-plate waveguide (PPW) resonance modes between reference planes. PCBs generally include lots of via-holes and the resonances are coupled through the via-holes [2]. Influences from plane waves to PCBs with different dielectric materials were researched [3] but effects by PCB resonances were not considered. Hence, in this paper, the coupling effects from plane wave to a target PCB including a via-hole are analyzed by measurements according to PCB orientations.

II. MEASUREMENT RESULTS

A target PCB having a signal trace as well as a via-hole is fabricated (size = 36 mm × 24 mm × 3.04 mm, $\varepsilon_r = 3.5$), and measured using vector network analyzer (VNA) to assure a resonance mode generation. A transmission characteristic (S_{21}) of an ideal trace should be almost 0 dB but when noise couplings are occurred at some frequencies, it becomes below 0 dB at those frequencies. The dominant resonance mode of the fabricated PCB is TM_{10} at 2.4 GHz and it is clearly observed using VNA as shown in Fig. 1.

Coupling effects from plane wave according to PCB orientations are measured using VNA and a dual ridged horn at an anechoic chamber. Fig. 2 represents a configuration of the measurement system. VNA is connected between DRH and one port of the signal trace using RF cables, and a 50 Ohm terminated load is connected to another port of trace. Fig. 3(a) and Fig. 3(b) describe measured coupling effects from vertically and horizontally polarized plane waves, respectively. High level of coupling effects are measured around 2.4 GHz regardless of polarizations and the incident angle, except for a front propagation (theta = 90°) of the horizontally polarized plane wave because it hardly generates resonance modes between reference planes of the target PCB.

This work was supported by Agency for Defense Development, Daejeon, Republic of Korea.

III. SUMMARY AND CONCLUSION

The incident fields generate the PPW resonance modes which are coupled through via-holes of traces at PCBs. Vertically and horizontally plane waves are excited toward a target PCB to measure coupling effects according to its orientations and it found that high coupling effects are occurred by both of plane waves regardless of the incident angle, except for a front propagation of the horizontally polarized plane wave. PCBs are usually located in metal enclosure then its orientation can be adjusted properly to decrease coupling effects if field distributions inside enclosures are well analyzed.

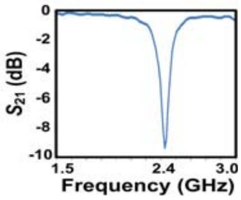

Figure 1.
Transmission characteristic of the signal trace.

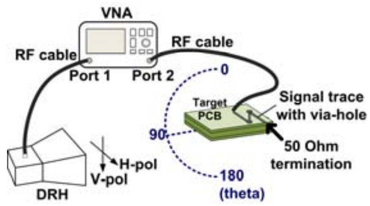

Figure 2.
Measurement configuration at the anechoic chamber.

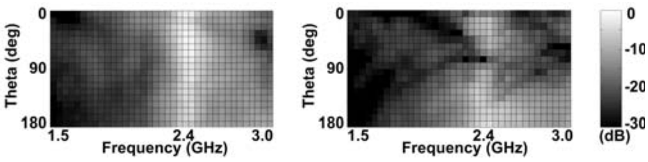

(a) (b)

Figure 3. PCB coupling effects from (a) vertically polarized plane wave and (b) horizontally polarized plane wave

.REFERENCES

[1] D. Hockanson and S. Radu, "An investigation of the effects of PCB module orientation on radiated EMI," in *Proc. IEEE Int. Electromagn. Compat. Symp.*, Aug. 1999, vol. 1, pp. 399–404.

[2] H.-D. Kang, H. Kim, S.-G. Kim, and J.-G. Yook, "A localized enhanced power plane topology for wideband suppression of simultaneous switching noise," *IEEE Trans. Electromagn. Compat.*, vol. 52, no. 2, pp. 373–380, May 2010.

[3] F. Brauer, C. Klunder, and J. L. Haseborg, "The influence of different PCB materials on the coupling behavior of high power electromagnetics," in *Proc. IEEE Int. Electromagn. Compat. Europe Symp.*, Jun. 2009, vol. 1, pp. 1–4.

Parametric Characterization of Electromagnetic Energy Production From Over-Voltaged Spark Gaps*

Artem Kuskov, Sydney Horne,
Ahmed Elshafiey, Salvador Portillo
Department of Electrical and Computer Engineering, University of New Mexico
Albuquerque, NM 87131-0001, USA
edls@unm.edu

Abstract— **Spark gap based high power microwave sources have been actively developed as possible high power microwave (HPM) sources for directed energy applications for over two decades. These sources rely on the fast rising time varying current and as such are dependent on the geometry and the overall LCR characteristics of the source and input pulse. Due to the geometric considerations of an over-voltaged spark gaps the resultant spectral output is generally in the broadband regime [1]. This paper presents our preliminary work on developing a test bed for spark gap based HPM sources, initial field measurements characterising this test bed and preliminary particle in cell and time and frequency domain models that attempt to capture the physics of these spark gaps with respect to electromagnetic energy production.**

Keywords-high power microwaves, spark gap sources, pulsed power

I. Introduction

The high power microwave, plasma and beam physics group at the University of New Mexico, Electrical and Computer Engineering Department is actively pursuing a physics based approach to understanding the generation of electromagnetic energy for directed energy applications. As part of these efforts a modular spark gap test bed is being developed to facilitate the measurement of plasma streamers and their characteristics and the concomitant production of electromagnetic energy.

II. Test Bed and Field Measurements

Our Spark gap based test bed is a modular system comprised of a variable separation between electrodes and the capability to vary the electrode shape. The main housing is made up a dielectric with a low attenuation coefficient in the 300-900 nm range. It is designed to hold relatively high pressures using N_2 as the inter-electrode dielectric. The optical transmission of the housing is needed as future work will include time resolved spectral and density measurements of the breakdown which in turn will be tied to the net electromagnetic radiation production.

The pulsed power driver, which is capable of delivering up to 50 kV in single stage mode will described along with its spice model. The pulsed driver is also of modular design, incorporating a pulse forming network (PFN) as part of the main circuit. This PFN is of type E design with parallel LC discrete components.

Preliminary data for the angular distribution of electromagnetic energy production, in absolute units will be presented. The Electric fields will be measured directly using a D-dot and Balun combination from Prodyn Corp. Additional UNM built D-dots, and calibrated to the Prodyn sensor, will be fielded to measure the angular fields. The fields spectral content dependence on the LCR circuit, voltage and resultant dI/dT of the test bed, which also includes the spark gap shape will be shown.

III. Numerical Modeling

Preliminary particle in cell numerical model is presently being designed. A parametric scan of various electrode geometries and AK gaps will be conducted and its results fed back into the experimental parts of this work. Future work will include not just the geometric and pulsed power dependence of the generated RF but additional work will focus on the atomic physics of the spark channels to gain further understanding of the spark gap process and how this affects the electromagnetic energy production.

Due to the varying needs of directed energy applications a narrowband or mesoband bandwidth may be needed. This has been the motivation to conduct time domain and frequency domain numerical modeling of geometric structures to produce this narrowband content.

References

[1] F. Sabbath, D.V. Giri, *Ultra-Wideband, Short Pulse Electromagnetics* Vols 1-10 (Springer).

* Work supported by AFOSR Grant FA9550-11-1-0200

Electromagnetic Modeling of Hot-Wire Detonators

Michael Lambrecht
Air Force Research Laboratory, Directed Energy Directorate, Kirtland AFB, NM, USA

Edl Schamiloglu
Department of Electrical and Computer Engineering, University of New Mexico, Albuquerque, NM, USA

A modeling technique has been developed to determine the electromagnetic (EM) characteristics of hot-wire detonators in order to quantify possible effects of impinging EM radiation. The analysis includes both analytical and numerical models. The analytical model uses transmission line theory to represent the detonator as a cascaded transmission line incorporating several different sections and calculates both differential and common mode impedances as well as resonant frequencies. The numerical model uses ICEPIC (Improved Concurrent Electromagnetic Particle In Cell), a finite-difference-time-domain EM solver, to determine these same parameters for comparison. The models are synergistic as the analytical model has been modified using additional circuit elements whose values were found using ICEPIC. This combination produces an improved analytical model that can be run nearly instantaneously on a PC for a wide range of hot-wire detonators to determine possible variations in radio frequency response. Experimental measurements on live detonators have been used to validate the models.

Keywords-EED, IED, Blasting Cap, FDTD, PIC

High-Altitude Electromagnetic Pulse – The Threat to the Electric Power Grid Updated

William A. Radasky

Metatech Corporation
Goleta, California USA
wradasky@aol.com

***Abstract*— A nuclear burst detonated in space over any of the continents in the world would create a high-altitude electromagnetic pulse (HEMP) that could cause the functional collapse of the exposed electrical power grids. As a result, major infrastructures that depend on the power grid such as communications, transportation, financial services, emergency services, energy distribution, food and water could also be disrupted or extremely impaired.**

Keywords-HEMP, Power Grid, Standards, Critical Infrastructures

I. INTRODUCTION

The United States Congress formed a Commission in 2002 to examine the impact of nuclear weapon generated electromagnetic pulse (EMP) on the United States. The work performed by the EMP Commission from 2002-2008 was groundbreaking in terms of studying the impact of HEMP on the critical civil infrastructures of the United States and is applicable to critical infrastructures in modern societies.

This paper updates the public information available concerning HEMP and its likely effects on the electronics operating the power grid since 2008 including work performed for the Federal Energy Regulatory Commission (FERC) and the Special Issue on HEMP in the IEEE EMC Transactions. Discussion and references will be provided in the presentation.

II. THE HEMP TIME WAVEFORM

The high-altitude electromagnetic pulse (HEMP) is defined as a series of electromagnetic waveforms that are generated from a nuclear detonation at altitudes above 30 km and propagate to the Earth's surface.

It is important to understand that HEMP is not described as a single pulse, but rather as a series of waveforms covering times from nanoseconds to hundreds of seconds. After years of research it has been determined that three main waveforms are generated due to different nuclear and atmospheric mechanisms, as defined by the IEC and are shown in Figure 1.

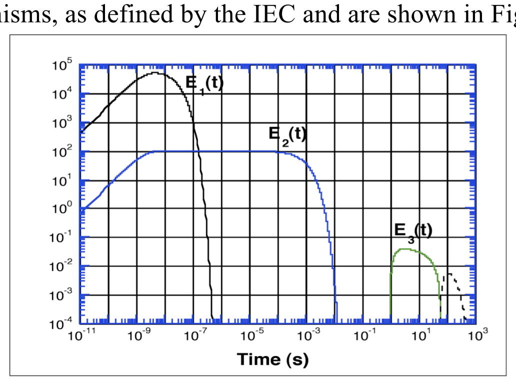

Figure 1. Three portions of the HEMP electric field waveform in volts/meter from IEC 61000-2-9.

The early-time waveform is referred to in Fig. 1 as E1, the intermediate-time waveform is referred to as E2 and the late-time waveform is known as E3.

III. THE EMP COMMISSION AND THE POWER GRID

While the EMP Commission examined the impacts of HEMP on all portions of the critical infrastructures, they determined that the power system was the most critical due to its direct support of the other major infrastructures such as communications, transportation, financial services, emergency services, energy distribution, water/food, etc. Their conclusions regarding the power system were:

1) HEMP-induced functional collapse of the electrical power grid risks the continued existence of U.S. civil society.

2) Early-time HEMP (E1) transients are likely to exceed the capabilities of protective safety relays.

3) Late-time HEMP (E3) could induce currents that create significant damage throughout the grid.

4) The national electrical grid is not designed to withstand near simultaneous functional collapse.

5) Procedures do not exist to perform a "black start" after an EMP attack, as restart would depend on telecom and energy transport, which depend on power.

6) Restoration of the national power grid could take months to years.

7) HEMP-induced destruction of power grid components could substantially delay recovery.

The EMP Commission's overall power system conclusion was: "Widespread functional collapse of the electric power system in the area affected by EMP is likely."

While the Commission felt that there were approaches available to deal with many of the problems raised above, it was not clear who should lead the effort to mitigate the threat of HEMP on the power grid.

One option in the opinion of this author is to develop protective methods, operational responses, and restoration approaches for the power system. The best approach to deliver this information to manufacturers and operators would be to develop openly available standards that deal with the problem. Fortunately much of this work has been underway in the IEC for more than 20 years. Details of the existing standards will be discussed in the presentation. In addition a substantial list of references will be provided for those interested in pursuing this subject in more detail.

Effect of Magnetic Field Distribution on MDO Operation

Jeremy McConaha, Chris Leach, Sarita Prasad, and Edl Schamiloglu

Department of Electrical and Computer Engineering

The University of New Mexico, MSC01 1100, 1 University of New Mexico, Albuquerque, NM 87131 USA

***Abstract*— A high efficiency relativistic magnetron with diffraction output (MDO) was designed at the University of New Mexico (UNM) and its experimental verification is underway. In this paper we explore the effect of magnetic field variation along the interaction space on MDO [1] operation. Two magnetic field distribution scenarios were studied in MAGIC [2]: 1) nearly 100% uniformity and 2) 90% uniformity. These results will be presented. Furthermore, the recently-constructed pulsed discharge circuit used for energizing the electromagnets will also be described.**

Keywords-relativistic magnetron; MDO

I. Introduction

It was necessary to adapt a previously-existing Helmholtz coil pair to provide the magnetic field necessary for the MDO operation [1]. However due to the physical size of the existing coils and the constraints it presented, the spacing between the coils needed to be reduced. As such, it was necessary to explore the effects of magnetic field non-uniformity on the operation of the MDO. This was accomplished by performing MAGIC [2] simulations with a variety of magnetic field configurations, some with as much as 10% variation in the field distribution, in the hopes of maintaining the high performance of the device. MAGIC is a 3-dimensional fully relativistic, fully electromagnetic particle-in-cell code. An electromagnetic discharge circuit was built to generate this field.

II. Simulation Setup

The simulations in MAGIC were performed by modifying the magnetic field profile, both by adjusting the spacing between the coils to either 13.2 cm or 8.34 cm, and by varying the peak magnitude of the magnetic field between 0.37 T to 0.47 T in 0.02 T increments. These variations were used to cause a non-uniformity of roughly 10% along the interaction space of the device. The results of these simulations can be seen in Fig.1. Output microwave power, total current, and total efficiency were measured. The operating mode of interest is the $4\pi/3$ mode, although some results might fall outside of this for completion.

This work was supported by a grant from ONR Code 30, SAAET.

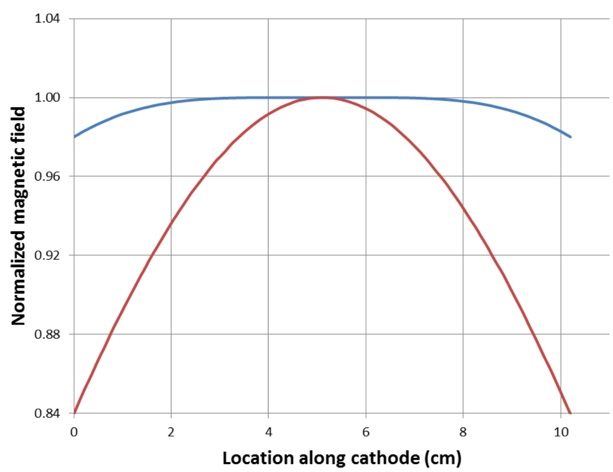

Figure 1. Normalized magnetic field distribution for a Helmholtz coil pair (blue) and a modified Helmholtz coil pair configuration (red) along the interaction space of the cathode.

III. Electromagnet Circuit

The electromagnetic discharge circuit was designed to provide a maximum 0.69 T magnetic field. This circuit consists of a 1.6 mF capacitor bank with maximum charging voltage of 3 KV. The capacitors are discharged into the coils by means of an optically-triggered thyristor switch.

IV. Conclusion

For the narrow range of magnetic fields studied, the results of the simulations with a magnetic field variation of up to 10% shows that there are only minor effects on the operation of the MDO. Thus we can conclude that the MDO is a robust system, with good tolerance to variations in the insulating magnetic field. However further research into the effects of larger variations in the insulating magnetic field will be presented.

References

[1] M.I. Fuks and E. Schamiloglu, "70% efficient relativistic magnetron with axial extraction of radiation though the horn antenna," *IEEE Trans Plasma Sci.,* vol. 34, 1302-1312 (2010).

[2] B. Goplen, L. Ludeking, D. Smithe, and G. Warren, "User-configurable MAGIC for electromagnetic PIC calculations," *Comp. Phys. Commun.,* vol. 87, pp. 54-86 (1995).

Prospects of Split Ring Resonators for the Generation of High Power Microwaves

Sarita Prasad, Alan Lynn, Kost′ Ilyenko, Mikhail Fuks and Edl Schamiloglu

University of New Mexico

Department of Electrical and Computer Engineering
Albuquerque, NM 87131, USA
sarita@ece.unm.edu

Abstract— **In this work we explore several configurations of split ring resonator (SRR) interaction structures for the generation of high power microwave (HPM) radiation. The 3-dimensional code MAGIC was used to initiate the design and optimization process of this novel device. An electron beam was propagated along the axis of the SRR periodical arrangement. The response of the structure was evaluated by measuring the output power and frequency. The preliminary results are presented.**

Keywords-split ring resonator; HPM; Metamaterials

I. INTRODUCTION

Recently, there has been interest in exploring metamaterials for HPM generation. Split ring resonators are commonly used as periodic arrays to serve as building blocks for bulk metamaterial structures that exhibit non-conventional properties like negative permeability and negative permittivity.

We used the 3-dimensional fully relativistic, fully electromagnetic particle-in-cell code MAGIC [1] for studying the effect of the SRR's when an annular electron beam concentric to it is allowed to propagate through. The SRR configuration used for this study is similar to the Broadside-Coupled SRR geometry. The rings are arranged in a longitudinal manner and the cuts in the consecutive rings are 180^{o} out of phase.

Two geometrical variations were studied. The main difference between the two approaches lies in the way the SRR's were suspended in the cylindrical waveguide. From the results obtained thus far one design shows less mode competition and the excitation of a low order TE_{21} mode but outputs very low power which is attributed to the mode being evanescent in the waveguide. While the other design exhibits higher output power, higher mode competition and a higher order radiated mode. It was also seen in simulations that the former design was very prone to instabilities when the beam current exceeded 2 kA.

II. SIMULATION SETUP

Two SRR configurations are explored for HPM generation. Figure 1 (a) and (b) show the SRR design variations.

This research was supported by AFOSR MURI Grant FA9550-12-1-0489 and US Army Aviation & Missile Res., Dev., & Eng. Center RDMR-WSS grant Phase I A11A- 001-0471.

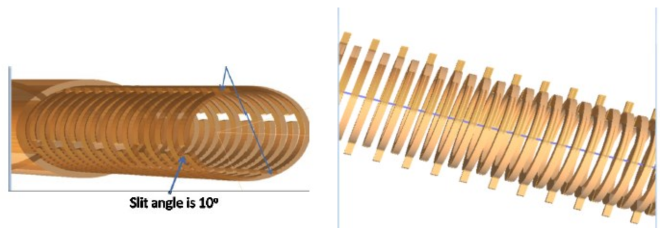

Figure 1. Schematic of the SRR design 1 (left) and design 2 (right).

In the first design the SRR's are electrically connected by means of a rod that is then connected to a cylindrical waveguide. In the second design the SRR's are connected directly to the cylindrical waveguide by means of alternating conducting tabs. For both cases the radius of the cylindrical waveguide was set to 2.5 cm.

Figure 2 shows the mode pattern measured at the waveguide output port for the two designs and their corresponding fast Fourier transforms (FFT).

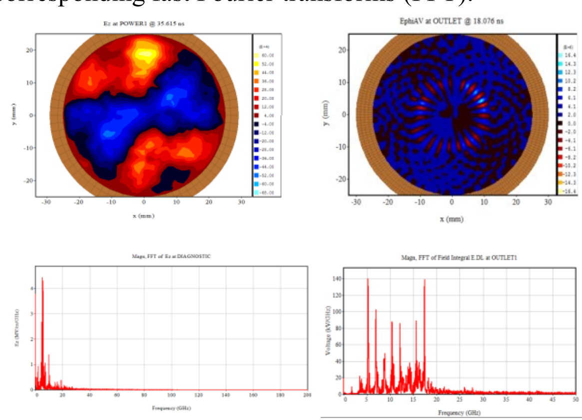

Figure 2. Mode pattern and it's corresponding FFT detected at the output port for design 1 (left) and design 2 (right).

III. CONCLUSION

We present the preliminary results on the prospects of using SRR's for HPM generation. Understanding and analysis of these results will lead towards the design of a more robust system.

REFERENCES

[1] MAGIC ATK Mission Research, Newington, VA [Online]. Available: http://www.mrcwdc.com/Magic/.

Swept CW Testing of Large Systems

William D. Prather
Air Force Research Laboratory
Directed Energy Directorate
Kirtland AFB NM, USA
william.d.prather@ieee.org

Jory Cafferky
TEAM Technologies, Inc.
EME Programs
Albuquerque NM
jcafferky@team-technologies.com

Jay Anderson
Oklahoma City ALC
Tinker AFB OK, USA

Michael Rooney
Defense Threat Reduction Agency
Ft. Belvoir, VA

***Abstract*—Methods of using swept CW illumination to measure the penetration of electromagnetic waves into a large system have been greatly improved in recent years. The testing is low level, harmless to the system, and less costly than full threat-level EMP testing. Comparisons with measurements in full-scale EMP simulators is quite good with the CW measurements often revealing more detailed information than can be had from a pulsed EMP simulator and transient digitizers. This paper addresses the use of low-level swept CW testing as an engineering tool for measuring shielding design and also for hardness surveillance afterwards.**

Keywords-EMP, CW, swept CW, system test

I. Introduction

With a correctly designed wideband antenna, low-level swept CW illumination can be used effectively to measure the integrity of the shielding protection on large systems such as aircraft. The CW measurement system can measure the magnitude and phase of cable currents on the aircraft normalized to the incident field so that the results can be extrapolated to an EMP threat or any other waveform within the bandwidth of the measurement.

II. CW Measurements

The sensitivity of the CW system allows one to diagnose problems and understand the performance of a shielded system or a test site more clearly than is possible using a threat-level pulse system and transient digitizers.

This work was sponsored by the Air Force Research Laboratory, Defense Threat Reduction Agency, Oklahoma City Air Logistics Center, Naval Air Test Center at Patuxent River, and the Navy Surface Warfare Center at Dahlgren.

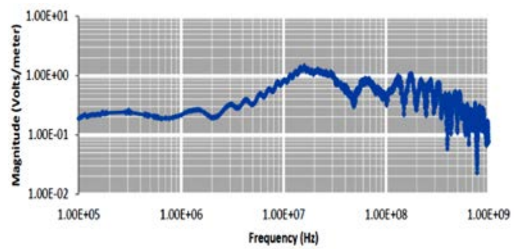

Fig. 1. Measured electric field.

III. CW-to-Pulse Comparison

If the field pattern in the CW and pulse illuminations is uniform, and the CW radiated spectrum is flat, the final CW and pulse measurements on the aircraft will compare very well.

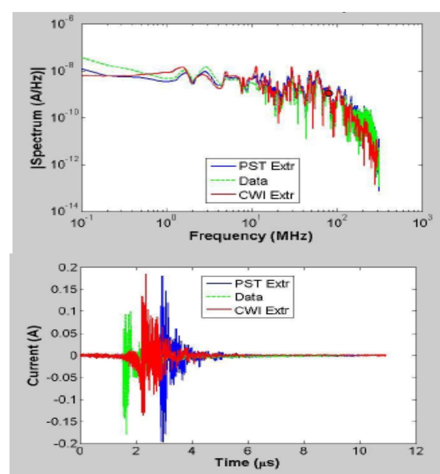

Fig. 2. CW-to-pulse comparison. Red = extrapolated CW. Blue = extrapolated pulse. Ignore the green (raw data).

References

[1] W.D. Prather, et al, "Elliptic CW Illumination System," AFRL-PS-TR-2013-0009, Air Force Research Laboratory, Jan 13 and published as Sensor & Simulation Note 559, University of New Mexico.

A Simulation Tool for the Stochastic Electromagnetic Field Coupling to a Uniform Transmission Line

Mathias Magdowski
Chair of Electromagnetic Compatibility, Institute for Medical Engineering
Otto-von-Guericke-University
Magdeburg, Saxony-Anhalt, Germany
Email: mathias.magdowski@ovgu.de

***Abstract*—A statistical tool will be presented that allows to calculate the differential-mode current coupled to a transmission line using a stochastic plane wave excitation in the frequency domain. The field model is based on a Monte Carlo approach that approximates the well-known plane wave integral representation for fields inside reverberation chambers. A fixed stirrer position or a fixed electromagnetic boundary condition is formed by a certain number of plane waves with random wave vectors, polarizations and phases. A given number of boundary conditions can be simulated and the mean value, the standard deviation, the probability density function, the cumulative distribution function, or the correlation of the current along the line can be analyzed. The dimensions of the straight and uniform double wire transmission line as the length, the line separation and the wire radius can be arbitrarily adjusted. Variable resistances can be set to terminate both line end. The average electric field strength inside the reverberation chamber can be defined in terms of the quality factor, the input power and the chamber volume. Many numerical results can be compared to analytical expressions from the literature. The tool was developed in MATLAB and features a multilingual graphical user interface.**

***Keywords*—electromagnetic coupling; statistical fields; reverberation chambers; statistical distributions; transmission lines; correlation; differential-mode current**

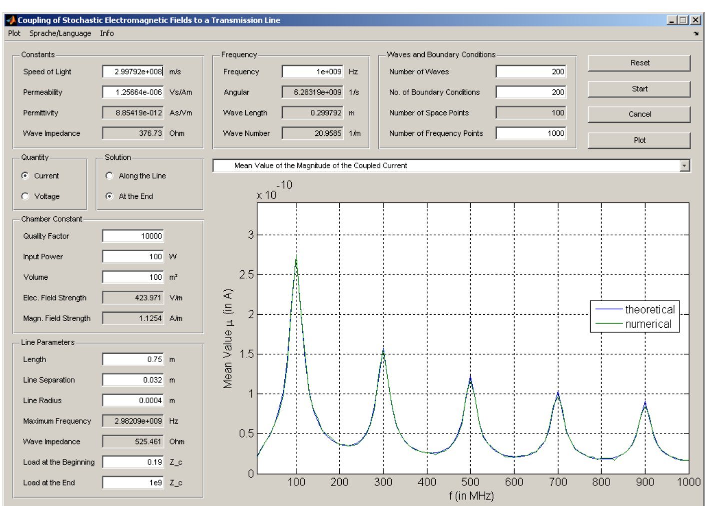

Figure 1. Screenshot of the graphical user interface.

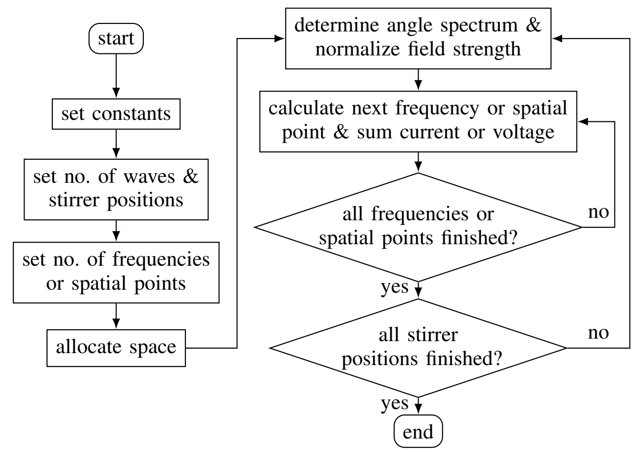

Figure 2. Schematic of the program flow chart of the field generator.

References

[1] D. A. Hill, “Plane wave integral representation for fields in reverberation chambers,” *IEEE Trans. Electromagn. Compat.*, vol. 40, no. 3, pp. 209 – 217, Aug. 1998.

[2] M. Magdowski, S. V. Tkachenko, J. Nitsch, and R. Vick, “Simulation of the stochastic electromagnetic field coupling to a transmission line using a Monte-Carlo method,” in *ESA Workshop on Aerospace EMC*, Florence, Italy, Mar. 2009, pp. 1 – 6.

[3] M. Magdowski, *Entwicklung und Validierung eines Werkzeugs zur Berechnung der elektromagnetischen Einkopplung von stochastischen Feldern in Leitungsstrukturen*, 1st ed., ser. Res Electricae Magdeburgenses, Magdeburger Forum zur Elektrotechnik. Magdeburg: Nitsch, Jürgen and Styczynski, Zbigniew Antoni, 2008, no. 29.

[4] M. Magdowski, S. V. Tkachenko, and R. Vick, “Coupling of stochastic electromagnetic fields to a transmission line in a reverberation chamber,” *IEEE Trans. Electromagn. Compat.*, vol. 53, no. 2, pp. 308 – 317, May 2011.

[5] M. Magdowski and R. Vick, “Closed-form formulas for the stochastic electromagnetic field coupling to a transmission line with arbitrary loads,” *IEEE Trans. Electromagn. Compat.*, vol. 54, no. 5, pp. 1147 – 1152, Oct. 2012.

[6] H. Zhang, X. Zhao, L. Yan, C. Liu, and K. Huang, “Some amendments to ’Field-to-Wire Coupling in an Electrically Large Cavity: A Semianalytic Solution’,” *IEEE Trans. Electromagn. Compat.*, vol. 54, no. 1, pp. 232 –234, Feb. 2012.

[7] P. De Doncker and R. Meys, “Electromagnetic coupling to transmission lines under complex illumination,” *Electronics Letters*, vol. 40, no. 1, pp. 11–13, 2004. [Online]. Available: http://link.aip.org/link/?ELL/40/11/1

Experimental Studies of a Relativistic Backward Wave Oscillator with Gaussian Radiation

Ahmed M. Elfrgani, Sarita Prasad, Mikhail I. Fuks, and Edl Schamiloglu
Department of Electrical and Computer Engineering, MSC01 1100
University of New Mexico,
Albuquerque, NM, USA
elfrgan@unm.edu

***Abstract*— A high power Gaussian radiation is always attractive for many applications such as short pulse radar, plasma diagnostics, and sounding systems. An X-band relativistic backward wave oscillator (RBWO) is proposed with a two-spiral corrugated Bragg reflector to provide such a radiation. BWOs are typically known to radiate in the TM_{01} mode, where a cavity or cut-off section reflector is used. A Bragg reflector has been designed and optimized using the fully electromagnetic, relativistic particle-in-cell (PIC) code MAGIC. Such a reflector converts the operating TM_{01}-mode of the BWO to the forward TE_{11}-mode with a Gaussian microwave beam at the output. The RBWO was driven by a voltage pulse that has a half sine wave-like shape, 460 kV amplitude, and FWHM duration of 12 ns (SINUS-6 Accelerator). With these parameters a microwave power of 330 MW at a frequency of 9.9 GHz in a clean TE_{11} mode pattern was detected at the output of the simulations.**

Keywords- backward wave oscillator; Bragg reflector; linearly polarize

I. Introduction

A backward wave oscillator (BWO) is an O-type Cerenkov device that is designed to effectively convert electron beam energy into electromagnetic radiation. This electromagnetic energy is generated with negative group velocity, where the wave is traveling in a direction opposite to that the electron beam, with a power varied from several 100 MW to several GW. The output mode pattern of the BWO is the TM_{01} mode where the field distribution is a doughnut shape (i.e., with a hole at the axis of the mode pattern). In order to make the RBWO more applicable in scientific research and for some practical applications, a two-spiral corrugated Bragg reflector has been used downstream of the cathode as shown in Fig. 1. The Bragg reflector allows the device to radiate a TE_{11} mode (a narrow Gaussian-like mode) at the axial output.

II. RBWO with BRAGG REFLECTOR

The oscillator consists of two slow wave structures (SWS) with sinusoidal corrugations. BWO-SWS is an axisymmetric sinusoidal corrugation while Bragg-SWS is a combination of left- and right-single-fold spiral corrugations. The SWSs can be described by

$$R(\theta,z)=R_0+ l_0*\sin(h*z + m*\theta), \quad (1)$$

where z and θ are the axial and azimuthal coordinates, respectively. R_0 is the average radius; l_0 is the amplitude of the corrugation; $h=2\pi/d$ and d is the axial periodicity of the corrugations; and m is the number of folds. The dimensions of the SWSs are summarized in Table I.

TABLE I. THE PERIODIC STRUCTURES DIMENSIONS

Quantity	The SWS Dimensions in cm	
	BWO-SWS	*BRAGG-SWS*
R_0	1.74	2.03
l_0	0.19	0.25
d	1.3	1.74
m	0	±1
Lenght	9*d	8*d

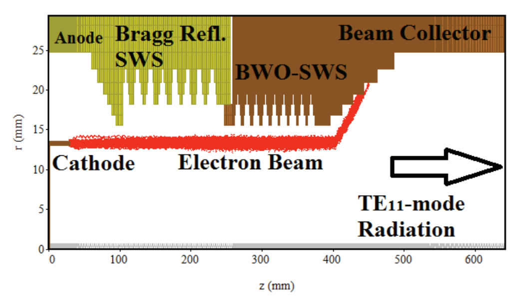

Figure 1. Design of the BWO with Bragg reflector.

This research supported by AFOSR Grant FA9550-11-1-0200.

References

[1] A. Elfrgani, S. Prasad, M. Fuks, and E. Schamiloglu, “Relativistic BWO with Linear Polarized Gaussian Radiation Pattern,” IEEE Trans. Plasma Sci. (under review, 2014).

[2] E. B. Abubakirov, J.-P. Brasile, A.N. Denisenko, M.I. Fuks, N.F. Kovalev, A.V. Saveljev, M. Simon, E.I. Soluyanov and V.V. Yastrebov, “Oversized Relativistic BWO with Selective Bragg Mode Converter,” Digest of Technical Papers of the International Workshop on HPM Generation and Pulse Shortening. Edinburgh, UK: 1997, pp. 179-183.

Electromagnetic Simulation on Emerging Hardware Architecture

Peter Stoltz, Eric Hallman, Kristian Beckwith
Tech-X Corp.
Boulder, CO 80212, USA
pstoltz@txcorp.com

Dmitry Gorelov, Chase Boulware
Niowave Inc.
1012 N Walnut St, Lansing Charter Township, MI 48906

***Abstract*— We will present results for porting electromagnetic simulation tools to emerging hardware accelerators, such as the graphics processing unit (GPU) or many integrated core (MIC) architecture. We will show application of these hardware accelerators to simulations of rf cavity structures. We will also discuss how we are working to integrate these accelerators into the industrial design process to create desktop supercomputing for engineers.**

Keywords-graphics processing unit, many integrated core, supercomputing

I. Introduction

Electromagnetic systems, such as those for high power microwave generation or high current electron beam generation, rely on modeling as one of the most effective ways to reduce design costs. Frequently the level of detail required to adequately model these devices necessitates using high performance computing power. However, many high performance modeling tools are too difficult for design engineers to use on a daily basis. The goal, therefore, of a new project underway between Niowave, Inc. researchers and Tech-X Corp. researchers is to improve the usability of high-performance computing software to make the software more effective in the electromagnetic component design process.

II. Motivation

Electromagnetic systems benefit from detailed numerical modeling. For instance, one might hope to understand in detail how a system might oscillate at unwanted frequencies, such as higher-order modes (HOMs). In a case of particular interest to the ship-board free electron laser community, researchers have designed a 700 MHz cavity as a high-current electron source, but researchers are concerned that the beam may drive the cavity at its many higher modes.

The implications of these induced fields at unwanted frequencies have been extensively studied in the context of superconducting accelerators because they add to the cryogenic load and can cause beam instabilities. Up until now, this analysis has almost always been performed for constant-velocity particles. To properly design a high-brightness, high-current superconducting electron source requires a self-consistent approach that calculates the driving of HOMs by an electron beam which is accelerated from rest to the speed of light over a distance on the order of a few cm.

This process requires the use of high-performance computing resources to be efficient. The resolution of the cavity structure often requires full use of available computing hardware, either through parallel computing or hardware acceleration such running on a GPU. Parameter scans requiring many separate simulations may be needed which will require sufficient computing resources and simulation software specifically designed to allow parameter scans.

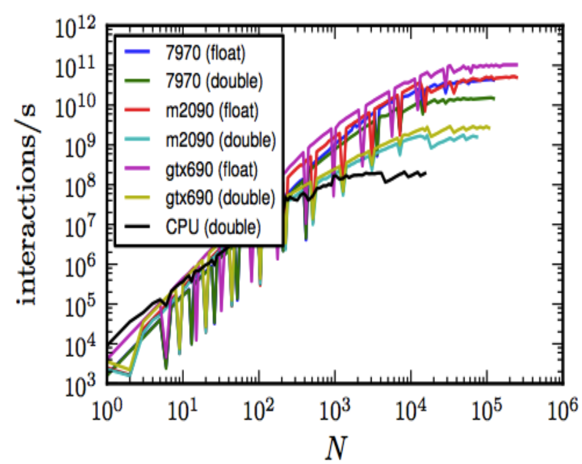

Figure 1 . Speedup versus number of compute cores for particle space charge calculations in free space (no metallic boundaries). We performed these space charge calculations on various multi-core CPU (black line) and GPU (colored lines) architectures. The GPUs in this work are the AMD 7970, the NVidia Tesla m2090, and the NVidia gtx690, all in both floating point and double precision. Determining what hardware performs best for more detailed electromagnetic applications is a main thrust of this new research effort between Tech-X Corp. and Niowave, Inc.

III. Results

As a first result, we show in Fig. 1 some preliminary work for speedup versus number of compute cores for particle space charge calculations in free space (no metallic boundaries). We performed these space charge calculations on various multi-core CPU (black line) and GPU (colored lines) architectures. The GPUs in this work are the AMD 7970, the NVidia "Tesla" m2090, and the NVidia gtx690, all in both floating point and double precision. Determining what hardware performs best for more detailed electromagnetic applications is a main thrust of this new research effort between Tech-X Corp. and Niowave, Inc.

Sectional Cylindrical Waveguide with longitudinally distributed slots

Ali Harmouch, Hassan Haddad,
Mustapha Ziade
Doctoral School,
Lebanese University,
Tripoli, North, Lebanon
E-mail: harmush_ah@hotmail.com

***Abstract* — Base station Cellular Systems require omni-directional efficient antennas to provide an acceptable service within the cell site. Conventional antennas used for this purpose are mainly micro-strip patch antennas in the form of a circular array. However, these antenna elements suffer from low efficiency due to the additional losses involved in the feeder line as well as in the material from which the patch antenna is formed. These major drawbacks can be eliminated by introducing a sectional slotted waveguide array that consists of N longitudinally distributed slots at specific positions, and with specific dimensions in order for the antenna to provide high directional efficiency, compactness, high wind resistance and surely high power handling capability.**

A series of simulation results have been done on the proposed antenna at the desired 2.4GHz frequency and show a significant gain of about 15dBi over the desired frequency band of interest.

keywords - Sectorized, Sectional, slotted waveguide, radiation efficiency, array, gain, bandwidth, wind resistance.

I. Introduction

Antennas, today, are used in many systems especially in wireless internet communications and Radar applications where high power handling capability, high gain, proper polarization along with reliable mechanical characteristics are needed. However, these parameters are very hard to simultaneously optimize, there is always a trade-off in between. In this paper, a Sectional Cylindrical Slotted Waveguide Antenna (CSWA) is presented. The purpose of this paper is to provide an optimized version of cylindrical slotted waveguide antennas by simply selecting the optimum position, number, shape and size of the slots within the waveguide's sectional wall. Such configurations are suitable to be used in Wireless internet distributing systems and radar applications. Simulation results along with Experimental validations will be conducted at the 2.4 GHz frequency demonstrating high effectiveness in terms of directional efficiency given a reduced cost, simplicity of fabrication with optimized size and shape [1,2].

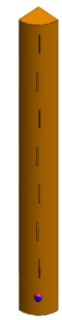

Figure 1. Simulated Design of a 7-slots Sectional Cylindrical Waveguide

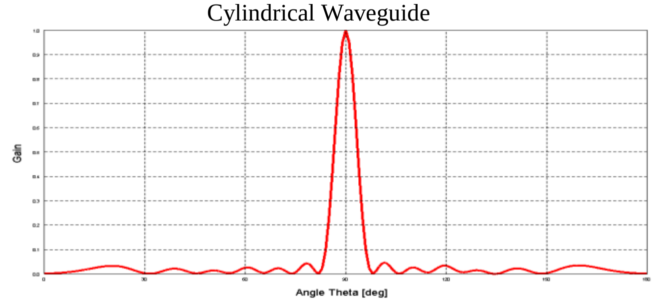

Figure 2. Normalized Linear Rectangular Plot of the Radiation Pattern of 7-slots Sectional Cylindrical Waveguide.

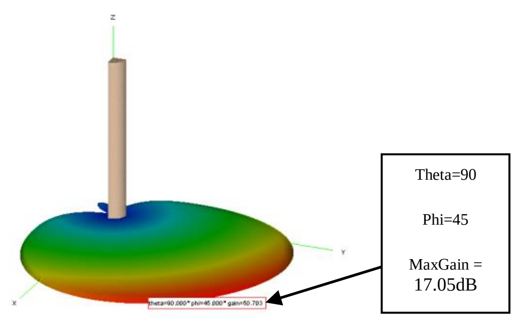

Figure 3. Simulated 3D Radiation Pattern of a 7-slots Sectional Cylindrical waveguide.

References

[1] A. Elsherbeni, D. Kajfez, and S. Zeng, "Circular sectoral waveguides," *IEEE Antennas and Propagation Magazine*, vol. 33, no. 6, pp. 20–27, Dec. 1991.

[2] N. Pasri, C. Phongcharoenpanich, and M. Krairiksh, "Design of a circumferential slot antenna on a sectoral cylindrical cavity excited by a probe," in *IEEE Antennas and Propagation Society International Symposium, 2004*, vol. 3, pp. 2337–2340 Vol.3.

ID 152

Modeling and Experiments of High Power Radio-Frequency Effects on Printed Circuit Boards and their Embedded Chip Elements

Manuel J. Rivera[1], Ryan Schlegel[1], Xu Gao[2], Chunchun Sui[2], Karan Sharma[2], Daryl Beetner[2], Joe Yakura[3], Lisa Andhivahis[4], Sameer Hemmady[1]
[1] TechFlow Scientific, 2155 Louisiana Blvd NE, Suite 4200, Albuquerque NM 87110
[2] Dept. of Electrical and Computer Eng., Missouri University of Science and Technology, 141 Emerson Electric Co. Hall, 301 W. 16th St. Rolla, MO 65409
[3]Air Force Research Laboratory/RDHE, 3550 Aberdeen Blvd SE, Kirtland AFB, NM 87117
[4] Defense Threat Reduction Agency, J9-NTE, 8725 John J Kingman Rd #6201, Fort Belvoir, VA 22060

Abstract— **The ability of high power microwaves (HPM) to upset electronic systems through intentional electromagnetic interference (IEMI) is well recognized. We describe our ongoing technical efforts under the Air Force Research Laboratory's (AFRL's) 3 year-long High Power Microwave Technological Electromagnetic Susceptibility with Laboratory Applications (HPMTESLA) Call 0005 program to advance the state-of-the-art in theoretical, modeling and simulation (M&S), and experimental efforts to understand and eventually predict the effects of high power Radio-Frequency (RF) and electromagnetic pulse (EMP) energy on digital electronic devices comprising printed circuit boards (PCBs) and their embedded chipsets. Through MOSIS, we have designed and fabricated several test structures and embedded digital circuits which are ubiquitous in larger digital electronic systems (such as delay line loops, ring oscillators, memory modules) utilizing modern day semiconductor process technologies of varying scales. In this presentation, we will focus on the direct injection of HPM and EMP-like waveforms into various nodes of a ring oscillator/inverter chain and discuss the observed upset phenomenology. Finally, we will describe our on-going work on building a predictive physics-based analytical model to describe the observed upset phenomenology. Such analytical models can be incorporated into circuit design simulators to gain a predictive capability towards upset of larger digital electronic systems exposed to HPM/EMP stress.**

Keywords-High Power Microwaves; EMI; EMC; Directed Energy; Electromagnetic Pulses; Integrated Circuits;

I. Introduction

It has been widely noted in the RF effects community that susceptibility to IEMI-induced upset of computer electronics can be considered at a wide spectrum of integration levels. At one end of the spectrum, the Air Force Office of Scientific Research (AFOSR) sponsored Multi-University Research Initiative (MURI)-2001 program **[1]** focused on a number of areas, including most prominently, the formulation of some physics based, analytic sub-models to explain experimentally-observed, upset phenomenology of elemental semiconductor devices (gates and transistors) due to direct IEMI injection. At the other end of the spectrum, TechFlow Scientific has just completed execution of the Air Force Research Laboratories (AFRL)-sponsored HPMTESLA Call 0006 SOO3 **[2]** study to create and develop a functional diagnostic toolkit to determine the state of a personal computer (PC) (comprising billions of elemental devices) after a free-field HPM induced upset. The research program being executed by the TechFlow Scientific team under the HPMTESLA Call 0005 solicitation is bridging a critical intellectual chasm in the HPM effects community between the physics-based explanations, commonly used for describing RF-upset in direct-IEMI-injection testing of elemental electronic components, and the more functional based explanations describing the erroneous operational behavior of PCs and higher-level systems to free field HPM exposure. By designing and fabricating test circuits, accurate physics-based analytic models can be derived to describe the observed upset phenomenology due to IEMI. These models can be subsequently scaled to higher levels of electronic circuit complexity to understand and eventually predict the observed upset phenomenology of more complex electronic systems comprising cascaded sections of these fundamental circuits.

II. Test Setup

The Test IC is designed and fabricated using the 0.5 micron ON Semiconductor process. Four circuits ubiquitous in digital electronics were implemented in this test IC. They include an inverter chain, a delay lock loop (DLL), a Static Random Access Memory (SRAM) unit, and a crystal oscillator (Figure 3). IEMI directly injected on to power or I/O lines can cause errors in each of these circuits that may disrupt the sub-circuit operation and functionality. As part of this study, we have parsed the upset phenomenology into analog domain upsets and digital domain upsets, for which we are developing analytic physics-based upset models.

III. Results

Figure 1 shows some representative results on the variation of the natural oscillation frequency of the inverter chain circuit due to an electrically fast transient injected on the power supply line, along with predictions from our analytic model.

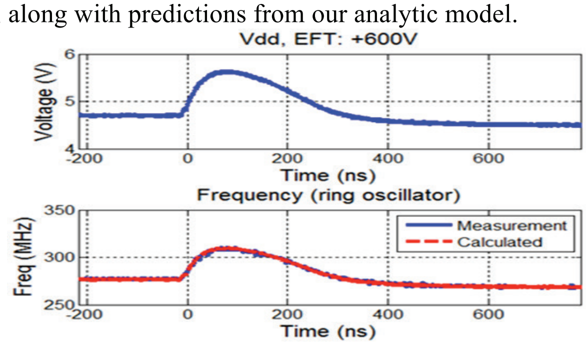

Figure 1: Variation in natural oscillation frequency due to injected EFT (blue- experiments, red- predictive model).

References

[1] www.ireap.umd.edu/MURI-2001/FinalReport-103106/MURI01FinalReport-06.pdf

[2] S.Hemmady, "RF Upset of Digital Systems", Final Technical and Scientific Report, AFRL-RDHE, Submitted Dec. 2013.

Tracking Electromagnetic Interference in an Urban Environment on the World Wide Web

Dr. Osman Cerezci
Department of Electrical & Electronics Engineering,
Sakarya University
Sakarya, Turkey
cerezci@sakarya.edu.tr

Dr. A. Yasin Citkaya
Department of Innovation and R&D Strategies
NETAS Telecommunications Inc.
Istanbul, Turkey
ycitkaya@netas.com.tr

***Abstract*— Electromagnetic radiation stemming from base stations and high voltage power lines in the vicinity of houses is considered as one of the most concerning source. That is the reason why the study of "Tracking Electromagnetic Interference from base stations via GPS coordinates on the world wide web" is carried in Nilufer municipality in Turkey to inform public. Thanks to this project[1], the public living in Bursa-Nilufer municipality can go into web platform to see how many base stations are present in the neighborhood and to follow the present electromagnetic radiation density.**

Keywords- electromagnetic radiation; web; base station; analysis

I. Introduction

High speed data transfer need in mobile communication has triggered planning and installation of new base stations; as a result of which electromagnetic radiation exposure is on rise. The studies illustrating exact findings of health effects of electromagnetic radiation due to mobile base stations and radio-television transmitters are not completed yet, due to the fast developing mobile communication technologies and the relatively slow enhancements in scientific research. That is why people have become more concerned and started to demand information about electromagnetic radiation sources and density levels in their neighborhood.

II. Measurements

In this study, more than two hundred measurement analyses have been carried out to assess electromagnetic radiation levels near houses, schools, offices and children playing fields of high daily occupation in the city. For radiofrequency signals, Narda NBM550 broadband field meter with EF0691 isotropic E-field probe and Narda SRM3006 selective radiation meter with 27MHz-3GHz isotropic E-field probe are used, whereas for ELF band magnetic field measurements, Narda ELT400 with 1Hz-400kHz field probe is used. Figure 1 illustrates a sample continuous and long duration measurement in a house which is across a base station. The study also focuses on the development of the web system enabling public to reach electromagnetic radiation density stemming from base stations. People logging their location in web will be able to see measurement results on Google maps, all base stations and their distances in 300 meters radius. Furthermore, system enables to get antenna directions, base station EMF values and measurement dates, as shown in Figure 2.

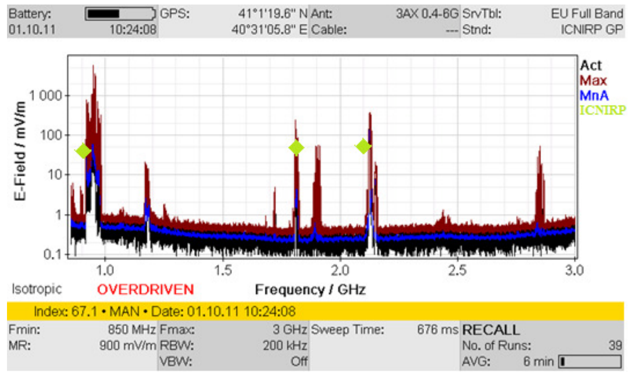

Figure 1. EMR density with respect to frequencies in a house across a base station

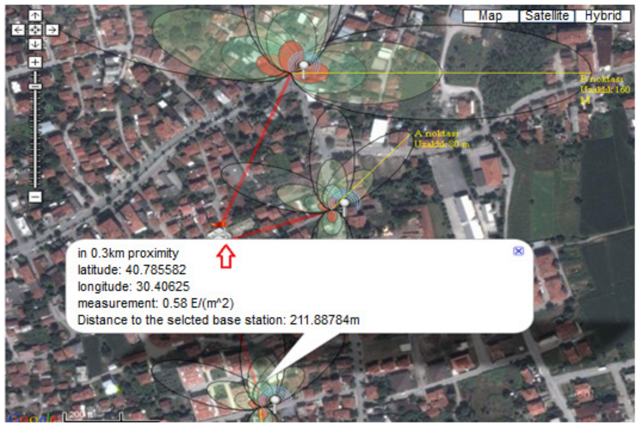

Figure 2. Representation of base stations in the web application

III. Findings and Discussion

In this study, measurements for 228 base stations located in Nilufer/Bursa municipality with population around 300,000 have presented that 95% of indoor electric fields are found to be below 3V/m, which is much lower than the maximum ICNIRP safety limits (42V/m for 900MHz, 58V/m for 1800MHz, and 61V/m for 2100MHz).

When the measurements are repeated in the following year, it has been found out that EM radiation levels have considerably increased due to new base station installations in specific areas. These long duration onsite measurements, which are also disclosed in the web, contribute to public information and conscious.

References

[1] O. Cerezci, Nilufer Municipality Electromagnetic Pollution Report, Nilufer Municipality Publications, 2012.

Study of Electromagnetic Risk Analysis in Hospitals

Dr. Osman Cerezci
Department of Electrical & Electronics Engineering,
Sakarya University
Sakarya, Turkey
cerezci@sakarya.edu.tr

Dr. A. Yasin Citkaya
Department of Innovation and R&D Strategies
NETAS Telecommunications Inc.
Istanbul, Turkey
ycitkaya@netas.com.tr

***Abstract* — Widespread usage of electrical devices has increased the focus on the necessity to assess and regulate electromagnetic radiation in especially sensitive areas like hospitals and health clinics. These sensitive places are where both patients and also staff are uncontrollably exposed to negative effects of electromagnetic radiation due to intensive diagnosis and treatment appliances operating in clinic environment. In this regard, European countries established the standard EU2004/40 to regulate electromagnetic environment assessment. This study mainly focuses on electromagnetic field assessment by conducting both low and high frequency electromagnetic field measurements in a selected hospital in Turkey. Then the measurement results will be discussed in the scope of EU 2004/40 directive to achieve satisfactory preventive measures.**

Keywords- electromagnetic radiation; hospital; risk; analysis

I. INTRODUCTION

In order to characterize the electromagnetic fields in hospitals, it is necessary to determine the locations and specifications of indoor appliances, electrical installations and wiring, and also outdoor electromagnetic radiation sources, such as base stations, high voltage transmission lines and transformers. Hospital areas near corridor intersections, emergency rooms, operating rooms, vicinity of MRI appliances, diathermy units are hot spots in terms of electromagnetic radiation intensity.

Due to rapid increase in mobile telecommunication adaptation, mobile phone signals in the hospitals create interference for biomedical appliances [1, 2]. That is why there has been restrictive guidance for GSM frequency electromagnetic radiation levels by ICNIRP. In this study, both high and low frequency electromagnetic fields are measured in a city hospital, where indoor antennas present and 380kV high voltage power transmission lines are in the vicinity by 20-30 meters.

II. MEASUREMENTS AND METHODOLOGY

Due to hospital's intense working conditions, measurements are carried out in different places of the hospital, with high focus on patient comfort and hygienic conditions. Wide band high frequency measurements are carried out with PMM8053 and 100 kHz–3 GHz probe; while frequency selective measurements are realized with Advantest 9 kHz–3 GHz spectrum analyzer and other appropriate antennas. Holaday HI3604 model 30 Hz–2000 Hz field meter is used in low frequency measurements.

In Fig. 1, electromagnetic field measurement near the diathermy machine in hydrotherapy room is presented. Figure 2 illustrates magnetic field strength measurements, together with extreme values, obtained at 38 different spots in the first building. Therefore, these figures not only reveal the electromagnetic effect of 380kV power transmission lines which are at a distance of 20-30 meters to the hospital buildings, but also the EM fields created during medical appliance operations.

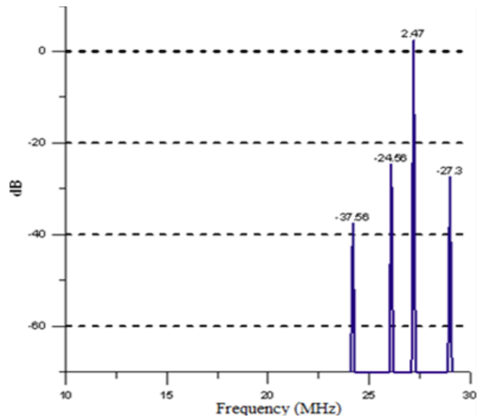

Figure 1. Hydrotherapy room measurements from 1m distance

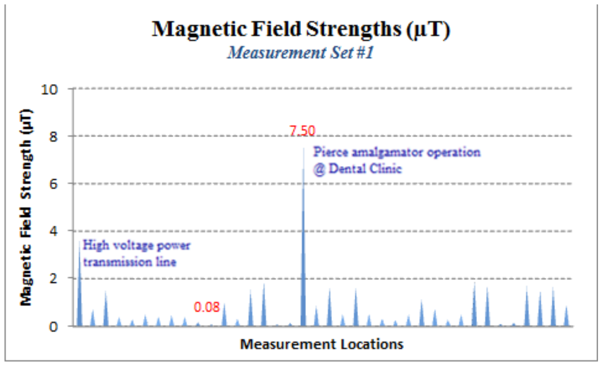

Figure 2. Electromagnetic field measurements in the hospital building #1

III. DISCUSSIONS AND CONCLUSION

It has been observed through the analysis of ELF and HF electromagnetic field measurements that the results are within the ICNIRP limits (for high voltage transmission lines 5000V/m, for GSM frequencies 42-61V/m). The 380kV high voltage power transmission lines outside the hospital create ELF magnetic field whose value is found to be quite larger than 1µT. The measurement results due to high voltage power transmission lines around the hospital exceed the ICNIRP safety values. For this reason, a corridor of 30m on both sides of the transmission line should be prevented from human presence for example with fences etc. to minimize unintended electromagnetic radiation exposure. Additionally, keeping other patients away from the diathermy device operating in the hydrotherapy room would be useful to minimize unwanted radiation exposure.

REFERENCES

[1] H. W. Ott, Electromagnetic Compatibility Engineering, Wiley, 2009.

[2] J.L. Silverberg, "Performance Degradation of Electronic Medical Devices Due to Electromagnetic Interference", Compliance Eng., pp 25-39, 1993.